# Evaluating B cell phenotype and function in the tumor microenvironment of head and neck cancer

by

**Ayana Tene' Ruffin**

BS, Towson University, 2015

MS, Towson University, 2017

Submitted to the Graduate Faculty of the

School of Medicine in partial fulfillment

of the requirements for the degree of

Doctor of Philosophy

University of Pittsburgh

2022

UNIVERSITY OF PITTSBURGH

SCHOOL OF MEDICINE

This dissertation was presented

by

**Ayana Tene' Ruffin**

It was defended on

July 26, 2022

and approved by

Dario A.A. Vignali, PhD
Frank Dixon Chair in Cancer Immunology, Vice Chair and Professor, Immunology

Mark J. Shlomchik MD, PhD
UPMC Endowed and Distinguished Professor, Chair, Immunology

Walter Storkus, PhD
Professor, Dermatology, and Immunology

Geetha Chalasani, MD
Associate Professor, Medicine, and Immunology

Timothy F. Burns, MD PhD
Associate Professor, Medicine, Hematology-Oncology

Dissertation Director: Tullia C. Bruno, PhD
Assistant Professor, Immunology

Copyright © by Ayana Tene’ Ruffin

2022

**Evaluating B cell phenotype and function in the tumor microenvironment of head and neck cancer**

**Ayana Tene' Ruffin, PhD**

University of Pittsburgh, 2022

B lymphocytes (B cells) are crucial for producing antibodies that provide lifelong protection against invading pathogens. Prevalence of B cells in human solid tumors correlates with favorable outcomes and can predict response to current immune checkpoint inhibitors (ICI). However, their role in immune responses to solid tumors remains understudied. To determine the therapeutic potential of B cells, it is critical to characterize B cell phenotype and function within different tumor microenvironments (TMEs).

Patients with HNSCC caused by human papilloma virus (HPV+) have significantly higher germinal center like (GC-like) B cells and tertiary lymphoid structures (TLS) in their tumors compared to carcinogen driven HNSCC tumors (HPV-)which correlated with better overall survival. Patients had superior outcomes in both etiologies when their TLS contained GCs. Semaphorin4a (Sema4a) marks GC-like B cells and its expression increases as naïve B cells differentiate into GC-like B cells in HNSCC **(Chapter 3).** Class-switched (SW; CD27+) memory B cells (MBC), which can be products of GCs are increased in both HPV+ and HPV- HNSCC tumors and peripheral blood (PBL) compared to inflamed tonsil and healthy donor PBL. I also report an increase in a two extrafollicular, or GC independent B cell subpopulations termed double negative 2 (DN2) ($CD11c^{+}CD27^{-}$ $IgD^{-}$ $CD21^{-}$) and double negative 3 (DN3) ($CD11c^{-}CD27^{-}$ $IgD^{-}$ $CD21^{-}$) in HNSCC

patients.DN3 B cells are increased in locally advanced (LA) HNSCC tumors with higher tumor stage and more prevalent in HPV- patients but DN2s are absent in HNSCC tumors. DN3 are also abundant in PBL of patients with metastatic melanoma (MEL) and lung cancer while DN2s were abundant in HNSCC and Lung cancer PBL. Higher frequency of circulating DN3 was observed in MEL patients with progressive disease. Lastly, I show that DN3 and DN2 B cells are less functional than SW MBC (**Chapter 4).**

Taken together, my findings suggest that the presence of GC B cells and TLS formation in the TME may be indicative of having an enhanced anti-tumor response mediated by T cells and overall better control of disease. Accumulation of intratumoral and circulating DN3 B cells may be indicative of an immunosuppressive microenvironment.

## Table of Contents

**Preface** ..... xvi

**1.0 Introduction** ..... 1

**1.1 Cancer** ..... 2

**1.1.1 Cancer immunity cycle** ..... 3

**1.2 Head and Neck Squamous Cell Carcinoma** ..... 5

**1.2.1 Etiologies of Head and neck cancer** ..... 5

**1.2.2 The role of HPV viral proteins in HNSCC development** ..... 7

**1.2.3 Unique ecosystems of HNSCC: one disease; two microenvironments** ..... 8

**1.2.3.1 Using The Cancer Genome Atlas to evaluate differences in immune cells and immune related genes and their impact on survival in HNSCC** ..... 9

**1.2.3.2 Functional CD8 and CD4 effector T cells are key to a robust immune response in HPV+ and HPV- disease** ..... 12

**1.2.3.3 Regulatory T cells drive immunosuppression in the HNSCC TME** ..... 14

**1.2.3.4 Innate immune cells complement adaptive immunity in the HNSCC TME** ..... 17

**1.2.3.5 Stromal tissue is an important regulator of the HNSCC TME** 21

**1.3 B lymphocytes** ..... 26

**1.3.1 B cell differentiation and subsets** ..... 27

1.3.1.1 Germinal centers ..... 28
1.3.1.2 Tertiary Lymphoid structures ..... 31
1.3.2 B cell function ..... 32
1.3.2.1 Antibody mediated effector function ..... 32
1.3.2.2 Antibody-independent effector function ..... 33
1.4 Harnessing B Cells and TLS for Antitumor Immunity ..... 35
1.4.1 Mouse versus Human cancer studies: Are B Cells Friend or Foe? ..... 35
1.4.2 Clinical significance of B cells and TLS in human tumors ..... 37
1.4.3 Significance of TLS subtypes in the TME ..... 38
1.4.4 How do tumor infiltrating B cells contribute to tumor immunity? ..... 42
1.4.4.1 Targets of tumor-reactive antibodies ..... 43
1.4.4.2 Antibody-mediated effector mechanisms ..... 45
1.4.4.3 Antigen presentation ..... 46
1.4.4.4 Cytokine production ..... 47
1.4.4.5 Direct Tumor lysis ..... 48
1.5 Questions to address ..... 51
2.0 Methods ..... 53
2.1 Human subject details ..... 53
2.2 Method details ..... 54
2.2.1 Blood and tissue processing ..... 54
2.2.2 Flow cytometry-based cell sorting ..... 55
2.2.3 Single-cell RNAseq Library Preparation and Sequencing ..... 55
2.2.4 Processing and clustering of single-cell RNAseq data ..... 56

**2.2.5 Identification of cell types in single-cell RNAseq.....57**

**2.2.6 Quantification of differences in cell frequencies across clusters....58**

**2.2.7 Gene set enrichment analysis of B cells .....58**

**2.2.8 Survival analysis using The Cancer Genome Atlas.....59**

**2.2.9 Pseduotime analysis of B cells .....59**

**2.2.10 Adaptive B cell receptor Sequencing.....60**

**2.2.11 Surface and intracellular antibody staining of patient and healthy donor cells .....61**

**2.2.12 High dimensional spectral cytometry .....61**

**2.2.13 Single-plex immunohistochemistry.....62**

**2.2.14 Cytoscape analysis .....63**

**2.2.15 Immunofluorescence analysis .....63**

**2.2.16 Immunofluorescent confocal microscopy .....64**

**2.2.17 Statistical analysis.....65**

**2.2.18 Data availability .....65**

**2.2.19 Code availability.....66**

**2.2.20 BCR signaling assay.....66**

**2.2.21 Mitotracker and 2-NBDG staining.....67**

**2.2.22 Extrafollicular B cell differentiation assay.....67**

**2.2.23 Antibody production and ASC differentiation assay .....68**

**2.2.24 In vitro antigen presentation assay .....68**

**3.0 B cell signatures and tertiary lymphoid structures contribute to outcome in head and neck squamous cell carcinoma ..... 69**

3.1 Summary ..... 69
3.2 Introduction ..... 70
3.3 Results ..... 73
3.3.1 Distinct TIL-B transcriptional signatures in HNSCC are revealed by single cell RNA sequencing ..... 73
3.3.2 Germinal center TIL-Bs and tertiary lymphoid structures are increased in HPV+ HNSCC ..... 78
3.3.3 SEMA4A expression is associated with GC B cell differentiation and TLS with GC in HNSCC ..... 83
3.3.4 Dissection of germinal center B cell reactions reveals distinct waves of gene expression ..... 91
3.3.5 Tertiary lymphoid structures are associated with better survival in HNSCC ..... 95
3.4 Discussion ..... 99
3.5 Author contributions ..... 103
4.0 Prevalence of intratumoral and circulating extrafollicular b cells is associated with disease progression in cancer patients ..... 104
4.1 Summary ..... 104
4.2 Introduction ..... 105
4.3 Results ..... 109
4.3.1 Extrafollicular derived B cell subpopulations are abundant in cancer patients and may predict disease outcome ..... 109

4.3.2 Tumor location and environment may drive extrafollicular responses in HNSCC ..... 115
4.3.3 Intratumoral and circulating extrafollicular-derived MBCs have markedly reduced effector function compared to GC-derived MBC ..... 118
4.3.4 Circulating DN3 and DN2 share a B cell exhaustion-like expression profile that may be driven by Th1 cytokine signals in cancer patients ..... 125
4.4 Discussion ..... 134
4.5 Author contributions ..... 140
5.0 Future directions ..... 141
5.1 Summary ..... 142
5.1.1 B cell-based immunotherapy: The next generation ..... 143
5.1.1.1 Effects of current therapies on B cells ..... 144
5.1.1.2 How do we target B cell and TLS as a form of immunotherapy? ..... 145
Appendix A ..... 154
Appendix B ..... 171
Bibliography ..... 181

## List of Tables

**Table 1: Clinical characteristics of prospective patient cohort for single-cell RNAseq and immunofluorescence (Cohort 1) ..... 167**

**Table 2: Clinical characteristics of prospective patient cohort for spectral flow cytometry and protein validation (Cohort 2) ..... 168**

**Table 3: Clinical characteristics of retrospective patient cohort for IHC and TLS analysis (Cohort 3) ..... 169**

**Table 4: Flow cytometry antibody panels (Chapter 3) ..... 170**

**Table 5: Flow cytometry antibody panels (Chapter 4) ..... 172**

## List of Figures

**Figure 1: New targets for T cells in the HNSCC TME ..... 16**

**Figure 2: Innate cell interactions generate inflammatory signals that drive HNSCC patient outcome ..... 20**

**Figure 3: The stromal microenvironment is functionally important for the HNSCC TME ..... 25**

**Figure 4: B cells and TLS are heterogeneous within the tumor microenvironment ..... 41**

**Figure 5: Potential Anti-tumor roles for B cells in the tumor microenvironment .. 50**

**Figure 6: Differences in tumor infiltrating B cell and helper CD4+ T cells between HPV- and HPV+ HNSCC contribute to survival. ..... 77**

**Figure 7 : High dimensional flow cytometry and immunohistochemistry reveal distinct TIL-B phenotypes and increased tertiary lymphoid structures in HPV+ HNSCC. ..... 82**

**Figure 8: Differentially expressed ligands and receptors in HNSCC and modeling of GC differentiation identify SEMA4A as associated with development and maturation of GC. ..... 88**

**Figure 9: Sema4a expression is increased in GC TIL-Bs in TLS in HNSCC..... 90**

**Figure 10: Cyclical pseudotime modeling of germinal center B cell reactions reveals waves of gene expression. ..... 94**

**Figure 11: Increased TLS with GC within HPV+ HNSCC patients correlate with increased patient survival..... 98**

**Figure 12: Increased presence of intratumoral and circulating extrafollicular B cells is associated with disease progression and may be predictive of disease outcome in cancer patients. ..... 114**

**Figure 13: Presence of tissue-resident DN3 B cells is increased in HPV- tumors ..... 117**

**Figure 14: Circulating and intratumoral extrafollicular B cell subsets are hyporesponsive to BCR stimulation ..... 122**

**Figure 15: Circulating and intratumoral GC and EF B cell subsets are isotype-switched but EF B cells are poor antibody producers ..... 123**

**Figure 16: Hyporesponsiveness of intratumoral DN3 B cells to stimulation may be due to mitochondria stress and glucose avidity ..... 124**

**Figure 17: Circulating DN3 and DN2 B cells in cancer patients co-express Tbet, Tox, and inhibitory receptors but intratumoral DN3 B cells do not..... 130**

**Figure 18: scRNA seq analysis of cytokines in HPV+ and HPV- HNSCC tumors and PBL ..... 131**

**Figure 19: TLR7 and cytokines induce differentiation of Naïve B cells and SW MBCs into DN3, DN2 and ASC in vitro ..... 132**

**Figure 20: Summary of ex vivo function and proposed origin of EF MBC subsets in cancer ..... 139**

**Figure 21: Targeting B cells and TLS for cancer immunotherapy ..... 152**

**Appendix Figure 1: Validation of a combination Wilcoxon rank sum test and clustering based method for identification of cell types ..... 155**

**Appendix Figure 2: Identification of cell types from patients and controls using the combination Wilcoxon rank sum test and clustering based approach. .... 157**

**Appendix Figure 3: Statistical assessment of observed versus expected number of cells in germinal center and plasma cell clusters. ..... 159**

**Appendix Figure 4: Relationship between germinal center cell states and TFH cells in samples from The Cancer Genome Atlas..... 160**

**Appendix Figure 5: Adaptive BCR sequencing reveals no difference in clonality or other metrics between HPV– and HPV+ TIL. ..... 161**

**Appendix Figure 6: B cells are significantly increased compared to plasma cells in HNSCC patients. ..... 163**

**Appendix Figure 7: Additional high dimensional analysis of HNSCC cohort 2… 164**

**Appendix Figure 8: Flow cytometry gating strategy for B cell and T cell profiling. ..... 165**

**Appendix Figure 9: Multivariate survival analysis for TLS, HPV status, and disease burden. ..... 166**

**Appendix Figure 10: Comparision of germinal center and extrafolliicular B cell differentiation pathways ..... 173**

**Appendix Figure 11: Comparision of DN2 MBC phenotype in different diseases ..... 174**

**Appendix Figure 12: Additional quantification and clinical correaltion of GC and EF derived B cell subsets..... 175**

**Appendix Figure 13: Clinical correlation of EF subsets in Lung cancer patient cohort ..... 176**

**Appendix Figure 14: Quantification of B cell exhaustion-like program in SW, Naïve, DN1 subsets ..... 177**

**Appendix Figure 15: Gating stategy for in vitro EF differentiation assay ..... 178**

**Appendix Figure 16: in vitro antigen presentation assay ..... 180**

## Preface

This journey to becoming a professional scientist has not been easy but it has been the most rewarding thing I've done in my life thus far. To be the first in my family to successfully pursue both undergraduate and graduate level education is something I am extremely proud of. I am very grateful for all those who took have taken on the role of mentor and continue to help guide me along this path. I have made many friends along the way who have provided support in so many ways. I have had an amazing PhD experience that I will look back fondly on for years to come. I would like to use this space to share my gratitude for the village of people who made this work possible.

I would first like to thank my mentor Dr. Tullia Bruno. Tullia, working for you has been nothing short of an amazing experience. You have helped transform me into a more thoughtful scientist and I am a better public speaker because of your mentorship. Your kindness and compassion really helped me get through the tough years of graduate school. Thank you for always being there and advocating for me especially when I was unable to advocate for myself. You taught me to be fearless and go after what I want. I want to thank you for giving me the space to explore my own Ideas and cheering me up when things didn't go the way we planned. You're a rockstar scientist and have taken the field of cancer immunology by storm. It's amazing to see the field take notice. I have learned so much about starting and running a research lab from you that I know I will be able to use the tools you have gifted me to start my own program in the not-so-distant future and perhaps one day we will collaborate on a project. You have a knack for cultivating teams and I am so proud to be one the first to graduate from the Bruno lab

team. I can't wait to see how far the lab goes and what you guys discover. You always remind me of how proud you are of my accomplishments, and I am equally proud of you for all that you've done in just the span of my PhD all while growing and raising two adorable little humans! I know you will continue to be at the forefront of translational research, and I can't wait to see what you create in terms of a B cell-based therapy. Go forth and be fierce!

When I came to Pitt in 2017, I knew I wanted to study immune cell biology and do translational research. I didn't know what that would entail exactly, and I also did not anticipate that I would get to work with so many leaders who are pushing the field forward. I would like to thank my thesis committee: Drs Walter Storkus, Geetha Chalasani, Mark Shlomchik, Timothy Burns, and Dario Vignali for their invaluable guidance and encouragement throughout my graduate career. Mark and Geetha, your B cell expertise has been so crucial to the completing my thesis work and I am grateful that I got to work with two experts and now at the end of my PhD I feel like I have a great grasp on B cell biology to take with me on my next endeavor. Walt, Tim, and Dario, you have all taught me what it means to take our bench work and bring it to bedside. I have learned how to think more deeply about the basic and translational science we are doing and what it means for patients from each of you. Your support and sometimes tough questions have really helped mold me into a better scientist and I am happy that I got to know and work with you all.

To the Vignali Lab, Thanks for allowing me to be an honorary Vignali Lab member for a little while and brining B cells to your T cell space. I admire many things about how Dario structures and directed research in his lab, and I am grateful that I got to participate

and learn from such a prominent leader in the field. I had fun working with you all and helping plan lab retreats and learning from your lab meetings/ focus groups. Tony, Feng, Sayali, Chris, and Ashwin it was a pleasure to get to know all of you and you each taught me something that made me a better scientist. You are all immensely talented and I hope our paths continue to cross in the future at conferences and maybe potential collaborations!

To the Bruno Lab past and present, Ian, Hye Mi, Sheryl, Asia, Noor, Zel, Anjali, Grant, Mia, Xiang, Alex, and Caleb It has been a pleasure working with all of you. I have learned so much from each of you and mentoring you all has made me a better scientist and lab mate. I am happy that I was able to be a mentor and a source of information to help you in the lab. You each have added something special to the group and I love seeing you all grow and do great work. Can't wait to see what you guys discover in the future! We will have to reunite at conferences in our Bruno lab swag!

Original "OG" PMI class, Sid, Ronal, T, Amie, Steph, Jess, Allison, Sean, Kristin, Ellyse, and Pam can't believe we are at the end of our journey here at Pitt! Thanks for all the wine nights, game parties, vacations, and science conversations. I know that we will continue to be friends and colleagues long after we graduate from Pitt.

Lastly, I'd like to thank my family and friends for all their support. I hope I have made you all proud. Thank you for supporting my dreams no matter how big or small. To my mom, who is my biggest cheerleader thank you for celebrating every win and comforting me when the journey got difficult. To my partner in life, Donte Hill, thank you for being my best friend all these years. I am lucky to be on this journey with you and I couldn't have reached this point without your support. During the hardest part of this

journey, you reminded me that I worked hard to get here against all the odds we grew up in and I can do anything if I put my mind to it. To all my friends back home, Freddy, Curtis, James, Danielle, Tarica, Lauren, Shakela, Talaysia and so many others, your support has been so comforting and can't wait to celebrate this accomplishment with you all.

# 1.0 Introduction

Portions of subsection 1.2 (1.2.3-1.2.4) are unpublished but were compiled, submitted in a review article that is under review at *Nature Reviews Cancer* titled:

**Ruffin AT**, Li, H, Vujanovic, L et al. Improving head and neck cancer therapies by immunomodulation of the tumor microenvironment. *Nature Reviews Cancer*. *In Revision.*

Portions of this chapter (1.4-1.6) were compiled and published in the second edition of *Cancer Immunotherapy: Principles and Practice* in the following book chapter *Cancer:*

**Ruffin AT**, Bruno TC. Harnessing B cells and tertiary lymphoid structures for antitumor immunity. In: Butterfield LH, Kaufman HL, Marincola FM, Ascierto PA, Puri RK, eds. Cancer immunotherapy principles and practice. New York, NY: Springer Publishing Company; 2021. doi:10.1891/9780826137432.0042. Copyright license ID (1223908-1)

## 1.1 Cancer

Cancer is a chronic, complex and heterogenous disease that develops when normal cells in the body grow uncontrollably, spread, and destroy the normal existing tissue. Cancer can develop from almost any cell in the body and is caused by changes in genes that control cell function and growth. These changes can be induced by (1) failure to repair errors that occur during DNA replication during the cell proliferative cycle, (2) damage to DNA caused environmental carcinogens such as UV radiation from the sun or chemicals in food and tobacco products, (3) inherited genetic abnormalities and (4) infection with cancer causing (oncogenic) viruses ,(5) epigenetic modifications[1]. Cancers fall into two main categories: (1) hematological (blood) cancers: which develop in white blood cells (leukemias, lymphomas and multiple myeloma) or (2) solid tumor cancer: which develop in body organs and tissues such as breast, lung, and liver[2,3].

Hanahan and Weinberg originally proposed six biological properties (hallmarks) that normal cells adopt during the development into tumors including: (1) sustaining proliferative signaling, (2) evading growth suppressors, (3) resisting cell death, (4) enabling replicative immortality, (5) inducing angiogenesis, and (6) activating invasion and metastasis[4]. Discovery of these features of cancer cells through a vast amount of cancer research studies established the foundation for our understanding of cancer and provided instruction for the design anti-cancer therapies. Over a decade later , following a growing body of evidence, two additional hallmarks were added (7) deregulating cellular energetic (reprograming cellular metabolism) and (8) evading immune destruction[5]. Additional characteristics of tumors including genomic instability and mutation and tumor promoting inflammation have been implicated in enabling tumors to grow and progress.

Recently, several additional hallmarks have been proposed including (9) cell plasticity and disrupted differentiation, (10) non-mutational epigenetic reprogramming and (11) presence of polymorphic microbiomes within tumors[6]. This ever-growing list of hallmarks reinforces the fact that cancer research is ever-growing and there is still much to learn about tumor biology.

Cancers are diverse “ecosystems” composed of many different cell types and non-cellular components. This can include tissue resident normal cells and malignant cells, infilitrating immune cells, stromal cells, extracellular matrix, blood vessels, cytokines, chemokines, and growth factors. This collection of cellular and non-cellular components constitutes the tumor microenvironment (TME)[7–9]. The TME plays an important role in development, progression, and metastasis of tumors. The TME is also inherently complex, and components vary across tumor types and even within a given tumor type. Increasing focus has been placed on understanding the role of immune cells in these environments given the success of cancer therapies that harness the immune system’s ability to detect and destroy cancer cells. These therapies are collectively known as immunotherapies.

### 1.1.1 Cancer immunity cycle

There is a series of ordered events that must occur for the immune system to effectively kill cancer cells referred to as the cancer immunity cycle[10]. These events include in order: (1) release of cancer antigens, (2) cancer antigen presentation by antigen presenting cells (dendritic cells (DCs)/APCs), (3) Priming of T cells by APCs, (4) trafficking of T cells to tumors, (5) infiltration of T cells into tumors, (6) recognition of

tumors to by T cells, (7) killing of cancer cells. Cancer cells evolve mechanisms to subvert one or more of these important events, thus the cancer immunity cycle does not perform optimally in cancer patients[10]. Current cancer treatments including immunotherapies are designed to antagonize cancer immune evasion mechanisms. For example, there are several chemotherapies drugs that induce DNA damage such as oxaliplatin and cyclophosphamide that can initiate the immunogenic cell death (ICD) of tumor cells leading to the exposure of damage associated molecular patterns (DAMPs) such as calreticulin (CALR), heat-shock proteins (HSPs) and high-mobility group box 1 (HMGB1) and the release of cancer antigens which alert the surveilling immune system to respond to danger[11,12]. On the other hand, tumor cells upregulate inhibitory ligands such as programmed cell death ligand (PDL1) which binds to the inhibitory receptor programmed cell death protein 1 (PD1) on T cells effectively inhibiting their ability to kill tumor cells and to remain alive in the TME. Immune checkpoint blockade (ICB) is a class of immunotherapy drugs (monoclonal antibodies; mAb) that block the interaction of inhibitory ligands and their receptors such as PD1-PDL1 to allow T cells to function properly in tumors over extended periods of time[10,13,14]. We are learning that there isn't a "one-size" fits all treatment for cancer. In fact, some treatments such as anti-PD1 only work in some cancer types, and within in each cancer type some patients fail to respond at all to specific treatments. I would assert that expanding our understanding of how the cancer immunity cycle is affected in different tumor types is paramount for designing new treatments and determining how to effectively combine cancer treatments to achieve maximal benefit for patients.

## 1.2 Head and Neck Squamous Cell Carcinoma

My dissertation research mainly focuses on one type of cancer known as head and neck cancer.

### 1.2.1 Etiologies of Head and neck cancer

Head and neck squamous cell carcinoma (HNSCC) is the 6$^{th}$ most common cancer type worldwide with incidence rates expected to increase by 30% by 2030[2,15,16]. HNSCC develop in the mucosal epithelium of the oral cavity, pharynx, and larynx. Within in the oral cavity, tumors can originate in the lips, buccal mucosa, hard palate, anterior tongue, floor of the mouth and retromolar trigone[15]. The pharynx can also be subdivided into distinct anatomical sites where tumors can arise which include the nasopharynx, oropharynx (palatine tonsil, lingual tonsil, base of tongue, soft palate, uvula) and hypopharynx[15]. Tumors that originate in the oral cavity, larynx, hypopharynx are primarily driven by persistent tobacco consumption, alcohol abuse or both[15]. Tumors that occur in the oropharynx are driven by infection with high-risk human papilloma virus (HPV)[15,17]. Thus, HNSCC tumors can be classified as HPV-negative (HPV-) and HPV-positive (HPV+).

Normal mucosal epithelial cells develop into HNSCC via an ordered series progression of events initiated by genetic mutation in and/or degradation of key signal transduction molecules and/or amplification of key pathways associated with cell growth, survival, and metastasis. These events include: (1) hyperplasia, (2) dysplasia, (3) carcinoma in situ and (4) invasive carcinoma. Although the majority of head and neck

cancers are squamous cell carcinomas, the two causative agents of HNSCC promote a genetically and biologically heterogeneous cohort of tumors[15,18,19]. HPV- HNSCC is driven by activating or inactivating mutations in multiple oncogenes and tumor suppressor genes (TSGs)[15,18]. However, HPV+ HNSCC is driven by changes in proteins encoded by oncogenes and TSGs that are rendered in active or amplified by HPV viral proteins[20,21]. In fact, genomic analysis of HPV+ and HPV- tumors revealed that HPV+ tumors have a significantly lower mutational burden and less allelic loss compared to HPV-[19,22].

Oncogenes encode for proteins that potentiate cancer development and progression[23]. TSGs encode for proteins that regulate cell cycle, growth, and the DNA damage response. Mutation in TSGs often leads to loss-of function in these proteins[23]. The TSGs that are commonly mutated in HPV- HNSCC include TP53 (encodes p53), CDKN2A (Cyclin Dependent Kinase Inhibitor 2A), PTEN (Phosphatase and tensin homolog), RB1 (encodes retinoblastoma protein pRb), NOTCH1 and FAT1 (FAT atypical cadherin 1)[15,18,19]. Oncogenes that are commonly mutated include EGFR (epidermal growth factor receptor), PIK3CA (phosphatidylinositol 3- kinase subunit-α)[19,22]. Of note, mutated oncogenes and TSGs have been identified HPV+ tumors including EGFR, FGFR2/3 (Fibroblasts growth factor receptor 2 and 3), KRAS, BRCA1/2, CCND1 (cyclin D1), PIK3CA and TRAF3 (tumor necrosis factor receptor associated factor 3), NOTCH1, DDX3X (DEAD-box helicase 3 X-linked) and MLL/23 (a histone methyltransferase)[19,22].

### 1.2.2 The role of HPV viral proteins in HNSCC development

Disease- associated high-risk HPVs are small, double stranded DNA viruses that integrate into the human genome at a single site which can vary across patients. HPV-16 is the most predominant HPV type identified in HPV+ HNSCC tumors. HPV-18, -33, -31- and -52 are found in a small subset of HPV+ HNSCC patients[20,24]. In contrast to HPV- HNSCC, cell cycle regulators such as p53, PTEN and retinoblastoma protein (pRb) are not mutated in HPV+ HNSCC but rather rendered inactive by HPV viral proteins E6 and E7[20,24]. Additionally, signaling pathways that promote cell survival and growth such as Wnt, Notch, EGFR, and Akt are activated by HPV E6/ E5[20,24,25].

E6 induces proteasomal degradation of p53 via cellular ubiquitin ligase E6AP (E6-associated protein). E6 can also inhibit additional tumor suppressor genes that contain a PDZ domain (PDZ proteins) via proteasome degradation. E6 has a PDZ binding motif (at the extreme C-terminus) which is not found in E6 proteins in non-carcinogenic HPV-types[26,27]. Degradation of these proteins via E6 leads to persistent PI3K/AKT signaling which promotes cell survival and growth. E7 deregulates pRb pathway via several mechanisms: (1) preventing binding of pRb to transcription factor E2F1 allowing increased entry into cell cycle, (2) promoting the degradation of pRb via cellular ubiquitin ligase cullin 2, (3) binding to E2F1 thereby increasing its activity and blocking the activity of the E2F1 transcriptional suppressor E2F6. E6 and E7 both deregulate microRNAs ,which exhibit tumor suppressor activity. The function of HPV E5 function has not been well characterized as those for , E6/E7, but some studies have revealed that E5 increases activation of EGFR signaling and inhibits the Fas/FasL apoptosis pathway[24,28,29]. E5 can also enhance the carcinogenic effects of E6 and E7[20,24]. While the viral E6 and E7 genes

are integrated into the host genome and are always expressed in HPV+ tumors, HPV E5 is not integrated but instead expression is retained in episomes[24]. Transcriptional analyses of HPV+ tumors have revealed that only a fraction patients retain E5 expression[30].

### 1.2.3 Unique ecosystems of HNSCC: one disease; two microenvironments

In addition to the unique molecular changes in the tumor cells, HPV+ and HPV- tumors have unique stromal compartments, differing in infiltration of immune cells and non-cellular components. The importance of these differences is underscored in the fact that HNSCC patients with HPV+ tumors have had historically more favorable survival rates in the locally advanced (LA) setting and superior response to chemotherapy/radiation than HNSCC patients with HPV- tumors[31,32]. Only a subset of patients with recurrent (R) and metastatic (M) (R/M) disease respond to immunotherapy[33,34]. Understanding the diverse interactions of tumors and components of their TME is expected to ultimately lead to the development of improved anti-cancer therapies and novel combinatorial strategies to improve patient survival. Researchers investigating components of the TME in HNSCC have determined that HPV+ and HPV- HNSCC tumors have distinct TMEs[30,35,36]. The HNSCC TMEs provides researchers a unique opportunity to study how distinct drivers of cancer affect tumor immunity within the same disease. Additionally, comparing the TME's of patients with LA-HNSCC versus RM-HNSCC may provide insight into the factors that impact better responses biomarkers that may prevent recurrence in patients. In the following sections, I summarize and compare the advances made in dissecting the immune and non-immune compartments within

HPV+ and HPV- TMEs and discussing how these differences may affect patient outcomes.

#### 1.2.3.1 Using The Cancer Genome Atlas to evaluate differences in immune cells and immune related genes and their impact on survival in HNSCC

To address these knowledge gaps, researchers have employed state-of-the-art techniques and analyses such as bulk RNA sequencing (RNA-seq), single-RNA sequencing (scRNA-seq) and flow cytometry to determine the composition of immune and non-immune cells within HPV+ and HPV- HNSCC tumors in both the LA and R/M settings. The Cancer Genome Atlas (TCGA) is a database that contains genomic sequencing data of primary tumors from patients with over 33 different forns of cancer types representing a valuable resource to understand global changes in various aspects of tumor biology. The HNSCC cohort in TCGA (97 $HPV^+$, and 423 $HPV^-$ patients) contains bulk RNAseq data collected from tumor specimens resected from the different anatomic sites of the head and neck. This rich resource has allowed for improved understanding of the immunogenomic landscape differences that exist between these two TMEs and how this is shaped by clinical features including HPV status, tumor stage, mutational burden, tobacco, and alcohol use.

Several reports using gene set enrichment analysis (GSEA) and unsupervised clustering to deconvolute and identify cell types, have stratified HNSCC patients in the TCGA cohort based on immune signatures: cold (no immune infiltrate), or lymphocyte (enrichment for CD4+ T, CD8+ T, B cells and plasma cells) and myeloid/dendritic cell (DC) (enrichment of neutrophils, macrophages, monocytes, DCs, T regulatory cells (Tregs) and eosinophils)[37–40]. In terms of total abundance of each individual cell type,

HPV$^+$ HNSCC had a significant increase in frequencies of B cell, plasma cells, T helper type 1 CD4+ T cells (Th1), T helper type 2 CD4+ T cells (Th2), natural killer cells (NK) and CD8+ T cells compared to HPV$^-$ HNSCC. Monocytes, macrophages, natural killer T cells (NKT), and neutrophils were higher in HPV$^-$ HNSCC[37,38,40]. There have been conflicting reports regarding Treg abundance in HNSCC. One study reported there to be a higher abundance of Tregs in HPV$^+$ HNSCC based on bulk RNAseq analysis while another reported no significant difference[37,38]. Overall, lymphocyte gene signatures correlated with a longer overall survival rate compared to the other signatures, especially within the HPV$^+$ cohort of patients. Immune cold and myeloid/DC gene signature enrichment correlated with later stage III-IV and shorter overall survival[37,38,40]. Having an increased molecular signature associated with smoking, (defined by the mutational processes in each tumor attributable to tobacco smoking), correlated with poor immune infiltration in both HPV$^+$ and HPV- tumors and high total non-synonymous mutational burden[38].

Comparing individual differentially expressed immune related genes (IRGs) in the TCGA-HNSCC cohort revealed a total of 65 IRGs that were associated with prognosis, 56 of which were significantly associated with overall survival rates in HPV$^-$ HNSCC[39,41]. In this IRG prognosis model, SEMA3G, GNRH1, TNFRSF4 and ZAP70 were positively correlated with overall survival (OS). PLAU, SH2D1A, CCL26, DKK1, GAST, PDGFA and STC1 were negatively correlated with OS. Further, there was a 32% five-year survival rate for patients who expressed negatively correlated genes[41]. This study focused on HPV$^-$ HNSCC tumors with have low immune cell infiltration. Indeed, TCGA analyses that have focused on both TMEs have uncovered significant differences in several other

immune pathways. For example, CD8+ T cells express significantly upregulated expression of programmed death protein 1 (PD-1), T-cell immunoglobulin and mucin domain-3 (TIM3), lymphocyte-activation protein 3 (LAG3), and T cell immunoreceptor with Ig and ITIM domains (TIGIT) in $HPV^+$ vs $HPV^-$tumors[35,42–45]. In addition, CD8+ T cells in $HPV^+$ tumors also showed higher expression of T cell activation marker CD137 (4-1BB), and ectonucleotidase CD39 compared to $HPV^-$ tumors[46]. KIR inhibitory receptor genes that inhibit NK cell function are increased in $HPV^+$ tumors genes expressed on B cells such as CD200, VCAM1, BCL2 and ICOSLG are also increased $HPV^+$ patients[35,38].

Bulk RNAseq datasets such as the ones in the TCGA require deconvolution to identify cell types within samples and thus may underrepresent the composition and distribution of certain cell types within a given sample[47–50]. Thus, these analyses have limited ability to detect intratumoral heterogeneity and cell-to-cell variability based on gene expression. Further, differences in transcript quantification, read depth and sequencing platforms can compromise the reproducibility of TCGA analyses[48,50]. The development of single cell scRNAseq has revolutionized transcriptomic analysis of all cellular populations in the HNSCC TME Specifically, scRNAseq can uncover rare cell populations, novel protein-protein interactions, and track differentiation of cell types within a specific cell lineage[47,50]. Indeed, scRNAseq analyses paired with high dimensional flow cytometry and spatial multispectral imaging have revealed immense differences among innate and adaptive immune cells within $HPV^+$ and $HPV^-$ HNSCC tumors that were not captured by initial bulk TCGA analyses[30,36,51].

#### 1.2.3.2 Functional CD8 and CD4 effector T cells are key to a robust immune response in HPV+ and HPV- disease

CD8+ T cells play a pivotal role in controlling viral infections and eradicating tumor cells. They can recognize antigens presented by tumor cells in the context of MHC class I complexes and directly kill them by releasing proinflammatory cytokines such as interferon gamma (IFN-γ) and tumor necrosis factor alpha (TNF-α), and cytolytic granules containing perforin and granzymes. While there is a considerable decrease in the overall abundance of CD8+ T cells in $HPV^-$ HNSCC, those patients with comparable proportions of CD8 T cells to $HPV^+$ tumors tend to have favorable outcomes[52–54]. However, in cancer and chronic infection, T cells can become dysfunctional, (i.e. exhausted) exhibiting a hierarchal loss of effector function (IL-2, TNF-$\alpha$, and IFN-$\gamma$ production) and increased co-expression of the immune inhibitory receptors (IRs) PD-1, TIM3, LAG3, CTLA4, and TIGIT[55–58] . Recent scRNAseq that compared global changes in transcriptomic profiles of CD8+ TIL revealed five broad cell states in $HPV^+$ and $HPV^-$ disease, including cycling, cytotoxic, pre-dysfunctional or early activated, and terminally exhausted T cells[30,36]. Diffusion pseduotime analysis (DPT) which determines development relationships between cell populations revealed that CD8+ T cells follow a shared differentiation trajectory in $HPV^+$ and $HPV^-$ HNSCC moving from early activated CD8+ T cells toward terminally differentiated CD8+ T cells marked by co-expression of IRs[36]. Shared transcriptional profiles of exhausted CD8+ T cells have also been reported in paired LN metastases of LA treatment naïve $HPV^-$ HNSCC patients[51].

Recent high dimensional immune profiling studies using scRNAseq revealed that CD8+ TILs are a phenotypically and functionally diverse population within the antigen-

specific pool. scRNAseq analysis of HPV-specific T cells sorted from HPV$^{+}$ tumors and paired metastatic lymph nodes were composed of three distinct subsets: stem-like (PD-1$^{+}$TIM-3$^{-}$CD39$^{-}$TCF7$^{+}$), transitory (PD-1$^{+}$IFN-γ$^{high}$) and terminally differentiated (PD-1$^{+}$TIM-3$^{+}$CD39$^{+}$)[59]. TCR clonotypes directed at HPV proteins E2, E5 and E6 were shared amongst the three subsets which suggests that terminally differentiated CD8+ T cells derive from stem-like CD8+ T cells[59]. HPV-specific stem-like CD8+ T cells effectively proliferate upon in vitro stimulation with HPV peptide stimulation and immune checkpoint inhibition (ICI)[59]. This may imply that strategic reinvigoration of HPV-specific stem-like CD8+ T cells by ICI will benefit HPV$^{+}$ HNSCC patients. Stem-like CD8+ T cells are also present in HPV- HNSCC tumors and produce abundant levels of TNF-α, although their antigen specificity remains poorly understood[60]. More work is needed to determine how and if non-viral neoantigen-specific CD8+ T cell differentially contribute to response to therapy in both patient cohorts.

CD4+T cells are also essential for eliciting anti-tumor immune responses through their differentiation into distinct effector subtypes upon antigen stimulation and secretion of different cytokines supporting CD8 T cell and myeloid cell responses[61,62]. . Th1 CD4+ T cells produce proinflammatory cytokines, particularly IFN-γ and TNF-α, which induce MHC-class I and class II expression in the TME, thereby enhancing tumor antigen recognition by other immune effector cells, leading to increased killing of tumor cells[61,62]. T helper 17 (Th17) cells produce IL-17, IL-2, IL-8 and TNF-α and play an important role in protection against pathogens[63]. Both pro- and anti-tumor roles have been described for Th17 in both mouse and human cancer, although studies are limited for human tumors[64]. Higher numbers of Th1 CD4+ T cells are observed in HPV$^{+}$ HNSCC in comparison to

HPV- HNSCC. RNAseq analyses demonstrated that CD4+ TILs have higher RNA expression of Th1 marker TBX21 (encodes transcription factor T-bet and regulate IFN-γ production) as well as Th17 marker RORA and RORC in HPV+ vs HPV- HNSCC[65]. Further, HPV-16-specific CD4+ T cells predominantly express IFNγ and IL17, suggesting that Th1 and Th17 cells are enriched in the HPV+ TME[66,67]. In addition, HPV-16-specific CD4+ T cells release IFN-γ and TNF-α and synergize with cisplatin-based therapy to control tumor cell growth, highlighting their importance in patients' responsiveness to cancer therapies[68]. Th17 cells also accumulate in patient peripheral blood (PBL) and tumor draining lymph nodes (LNs) of HNSCC patients with primary HNSCC tumors express Th17 inducing cytokines IL-6, IL-23 and IL-1β[69,70]. Functionally, Th17 cells were able to suppress HNSCC tumor growth and decrease production of angiogenesis proteins by HNSCC tumor cells in vitro[69,70]. Future studies should further evaluate the antigen specificity and function of Th17 cells in both TMEs to determine their impact on patient outcomes. CD4+ T follicular helper cells (Tfh cells), which express CXCR5 and PD-1 produce the chemokine CXCL13, which is important for recruiting B cells and CD8+ T cells into the tumor[71–73]. Tfh cells are important for activation and maturation of B cells through IL-21 production and expression of costimulatory ligands such as inducible T-cell costimulatory (ICOS) and CD40 ligand[74,75]. Recent scRNAseq analysis demonstrated that a Tfh gene signature is enriched in HPV+ HNSCC and correlate with improved progression-free survival[36,76]

#### 1.2.3.3 Regulatory T cells drive immunosuppression in the HNSCC TME

Tregs are a subset of CD4+ T cells defined by their expression of the transcription factor Foxp3 (forkhead box protein 3) and CD25 expression, and they actively suppress

immune effector cell function and promote tumor progression[77]. Tregs exert immunosuppressive functions in tumors via their secretion of inhibitory cytokines, such as IL-10, IL-35 and TGF-β, upregulation of IRs, disrupting metabolism via CD39 and CD73 (catabolizing ATP), and depriving the local TME of IL-2 via high CD25 expression[77–79]. Tregs are present in PBL and tumors of HNSCC patients[79–81]. $HPV^+$ HNSCC patients have higher frequencies of intratumoral Tregs but recent scRNAseq analysis demonstrated that Tregs share transcriptomic profiles in $HPV^+$ and $HPV^-$ HNSCC[36]. Interestingly, Tregs exhibit unique transcriptional cell states distinguished by enrichment of IFN-response genes or tumor necrosis factor receptor (TNFR) family genes[36]. IFN-response genes correlated with early activation of Tregs while TNFR genes such as glucocorticoid-induced TNFR-related protein (GITR), 4-1BB, and OX40 were expressed later in differentiation suggesting reciprocal control of Treg effector function[36]. Key IRs, such as CTLA4, have also been described on Tregs in HNSCC[82]. CTLA4 expression is high on intratumoral Tregs in HNSCC patients and is further upregulated after cetuximab treatment[82] Expression of neuropillin-1 (NRP1) on intratumoral Tregs was shown to correlate with GITR and 4-1BB expression on Tregs[80]. NRP1+ Tregs have enhanced suppressive function and correlate with overall poor prognosis in HNSCC patients[80]. NRP1 expression on Tregs is driven by T cell activation signals and can be reduced by inhibiting molecules within the TCR signaling pathway[80]. Taken together, these data suggest that Tregs have diverse mechanisms to reinforce an immunosuppressive TME in HNSCC patients and thereby specifically inhibiting Tregs in the HNSCC TME may enhance immuno-therapeutic response. **(Figure 1)**

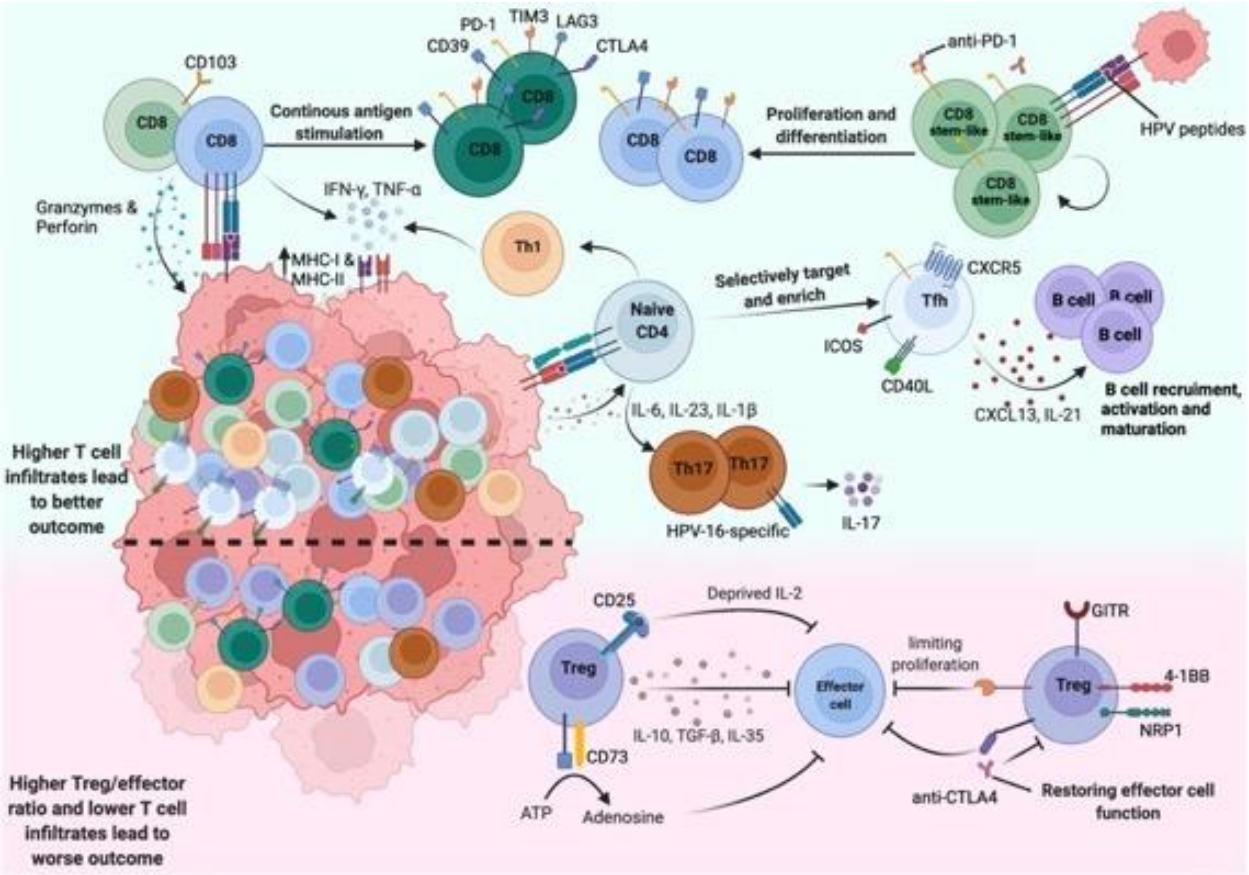


**Figure 1: New targets for T cells in the HNSCC TME**

CD8+ T lymphocytes can directly lyse target cells via releasing granzymes and perforin in an antigen-directed manner. Chronic engagement with tumor antigen leads to a dysfunctional state characterized by high immune checkpoint receptor expression (PD-1, TIM3, LAG3, and CTLA4). HPV-16-specifc CD8+PD-1+ T cell population in HPV+ tumors contain a stem-like CD8+ T cell subset. These cells are capable of proliferating and differentiating into effector cells upon HPV peptide stimulation and represent a population of future therapeutic targets. CD4+ T lymphocytes recognize MHC-II antigens and differentiate into different subtypes upon antigen stimulation. Higher number Th1 and Th17 cells are found in HPV+ tumors. Th1 cells release IFN-$\gamma$ and TNF-a and promotes MHC-I and MHC-II upregulation on cancer cells, facilitating tumor elimination. IL-17 releasing Th17 cells are induced by IL-6, IL-23 and IL-1$\beta$ produced by primary tumor cells. CXCR5+PD-1+ICOS+CD40L+ Tfh cells produce CXCL13 and IL-21, recruiting B cells into TME. Tfh cells are essential for B cell activation and maturation in tumors and their presence is associate with better outcome. Tregs play immunosuppressive role in TME. Tregs can suppress effector cells through releasing IL-10, TGF-$\beta$ and IL-35. Tregs express high CD25, which deprives local IL-2 necessity for effector cell

activation and survival. Tregs also express CD39 and CD73 which convert extracellular ATP to adenosine and impair effector T cell function. Co-expression of 4-1BB, GITR, and neuropilin-1 (NRP1) on intratumoral Tregs demonstrated an enhanced suppression function. Immune checkpoint receptors are reported expressed by Tregs in HNSCC, such as TIM3 and CTLA-4. Both are highly expressed by intratumoral Tregs and able to suppress effector cell functions. Therapeutically targeting Tregs may help rejuvenate effector cell function. Created in Biorender.com (Housayin Li)

#### 1.2.3.4 Innate immune cells complement adaptive immunity in the HNSCC TME

Natural killer (NK) cells are crucial mediators of innate immunosurveillance and elimination of infected cells and tumor cells. NK cells express a host of activating receptors (NKG2D, NKp46, NKp30) which allow NK cells to detect and mediate killing of infected and cancerous cells. They also express a repitoire of inhibitory receptors (KIR family and NKG2A) that prevent NK cells from killing healthy "self" tissue. Tumor cells often upregulate NK inhibitory receptor ligands to evade destruction. NK cells can mediate anti-tumor immunity via three mechanisms: (1) granule-dependent killing (mediated by perforin, granzyme B), (2) death receptor-dependent killing (mediated by transmembrane FasL, LTα1β2, TNF and TRAIL) and (3) antibody-dependent cellular cytotoxicity (ADCC; mediated by CD16/FcγRIII)[83,84]. NK cells can also orchestrate adaptive anti-tumor immunity as they can recruit (CCL5, XCL1 and XCL2) and activate dendritic cells (DC) via cytokine release (IFN-γ, TNF, GM-CSF, Flt3 ligand)[85,86] NK cells can be divided into two major subsets, $CD56^{bright}CD16^{-}$ and $CD56^{dim}CD16^{+}$. $CD56^{bright}CD16^{-}$ cells are primarily known for their regulatory/cytokine-producing capacity, while $CD56^{dim}CD16^{+}$ cells are best known for their cytotoxic capacity[38,87] Comparative transcriptomic analyses indicate that HNSCC have the highest median $CD56^{dim}$ NK cell infiltration of any major tumor type[38]. HPV+ HNSCC have more tumor-infilitrating NK cells than HPV- HNSCC

however NK infiltration is associated with improved disease-free and overall survival independent of HPV status[38,88].

Dendritic cells (DCs) are regarded as the bridge between innate and adaptive immune responses. DCs are critical for the initiation and functional polarization of tumor antigen-specific immunity as they are considered the most potent antigen-presenting cell (APC). DCs also secrete a host of chemokines (CXCL9, CXCL10) and cytokines (Il-12, TNFa, IL1, IFNs) that recruit and activate T cells and NK cells. DCs are a heterogeneous population with multiple functionally distinct subpopulations[89–91]. Recent scRNA seq revealed that tumor infilitrating DCs can be divided into several major subsets: conventional DCs (cDC) subsets (cDC1 and cDC2), a plasmacytoid DC (pDC), a monocyte-like inflammatory DC (MoDC), and DC3[92,93]. This classification based on distinct gene profiles was shown to be conserved across several human tumors (NSCLC, Breast, Liver, colorectal and Ovarian). In HNSCC, DC infiltration is directly associated with increased T and NK cell infiltration, decreased rates of tumor dissemination and improved patient survival[94,95]. Available studies suggest that $HPV^+$ tumors may have higher frequencies of tumor-infiltrating DC than $HPV^-$ ones, however increased DC infiltrate positively correlated with improved outcome only in patients with $HPV^-$ disease[96].

Macrophages are monocyte derived APCs capable of stimulating antigen-specific T cell responses. Macrophages are generally categorized into two functionally distinct subtypes: M1 and M2 macrophages[97]. M1 macrophages are induced by Th1-cytokines such as IFN-γ and produce pro-inflammatory cytokines, including IL-12, IL-1, IL-23, TNF-α and stromal cell-derived factor 1α (SDF1α) which support CD8 , NK cell and Th1 responses. M2 macrophages are skewed by Th2-cytokies such as IL-4 and IL-13 and

they promote tissue remodeling and wound healing, by producing IL-1β, IL-10, arginase-1 matrix metalloproteinases (MMPs), TGF-β and vascular endothelial growth factor (VEGF) which in turn also suppress effector T cell function. Tumor-associated macrophages (TAM) are one of the major immune populations that infiltrate cancers[98–100]. In HNSCC, macrophage infiltration was elevated in tumors vs. to normal mucosa ,where the correlated with R/M disease and poor patient outcome. By scRNAseq, flow cytometry and multispectral imaging, TAM were identified as the primary contributors of PD-L1 within the HNSCC TME, regardless of disease etiology[30]. Not only do TAM express the highest levels of PD-L1 on their cell membrane, but PD-L1$^{+}$ macrophages have been shown to co-localize with CD8+ T cells within the HNSCC TME[30]. **(**Figure 2**)**

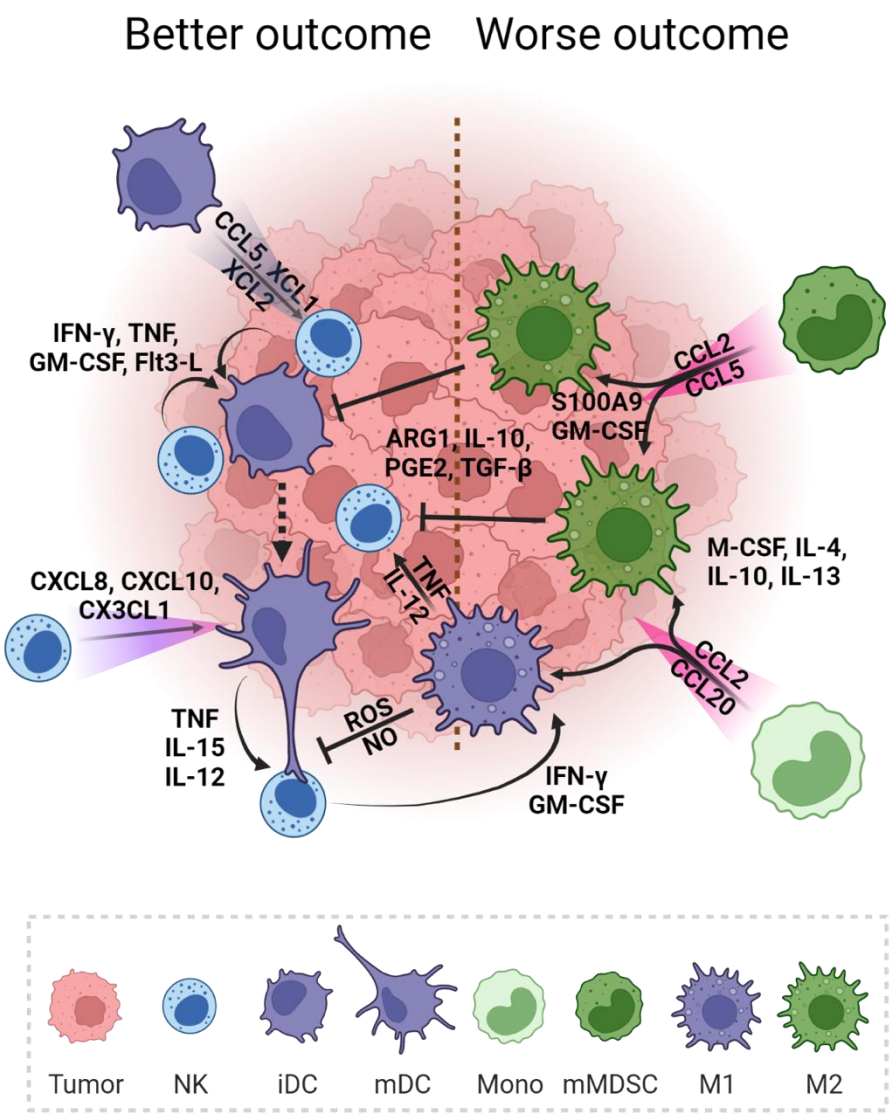


**Figure 2: Innate cell interactions generate inflammatory signals that drive HNSCC patient outcome**

HPV⁺ tumors generally have greater level of innate immune infiltrate, which correlates with better clinical outcome. Enhanced NK cell and DC infiltrates correlate with better patient survival. Tumor-infiltrating NK cells can recruit immature DC (iDC) into the tumor by releasing CCL5, XCL1 and XCL2. Once in the tumor, iDC can take up cell debris from killed tumor cells, which is the first step required for effective antigen presentation. As antigen-loaded DC start to mature, they can engage and crosstalk with NK cells via cell-cell contact. NK cells enhance DC maturation and polarization through the release of IFN-γ, TNF, GM-CSF and Flt3-L. Maturing DC (mDC) in turn enhance NK cell activation through IL-12 secretion, as well as cell-

cell contact mediated by transmembrane TNF and IL-15. Furthermore, they release a number of chemokines, including IL-8/CXCL8, IP-10/CXCL10 and fractalkine/$CX_3CL1$ that enhance the number of NK cells infiltrating the tumor. Monocytes can differentiate into anti-tumor M1 and immunosuppressive M2 macrophages depending on the inflammatory signals they receive within the TME. M-MDSC can further differentiate into M2 macrophages under the influence of endogenous S100A9 and exogenous GM-CSF. M2 macrophages have a variety of mechanisms by which they can suppress NK cell and DC activation and skew their polarization towards an immunoregulatory phenotype. M1 macrophages that can activate NK cells by IL-12 and TNF production, can also inhibit NK cell function by ROS and NO release. Created in Biorender.com

#### 1.2.3.5 Stromal tissue is an important regulator of the HNSCC TME

Non-immune cells such as fibroblasts and mesenchymal stem cells are also heterogeneous and variable in these TMEs and they have only recently been included in scRNAseq landscape analyses[30,101]. scRNAseq performed on treatment naïve HNSCC patients with primary tumors and LN metastasis revealed heterogeneity amongst tumor cells in patients with $HPV^-$ HNSCC tumors[51]. Seven expression patterns related to cell cycle, hypoxia, and epithelial genes and partial epithelial to mesenchymal transition (pEMT) were observed. Notably, pEMT high cells were spatially localized to the leading edge of primary tumors near cancer-associated fibroblasts (CAF) and expressed higher numbers of ligands that correspond to receptors expressed by malignant cells, particularly interactions important for pEMT transition[51,102]**.** In late stage HNSCC tumors, up to 80% of the cellular composition are fibroblasts which highlights the importance of understanding their role in the TME. Fibroblasts can have several key functions in normal settings: (1) secreting collagen and fibrous macromolecules that build the ECM, (2) maintenance of tissue homeostasis, (3) recruitment of immune cells via secretion of

cytokines, chemokines, and growth factors, (4) regulation of cell mobility within in tissue through degradation of the ECM via matrix metalloproteinases (MMPs), and (6) metabolic reprograming. CAF have been reported to be quite variable in human solid tumors and thus differ in function[9,98,103–105].

The heterogeneity of CAFs in HNSCC was recently characterized in two independent scRNAseq studies[30,101]. In the first study, eight CAF subpopulations were uncovered based on GSEA[101]. Seven of these subpopulations were significantly enriched in HNSCC compared to normal tissues. Three of the subclusters including myofibroblasts, EMT+ CAF, MHCII+ CAF were associated with poor overall survival. Pathway enrichment analysis revealed that these three populations had distinct biological functions related to cyclic guanosine monophosphate-dependent protein kinase (cGMP-PKG) signaling pathway/oxytocin signaling pathway, oxidative phosphorylation/ECM receptor interaction and antigen processing and presentation, respectively[101]. Distinctions between $HPV^+$ and $HPV^-$ HNSCC were not made in these analyses. In our scRNAseq study, we identified nine subpopulations of fibroblasts which could be grouped into three major subgroups: classical CAFs, normal/activated fibroblasts (NAF) and elastic fibroblasts[30]. Classical CAF were enriched for genes such as fibroblast activation protein (FAP), platelet-derived growth factor receptor (PDGFRA), lysyl oxidase (LOX), and MMPs. NAF showed a low expression of CAF markers. Elastic fibroblasts were enriched for tropoelastin (ELN), fibrillin1 (FBLN1), and microfibril associated protein 4 (MFAP4). The elastic CAF gene signature correlated with poor overall survival in $HPV^+$ but not $HPV^-$ HNSCC. $HPV^+$ patients with both low frequency of elastic fibroblasts and classical CAF signature had superior overall survival[30].

Functional analysis of HNSCC patient derived CAF revealed that CAFs secrete hepatocyte growth factor (HGF) which promotes glycolysis in HNSCC tumor cells[106,107]. HNSCC tumor cells in turn secrete fibroblast growth factor basic (FGFb) which induces oxidative phosphorylation, proliferation, and migration of CAFs by binding to fibroblast growth factor receptor (FGFR). HGF regulates glycolysis in HNSCC tumor cells via c-Met tyrosine kinase receptor expressed on HNSCC tumor cells. Inhibiting both c-Met and FGFR with small molecule inhibitors attenuated CAF-associated HNSCC tumor growth. Interestingly, in 2D and 3D cultures, $HPV^-$ HNSCC cell line conditioned media could activate normal oral fibroblasts to secrete HGF, IL6 and IL8 as well induce cell migration by fibroblasts while $HPV^+$ HNSCC cell lines could not[104,108]. Future studies should explore the secretory profile, proliferation, and migration potential of CAFs in ex vivo $HPV^+$ and $HPV^-$ HNSCC tumors. The metabolic relationship between CAFs and tumor cells in HNSCC could be a potential targetable axis and enhance current ICI. However, the metabolic relationship between CAFs and immune cells has not been fully elucidated. Notably, the heterogeneity in CAF phenotype and function can be patient specific and might provide a barrier for therapeutic targeting of CAFs[30,102,105].

Mesenchymal stromal cells (MSCs) are also referred to as mesenchymal stem cells because of their potential to differentiate into osteoblasts, chondrocytes, adipocytes, or myocytes depending on environmental conditions[9,109]. This capability makes MSCs extremely important for tissue repair and regeneration. MSC can also ameliorate tissue damaging inflammation and immune responses through inhibition of both innate and adaptive immune cells and induce immune tolerance. This is mediated by secretion of immunosuppressive soluble factors such as prostaglandin E2 (PGE2), TGF-β,

indoelamine 2,3 dioxygenase (IDO), and sHLA-G and expression of inhibitory and apoptotic ligands such as PDL1, Galectin 1/9, FasL[109,110]. In malignant stroma, MSCs promote tumor progression and metastasis[111].

MSC are increased in HNSCC tumors compared to normal tissue, and when isolated from HNSCC patients, they inhibited in vitro cell proliferation and cytokine production by polyclonally stimulated CD4+ and CD8+ T cells[112]. HNSCC tumor derived MSCs were also shown to inhibit T cell proliferation via IDO production and have a similar phenotype to normal bone-marrow derived MSCs[112]. Direct comparisons of MSCs in $HPV^+$ vs $HPV^-$ tumors were not performed in this study most likely due to limited patient cohort. However, of the thirteen patients analyzed, eleven of the tumors occurred in traditional $HPV^-$ sites. HNSCC-derived MSCs have also been reported to support survival of tissue resident memory T cells (Trm cells) through secretion of IL-7 and IL-15[113]. Ex vivo, tissue residence markers (CD69 and CD103) were increased on CD4+ and CD8+ T cells in HNSCC and normal tissues compared to PBL. Co-culture of HNSCC-derived MSC with healthy donor T cells increased CD69 and CD103 expression and migration of T cells. Vascular cell adhesion protein 1 (VCAM1) was shown to mediate interactions with HNSCC derived MSCs and T cells and blocking VCAM1 inhibited upregulation of Trm markers[113]. Again, distinctions between $HPV^+$ and $HPV^-$ MSCs were not made, however, these studies suggest HNSCC MSCs may have both pro- and anti-tumor roles and their function in the TME warrants further investigation. **(**Figure 3**)**

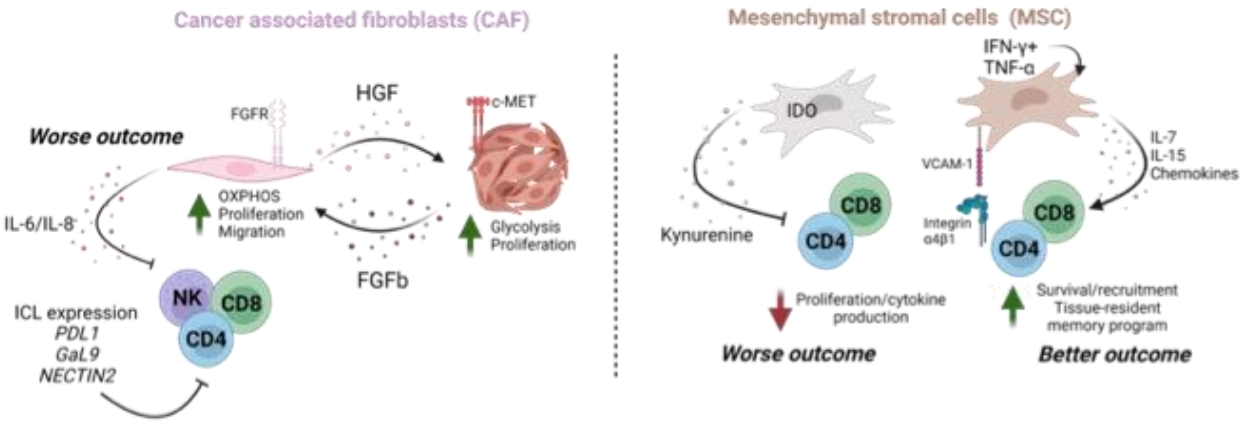


**Figure 3: The stromal microenvironment is functionally important for the HNSCC TME**

The HNSCC tumor microenvironment (TME) consists of a diverse stromal cell compartment that interacts with neighboring tumor cells and infiltrating immune cells. These interactions primarily promote tumor growth, progression and metastases but under some conditions can provide a supportive environment for immune cells and recruit immune cells to the HNSCC TME. CAFs and tumor cells have a metabolic relationship mediated by hepatocyte growth factor (HGF) and fibroblast growth factor basic (FGFb) which increases oxidative phosphorylation (OXPHOS) in CAFs and glycolysis in tumor cells. This leads to IL-6 and IL-8 production by CAFs which suppress immune cell function. CAF also express several immune checkpoint ligands including programmed death-ligand 1 (PDL1), galectin 9 (GaL9) and nectin cell adhesion molecule 2 (NECTIN2) which interact with corresponding inhibitory receptors on NK and T cells. Mesenchymal stromal cells (MSCs) can also suppress immune cell function *in vitro* via indoleamine-pyrrole 2,3-dioxygenase (IDO) which metabolizes tryptophan into kynurenins which are cytotoxic to T cells and NK-cells. On the other hand, some *in vitro* studies suggest that MSC can support tissue-resident memory T cells via IL-17 and IL-15 production in the presence of IFN-γ and TNF-α. Taken together, combining immune checkpoint therapy with therapies that target the stromal compartment may improve patient outcomes in HNSCC .

## 1.3 B lymphocytes

B cells and their antibodies (immunoglobulins) are the key components of the humoral arm in the adaptive immune response to invading pathogens. B cells express the B-cell receptor (BCR) which is a transmembrane protein consisting of a membrane bound immunoglobulin (Ig) molecule and signal transduction proteins CD79A/B[114]. The gene segments of the BCR are rearranged early in B cell development and subsequently mutated (somatic hypermutation) in later maturation stages to generate a pool of B cells expressing antibodies that can recognize an almost unlimited number different antigen. CD79A/B allow for antigen-driven signaling in B cells via the BCR which induces B cell proliferation, maturation, and other effector functions such as, secreting Igs, cytokine production and antigen presentation[114–116]. B cells are diverse in phenotype as well which is a result of the development and maturation stages that B cells undergo. Additionally, environmental factors such as cytokines and growth factors affect the type of B cell response that is generated. Successful vaccination strategies hinge on eliciting B cells to mature into long-lived memory and plasma cells that generate diverse antibody repertoires to resolve infections[117–119]. Defects in B cell development and maturation result in autoimmune disorders, B cell lymphomas, and allergies. B cells also participate in immune responses against cancer. B cells have been found to infiltrate a variety of human solid tumors including, breast, melanoma, pancreatic, ovarian, lung, liver and head and neck cancers[36,120–125]. Both pro and anti- tumor roles have been proposed for B cells but their function and antigen specificity in tumors remains understudied[126–129].

### 1.3.1 B cell differentiation and subsets

B cell differentiation and maturation steps begin in the bone marrow (BM) resulting in egress of immature B cells ($CD19^+CD20^+CD10^{+/-}$) characterized by expression of unmutated immunoglobulin (Ig) isotypes, IgM and IgD[114,130]. These cells are referred to as transitional B cells. All mature B cell subsets develop from transitional B cells. Three subsets of transitional B cells can be found circulating in the blood: T1, T2 and T3. T1 and T2 express $CD10^+$ and have high expression CD38 and CD24 while T3 lose expression of CD10 and have lower CD38 and CD24 expression[131]. Transitional B cells regularly migrate into secondary lymphoid organs (SLOs) including the spleen, lymph nodes (LNs), tonsils, Peyer patches, and mucosal tissues and receive further maturation signals[114,130]. T2 B cells within the spleen have been shown to develop into marginal zone (MZ) B cells or follicular (FO) B cells depending on BCR specificity and signal strength[132,133]. These fate decisions are mediated via signal transduction pathways Notch2 and canonical nuclear factor-κB (NF-κB) respectively[134]. Human MZ B cells can be distinguished by expression of CD1c, CD21, IgM, CD27, low IgD expression, and transmembrane activator, calcium modulator, and cyclophilin ligand interactor (TACI). FO B cells also express TACI and are characterized by expression of CD23, low IgM and CD21, high expression of IgD and CXCR5[135]. Both MZ B cells and FO B cells express B-cell activator of the TNF-a family receptor (BAFF-R)[114,136]. Expression of BAFF-R and TACI are important for survival of B cells in the periphery. Patients with BAFF-R and TACI deficiencies have impaired responses to T cell-independent antigens, low levels of circulating B cells and serum IgM and IgG antibodies levels[114,136]. FO B cells participate in T- cell dependent immune responses and reside in spleen and other SLOs, while MZ

B cells are mainly found in the spleen and participate in T cell independent immune responses mainly against polysaccharide antigens expressed on bacteria. T cell dependent antigens include proteins, polypeptides, hapten-carrier complexes, erythrocytes, and antigens with diverse epitopes which all require interaction between B cell and T cell to induce an antibody response[137,138]. When FO B cells engage with T dependent antigens and receive maturation signals from T cells this typically results in secondary follicle formation (germinal centers)[134].

#### 1.3.1.1 Germinal centers

Germinal centers (GCs) are transient specialized microstructures that develop in SLOs and are responsible for generating memory B cells (MBC) and plasma cells (PC) that have a stronger binding capability (high affinity) for the cognate antigen that their BCR recognizes[139]. MBC and PC generated from GCs can be detected as early as a few days after antigen encounter and persist in a resting state in BM and SLOs for life until rechallenged[140]. This allows for quick resolving of active infections and life-long protection against disease developing from reinfections. The importance of GCs is underscored in people with immunodeficiencies such as common variable immunodeficiency (CVID)[141,142]. These patients have high susceptibility to infection and ultimately develop inflammatory diseases because they are unable to resolve infections due to the absence of B cells and/or lack antigen specific Igs[142].

The GC reaction is a dynamic process that is initiated when a mature-naïve B cell encounters its cognate antigen. B cells can directly bind free floating soluble antigen, and peptides or bind antigen presented by follicular dendritic cells (FDCs), macrophages or dendritic cells (DCs) within the B cell follicle via their BCR[143]. Signaling via the BCR

increases expression of MHCII and CCR7, which allows B cells to migrate following a chemokine gradient via CCL19 and CCL21 to the T cell zone to receive T cell 'help'[139,144]. The T cell zone in SLOs is positioned adjacent to B cell follicles and where they meet is known as the T-B border. Within the T cell zone, there are naïve CD4+ T cells and DCs. When DCs present antigen and provide activation signals to naive CD4+ T cells, they differentiate into the appropriate T helper subset depending on the stimulus. Naïve CD4+ T cells that commit to the T follicular helper ($T_{FH}$) linage participate and facilitate GC reactions.

The GC reaction is distinguished histologically by the organization of B cells into two zones: (1) dark zone (DZ) and light zone (LZ) where distinct B cell maturation events occur[144,145]. DZ B cells are referred to as centroblasts and express CXCR4. LZ B cells are referred to as centrocytes and express CD86. In the DZ, B cells undergo rapid proliferation and mutation of the variable (V) region of the heavy and light chains of the Ig which is known as somatic hypermutation (SMH). SHM is mediated by activation-induced cytidine deaminase (AID) which induces DNA mismatch pair by converting cytidine (C) to Uracil (U). This is corrected by base excision repair enzyme (uracil-DNA glycosylase) and error-prone DNA polymerases insert a base causing a mutation. In the LZ, B cell clones are selected for their ability to bind strongly to foreign antigen by FDCs and $T_{FH.}$ Class-switch recombination (CSR) is a process in which the heavy chain gene locus of the Ig is replaced to allow expression of one of the five Ig isotypes (IgM, IgA, IgG, IgE, IgD) which is also mediated by AID and alternative splicing for switching out IgD for IgM. CSR was thought to occur strictly in the LZ of the GC but recent studies using transgenic mouse

models revealed that CSR is triggered prior to commitment of activated B cells into GC B cells or plasmablasts and is greatly diminished in GCs[146]. .

Since B cells in the GC are undergoing unparallel amounts of proliferation and potentially dangerous DNA damage, the GC reaction is tightly regulated by a host of transcription factors, cytokines/chemokines, and the coordination of cell-cell interactions. B cell lymphoma 6 protein (BCL6) is considered the master transcription factor that regulates GC commitment in both GC B cells and TFH which is evident in the fact that BCL6 deficient mice fail to form GCs. BCL6 acts as a transcriptional repressor to suppress genes involved in DNA-damage sensing as well as cell cycle regulators to allowing for expansion and SHM of GC B cells. BCL6 also controls CXCR4 expression and sphingosine-1 phosphate receptor type 1 (S1PR1) to allow B cells to cycle through DZ and LZ and traffic out of the follicle respectively[139,144,147,148]. MEF2B, IRF8, IRF4 are transcription factors that control BCL6 expression and are important for initiation of GC reactions[149,150]. FOXO1 is essential for polarization of the GC and formation of the DZ and regulates BATF which regulates BCL6 and AID expression[151].

The major stromal cells involved in GC reactions are FDCs, CXCL12-producing reticular cells (CRCs), and fibroblast reticular cells (FRCs)[147,152–154]. FDCs are defined by high expression of complement receptors-1 and -2 (CD35 and CD21). FDCs produce CXCL13 and BAFF which recruit B cells and TFH via CXCR5 and support survival in the B cell follicle respectively. FDCs also act as APCs to B cells. FDCs express vascular cell-adhesion molecule1 (vCAM1) and intercellular adhesion molecule 1 (ICAM1) as well as Fc receptors which allow for strong interactions with migrating B cells and capture and presentation of antibody-bound antigen respectively[143]. Depending on BCR signal

strength from antigen presented on FDCs GC B cells may return to the DZ , differentiate in the LZ or undergo apoptosis[139,147,155] FRCs support and establish the T-cell zone by producing CCL19, CCL21, and CXCL12 which recruits T cell and DCs.

### 1.3.1.2 Tertiary Lymphoid structures

TLS are ectopic lymphoid aggregates that form at the sites of chronic inflammation in non-lymphoid tissues, including tumors.[156] TLS have been associated with antitumor immune responses in cancer patients as the absence of TLS is associated with worse outcomes[157,158]. TLS share many structural characteristics with SLOs including T cell-rich immune clusters, B cell follicles consisting of naïve B cells, specialized blood vessels called high endothelial venules (HEVs), mature dendritic cells (DCs), and follicular dendritic cells (FDCs)[157,159]. Murine studies suggest that TLS formation in non-lymphoid tissues occurs by similar mechanisms of SLO neogenesis[156,160]. In SLO neogenesis, $CD4^+CD3^-RANK^+IL\text{-}7R\alpha^{hi}$ lymphoid tissue inducer (LTi) cells are recruited to sites of inflammation by local production of CXCL13 and IL7 by immune or tissue-resident stromal cells[156,161,162]. LTi cells also express lymphotoxin $LT\alpha_1\beta_2$ which binds LTβR (lymphotoxin beta receptor) on stromal cells[125,157,162]. This interaction leads to the production of chemokines CCL19, CCL21, CXCL12 and CXCL13 as well as vascular endothelial growth factor C (VEGFC), which recruits B cells, T cells and DCs and supports the development of HEVs[125,156,161,162]. While LTi cells are required for SLO development in the LN, spleen, and Peyer's patches, $CD4^+$ T helper 17 cells (Th17), M1-polarized macrophages, and B cells can induce TLS formation in the absence of LTi cells[163,164]

### 1.3.2 B cell function

B cells mediate their functions through both antibody dependent and antibody independent mechanisms.

#### 1.3.2.1 Antibody mediated effector function

Antibody effector functions are an important part of the humoral immune response against invading pathogens[165–167]. There are five main classes of antibody isotypes: IgM, IgD, IgA, IgG, IgE. Human IgG can be further divided into four subclasses: IgG1, IgG2, IgG3, IgG4. IgA can also be divided into two subclasses: IgA1 and IgA2. Antibodies directly neutralize pathogens and pathogen-derived products as well as recruit immune cells to destroy infected cells or tumor cells. They can also activate the complement system which is an innate surveillance system comprised of more than 15 soluble proteins that mediate destruction of microbial pathogens[168]. Antibody effector functions are mediated by the Fc portion of antibodies, which interacts with complement proteins or Fc-receptors (FcR) expressed on innate immune cells such as NK, neutrophils, eosinophils, macrophages, and DCs[165,166] The major Fc-mediated effector functions include: (1) antibody-dependent cell-mediated cytotoxicity (ADCC), (2) antibody-dependent cellular phagocytosis (ADCP), and (3) complement-dependent cytotoxicity (CDC)[165,166] In addition to Fc-mediated effector functions, antibodies can form immune complexes which can: (1) activate degranulation of neutrophils and eosinophils (cytokine/chemokine release; reactive oxygen species (ROS)), (2) induce DC maturation which can skew T cell responses, (3) activate macrophages, and (4) regulate B cell antibody responses[165,166].

IgG is the most predominant circulating isotype accounting for 10-20% of human plasma protein[169]. IgG3 has a shorter half-life than IgG1 as it has a higher binding affinity to FcRs[169,170]. It is typically produced early in the course of infection. However, both IgG1 and IgG3 are effective at neutralizing viruses while IgG2 respond to polysaccharide antigens on encapsulated bacteria[165,169]. IgG4 and IgE are effective against large extracellular parasites. IgM has a high avidity for antigens with repetitive binding motifs such as lipopolysaccharide (LPS) and strongly activates CDC[165]. IgA1 and IgA2 respond to pathogenic bacteria in mucosal surfaces such as intestines, stomach, lungs, and genital areas. IgA2 more potently activates neutrophils and macrophages than IgA1 which has been attributed to the different glycosylation patterns of the Fc region on these isotypes[171].

Switching from one isotype to another is mediated both by antigen driven signaling through the BCR but also through signals from costimulatory molecules CD40 and BAFF-R. CD40 and BAFF signals lead to activation of canonical and non-canonical NFKβ signaling which induces AID expression[136,172,173]. Cytokines also play an important role in isotype switching. in vitro human B cell studies show that IL-4 and IL-13 induces CSR to IgG1, IgG4 and IgE. IL-10 and IL-21 induce IgG1, IgG3, IgA CSR. IL-10 synergizes with TGFβ to induce IgA production. IL-12 induces IgM+ B cell differentiation[172].

#### 1.3.2.2 Antibody-independent effector function

In addition to secreting antibodies, B cells can perform additional effector function such as antigen presentation, cytokine production and some B cell subsets have cytotoxic capabilities. There are several key features of B cells that makes them an effective professional APC: (1) BCR-mediated endocytosis: High-affinity BCRs produced after GC

reactions allow B cells to concentrate small amounts of antigen and internalize them faster than DCs which allows for efficient antigen presentation, (2) HLA-DO expression: inhibits HLA-DM allowing loading of MHC II peptides to occur in the MHC class II-enriched compartment (MIIC) where BCR:antigen complexes can be degraded and processed, (3) BCR signaling: antigen binding to BCR sends internal signals to B cell for activation, directs antigen processing machinery, and upregulates expression of costimulatory molecules CD40, CD86 and MHC II[138,174–176]. While antigen presentation by resting B cells induces immune tolerance, antigen presentation by human B cells activated with CD40 stimulation can boost memory T cell responses and prime naïve T cell response against neoantigens ex vivo[177–179].

B cells primed by $CD4^+$ T helper 1 (Th1) T cells or $CD4^+$ T helper 2 (Th2) T cells can polarize B cells to produce IFN-γ, TNF-α, and IL-12 (Th1 effector) or IL-2, IL-13, IL-6, and IL-4 (Th2 effector) cytokines, respectively[115,180]. Th1 effector cytokines promote Th1 T cells, NK cell and M1 macrophage responses. Th2 effector cytokines promote Th2 T cells, M2-macrophages and Tregs. However, IL-6 is also important for TFH differentiation[181]. B cells can also produce the regulatory cytokine IL-10 when stimulated with TLR ligands (TLR7 or TLR9) and with CD40 stimulation in the presence of various cytokines[182–184]. While IL-10 and other suppressive cytokines (IL-35, TGFβ) production in T cells is restricted to Tregs, IL-10 can be produced by multiple B cell subsets[184–186]. Additionally, IL-10 producing B cells also co-express proinflammatory cytokines IL-6 and TNF-α[184]. Human B cells were shown to produce functional granzyme B in the presence of BCR and IL-21 stimulation but without CD40 ligation[187,188]. Granzyme B-producing B cells can induce apoptosis when cultured with tumor cells in vitro but have also been

shown to inhibit CD4+ T cell proliferation[187–189] . Lastly, B cells can express several death receptor ligands such as tumor necrosis factor-related apoptosis-inducing ligand (TRAIL) ,which provide B cells with cytotoxic capabilities[190–194].

## 1.4 Harnessing B Cells and TLS for Antitumor Immunity

### 1.4.1 Mouse versus Human cancer studies: Are B Cells Friend or Foe?

Within the last decade, several studies have highlighted that increased infiltration of B cells in human solid tumors is associated with favorable outcomes in a variety of cancers[122,123,195–198]. However, B cells have been overlooked as a potential target for immunotherapy. In fact, mechanistic studies interrogating how B cells contribute to anti- or protumor immune response in humans are very limited despite their abundance within the TME. Perhaps this neglect of B cells as an immunotherapeutic target can be attributed to the contradictory evidence regarding B cell function in the TME in pre-clinical mouse models[126,199]. Most mouse models demonstrate that B cells promote tumor progression or play no role in the antitumor immune response. For example, in melanoma and sarcoma murine models, depletion of B cells enhanced $CD8^+$ T cell antitumor reponses[200]. However, a different study demonstrated that depletion of B cells in a B16 melanoma model significantly accelerated melanoma growth and metastasis and reduced the antitumor response of $CD4^+$ and $CD8^+$ T cells[199]. Depletion of B cells either genetically ($RAG^{-/-}$, μMT mice) or via therapeutic antibodies (anti-CD20; Rituximab)

overlooks the fact that B cells are a heterogenous population and it may be more physiologically relevant to enhance some B cell subsets while inhibiting others.

Pre-clinical mouse models will be needed to perform critical mechanistic studies to assess B cell function in the TME before B cell specific therapies can be generated and tested in the clinic. I would assert that murine cancer models that more closely mimic human cancer development and/or behavior would be most ideal to address these knowledge gaps. As such advances in human tumor immunology have prompted new approaches to studying B cells in preclinical murine cancer models. For example, lung adenocarcinoma (LUAD) patients who have enrichment for GC B cells and TFH had overall better survival[201]. To determine the mechanistic role of GC B cell and TFH in LUAD, Joshi et al developed a murine LUAD model that allows tumor cells to express a neoantigen that is recognized by both B cell and T cells or just T cells. In this model, tumors that expressed a B-T neoantigen induce GC formation and TFH differentiation and subsequently enhanced CD8 T cell control of tumor growth[201]. To interrogate the role of B cells in cancer further in vivo models and human studies, I would argue that it is important assess: (1) TIL-B maturation within a given TME and the antigen specificity that is acquired (2) determine how TIL-B subpopulations function, (3) identify key biomarkers to distinguish functional subsets from dysfunctional subsets, (4) identify key cell-cell interactions between TIL-Bs and other cell types. This will aid in clarifying the overall impact of B cells on tumor progression or tumor clearance within a given cancer type.

### 1.4.2 Clinical significance of B cells and TLS in human tumors

B cell infiltration in human solid tumors is associated with favorable outcomes in hepatocellular carcinoma (HCC), colorectal cancer (CRC), melanoma (MEL), pancreatic ductal adenocarcinoma (PDAC), breast cancer (BRCA), non-small cell lung cancer (NSCLC), esophageal cancer (ESCA), stomach adenocarcinoma (STAD), ovarian cancer (OV) and head and neck squamous cell carcinoma (HNSCC) patients[35,197,202–207]. TLS are also associated with better survival in at least ten different types of cancers including HCC, OV, HNSC, MEL, BRCA and NSCLC[196,198,206,208,209]. Thus, immunotherapies targeting B cells and TLS could potentially benefit multiple cancer indices and perhaps enhance responses to current T cell-focused therapies. Recently, B cells and their presence in TLS were shown to predict whether patients would respond to ICB[122,158,195]. Patients with high-risk resectable MEL and metastatic renal cell carcinoma (RCC) that responded to ICB had more B cells and TLS prior to and after treatment[122]. Additional studies corroborated these findings in MEL, demonstrating that TLS in MEL patients contained high densities of B cells and patients without TLS had worse outcomes while on ICB[158]. B cell-rich TLS are also predictive of response to ICB therapy in soft tissue sarcomas (STS) and B cells were shown to be the strongest prognostic factor in comparison to $CD8^+$ T cells in STS patients[195]. These complementary studies highlight the prognostic importance of B cells and TLS. More importantly, they emphasize the potential of B cells and TLS to inform whether patients should be treated with current immunotherapies.

### 1.4.3 Significance of TLS subtypes in the TME

TLS have been detected within the tumor bed but are more abundant in the invasive margin and stroma of the TME[157,162]. Significant variability in TLS organization and immune cell composition can be observed from patient to patient within a given cancer type and between different cancer types, suggesting that some TMEs are more conducive to TLS formation and maintenance[206,210–212]. For example, in treatment-naïve lung squamous cell carcinoma (LUSC) and non-metastatic colorectal carcinoma (nmCRC) patients, three distinct phenotypes of TLS were identified using multispectral immunofluorescence (mIF) : (1) early TLS (E-TLS): dense immune cell aggregates without FDCs, (2) primary follicle-like TLS (PFL-TLS); B cell clusters with FDCs but without GCs, (3) secondary follicle-like TLS (SFL-TLS): TLS with GCs (Figure 34.1)[210,213]. In nmCRC, high numbers of E-TLS and low numbers of SFL-TLS were associated with increased risk of recurrence[213]. Further, in LUSC, patients with high densities of TLS also had increased expression of genes involved in TLS formation such as CXCL13,CXCL12, LTB, CCL19, CCL21, IL7 and genes associated with the adaptive immune response including B cell (CD20, CD40) and T cell (CD3, CD8, IL-21, PD1) gene signatures[210]. In high-grade serous ovarian cancer (HGSOC), similar TLS phenotypes were described: (1) *Type I*: small aggregate of $CD20^+$ B cells , $CD4^+$ and $CD8^+$ T cells and some DCs, (2) *Type II:* larger aggregate of $CD20^+$ B cells , $CD4^+$ and $CD8^+$ T cells without clear zones or follicles, (3) *Type III:* defined B cell follicle with GC and a network of $CD21^+$ FDCs, discrete $CD4^+$ and $CD8^+$ T cell zones and HEV [206]. Active immune responses within TLS were observed in HGSOC patients by IHC staining of transcription factor BCL6, which regulates GC reactions and activation-induced cytidine deaminase (AID), which regulates

SHM of Ig genes and class switch recombination (CSR)[148,206]. Notably, patients with tumors containing $CD8^+$ and $CD4^+$ T cells and $CD20^+$ B cells and plasma cells had increased disease-specific free survival[206].

Oncogenic drivers such as environmental exposure to carcinogens or viral infection may influence the type of TLS present within a given TME. Viral and carcinogen stimuli can activate the lymphotoxin/CXCL13 pathway, which is key for TLS formation, however, chemical carcinogens present in tobacco can also suppress immune responses. While TLS and the key TLS associated inflammatory gene signatures are increased in virally associated cancers such as HNSC and HCC, whether viral infection in tumors plays a direct role in maturation of B cells and TLS remains unclear[120]. Further, there is a growing interest in understanding how organisms (microbiome) that live on barrier surfaces where tumors occur such as skin and colon affect tumor immunity[214]. While direct effects of the microbiome on intratumoral B cells and TLS in human solid tumors are largely unknown, early studies in murine models of CRC reveal that modifying the microbiome of CRC with colonization of *Helicobacter hepaticus* (Hhep) can drive microbiome specific TFH differentiation and TLS formation in CRC tumors[215].

Cancers caused by exposure to carcinogens such as UV exposure, tobacco and alcohol use often have an increased mutational burden, which has been associated with increased TLS and TLS-associated gene signatures[120,213,216]. It is clear from mouse and human studies that at least three key events are needed for TLS formation: (1) inflammatory cytokine expression, (2) lymphoid chemokine production by stromal cells, and (3) HEV development[160]. Future studies should investigate how oncogenic drivers play a role in initiation of these events as this may provide insight into why TLS formation

is absent in some TMEs. Additionally, it will be important to understand the stimuli and factors necessary for mature TLS (SFL-TLS) development and maintenance as this TLS phenotype is associated with better survival and reduced risk of recurrence. **(**Figure 4**).**

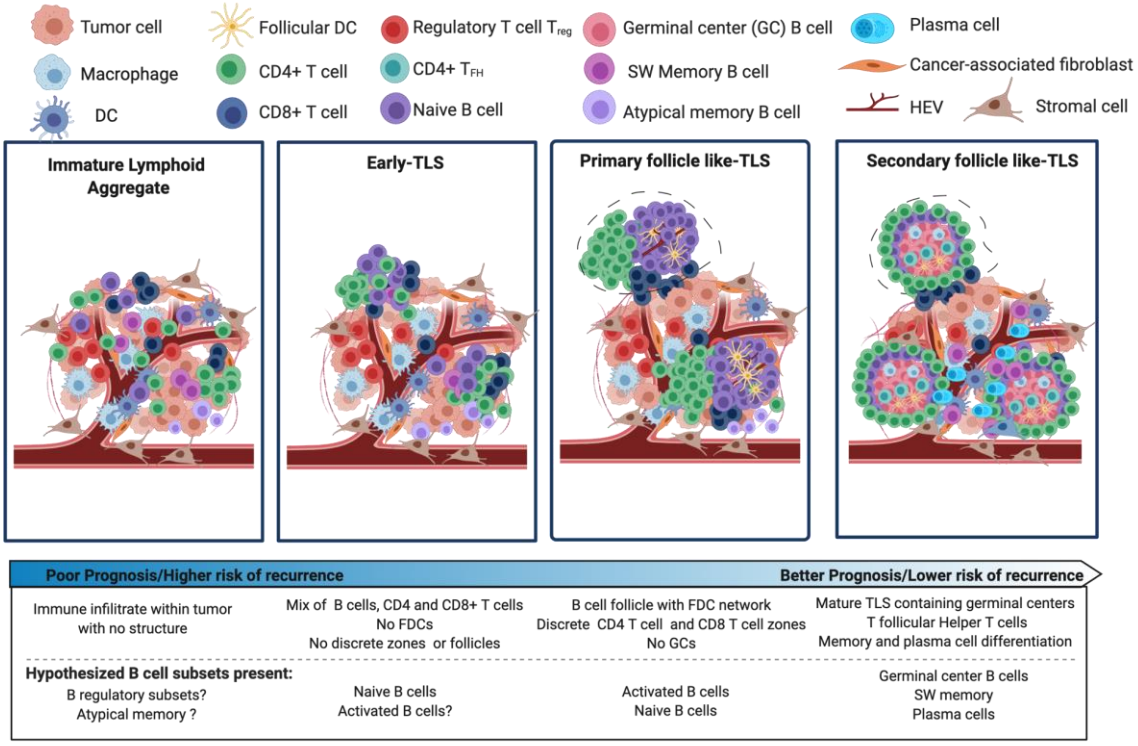


**Figure 4: B cells and TLS are heterogeneous within the tumor microenvironment**

The schematic depicts the different stages of tertiary lymphoid structures (TLS) maturation within the in the tumor microenvironment as well as the immune cell composition within each. Four distinct phenotypes of TLS have been identified in human tumors: (1) Immature lymphoid aggregates : small collections of B and T cells, with immature DCs scattered throughout the tumor with no organized structure formation. (2) Early-TLS: B cells and T cells begin to form larger aggregates but DCs remain undifferentiated. (3) Primary-follicle like : TLS begins to resemble primary B cell follicle in lymph-node with defined naïve B cell cluster with a network of FDC within the follicle, defined T cell zone and HEV formation. (4) Secondary-follicle-like: mature TLS with active germinal centers (GC), GC B cells can be found interacting with CD4+ T follicular helper cells. Class-switched memory B cells and plasma cells have been detected *in situ* in patients with mature TLS. Patients can have one or more of these TLS phenotypes with mature TLS correlating with better survival and reduced risk of recurrence. Intratumoral B cells within TLS are often identified using only CD20 staining , thus its not yet clear which B cell subsets are present in each type of TLS. Here, we hypothesize which B cell subsets could be present in ach TLS based on what is known about their function

and impact on overall patient survival. *DC: Dendritic cell, FDC: Follicular dendritic cell. HEV: High endothelial venule.* Created in Biorender.com

### 1.4.4 How do tumor infiltrating B cells contribute to tumor immunity?

While TIL-B and TLS correlate with better prognosis in many cancers, it is not yet clear why and how TIL-Bs provide a survival advantage to patients. Further, patients on ICB therapy have better outcomes when their tumors have high levels of TIL-B cells, however, the mechanisms by which TIL-Bs are supporting improved outcomes to ICB remain unclear. Nevertheless, insights into potential functions of TIL-Bs can be gained from other disease models such as autoimmunity, transplantation and infectious disease[116]. Additionally, some cancer studies have revealed that TIL-Bs can support antitumor immunity in several ways including: (1) producing tumor reactive antibodies, (2) presenting tumor-antigen to $CD4^+$ T cells, (3) providing co-stimulation to $CD4^+$ or $CD8^+$ T cells, (4) directly killing tumor cells via Fas/FasL or TRAIL pathway, (5) generating proinflammatory cytokines, and (5) inducing TLS formation. Alternatively, in some cancer indices, TIL-B cells can promote tumor progression by producing immunosuppressive cytokines (IL-10, IL-35, TGF-β), and adenosine and expression of inhibitory receptor ligands. It is not yet clear whether the same TIL-B cell subset can perform multiple functions or if there is a “division of labor” whereby multiple TIL-B cell subsets carry out distinct functions. Linking TIL-B phenotypes to distinct function will aid in the development of B cell-based immune therapies.

#### 1.4.4.1 Targets of tumor-reactive antibodies

TIL-B cells and TIL-PCs and circulating B cells and PCs can be a potent source of tumor-reactive antibodies, which recognize a variety of aberrantly expressed or mutated self-antigens and tumor-specific antigens[167,217,218]. Mucin 1 (MUC1) is a self-antigen that is overexpressed in its un-glycosylated form in several tumor types including OV, PDAC, gastric, BRCA, and NSCLC[219–223]. Serum IgG antibodies directed at MUC1 are associated with favorable prognosis in patients with early stage PDAC and BRCA[221–223]. Circulating antibodies to cancer/testis (CT) antigens such as melanoma-associated antigen1 (MAGE1) and new york esophageal squamous cell carcinoma-1(NY-ESO-1) are found in serum of HNSCC, OV, NSCLC, and esophageal adenocarcinoma (EAC)[128,224–226]. In NSCLC, intratumoral PCs also produce antibodies to MAGE proteins and NY-ESO-1[203]. Interestingly, serum antibodies to NY-ESO-1 and X antigen family member 1A (XAGE1) in NSCLC also correlate with better survival and response to anti- PD1 therapy[224]. In medullary BRCA, serum and intratumoral antibodies were also directed at intracellular self-antigens aberrantly exposed on the surface of apoptotic tumor such as β-actin[227,228]. Mutations to tumor suppressor gene p53 is a common feature of most human cancers and antibodies directed to mutated p53 can be detected in the sera of patients[229–233]. In some NSCLC patients, anti-p53 antibodies are associated with favorable outcomes[129,232].

Circulating antibodies to growth factor receptors that are overexpressed in tumors including human epidermal growth factor receptor 2 (HER2) and epidermal growth factor (EGFR) have also been detected[218,234–237]. Treatment naïve patients with BRCA have naturally occurring serum antibodies directed to the intracellular domain of HER2 and this

is associated with favorable outcomes[234]. The level of circulating anti-HER2 IgG is increased in patients treated with chemotherapy and trastuzumab, a HER2 monoclonal antibody[235]. While increased circulating antibodies to self-antigens (autoantibodies) are a sign of disease progression in autoimmune disorders, it is thought that they can be used as biomarkers for detection of early-stage cancer and a positive prognostic indicator in some indices including OV, CRC, HCC, BRCA and NSCLC[219,223,238–240]. However, there is some contradictory evidence demonstrating higher levels of circulating and intratumoral antibodies to tumor associated self-antigens are associated with poor prognosis in BRCA[241]. Additionally, antibodies can be directed at novel tumor specific antigens known as “neoantigens” as well as new epitopes of known antigens (cryptic epitopes) both of which are associated with improved survival[242,243]. Further, circulating antibodies from plasmablasts in metastatic MEL, LUAD, and RCC were shown to be reactive to autologous and heterologous tumor tissue and tumor cell lines, suggesting that shared tumor antigens are present in these cancer types[231,244].

Intratumoral and circulating antibodies can also be directed at viral proteins present in cancers caused by oncogenic viruses including HPV, hepatitis B (HBV), hepatitis C (HCV), Merkle cell polyomavirus (MCPyV)[226,245–249]. In $HPV^{+}$ HNSCC, intratumoral B cells and PCs produce IgG antibodies directed at E6, E7 and E2 HPV viral proteins[246]. Additionally, circulating antibodies to early (E2, E4, L1) and late (E6 and E7) HPV antigens are detected in HNSCC and oropharyngeal squamous cell carcinoma (OPSCC)[226,250]. Serum antibodies to HBV surface antigen (HBVsAg) and HCV core protein are prevalent in HCC patients[247–249]. HBV-specific intratumoral B cells are present in HBV driven HCC, however, they have an atypical memory phenotype and poor

antibody production[249,251,252]. Several technologies are available to study antigen specific B cells including: (1) *ELISPOT*, (2) *Flow cytometry*: using fluorescently labeled antigen probes, (3) *Reversed B-cell FluoroSpot assay*: uses recombinant tagged antigens and fluorescently labeled detection systems (streptavidin or IgG antibodies) to detect antigen specific IgG secreted by B cells. Given the role of antibodies in immune memory, more studies should assess antigen specificity of TIL-B cells and PCs and ways to increase tumor-specific antibody production[253–255].

#### 1.4.4.2 Antibody-mediated effector mechanisms

There is very limited evidence regarding the effector function of tumor-reactive antibodies within the TME of human solid tumors. However, we can hypothesize how tumor-specific antibodies can contribute to tumor immunity by taking cues from humoral responses to viral infection[165,166]. ADCC *in vivo* is thought to mostly be carried out by NK cells although, *in vitro* other innate immune cells such as monocytes and macrophages are also capable of ADCC[165]. ADCC is mostly mediated by IgG1 isotype which interacts with Fc gamma receptor III a (FcγRIIIa) or CD16a on NK cells causing release of granzyme b and perforin that lyse infected or tumor cells[165,166]. In MEL, MEL reactive antibodies derived from patients have been shown to be capable of ADCC *in vitro*[256]. Although not well studied in the context of intratumoral antibodies from B cells or PCs, ADCC is a key mechanism of action for therapeutic monoclonal antibodies[83,257,258259]. ADCC is carried out by phagocytic cells such as macrophages, which express a number of FcγR that interact with IgG1 antibodies bound to infected or tumor cells[165,166,260]. Additionally, antigen: antibody complexes can also bind FcγRs on macrophages which can allow them to uptake these complexes and present antigen to T cells[165,166]. It appears

that the complement system plays a complex role in the TME in murine models, but is severely understudied in human tumors[261,262]. During immune responses to infection, CDC is mediated by IgG and IgM antibodies which activate the complement pathway[165,166]. Classical complement protein C1q binds to antibodies on infected or tumor cells, which activates the complement cascade, ultimately leading to formation of membrane attack complex (MAC), which directly causes cell lysis[165,166,261]. Whether intratumoral IgG and IgM antibodies can mediate complement pathway activation in tumors and what effect this has on tumor immunity remains unknown. However, expression of classical and alternative complement genes can be found in a variety of tumors[261]. Future studies should focus on isolating TIL-B cells and PCs from patients, stimulating them to make antibodies and subsequently testing the effector function capabilities (ADCC, ADCP, CDC, immunomodulation) in vitro[257,259,263,264]. This may provide insight to the potential in vivo roles of tumor-specific antibodies.

#### 1.4.4.3 Antigen presentation

Although DCs are regarded as the main antigen presenting cell (APC) in immune responses to infection and tumors, DC function is often rendered dysfunctional by the immunosuppressive TME[90,91,265]. B cells are also a professional APC, however their role as APCs in human solid tumors remains understudied. It has been shown that activated B cells $CD21^{-}CD86^{+}$ are potent APCs while resting B cells ($CD21^{+}CD86^{-/lo}$) are more tolerogenic[266–268]. Indeed, in NSCLC patients, activated TIL-B cells were shown to be capable of presenting tumor antigen to $CD4^{+}$ T cells[127]. Additionally, activated TIL-Bs in NSCLC were shown influence $CD4^{+}$ T cell phenotypes[127]. CD40 stimulated B cells were able generate tumor-specific $CD4^{+}$ T cells after being pulsed with tumor associated

antigens gp100 and NY-ESO-1[179]. Cross presentation by B cells to $CD8^+$ T cells in humans has not been well investigated. However, activated B cells can promote $CD8^+$ T cell proliferation and survival independent of antigen via CD27/CD70 interactions[269]. In OPSCC, activated TIL-B cells and $CD8^+$ T cells are found in close proximity within TLS and depletion of B cells from tumor-derived cell suspensions resulted in decreased survival and functionality of $CD8^+$ T cells[270]. Activated, antigen-experienced ($CD27^+CD21^-CD86^+CD95^+$) TIL-Bs have been described in HNSCC, TNBC, NSCLC, and gastric cancer[127,128,198,203,226]. Thus, further investigation of the antigen presentation capabilities of different TIL-B subsets is warranted.

#### 1.4.4.4 Cytokine production

TIL-Bs also have the potential to shape tumor immunity via cytokine and chemokine production, although this has not been well investigated in human solid tumors[115,180,271,272]. In TNBC, TIL-Bs cells had higher mRNA expression of Th1 effector cytokines IFN-γ and TNF-α as well as compared to B cells from non-diseased lymph node and tonsils. Th2 effector cytokines IL-4 and IL-5 mRNA was also detected[198]. However, this study did not directly assess soluble protein production of cytokines by intratumoral B cells. In HCC, intratumoral MBC, located in the margin of the tumor, produced IFN-γ, IL12-p40 and granzyme B by flow cytometry and confocal microscopy[205]. Granzyme B production by B cells has been reported in the context of viral infection. In fact, B cells from patients recently vaccinated against tickborne encephalitis virus (TBEV) produce granzyme B when rechallenged with TBEV antigens[188]. Granzyme B production by B cells is driven by IL-21 and BCR stimulation in the absence of help from T cells through CD40 ligation[187]. Depending on the context, IL-21 induced granzyme B production by B cells

could be an important mechanism of killing tumor cells within the TME[187–189]. There is more evidence regarding the production of immunosuppressive cytokines (IL-10, IL-35, TGF-β) by intratumoral Breg subsets. IL-10 production is induced by intratumoral B cells when co-cultured with tongue squamous cell carcinoma (TSCC) tumor cell lines can induce differentiation of resting $CD4^+$ T cells into $T_{regs}$[273]. IL-10 production by intratumoral B cells has been detected in OV, CESC, HNSC, HCC and can suppress $CD4^+$ T cell and DC effector responses[200,226,274,275]. In HCC, IL-10 production by PD-$1^{hi}$ intratumoral $B_{regs}$ inhibit cytokine production by $CD8^+$ T cells[276]. IL-35 production by intratumoral B cells has been detected in STAD patients and is associated with disease progression of STAD[277]. Future studies should further assess soluble cytokine production by intratumoral B cells and cytokine production across intratumoral B cell subsets. Using different stimuli (tumor-specific vs polyclonal) may provide insight into how B cell cytokine production is influenced by different TMEs.

#### 1.4.4.5 Direct Tumor lysis

There is evidence that TIL-Bs are capable of killing tumor cells directly in the absence of antibodies through expression of death ligands: Fas Ligand (FasL) and TRAIL[191,194,205]. Expression of FasL has not been well characterized on intratumoral B cells in humans but increased expression of FasL on B cells is observed in infection models particularly on $CD5^+$ B cells. IL-10 and IL-4 can also regulate FasL expression. Human B cells express TRAIL following stimulation with CpG-A (ODN2007) and IFN-α and can directly kill tumor cells via TRAIL[192]. In HCC, intratumoral aMBC express TRAIL and granzyme B and were shown to kill HCC tumor cells in an in vitro co-culture[205].

Further studies are needed to solidify the cytotoxic function of intratumoral B cells. **(**Figure 5**).**

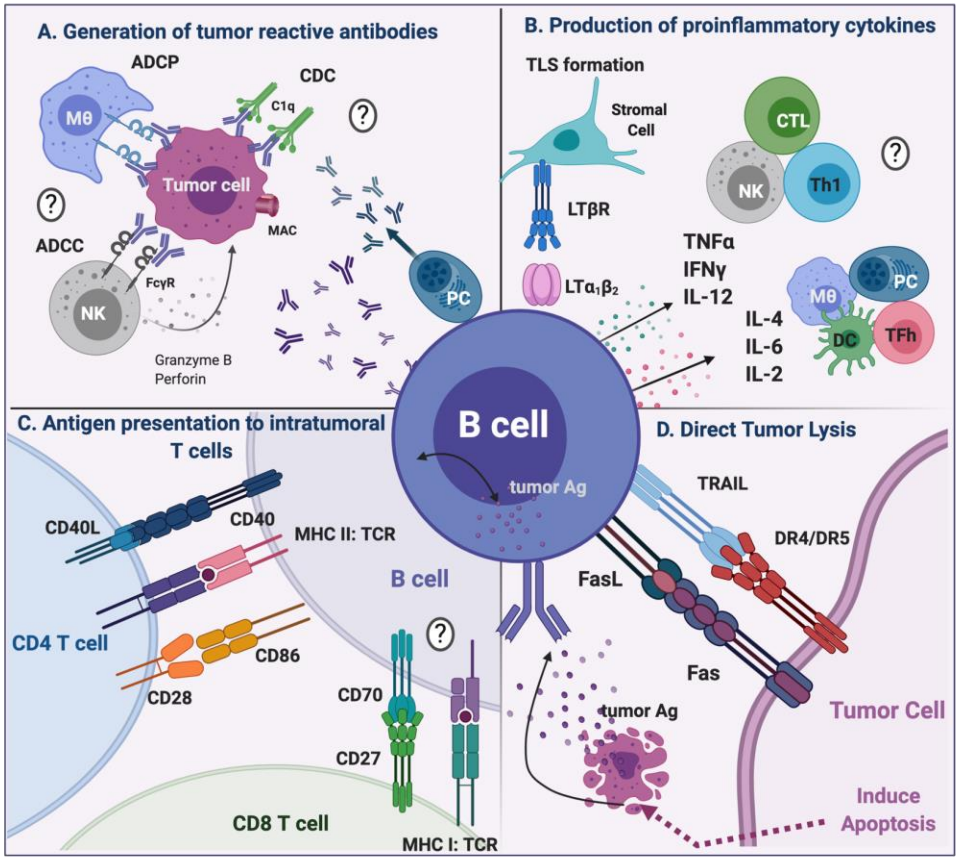


**Figure 5: Potential Anti-tumor roles for B cells in the tumor microenvironment**

B cells can potentially promote antitumor immunity in several ways: (A) Generation of tumor reactive antibodies: Intratumoral B cells and PCs can produce antibodies that are specific to surface proteins expressed on tumor cells . These antibodies are then recognized by the Fc-receptors on NK cells which can induce ADCC via the release of granzyme B and perforin or monocytes/macrophages which induces ADCP. Tumor specific antibodies can also opsonize tumor cells making them targets for CDC by complement cascade proteins such as C1q. (B) Production of proinflammatory cytokines: Intratumoral B cell can produce lymphotoxin ($LT\alpha_2\beta_1$) which interacts with LTβR on stromal cells. LTβR signaling leads to chemokine production by stromal cells initiating TLS formation. Th1 effector cytokines (TNF-α, IFN-γ, IL-12) produced by intratumoral B cells can support immune cells associated with antitumor function such as CTLs, NK cells, and Th1 cells. However, in some patients intratumoral B cells may produce more Th2 effector cytokines which typically support more suppressive populations but can also support DCs , PCs and TFH. (C) Antigen presentation to intratumoral T cells: Intratumoral B cells are found in close proximity

to CD4 T cells and CD8 T cell within TLS suggesting that they may be interacting. Intratumoral B cells have been shown to present tumor antigen via MHC II to $CD4^+$ T cells and costimulatory molecules associated with antigen presentation such as CD86 and CD40 are present on activated intratumoral B cells. Cross presentation of tumor antigen on MHC I by intratumoral B cells has not been investigated in humans but has been shown in mice models. In humans, intratumoral B cells can support intratumoral CD8 T cell function via CD27/CD70 interactions. (D) Direct tumor lysis: Intratumoral B cells can induce apoptosis in tumor cells through expression of TRAIL which only induces apoptosis in tumor cells leaving healthy cells intact, or expression of FasL which binds Fas which also induces apoptosis but is not necessarily restricted to tumors. Apoptosis of tumor cells can lead to exposure of intracellular tumor antigens that can be presented to T cells. *ADCC: Antibody-dependent cellular cytotoxicity ADCP: Antibody-dependent cellular phagocytosis CDC: Complement dependent cytotoxicity NK cell: Natural Killer cell LTβR: Lymphotoxin Beta Receptor Th1: T helper 1 Th2: T helper 2 CTL: Cytotoxic T lymphocyte DC: Dendritic cell PC: Plasma cell TFH: T follicular helper MHC II: Major histocompatibility complex II. MHC I: Major histocompatibility complex I. TRAIL: TNF-related apoptosis-inducing ligand.* Created in Biorender.com

## 1.5 Questions to address

Single agent immunotherapy approaches such as anti-PD1 have only improved care for a subset of patients with recurrent/metastatic HNSCC. Better predictors and targets to improve response are critically needed. Intratumoral B cell subpopulations can predict response to anti-PD1 therapy , which highlights the biomarker potential of B cells[122]. Further, recent studies have demonstrated that other components of the TME such as B cells and TFH cells within TLS may work in concert with CD8 T cells to enhance anti- tumor immunity[72,201]. Targeting B cells and TFH cells within TLS could complement CD8 T cell focused therapies in HNSCC. I will address the following questions to

determine the clinical significance and therapeutic potential of B cells, $CD4^+$ TFH and TLS in HNSCC: (1) what types of B cells , CD4+ T cells and TLS are present in HPV+ and HPV- HNSCC and do B cells, CD4+ T cells and TLS correlate with improved survival, (2) What is the ex vivo function of intratumoral and circulating B cell subpopulations in HNSCC (3) can circulating B cell subpopulations predict response to therapy? To address these questions, I utilized human tumor and blood specimens from HPV+ and HPV- HNSCC as well as blood specimens from metastatic melanoma and lung cancer patients who were later treated with anti-PD1 therapy. I hypothesize that B/T cell composition, transcriptomic profiles, and spatial location would be distinct between HPV+ and HPV- HNSCC. GC B cells, TFH, and TLS would be more prevalent in HPV+ HNSCC and correlate with favorable outcomes. Further, MBC subpopulations would also be distinct in HPV+ and HPV- HNSCC. Functional MBC populations would be more prevalent in HPV+ HNSCC. Dysfunctional MBC populations would correlate with poor response to anti-PD1.

# 2.0 Methods

## 2.1 Human subject details

All HNSCC, melanoma, lung cancer tissues and peripheral blood specimens and formalin-fixed paraffin-embedded and normal tissue samples were acquired under a University of Pittsburgh Cancer Institute Institutional Review Board (IRB)-approved protocols (99-069, 96-099 and 17-036) with written informed consent obtained from each patient in conjunction with the University of Pittsburgh Cancer Institute HNSCC and Melanoma SPOREs. Normal lymph nodes and spleen were collected from organ donors through a national organ donor program. Several patient cohorts were used for various aspects of this manuscript. Fig 6,8, 10 and Appendix A Fig 1-4 used the patient cohort[36] described in Table 1. This cohort consisted of consecutive patients undergoing surgical resection as treatment for head and neck cancer at the University of Pittsburgh, patients undergoing tonsillectomy as treatment for sleep apnea or tonsilitis, or healthy donors. Fig. 6 and 8 and Appendix A Fig 5-7, used the patient cohort described in Table 2, and consisted of patients undergoing surgical resection as treatment for head and neck cancer or patients undergoing tonsillectomy as treatment for sleep apnea or tonsilitis, or healthy donors. Fig.11 used the patient cohort described in 3 and consisted of a retrospective cohort of patients with formalin fixed paraffin embedded samples.

## 2.2 Method details

### 2.2.1 Blood and tissue processing

Peripheral blood was obtained by venipuncture and collected into tubes containing EDTA coagulant. Blood was processed into PBMC by Ficoll-Hypaque density gradient centrifugation. Briefly, whole blood was diluted and layered over Ficoll-Hypaque, followed by centrifugation at 400xg for 20 minutes with the brake set to off. PBMC were then collected and washed in complete RPMI (i.e. RPMI  10% fetal bovine serum and 1% penicillin/streptomycin). Tissues were collected from either HNSCC patients undergoing resection as treatment or sleep apnea or tonsillitis patient undergoing tonsillectomy. Tissues were collected directly into collection media (i.e. complete RPMI + 1% amphotericin B) in the operating room and were processed as soon as possible following surgery. Normal spleens were collected from organ donor patients who died from non-disease related reasons through an organ donor program. For transcriptional analysis, samples were processed within 2 hours of collection. Sample processing consistent of manually dissociating tumor tissue into approximately 1 mm pieces, then washing with cRPMI and passing the suspension over a 100 uM filter. The filter was then washed with cRPMI, and the cells were centrifuged at 500xg for 5 minutes. If significant numbers of red blood cells were present, red blood cell lysis was performed as per the manufacturer's instructions (BD Pharm Lyse).

### 2.2.2 Flow cytometry-based cell sorting

For experiments requiring cell sorting, cells were first stained in PBS with 2% FBS and 1 mM EDTA for 15 minutes, followed by centrifugation at 500xg for 5 minutes and staining with viability factor in PBS for 15 minutes. Cells were then centrifuged again, resuspended in PBS with 2% FBS and 1 mM EDTA, and sorted using a MoFlo Astrios High Speed Sorter (Beckman Coulter). Sort cells were collected directly in cRPMI. For single-cell RNAseq analysis, live CD45+ cells were sorted by using Fixable Viability Dye eFluor780 (eBioscience) and CD45 conjugated to PE (Biolegend, clone HI30). For in vitro assays, live B cells and CD4+ T cells were sorted using CD19 conjugated to PE-cy7 (Biolegend, clone HIB19), CD20 conjugated to PerCP-cy 5.5 (Biolegend, clone 2H7), CD27 conjugated to PE (Biolegend clone O323), IgD conjugated to Pacific Blue (Biolegend clone JAG-2), CD11c conjugated to APC (Biolegend, clone 3.9)

### 2.2.3 Single-cell RNAseq Library Preparation and Sequencing

Immediately following sorting, cells were centrifuged for 5 minutes at 500xg and were resuspended in PBS with 0.04% BSA. Cells were then counted using the Cellometer Auto2000 (Nexcelom) and loaded into the 10X Controller (10X Genomics) targeting a recovery of 2,000 cells per sample. Following bead/cell emulsification, RNA was reverse transcribed into cDNA. cDNA and was then purified by SPRI-bead selection and amplified, followed by fragmentation for library generated followed by 12 cycles of PCR amplification. The library quality was determined by Bioanalyzer analysis and concentration by KAPA qPCR DNA Quantification. Libraries were then pooled and

sequenced on a NextSeq500 (University of Pittsburgh Genomics Research Core) using a high-output kit.

### 2.2.4 Processing and clustering of single-cell RNAseq data

Following sequencing, raw Illumina reads were demultiplexed based on i7 indices (10X Genomics) using the mkfastq command of the CellRanger suite of tools (10X Genomics). Demultiplexed FASTQs were then aligned to the human genome (GRCh38) using the count command of CellRanger to generate cell/barcode matrices. Cell/barcode matrices were then read into Seurat (v2.3.4) for downstream analysis. Clustering was performed as an initial analysis step for several scRNAseq datasets using the workflow implemented in Seurat. Briefly, raw reads were normalized for library size per cell and log transformed. Highly variable genes were identified and selected, followed by scaling and center of data as well as regression out technical variables (i.e. number of genes per cell, percent of reads aligning to ribosomal genes per cell and percent of reads aligning to mitochondrial reads per cell). These scaled and centered expression values were then used as input into a principal component analysis to reduce the dimensionality of the data. The top principal components that explained the most variance in the dataset were heuristically selected as input for the fast interpolation-based t-SNE[278] and the Louvain-based clustering algorithm implemented in Seurat.

### 2.2.5 Identification of cell types in single-cell RNAseq

We initially sorted and sequenced all cells of the hematopoietic lineage (i.e. CD45+ cells), and were therefore needed to robustly identify B cells and $CD4^+$ $T_{conv}$ for downstream in-depth analysis. We did this using a two-step semi-supervised identification strategy. This strategy consisted of first identifying core transcriptional programs of the major lineages of the immune compartment. To do this, we downloaded publicly available single-cell RNAseq data of sorted immune lineages (10X Genomics; https://www.10xgenomics.com/resources/datasets/). We then clustered these cell populations as described above to identify lineage-specific clusters. Once these clusters were identified, we performed differential gene expression analysis using a Wilcoxon rank sum test to identify the top 20 genes associated with each cluster. These genes were defined as the core transcriptional profile of each lineage. We then used these genes as gene sets to test individual cells for enrichment of each immune lineage. Briefly, we used the log-fold change in gene expression as a metric and input these fold-changes into the Wilcoxon rank sum test for genes in each core lineage set versus genes outside that set, deriving a gene set score and p-value for each gene set for each cell. The core lineage gene set associated with the lowest p-value for each cell was then applied as that cell type. Following this test for each cell, we then examined clusters of cells in aggregate, and identified each cluster by the most common cell type enriched within that cluster. We then compared this two-step method (i.e. single-cell gene set enrichment testing and identification followed by aggregate identification of clusters) to the ground truth for each of the clusters know to be a sorted cell lineage using a confusion table from the R package

caret. B cells and CD4+ $T_{conv}$ were identified from all hematopoietic cells in our data set using this two-step method.

### 2.2.6 Quantification of differences in cell frequencies across clusters

We evaluated the enrichment of cells from a given sample type in each cluster by dividing the frequency of observed cells over expected cells in each cluster. The expected frequency of cells was calculated by assuming cells from each sample group were evenly divided across clusters. Analysis of variance was used to determine if the cell enrichment across groups was statistically significant, and Wilcoxon rank sum tests were used to determine if there were statistically significant differences in cell frequencies between HPV- and HPV+ TIL.

### 2.2.7 Gene set enrichment analysis of B cells

Gene set enrichment analysis was performed using the R package singleseqgset as previously described. Briefly, log-fold change in gene expression was calculated for all genes across B cell clusters and used as input for a variance inflation corrected Wilcoxon rank sum test to whether sets of gene were upregulated in a concerted manner within a cluster. B cell gene sets were curated based on biological relevance from the Molecular Signatures Database (C7 Immunology Gene Sets).

### 2.2.8 Survival analysis using The Cancer Genome Atlas

To determine if our gene sets were relevant for survival, we utilized bulk RNAseq data for HNSCC patients available through the TCGA and create an enrichment score for each signature from each patient as previously described[58]. Briefly, we derived genes sets that were reflective of the cell populations of interested and determined an enrichment score for each patient in the TCGA. Enrichment scores were calculated by using a Kolmogorov-Smirnov test comparing genes within the gene set of interest versus genes outside the given gene set. The gene set for B cell infiltration was defined by taking the top genes that were differentially expressed with a log fold-change >0.5 from the overall clustering used to define the major immune lineages. Gene sets for GC and plasma cells were derived by taking the top 200 differentially expressed genes by log fold-change from the two GC clusters and the two plasma cell clusters versus all B cells and CD4+ T cells (i.e. from cluster 17 and 18 for GC cells and 20 and 21 for plasma cells from Fig. 1a). We then stratified patients based on high versus low enrichment scores and performed Cox proportional hazards regression (see statistical analysis below).

### 2.2.9 Pseduotime analysis of B cells

Clustering analysis is useful for grouping cell types based on similar gene expression patterns but does not capture information related to developmental trajectories of cells. To assess developmental trajectories, we first embedded cells in a low-dimensional diffusion map (e.g. performed non-linear dimensionality reduction[279]. We then used the R package slingshot[280] to infer a pseduotime for each cell along the

developmental trajectory, and to infer individual trajectories. To evaluate whether genes were statistically associated with pseduotime, we performed LOESS regression using the R package gam, where we fit gene expression as a function of pseduotime along each trajectory. We focused on the trajectory that was characterized by progression from naïve B cells to germinal center B cells.

For pseduotime analysis of germinal center B cells, slingshot could not be used since it assumes a linear trajectory. Germinal center B cells are in a cycle between light and dark zones, and therefore require pseduotime inference based on a cyclical process. Therefore, a principal curve was fit along the circular trajectory to infer the pseudotime of each cell in this process. Genes were once again investigated for their relationship to pseudotime and were clustered based correlation of gene expression over pseudotime. An R package called “circletime” and accompanying vignette were created to encapsulate the code necessary to generate all aspects of the cyclical pseudotemporal analysis.

### 2.2.10 Adaptive B cell receptor Sequencing

Adaptive Biotechnologies’ immunoSEQ platform was used to perform a survey of B cell receptors (BCRs) from HNSCC patients. Total DNA was isolated from cryopreserved snap frozen tumor tissues using the QIAGEN DNeasy Blood and Tissue Kit and was used as input for the immunoSEQ platform. Analysis was performed using Adaptive’s analysis interface.

### 2.2.11 Surface and intracellular antibody staining of patient and healthy donor cells

Single cell suspensions from either HNSCC tissue, tonsillar tissue, HNSCC PBL or healthy donor PBL were stained with fluorescently labeled antibodies at 1:100 dilution (see Table 4 for antibody panel information), for 25 mins at 4°C in PBS (Thermo Fisher) supplemented with 2% FBS (Atlanta Biologicals) and 0.01% azide (Thermo Fisher) (FACS buffer). Cells were then washed with FACS buffer and spun down (1500 rpm, 5 min, RT). Cells were next stained using Fixable Viability Dye (eBioscience) in PBS to exclude dead cells. Cells were then washed with PBS and spun down (1500 rpm, 5 min, RT). For intracellular transcription factor staining cells were fixed using fixation/permeabilization buffer (eBioscience) for 20 mins at 4°C the washed with permeabilization buffer (eBioscience). Cells were then stained with fluorescently labeled antibodies. Flow cytometry measurements were performed on an LSR-II flow cytometer (BD) using BD FACS Diva software or Cytek Aurora using SpectroFlo software (Cytek). All data were analyzed using FlowJo.

### 2.2.12 High dimensional spectral cytometry

viSNE and FlowSOM analyses were performed on Cytobank (https://cytobank.org). FSC files for each sample type were first down sampled and concatenated in flowjo whereby each patients' FSC file contributed an equal number of total events to the concatenated file. Files were uploaded into Cytobank and traditional flow cytometry gating was performed to gate live CD19+ CD20+ B cells. viSNE analysis

was performed on CD19+ CD20+ B cells using proportional sampling cells from each concatenated FCS file to equal 100,000 total events with 1000 iterations, a perplexity of 30, and a theta of 0.5. The following markers were used to generate the viSNE maps: IgG, CD27, CD21, FcRL5, CCR1, Ki67, BAFFR, CD38, CD7, CD40, CD37, CCR6, CD72, IgD, ICAM1, CD180, CD72, CD86, CXCR4, Sema4a, CD83, CD18. The resulting viSNE maps were fed into the FlowSOM clustering algorithm. A new self-organizing map (SOM) was generated using hierarchical consensus clustering on the tSNE axes. The SOM contained 100 clusters and 10 metaclusters for B cells were identified.

### 2.2.13 Single-plex immunohistochemistry

Fresh tissues were formalin-fixed immediately followed surgical resection and were then embedded in paraffin. Tissues were processed as previously described[58]. Briefly, fixed tissues were then slide mounted, de-paraffinized using xylene and ethanol, and then re-fixed in formalin for 15 minutes followed by antigen retrieval. Slides were stained with the following antibodies: CD20 (Clone L26, ThermoFisher, 1:100, Cat# MA5-13141), CD4 (Clone D7D27, Cell Signaling, 1:100, Cat# 25229), CXCR5 (Clone D6L36, Cell signaling, 1:100, Cat# 72172), Tbet (Clone 4B10, Abcam, 1:100, Cat# ab91109). Quantification of cells and TLS were performed by a HNSCC pathologist. Specifics of these quantifications are outlined in Fig. Legends and definitions of a TLS were consistent across three independent pathologists.

### 2.2.14 Cytoscape analysis

We utilized Cytospace version 3.8.0 in conjunction with the top genes that shared temporal dynamics with *CD38* expression during differentiation from naïve B cells to GC B cells. The confidence score for interaction was set to 0.2, and the maximum number of additional interactors was set to 10. After pruning nodes that did not have any edges, we performed functional enrichment to identify biological functions associated with the interactions present in our network.

### 2.2.15 Immunofluorescence analysis

Fresh tissues were formalin-fixed immediately followed surgical resection and were then embedded in paraffin. Formalin fixed paraffin embedded tissue sections were cut at 5um thickness and mounted on slides. Briefly, sections were baked at 60$^{o}$C for 2 hours or overnight and deparaffinized using xylene and ethanol, followed by fixation in 10% neutral buffered formalin for 15 minutes. Tissues were then subjected to heat induced epitope retrieval (HIER) cycles in AR9 or AR6 citrate buffers (Akoya Biosciences). Post antigen retrieval, slides were blocked for 10 minutes with blocking buffer, followed by incubation with primary antibodies for 30 minutes in a humidified chamber at room temperature. Secondary antibodies conjugated to horseradish peroxidase were then added for 10 minutes. Separate opal detector fluorophores were used for each marker as follows: CD4 (Clone RM, BioCare Medical, Prediluted, Cat# API3209 AA)/Opal540, CD8 (Clone C8/144B, BioCare Medical, 1:200, Cat# ACI31160A)/Opal570, CD20 (Clone L26, Leica Biosystems, 1:200, Cat # CD20-L26-L-

CE)/Opal520, CD68 (Clone D4B9C, Cell Signaling, 1:800, Cat# 76437S)/Opal650, FOXP3 (Clone D608R, Cell Signaling, 1:250, Cat# 12653S)/Opal620 and Pan-cytokeratin (Clone AE1/AE3, Santa Cruz Biotech, 1:100, Cat# SC81714)/Opal690. Opal 7 color manual kit (including all opal fluorophores and DAPI) was purchased from Akoya Biosciences (Cat# NEL811001KT, 1:600 dilution). Final round of antigen retrieval was carried out to counterstain cells with spectral DAPI. Stained tissue sections were then mounted and sealed with Diamond Anti-fade mounting media (Thermo Fisher, cat # P36970). Following staining, slides were imaged as whole slide scans on the Vectra (Perkin Elmer). Regions of interest were selected from the whole slide scans, and slides were re-imaged to captures these regions at 10x magnification. Images were unmixed after scanning using inForm and Phenochart. Using FIJI, cell segmentation was performed with watershed analysis in each individual channel, and cells were assigned an x- and y-position on each slide associated with a given channel and assigned a cell type based on the channel. We then performed Delaunay triangulation to determine to odds of a cell interaction with another given cell type based on proximity[58,281].

### 2.2.16 Immunofluorescent confocal microscopy

Formalin-fixed paraffin-embedded (FFPE) 4 µm slides were deparaffinized, rehydrated, and processed for heat-induced antigen retrieval. Samples were then washed with PBS and blocked against nonspecific binding using universal blocking buffer for 1 hour at room temperature. Conjugated antibodies CD20/PE-cy7 (Clone 2H7, Biolegend, 1:50, Cat# 302312), BCL6/AF488 (Clone K112-91, BD Biosciences, 1:50, Cat# 561524) and SEMA4A/APC (Clone 5E3, Biolegend, 1:50, Cat# 148406) were diluted in 10%

universal blocking buffer (5µg/ml) and applied for 1 hour at room temperature. Samples were then washed with PBS and mounted with antifade media and left to dry overnight at 4 C°. All images were acquired on Nikon A1 confocal microscope and analyzed using Nikon elements NIS.

### 2.2.17 Statistical analysis

Analysis of variance (ANOVA) followed by pairwise t-tests was used to compare more than two groups of continuous variables. Two groups of continuous variables were compared by t-tests or Wilcoxon rank sum tests were indicated. Tukey's multiple comparisons test was performed following ANOVA where indicated. Survival analysis was performed by using Cox proportional hazards regression analysis, using either nominal values or stratifying continuous variables into nominal values. Stratification of continuous variables was performed using the "cutp" function of the R package survMisc. Correlations were performed using either Pearson's correlation or Spearman's correlation, as indicated. Correction for multiple comparisons using the false discovery rate was performed where appropriate. P values and false discovery rates were considered statistically significant when the two-sided type I error was 5% or less.

### 2.2.18 Data availability

Unprocessed FASTQ files for scRNAseq data are available through the Sequence Read Archive SRP226817 (https://www.ncbi.nlm.nih.gov/sra?term=SRP226817). Processed feature barcode matrices for all scRNAseq data are available through the

Gene Expression Omnibus with accession number GSE139324 (https://www.ncbi.nlm.nih.gov/geo/query/acc.cgi?acc=GSE139324). The bulk RNAseq and clinical data utilized for survival analysis from TCGA is available through the Broad Genome Data Analysis Center Firehouse (https://gdac.broadinstitute.org/). The gene barcode expression matrices from sorted cells are available through 10X Genomics website (https://www.10xgenomics.com/resources/datasets/). The Adaptive BCR sequencing data is available (**Appendix A)**

### 2.2.19 Code availability

For analysis, standard workflows from the R packages Seurat and Destiny were utilized for normalization, dimensionality reduction, clustering, and diffusion maps. We developed a new R package called circletime for the analysis of cyclical pseudotemporal processes (www.github.com/arc85/circletime; DOI: 10.5281/zenodo.4599815)[282].

### 2.2.20 BCR signaling assay

Single cell suspension of bulk lymphocytes from patient tumors and PBL or HD PBL from each donor were plated in a 96 well round bottom plate at a concentration of 5 × $10^5$cells per well, and stained for CD20, CD19, CD21, CD27 (Thermofisher), CD11c, LAIR1, FcRL5 , FcRL4 (Biolegend) at 4℃ in FACS buffer for 25 min. Cells were washed in FACS and incubated at 37℃ for 30 min in complete RPMI before adding anti-Ig-UNLB (Southern Biotech) at a final concentration of 20 µg/ml and incubating at 37℃ for 5 min.

Cells were washed with media and immediately fixed and permeabilized using 4% paraformaldehyde (PFA) diluted to 1.5% in 1X permeabilization buffer (ebioscience) for 45 mins at 4C. Cells were washed in 1X permeabilization buffer and stained with antibodies against phosphorylated Syk conjugated to Alexa Fluor 647 (AF647) (BDBioscience),phosphorylated BLNK conjugated to PE (BD Bioscience) and Tbet BV711 (see Table 5 for antibody panel information).

### 2.2.21 Mitotracker and 2-NBDG staining

Single-cell suspensions from tumor and PBL (approximately $1X10^6$/ ml) were placed in serum-free RPMI containing 2 μM 2NBDG and incubated at 37 C for 30 mins. Cells were washed 2X with complete RPMI and then stained with antibody cocktail including antibodies against CD20, CD19, CD21, CD27, CXCR5, FcRL5 and CD85J and 30nM of Mitotracker Deep Red FM dye (see Table 5 for antibody panel information)

### 2.2.22 Extrafollicular B cell differentiation assay

To test the ability of SW MBC or Naïve B cells to differentiate into extrafollicular subsets, SW and Naïve B cells were isolated from patient PBL via FACS sorting or CD27+ magnetic isolation kit (Stem cell) from HD PBL and stimulated under Th1 conditions as previously described[283]. Cells were plated at 20-30,000 cells/ well and stimulated with TLR7 agonist (R848) 1 ug/ml (Invivogen) BAFF 10 ng/ml, IL-21 10ng/ml, IL-2 50 units/ml and IFNg 20ng/ml (Peprotech), with or without 10 ug/ml goat F(ab')2 anti-human Ig- UNLB (Southern Biotech) for 3 days, cells were then washed and resuspended in fresh media

with R848 and cytokines but not anti-Ig- UNLB for an additional 4 days (Day 7) Cells were stained flow cytometry at Day 3 and Day7 with antibodies against CD19, IgD, CD27, CD11c, CD21, FcRL5, CD95, Tbet, Tox , CD72 and CD38 (See Table 5 for antibody panel information)

### 2.2.23 Antibody production and ASC differentiation assay

Purified B cell subsets were plated at 20,000 cells per well and cultured with CpG ODN 2006 (TLR9 agonist) (10ug/ml), soluble CD40 ligand (sCD40L) (1ug/ml) and cytokines: IL-2 (20 U/mL), IL-10 (50 ng/mL), and IL-15 (10 ng/mL) for five days. Cell culture supernatant were collected for Ig secretion analysis and cells were stained for CD27, CD138, CD38, IgD, and Ki67 (See Table 5 for antibody panel information). Detection of IgG1, IgG2, IgG3, IgG4, IgA, IgM and IgE was performed following the protocol for the Antibody Isotyping 7-Plex Human ProcartaPlex Panel (Thermofisher).

### 2.2.24 In vitro antigen presentation assay

Purified SW MBC and CD4+ T cells were plated at 10,000 cells per population per well and cultured for five days with or without the following reagents as previously described: anti-CD40 (4ug/ml) (Biolegend; clone 5C3) anti-CD28(1ug/ml) (Biolegend), anti-HLADR, DP DR (1ug/ml) (Biolegend). Some assays were performed using anti-HLADRa (1ug/ml) and therapeutic CD40 agonist (CDX-1140) (1ug/ml) from Celldex therapeutics.

# 3.0 B cell signatures and tertiary lymphoid structures contribute to outcome in head and neck squamous cell carcinoma

Data within this chapter were compiled and published in *Nature communications* in 2021 in the following manuscript:

**Ruffin, A.T**., Cillo, A.R., Tabib, T. et al. B cell signatures and tertiary lymphoid structures contribute to outcome in head and neck squamous cell carcinoma. Nat Commun **12**, 3349(2021). https://doi.org/10.1038/s41467-021-23355-x (*Open Access*)

## 3.1 Summary

Current immunotherapy paradigms aim to reinvigorate $CD8^+$ T cells, but the contribution of humoral immunity to antitumor immunity remains understudied. Here, we demonstrate that in head and neck squamous cell carcinoma (HNSCC) caused by human papillomavirus infection ($HPV^+$), patients have transcriptional signatures of germinal center (GC) tumor infiltrating B cells (TIL-Bs) and spatial organization of immune cells consistent with tertiary lymphoid structures (TLS) with GCs, both of which correlate with favorable outcome. GC TIL-Bs in $HPV^+$ HNSCC are characterized by distinct waves of gene expression consistent with dark zone, light zone, and a transitional state of GC B cells. Semaphorin 4a (SEMA4A) expression is enhanced on GC TIL-Bs present in TLS of $HPV^+$ HNSCC and during the differentiation of TIL-Bs. This study suggests that novel

therapeutics to enhance TIL-B responses in HNSCC should be prioritized in future studies to determine if they can complement current T cell mediated immunotherapies.

## 3.2 Introduction

Immunotherapies targeting the programmed cell death protein 1 (PD1) pathway are approved by the Food and Drug Administration for the treatment of several metastatic or unresectable cancers including head and neck squamous cell carcinoma (HNSCC), but only ~20% of patients achieve a clinical benefit, highlighting the need for new therapeutic targets[14,34]. Tumor infiltrating B cells (TIL-Bs) represent a possible new target to compliment T cell-based immunotherapies, as they are frequent in many human tumors and positively correlate with favorable patient outcomes[35,122,195,198]. Specifically, increased TIL-Bs have been reported in cancers caused by environmental exposure to carcinogens (i.e., tobacco, alcohol, UV exposure) such as lung cancer and melanoma as well as cancers caused by viral infection such as hepatocellular carcinoma (HCC) and Merkel cell carcinoma (MCC)[122,203,276,284,285]. HNSCC offers a unique avenue to study TIL-Bs in the tumor microenvironment (TME) as HNSCC cancer can be caused by both exposure to environmental carcinogens or infection with high-risk human papillomavirus (HPV)[286]. Patients with $HPV^+$ HNSCC have historically had better outcomes compared to $HPV^-$ patients[31,287]. While the mechanisms underlying this difference in outcomes remains unknown, TIL-B are more frequent in $HPV^+$ versus $HPV^-$ HNSCC[35,226,270]. Understanding B cell phenotypes and the spatial organization of immune populations in

the TME of patients in both viral and carcinogen induced cancers will provide critical insight into how TIL-Bs can be leveraged to enhance antitumor immunity.

Tertiary lymphoid structures (TLS) are immune aggregates with varying degrees of organization that form outside of secondary lymphoid organs (SLOs) in response to chronic inflammation or infection[288,289]. TLS are characterized by organization patterns similar to SLOs with defined T cell zones, B cell rich follicles and mature dendritic cells (DCs)[156,162]. TLS have been shown to also correlate with increased patient survival in many human tumors[125,290]. Recent studies have demonstrated that the presence of B cells and TLS in melanoma, renal cell carcinoma, sarcoma, and HNSCC are associated with better responses to immune checkpoint blockade (ICB)[122,158,195,196]. However, TLS are quite heterogeneous structures[206], and the composition of TIL-Bs within these structures has not been fully elucidated. Characterization of TLS in the TME, including their composition, spatial organization, and maturity would provide critical insight into the roles these structures play in antitumor immunity. Additionally, understanding the factors that drive formation of TLS would permit the identification of therapeutic avenues to foster an influx of antitumor TIL-Bs into the TME.

One feature associated with mature TLS is the formation and presence of germinal centers (GCs)[210]. GCs are typically found in SLOs and are responsible for producing affinity matured and class switched B cells that effectively recognize their cognate antigen, leading to memory B cells and durable humoral immunity. In humans, GC B cells are commonly identified as $CD38^+$ $IgD^-$ and transcription factor $BCL6^+$. GC B cells can be further divided into centroblasts (dark zone; DZ) and centrocytes (light zone; LZ) through expression of CXCR4 and CD86, respectively. In addition, recent studies have indicated

Semaphorin 4A (SEMA4A) expression on human GC B cells in SLOs[291]. However, SEMA4A expression on GC TIL-B has not been previously reported in human cancer. Ultimately, GCs within TLS in the TME are indicative of maximal engagement of the humoral arm of the immune system in antitumor immune responses. In support of this, GC-like TIL-Bs were found to be increased in melanoma patients who responded to ICB[122]. Understanding the features that drive TIL-Bs toward a GC phenotype and contribute to the development and maintenance of GCs within TLS in the TME would provide a path to enhancing antitumor immunity in patients.

Here, we demonstrate that TIL-Bs in $HPV^+$ and $HPV^-$ HNSCC have distinct transcriptional signatures. GC TIL-Bs and TLS with GC are increased in $HPV^+$ HNSCC patients and correlate with better outcomes. SEMA4A expression is increased on GC TIL-Bs compared to other TIL-B subsets and is associated with TIL-B differentiation and TLS containing GCs in HNSCC. GC TIL-Bs in $HPV^+$ HNSCC are characterized by distinct waves of gene expression consistent with dark zone, light zone, and transitional state of GC B cells. Overall, this study demonstrates the importance of TIL-B transcriptional signatures, phenotypes, and spatial patterning within the TME of patients with HNSCC, suggesting that this understudied lineage contributes to outcome and could be clinically targeted to increase antitumor immunity.

## 3.3 Results

### 3.3.1 Distinct TIL-B transcriptional signatures in HNSCC are revealed by single cell RNA sequencing

We first analyzed scRNAseq data generated from purified CD45+ cells (i.e. all immune cells) from a total of 63 samples, including paired PBL and TIL from 18 patients with HPV– HNSCC and 9 patients with HPV+ HNSCC **(Table 1, Cohort 1).** We developed and validated a two-step approach to robustly identify B cells and CD4+ Tconv **(**Appendix Figure **1; Methods).** We then bioinformatically isolated B and CD4+ Tconv and performed Louvain clustering (Methods) to reveal a total of 21 clusters **(Figure 6a).** Next, we visualized the association between sample type and transcriptional signatures by interrogating the Fast interpolation-based t-distributed stochastic neighbor embedding (FItSNE) of cells from each sample type **(**Figure **6b; Methods)**[278]. Differential localization in the FItSNE revealed distinct transcriptional profiles associated with each sample type **(**Figure **6b)**, and association between clusters and sample types **(**Figure 6**c).** Based on our cell type classifications **(**Appendix Figure 2**),** clusters 11 through 21 were B cells (Figure **6d),** while clusters 1 through 10 were CD4+ Tconv cells **(Figure 6e).** To ascertain the role of B cells in each cluster, we filtered gene sets from the Molecular Signatures Data Base Immunologic Signatures (C7) to eight gene sets associated with canonical B cell function (Methods). This gene set enrichment analysis revealed B cell clusters associated with naïve (clusters 11, 15, 16), switched memory (clusters 12, 13, 14, 19), GC B cells (cluster 17 and 18) and plasma cells (clusters 20 and 21) **(Figure 6f).** We observed statistically significant enrichment of GC TIL-Bs in the TME of HPV+ patients,

while plasma cells were not statistically different in HPV- versus HPV+ patients **(Appendix Figure 3).** We note that a subset of HPV- patients had higher levels of plasma cells **(Appendix Figure 3).** Interestingly, GC TIL-Bs and GC B cells from healthy tonsils were overlapping, suggesting that there is little difference between GC signatures despite being within the TME versus SLOs. We also investigated $CD4^+$ $T_{conv}$ and identified a cluster that was strongly associated with a $T_{FH}$ cell signature (i.e. high frequency and magnitude of *CXCR5, PDCD1, ICOS, CXCL13* expression; Figure 6**g).** These data ultimately revealed increased GC TIL-Bs in HPV+ patients and increased plasma cells in $HPV^-$ patients. Further, a $T_{FH}$ signature was more pronounced in HPV+ disease.

To assess whether B cell signatures were clinically significant, we utilized bulk mRNAseq expression data available through The Cancer Genome Atlas (TCGA; Methods) for HPV+ and HPV- HNSCC. Briefly, we scored each patient for enrichment of B cell signatures derived from our data (Methods). Genes reflective of an overall B cell signature were derived from differentially expressed genes associated with B cells versus other major canonical immune lineages (Supplementary Data 1), while genes for GC B cells and plasma cells were derived from their respective clusters in the analysis of B cells and $CD4^+$ $T_{conv}$ alone (Supplementary Data 2). We then determined if these gene signatures were associated with progression free survival (PFS). Overall, high B cell infiltrate and high enrichment for GC B cells were positively associated with longer PFS (HR 0.39 to 0.46; p values of 0.026 and 0.049, respectively; **Figure** 6**h).** Conversely, a high frequency of plasma cells trended toward shorter PFS (HR=2.0, p=0.12). We also found that enrichment scores for GC B cells from the light zone (LZ) were strongly correlated with those for $T_{FH}$ cells, while there was no relationship between dark zone

(DZ) and $T_{FH}$ enrichment scores (Appendix Figure 4). Taken together, these data suggest that TIL-Bs in the $HPV^+$ TME may be productively activated and receive $CD4^+$ $T_{FH}$ cell help.

Given the differences in transcriptional profiles between TIL-Bs from $HPV^+$ and $HPV^-$HNSCC, we performed bulk B cell receptor (BCR) sequencing via Adaptive **(Appendix Figure 5; Methods).** This analysis revealed no differences in measures of clonality or V-, D-, or J-gene usage between BCRs from $HPV^-$ and $HPV^+$ HNSCC. Thus, whether TIL-Bs recognize tumor antigens in both types of HNSCC or viral antigen in $HPV^+$ HNSCC will need to be further evaluated with more extensive cohorts or alternative assays in future studies.

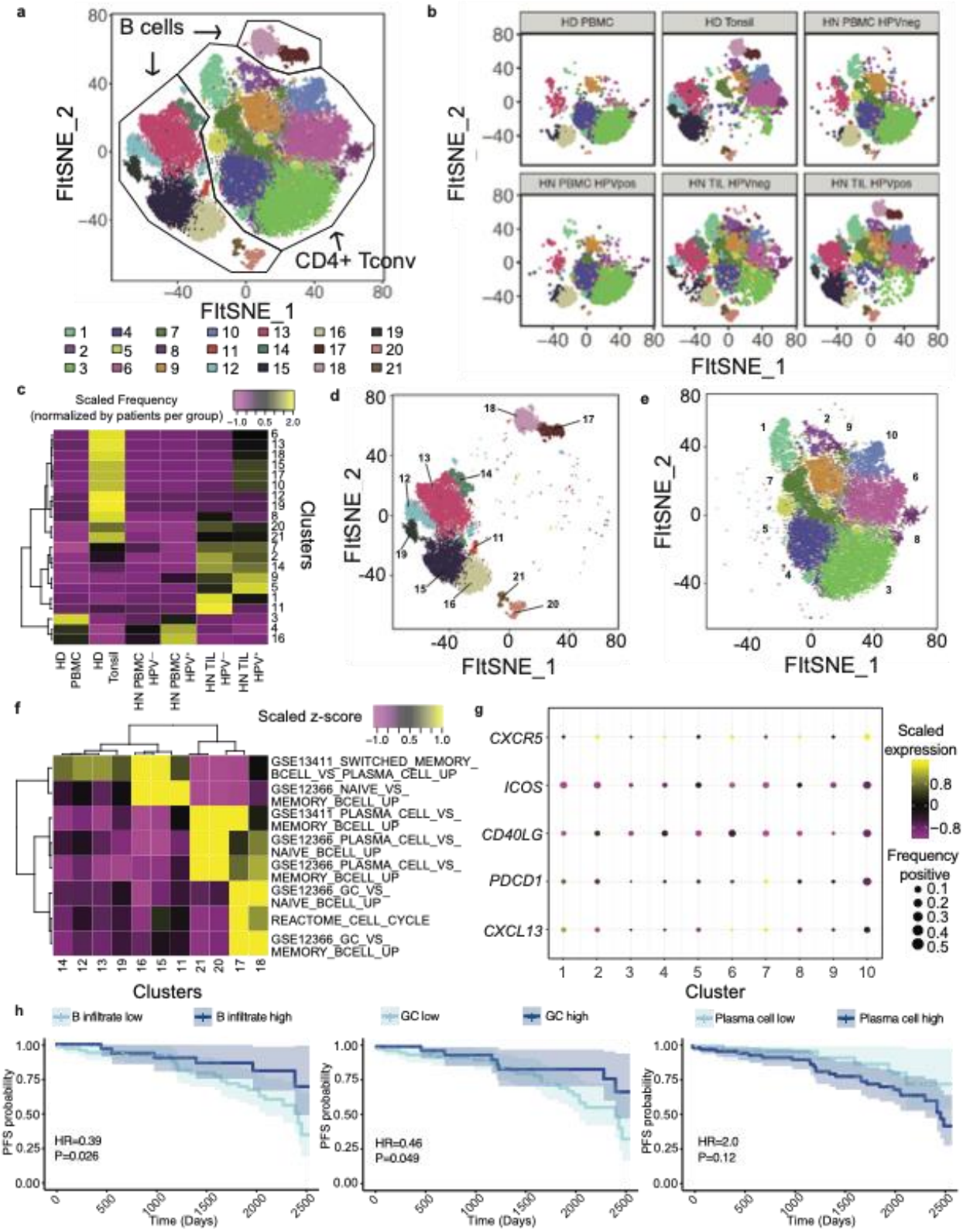
a
B cells
CD4+ Tconv
FItSNE_1
FItSNE_2
b
HD PBMC
HD Tonsil
HN PBMC HPVneg
HN PBMC HPVpos
HN TIL HPVneg
HN TIL HPVpos
c
Scaled Frequency
(normalized by patients per group)
Clusters
HD PBMC
HD Tonsil
HN PBMC HPV−
HN PBMC HPV+
HN TIL HPV−
HN TIL HPV+
d
e
f
Scaled z-score
GSE13411_SWITCHED_MEMORY_BCELL_VS_PLASMA_CELL_UP
GSE12366_NAIVE_VS_MEMORY_BCELL_UP
GSE13411_PLASMA_CELL_VS_MEMORY_BCELL_UP
GSE12366_PLASMA_CELL_VS_NAIVE_BCELL_UP
GSE12366_PLASMA_CELL_VS_MEMORY_BCELL_UP
GSE12366_GC_VS_NAIVE_BCELL_UP
REACTOME_CELL_CYCLE
GSE12366_GC_VS_MEMORY_BCELL_UP
Clusters
g
CXCR5
ICOS
CD40LG
PDCD1
CXCL13
Scaled expression
Frequency positive
Cluster
h
B infiltrate low
B infiltrate high
GC low
GC high
Plasma cell low
Plasma cell high
PFS probability
HR=0.39
P=0.026
HR=0.46
P=0.049
HR=2.0
P=0.12
Time (Days)

**Figure 6: Differences in tumor infiltrating B cell and helper CD4+ T cells between HPV- and HPV+ HNSCC contribute to survival.**

Unsupervised clustering of 16,965 B cells and 30,092 helper $CD4^+$ T cells (total of 47,057 cells) from all samples in patient cohort 1 (n=6 healthy donor PBMC, n=5 tonsils from sleep apnea patients, and paired blood and tumor specimens from n=18 patients with HPV- disease and n=9 patients with HPV+ disease). b. Same FItSNE plot as (a) but showing clusters by sample type. c. Heatmap showing the frequencies of cells recovered from each cluster by sample types, where the frequencies of cells were normalized by the number of patients assessed in each group. Tonsil samples, HPV- and HPV+ TIL were enriched for specific clusters. Statistical assessment of observed versus expected cell frequencies are detailed in Supplementary Fig. 3. d-e. FItSNE plot (d) showing the clusters containing B cells from (a), and the gene sets associated with specific functions for each cluster (e). Canonical B cell lineages, including naïve, switched memory, plasma cells and germinal center B cells were recovered. Interestingly, cells from HPV+ patients had GC B cells, while these cells were largely absent from TIL of HPV- patients. HPV- patients had a higher frequency of naïve and memory B cells. f-g. FItSNE plot (f) showing the $CD4^+$ helper T cells from (a), and a dot plot highlighting the present of cells with a T follicular-helper signature (cluster 10). h. Progression free survival (PFS) analysis derived from stratification of HNSCC TCGA patients based on enrichment scores for B cell infiltration, GC B cells, and plasma cells. Gene sets used to calculate enrichment scores were derived from our scRNAseq analysis and applied to bulk mRNAseq data from the TCGA (Methods). Cox proportional hazard models using a log-rank test were used for PFS analysis. The shaded regions represent 95% confidence intervals for the survival curves. Survival curves are derived from 111 HNSCC patients from the TCGA.

### 3.3.2 Germinal center TIL-Bs and tertiary lymphoid structures are increased in HPV+ HNSCC

As transcriptional analysis revealed differential enrichment of TIL-Bs in $HPV^+$ and $HPV^-$ HNSCC, we developed a spectral cytometry panel (Methods) to validate our scRNAseq findings at the protein level and to determine if there were any additional alterations in TIL-B subpopulations in HNSCC. We first quantified frequencies of TIL-Bs and plasma cells in HNSCC primary tumors (Table 2, Cohort 2), which revealed a significant increase in $CD19^+CD20^+$ TIL-Bs compared to plasma cells in the TME (Appendix Figure 6a-b). Next, we utilized our spectral cytometry panel to perform unsupervised clustering of B cells on a subset of HNSCC patients (**Cohort 2**). In these patients, we identified seven distinct B cell clusters: naïve B cells ($CD38^-IgD^+CD27^-$), $IgG^+$ switched memory B cells ($IgG^+CD38^-IgD^-CD27^+$), $IgG^-$ switched memory B cells ($IgG^-CD38^-IgD^-CD27^+$), activated switched memory ($CD38^-IgD^-CD27+CD21^-$),GC B cells ($CD38^+IgD^-BCL6^+Sema4a^+$), tissue-like memory B cells ($CD38^-IgD^-IgG^+CD27^-CD21^-FcRL5^+$) and antibody secreting cells ($CD38^{hi}CD27^+Ki67^{+/-}$) (Figure 7**a**, Table 2, Cohort 2). Tonsil and HPV+ HNSCC tumors were enriched for naïve, switched memory, and GC B cell clusters while HPV- tumors were enriched for switched memory clusters **(**Figure 7**a).** Of note, overall TIL-B density is increased in $HPV^+$ TIL compared to $HPV^-$ TIL Figure 7**a).** $HPV^+$ and $HPV^-$ PBL were enriched for naïve and switched memory B cell clusters **(Appendix Figure 7).** Interestingly, we observed that the tissue-like memory B cells were only present in the HNSCC PBL (**Appendix Figure 7**). To quantify differences in TIL-B subsets identified in our unsupervised clustering, we used standard flow cytometry gating and pooled data from additional HNSCC patients within Cohort 2 that were stained with

a modified flow cytometry panel (Methods). GC TIL-B were significantly increased in $HPV^+$ HNSCC compared to $HPV^-$ HNSCC **(Figure 7a).** We did not observe a significant difference in plasma cell frequency between $HPV^+$ and $HPV^-$ HNSCC patients **(**Figure 7**a).** We also did not observe a significant difference in naïve, activated or antibody secreting B cells in $HPV^+$ and $HPV^-$ HNSCC **(**Figure **7b).** Of note, total class-switched memory B cells ($CD38^-IgD^-$) are significantly increased in both $HPV^+$ and $HPV^-$ HNSCC when compared to normal and inflamed tonsils **(Figure 7b).**

As our transcriptional analysis of $CD4^+$ T cells in HNSCC tumors revealed an increased $CD4^+$ $T_{FH}$ cell signature in $HPV^+$ HNSCC, we sought to interrogate the frequencies of $CD4^+$ $T_{conv}$ lineages (i.e. $T_{FH}$, $T_{H1}$, regulatory $T_{FH}$, and $T_{regs}$) present in HNSCC patients by flow cytometry. We observed a significant increase in $T_{FH}$ within $HPV^+$ HNSCC patients compared to $HPV^-$ patients **(Figure 7c),** but $T_{H1}$ cells were not significantly different. Regulatory $T_{FH}$ ($CXCR5^+$ $FOXP3^+$) were not significantly different between $HPV^+$ and $HPV^-$ tumors (**Figure 7c).** $T_{regs}$ were significantly increased in $HPV^-$ HNSCC patients compared to $HPV^+$ HNSCC and normal and inflamed tonsils, and $CD8^+$ T cell frequencies were comparable **(Figure 7c).**

Although frequencies of cells quantified by flow cytometry are informative, evaluating spatial localization of cells *in situ* within the TME is an orthogonal approach that contextualizes the TME in which immune cells are located. We utilized a separate cohort (Table 3, Cohort 3) with significant patient follow up for these locational studies. We first used single-plex immunohistochemistry (IHC) to evaluate the number and location of TIL-Bs within different areas of the oropharynx. We observed that B cells predominantly infiltrated TLS regardless of HPV status and that TLS formation was

dictated by HPV status regardless of tissue sites i.e. tonsil vs. tongue **(Figure 7d-f).** Next, we evaluated frequencies of TLS in the tumor versus outside the tumor in $HPV^-$ and $HPV^+$ HNSCC **(Figure 7g).** $HPV^+$ tumors had a higher frequency of TLS within and adjacent to the tumor and the HPV+ tumors had a significant correlation with the total tumor area whereas $HPV^-$ tumors did not **(Figure** 7**h).** Further, the number of $CD4^+$ T cells and TIL-Bs in TLS were strongly correlated **(Figure 7i).** Finally, we found a higher frequency of $CXCR5^+$ immune cells (consistent with a $T_{FH}$ $CD4^+$ $T_{conv}$ infiltrate) in $HPV^+$ TIL versus $HPV^-$ TIL **(Figure** 7**j),** confirming that TLS likely foster GC reactions in the TME. Taken together, these flow cytometric and spatial data confirm that GC B cells and $CD4^+$ $T_{FH}$ are present within TLS and are more frequently found in $HPV^+$ HNSCC patients.

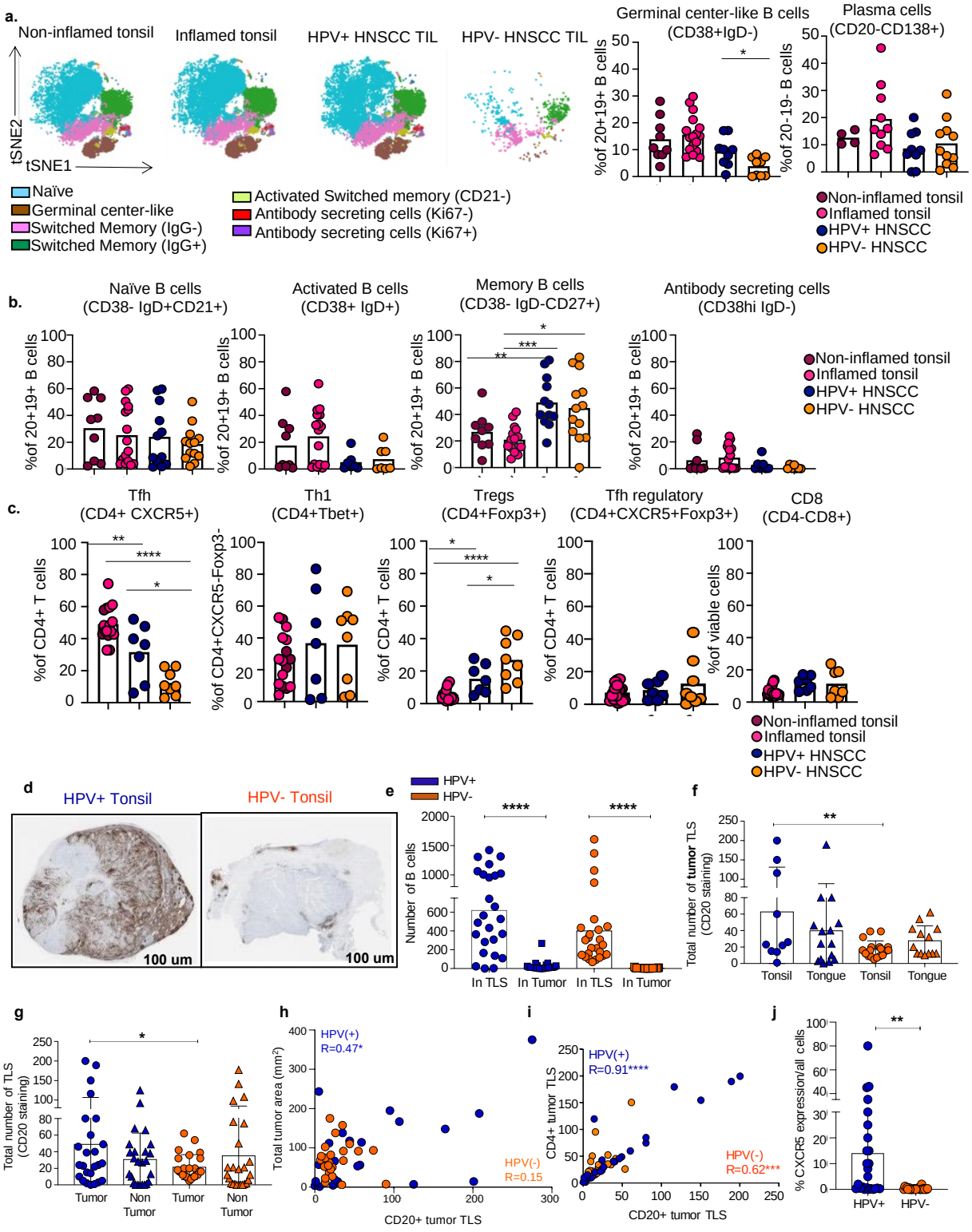
a.
Non-inflamed tonsil
Inflamed tonsil
HPV+ HNSCC TIL
HPV- HNSCC TIL
tSNE2
tSNE1
Naïve
Germinal center-like
Switched Memory (IgG-)
Switched Memory (IgG+)
Activated Switched memory (CD21-)
Antibody secreting cells (Ki67-)
Antibody secreting cells (Ki67+)
Germinal center-like B cells (CD38+IgD-)
%of 20+19+ B cells
Plasma cells (CD20-CD138+)
%of 20-19- B cells
Non-inflamed tonsil
Inflamed tonsil
HPV+ HNSCC
HPV- HNSCC
b.
Naïve B cells (CD38- IgD+CD21+)
Activated B cells (CD38+ IgD+)
Memory B cells (CD38- IgD-CD27+)
Antibody secreting cells (CD38hi IgD-)
%of 20+19+ B cells
c.
Tfh (CD4+ CXCR5+)
Th1 (CD4+Tbet+)
Tregs (CD4+Foxp3+)
Tfh regulatory (CD4+CXCR5+Foxp3+)
CD8 (CD4-CD8+)
%of CD4+ T cells
%of CD4+CXCR5-Foxp3-
%of viable cells
d
HPV+ Tonsil
HPV- Tonsil
100 um
e
HPV+
HPV-
Number of B cells
In TLS
In Tumor
f
Total number of tumor TLS (CD20 staining)
Tonsil
Tongue
g
Total number of TLS (CD20 staining)
Tumor
Non Tumor
h
Total tumor area (mm²)
HPV(+) R=0.47*
HPV(-) R=0.15
CD20+ tumor TLS
i
CD4+ tumor TLS
HPV(+) R=0.91****
HPV(-) R=0.62***
j
% CXCR5 expression/all cells

**Figure 7 : High dimensional flow cytometry and immunohistochemistry reveal distinct TIL-B phenotypes and increased tertiary lymphoid structures in HPV+ HNSCC.**

**a.** viSNE plots of B cells collected from non-inflamed and inflamed tonsils, HPV+ and HPV-HNSCC TIL and paired PBL (Supplementary Fig.7) were analyzed using Cytobank. Non-inflamed tonsil (n= 4), inflamed tonsil (n=6), HPV+ HNSCC (n=3), HPV- HNSCC (n=2). Bar plot displaying frequencies of GC B cells and plasma cells in non-inflamed tonsil (n=9), inflamed tonsil (n=16), HPV+ HNSCC (n=9), HPV- HNSCC (n=9). *P=0.02 Students 2-sided t test b. Bar plot for frequency of B cell subpopulations. Non-inflamed tonsil (n=9), inflamed tonsil (n=16), HPV+ HNSCC (n=12), HPV- HNSCC (n=13). **P=0.004, ***P=0.0009, *P= 0.03, One way ANOVA followed by Tukeys multiple comparisons test. c. Frequencies of T follicular helper (Tfh), regulatory T follicular helper (Tfhreg), regulatory T cell (Treg), T helper type 1 (Th1) and CD8 T cells in non-inflamed tonsil (n=6), inflamed tonsils (n=10), HPV+ TIL (n=7), HPV- TIL (n=8). *P=0.01,**P=0.009,****P<0.0001. *P=0.04, *P=0.03, ****P<0.0001. One way ANOVA followed by Tukeys multiple comparisons test. d. Representative CD20+ IHC on HPV+ and HPV- HNSCC tumors (4x magnification). e. B cell infiltrate counted within tumor bed compared to TLS. Total numbers from n=50, 25 HPV+, 25 HPV- were graphed. ****P< 0.0001, Student's 2-sided t test. f. Tumor TLS by site within the oropharynx (tonsil vs. tongue). Total numbers from n=50, 25 HPV+, 25 HPV - were graphed. **P= 0.0096, Student's 2-sided. Data are presented as mean values +/- SEM. g. Total number of tumor TLS and non-tumor TLS numbers in HPV+ and HPV- disease. Total numbers from n=50, 25 HPV+, 25 HPV- were graphed. *P=0.0249, Student's 2-sided t test. Data are presented as mean values +/- SEM. h. Correlation of $CD20^+$ tumor TLS with tumor area. Total tumor area ($mm^2$) for each patient tumor was calculated by a pathologist. *P< 0.05, non-parametric Spearman correlation. i. Total tumor TLS independently counted for $CD20^+$ and $CD4^+$ (n=50, 25 HPV+, 25 HPV-). ****P< 0.0001, ***P< 0.001, non-parametric Spearman correlation. j. Total CXCR5 was scored for all cell types (n=50, 25 HPV+, 25 HPV-).**P=0.0012, Student's 2 sided t test.

### 3.3.3 SEMA4A expression is associated with GC B cell differentiation and TLS with GC in HNSCC

To better understand differences between TIL-B in $HPV^+$ versus $HPV^-$ HNSCC, we next utilized our scRNAseq data to interrogate expression of ligands and receptors in the TME (Cohort 1). We found several ligands in the TME associated with each type of HNSCC **(Figure** 8**a)** and visualized the top 10 in each type of HNSCC **(Figure** 8**b-c).** Interestingly, we found that *SEMA4A* was enriched in HPV+ HNSCC and was largely restricted to GC B cell clusters (i.e. clusters 17 and 18, relative to other clusters). We performed a similar analysis with receptors, and found several receptors associated with GC B cells in $HPV^+$ TIL (e.g. *CD40* and *CXCR4*), and others associated with plasma cells in $HPV^-$ TIL (e.g. *CD63* and *LY96*) (**Figure** 8**d-f).**

We next used pseudotemporal modeling to better elucidate the dynamics of gene expression as cells progress from naïve B cells to GC B cells. These analyses are important not only to trace differentiation to GC B cells, but also organization of B cells into TLS, as naïve B cells must be pulled into a GC reaction to create a functional GC. Pseudotemporal modeling can be used to reconstruct differentiation trajectories from scRNAseq data based on smooth changes in gene expression that take place across cells as they transition from one state to the next. We found a trajectory from naïve to GC B cells (Figure 8**g),** which allowed us to infer a pseudotime ordering of B cells during differentiation from naïve to GC B cells. Interestingly, this analysis revealed that *SEMA4A* is associated with transition from naïve to GC B cells and shares similar dynamics of expression with *CD38* **(**Figure 8**h).** We also tracked the dynamics of genes associated with CD38 in order to infer putative protein-protein interactions using Cytoscape

(Methods) that may be taking place as B cells differentiate from naïve to GC B cells **(**Figure 8**h).** This analysis revealed extensive interactions, including interactions with *BCL6*, the master transcriptional regulator associated with GC B cells **(Figure** 8**i).** Functional enrichment revealed a variety of pathways associated with this interaction network, including Epstein-Barr infection as a top hit as well as several pathways associated with metabolic changes that occurring during progression to GC G cells (Supplementary Data 3). Taken together, this analysis revealed that *SEMA4A* expression is enriched in GC TIL-Bs, and the temporal expression of *SEMA4A* is associated with differentiation into GC TIL-Bs.

We next sought to interrogate whether SEMA4A has a similar expression pattern at the protein level on TIL-B (Cohort 2). Indeed, SEMA4A was co-expressed with CD38 as in the transcriptomic data (Figure **9a).** Additionally, SEMA4A was co-expressed with BCL6, a key transcription factor that regulates germinal centers in SLOs **(**Figure **9a and 10c).** We also found that SEMA4A mean fluorescence intensity (MFI) and frequency was significantly increased on GC TIL-Bs compared to GC and activated B cells in healthy donor tonsil via our high dimensional flow cytometry **(Figure** 9**a-b)**. In addition, SEMA4A MFI and frequency was significantly increased on GC TIL-Bs compared to memory or naïve TIL-Bs in HNSCC tumors **(Figure 9b).** Lastly, we observed an increase in costimulatory molecules such as CD40 and CD86 on activated TIL-Bs compared to naïve TIL-Bs in HNSCC tumors (**Figure 9a and Appendix Figure 7c)**, which we expect to be upregulated on B cell populations like GC and activated B cells for optimal antigen presentation. Pseudotemporal ordering in our scRNAseq data suggested that *SEMA4A* expression is increased during differentiation towards GC, meaning *SEMA4A* may play a

role in the progression of activated B cells. To interrogate this, we assessed whether there was a correlation between SEMA4A$^{+}$ activated B cells and SEMA4A$^{+}$ GC B cells and found a significant positive correlation between the two groups in healthy and inflamed tonsil. There was a trend towards a positive correlation between SEMA4A$^{+}$ activated TIL-B cells and SEMA4A$^{+}$GC TIL-Bs that did not reach statistical significance **(Figure 9d).** Overall, these data suggest that SEMA4A may play a role in development and maturation of B cells into GC B cells.

B cells entering the GC reaction begin in the dark zone (DZ) where they undergo expansion and somatic hypermutation[139,155]. Centroblasts then follow a CXCL13 gradient to enter the light zone (LZ), where they capture antigen presented on follicular dendritic cells (FDCs) which they present to CD4$^{+}$ $T_{FH}$ cells in order to undergo selection[139]. Since we observed significantly less GC TIL-Bs in HPV$^{-}$ HNSCC tumors, we sought to determine if there were any additional aberrations in SEMA4A expression on GC TIL-B cell subsets in HNSCC tumors. Specifically, we assessed expression on DZ or LZ GC TIL-Bs. SEMA4A was significantly expressed on LZ GC TIL-B cells in HNSCC tumors **(Figure 9e).** Further, SEMA4A$^{+}$ LZ GC TIL-Bs positively correlate with the frequency of total LZ GC TIL-Bs **(Figure 9f).** This suggest SEMA4A could be important in both the development of GC B cells and the interactions between LZ GC B cells and TFH cells in normal and tumor tissues. Using IHC, we confirmed the presence of SEMA4A and co-expression of the canonical GC transcription factor BCL6 with SEMA4A in tonsils. Interestingly, while SEMA4A is on B cells and myeloid cells in healthy donor (HD) tonsils and HPV$^{+}$ tumors, it is more restricted to macrophages (pink arrow) in HPV$^{-}$ tumors. To compliment the single plex IHC studies, we also performed 3 color confocal microscopy

to interrogate co-localization of Sema4a and Bcl6 within TLS in $HPV^+$ and $HPV^-$ HNSCC tumors **(Figure 9h).** Within HD tonsil GC and non-tumor GC (GC within tumor-adjacent normal oropharyngeal tissue), SEMA4A and BCL6 co-localize as expected **(Figure 9h).** Co-localization of these two markers and BCL6 expression in general is increased within TLS in HPV+ patients compared to TLS in HPV- patients (**Figure 9h**). Taken together, these data demonstrate that SEMA4A is associated with both activated and GC B cells in tonsil and the TME of patients with HNSCC, ultimately marking TLS with GC in $HPV^+$ patients due to its strong correlation with BCL6 expression. While SEMA4A may govern formation of GCs within TLS in HNSCC patients, further interrogation of this pathway is necessary to understand its role in TLS formation and maturity in the TME.

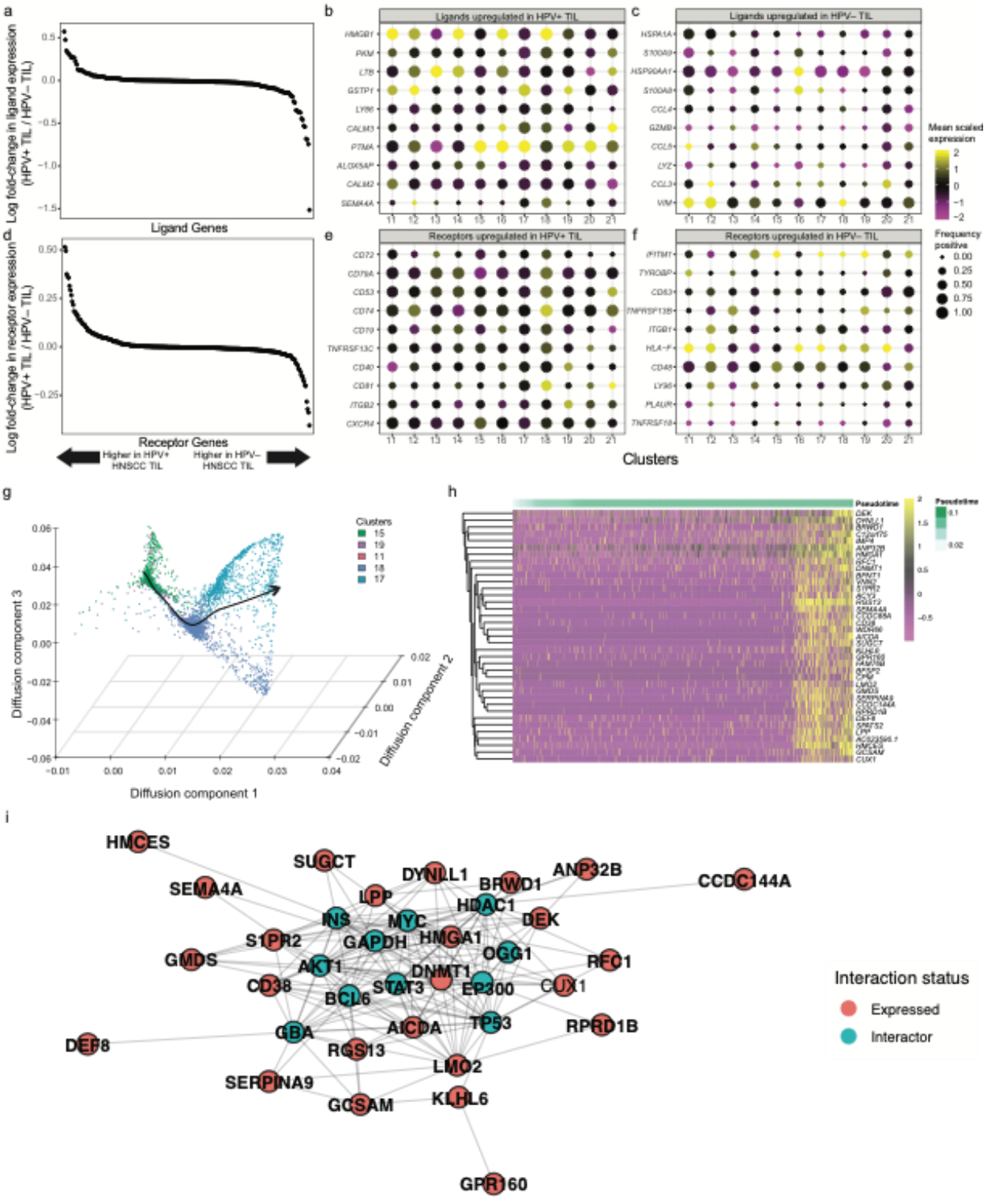
a
Log fold-change in ligand expression (HPV+ TIL / HPV− TIL)
Ligand Genes
b
Ligands upregulated in HPV+ TIL
HMGB1
PKM
LTB
GSTP1
LY86
CALM3
PTMA
ALOX5AP
CALM2
SEMA4A
c
Ligands upregulated in HPV− TIL
HSPA1A
S100A9
HSP90AA1
S100A8
CCL4
GZMB
CCL5
LYZ
CCL3
VIM
Mean scaled expression
d
Log fold-change in receptor expression (HPV+ TIL / HPV− TIL)
Receptor Genes
Higher in HPV+ HNSCC TIL
Higher in HPV− HNSCC TIL
e
Receptors upregulated in HPV+ TIL
CD72
CD79A
CD53
CD74
CD79
TNFRSF13C
CD40
CD81
ITGB2
CXCR4
f
Receptors upregulated in HPV− TIL
PTPRT
TYROBP
CD63
TNFRSF13B
ITGB1
HLA-F
CD48
LY96
PLAUR
TNFRSF1B
Frequency positive
Clusters
g
Clusters
15
19
11
18
17
Diffusion component 3
Diffusion component 1
Diffusion component 2
h
Pseudotime
i
HMCES
SUGCT
DYNLL1
ANP32B
BRWD1
CCDC144A
SEMA4A
LPP
HDAC1
INS
MYC
DEK
S1PR2
GAPDH
HMGA1
GMDS
OGG1
RFC1
AKT1
DNMT1
CD38
STAT3
EP300
CUX1
BCL6
TP53
RPRD1B
AICDA
GBA
DEF8
RGS13
LMO2
SERPINA9
GCSAM
KLHL6
GPR160
Interaction status
Expressed
Interactor

**Figure 8: Differentially expressed ligands and receptors in HNSCC and modeling of GC differentiation identify SEMA4A as associated with development and maturation of GC.**

a. Differential expression of ligands by B cells in the TME of HPV– and HPV+ HNSCC. Number of patient samples is the same as Fig. 1. b. Number of cells expressing ligands and magnitude of expression in HPV+ TIL-B by cluster. Consistent with GC B cell and formation of TLS, *LTB* was one of the top expressed ligands across HPV+ TIL-B. *SEMA4A* expression was largely restricted to clusters 17 and 18, which are GC TIL-B. c. Expression of top ligands by HPV- TIL-B included several chemokines (*CCL4* and *CCL5*). d. Differential expression of receptors by B cells in the TME of HPV– and HPV+ HNSCC. e. Top receptors expressed by HPV+ TIL-B including genes associated with GC function including *CD40* and *CXCR4*. f. Top receptors in HPV– B cells included CD63, which is associated with downregulation of CXCR4 and is suppressed by Bcl6. g. Diffusion map embedding of B cell associated with a lineage spanning naïve and GC B cells identified by slingshot (Methods). B cells are shown by their clusters identified in Fig. 1, and the line connecting the clusters denotes the differentiation trajectory with increasing pseudotime. h. Heatmap showing the top genes that are temporally associated with CD38 expression dynamics during progression from naïve B cells to GC B cells. *SEMA4A* follows the same expression dynamics as *CD38*. A total of 1000 cells were randomly sampled from the entire naïve cell to GC B cell dataset for visualization in the heatmap. i. Inferred protein-protein interactions from Cytoscape for the top genes that share temporal dynamics with CD38. Nodes represent genes, and edges in the network represent putative protein-protein interactions. BCL6, p53, AKT, and MYC were all inferred to be interacting with proteins encoded by genes that follow the expression dynamics of CD38. All analysis in this figure is derived from all patients in our scRNAseq cohort.

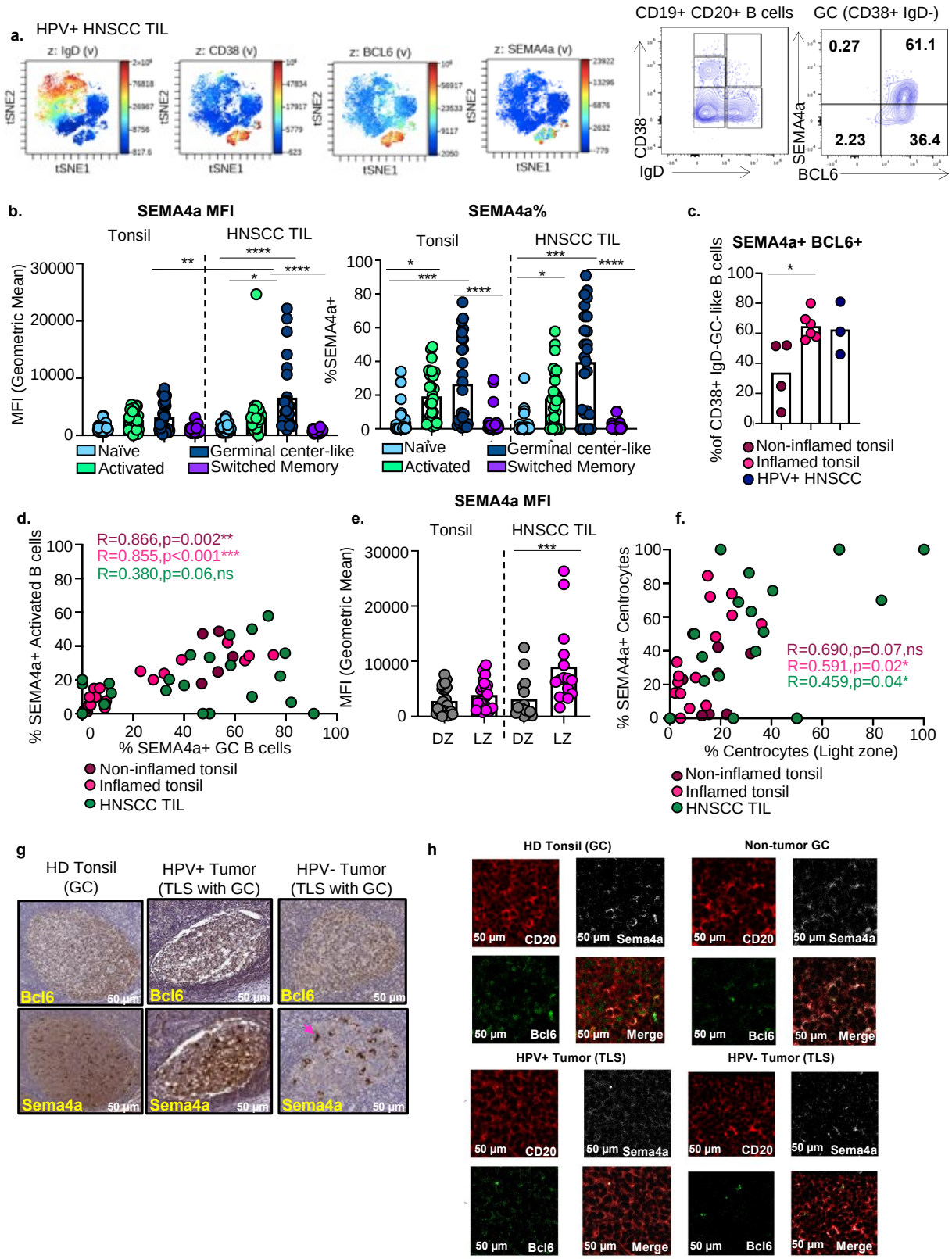
a.
HPV+ HNSCC TIL
z: IgD (v)
z: CD38 (v)
z: BCL6 (v)
z: SEMA4a (v)
tSNE1
tSNE2
CD19+ CD20+ B cells
GC (CD38+ IgD-)
CD38
IgD
SEMA4a
BCL6
0.27
61.1
2.23
36.4
b.
SEMA4a MFI
Tonsil
HNSCC TIL
MFI (Geometric Mean)
Naïve
Activated
Germinal center-like
Switched Memory
SEMA4a%
%SEMA4a+
c.
SEMA4a+ BCL6+
%of CD38+ IgD-GC- like B cells
Non-inflamed tonsil
Inflamed tonsil
HPV+ HNSCC
d.
R=0.866,p=0.002**
R=0.855,p<0.001***
R=0.380,p=0.06,ns
% SEMA4a+ Activated B cells
% SEMA4a+ GC B cells
Non-inflamed tonsil
Inflamed tonsil
HNSCC TIL
e.
SEMA4a MFI
Tonsil
HNSCC TIL
MFI (Geometric Mean)
DZ
LZ
f.
% SEMA4a+ Centrocytes
% Centrocytes (Light zone)
R=0.690,p=0.07,ns
R=0.591,p=0.02*
R=0.459,p=0.04*
Non-inflamed tonsil
Inflamed tonsil
HNSCC TIL
g
HD Tonsil (GC)
HPV+ Tumor (TLS with GC)
HPV- Tumor (TLS with GC)
Bcl6
Sema4a
50 µm
h
HD Tonsil (GC)
Non-tumor GC
HPV+ Tumor (TLS)
HPV- Tumor (TLS)
CD20
Sema4a
Bcl6
Merge
50 µm

**Figure 9: Sema4a expression is increased in GC TIL-Bs in TLS in HNSCC**

a. Individual viSNE feature plots demonstrating expression level of canonical markers used to identify B cell subpopulations in Fig. 2a. Number of samples is the same as Fig. 1. Representative flow plot showing traditional flow gating strategy for B cell subsets quantified in Fig. 2a-b and Sema4a co-expression with BCL6. CD19+CD20+ B cells were gated on CD38 and IgD. CD38+ IgD- (GC B cells) were than gated on Sema4a and BCL6 b. Bar plot showing geometric mean fluorescence intensity (gMFI) of SEMA4A on B cell subsets. Statistical analysis by ordinary one-way ANOVA followed by Tukeys multiple comparisons test. *P=0.02 **P= 0.0013, ***P=0.0007, ***P=0.0004, ****P<0.0001 Bar plot showing frequencies of SEMA4A positivity on B cell subsets. c. Bar plot comparing the frequency of $Sema4a^{+}$ $BCL6^{+}$ GC B cells. Statistical analysis by ordinary one-way ANOVA followed by Tukeys multiple comparisons *P=0.02. d. Scatter plot comparing the frequency of Sema4a+ GC-B cells to $Sema4a^{+}$ activated B cells. Statistical analysis by Spearman correlation. **P=0.002 ***P<0.001 ns; not significant e. Bar plot showing MFI of Sema4a on dark zone (DZ) and light zone (LZ) GC B cells. Statistical analysis by Students two-sided -T test (Mann Whitney) **P=0.001. f. Scatter plot comparing the frequency of $Sema4a^{+}$ light zone GC-B cells to total light zone GC B cells. Statistical analysis by Spearman correlation. *P=0.02, *P=0.04, ns; not significant g. Representative IHC for BCL6 and SEMA4A in HNSCC patients. BCL6 and Sema4a expression was compared in HPV+ and HPV- HNSCC patients to HD tonsil. Pink arrow is pathological characterization of macrophage. h. Confocal imaging of TLS in HPV+ and HPV- tumors compared to GC in HD tonsil. CD20, SEMA4A and BCL6 were co-localized to visualize co-expression of SEMA4A and BCL6 which mark GC in HD tonsil. Scale bar is 50 µm for all images.

### 3.3.4 Dissection of germinal center B cell reactions reveals distinct waves of gene expression

Since a better understanding of GC reactions has implications for antitumor immunity and effective humoral immunity in infection and vaccination, we performed an in-depth transcriptional dissection of GC reactions. To achieve this, we first bioinformatically isolated GC B cells and re-clustered them to reveal more subtle differences within the canonical GC populations **(**Figure 10**a).** This analysis revealed 6 clusters with distinct gene expression patterns **(**Figure 10**a).** Typical pseudotime algorithms assume a linear differentiation trajectory, but with GC B cells we expect a cyclical process as B cells toggle between LZ and DZ interactions for optimal B cell maturation. Thus, we developed a computational approach (see Methods) to capture the cyclical nature of this process. First, we embedded cells in a diffusion space, yielding a cyclical topology (Figure 10**b and Methods).** We then connected each cluster via their centroids and fit a principal curve to infer a pseudotime score for each cell in the GC Figure 10**c).** We then evaluated genes associated with GC progression, and identified not only DZ and LZ reactions, but also a transitional state for TIL-Bs within our cyclical GC model **(**Figure 10**d).** When viewed as a function of pseudotime, we found 3 distinct waves of expression associated with each of these GC states within the cyclical process (Figure 10**e).** The first phase consisted of expression of canonical LZ genes such as *CD22* and *HLA-DRB1*, followed by a wave of transitional genes consisting of *CXCR4* and *TCL1A*, followed by a final wave of cell cycle genes which are consistent with the proliferative nature of DZ B cells. Importantly the code utilized for this computational approach is publicly available in an R package called “circletime”[282].

Using the top differentially expressed genes of each GC cell state (DZ, LZ and transitional [TZ]) we sought to validate these GC cell states in normal SLO tissue and HNSCC via flow cytometry. The key genes that were upregulated on DZ were CXCR4, CD27, CD72, CCR1. We identified upregulation of CD40, CD37, CD7, and CD180 on LZ as well as CD83, ICAM1, CCR6 and CD18 on TZ. Using the classical gating strategy for human GC B cells ($CD38^+$ $IgD^-$ $BCL6^+$), we first assessed CXCR4 and CD86 expression as these canonically define DZ and LZ GC B cells **(**Figure 10**f).** We observed DZ GC B cells ($CXCR4^+$ $CD86^-$), TZ, ($CXCR4^+$ $CD86^-$) and LZ ($CXCR4^-$ $CD86^+$) in $HPV^+$ HNSCC and normal and inflamed tonsils **(**Figure 10**f,** Appendix Figure 8**).** While we observed protein expression of CD37, CD7, CD72, CCR6, CD18 and CD180 on GC B cells in tonsils and $HPV^+$ HNSCC, we observed no significant difference in expression of these markers between the three distinct GC cell states **(Appendix Figure 7).** GC B cells in the DZ undergo rapid proliferation, thus we next looked at Ki67 expression in each GC B cell population. Surprisingly, we observed significantly higher Ki67 expression in the TZ GC B cells compared to DZ or LZ in both tonsils and $HPV^+$ HNSCC **(**Figure 10**h-i).** These data suggest that TZ GC B cells may be the population undergoing proliferation in GCs in human tonsils and $HPV^+$ HNSCC tumors. CD83 is also used to distinguish DZ and LZ in human and mice with expression being predominantly on LZ GC B cells[145,292]. Recently, a cell state for GC B cells termed “gray zone (GZ)” that co-expresses CXCR4 and CD83 was identified using RNA-sequencing and flow cytometry in mice[292]. When we assessed CD83 expression on DZ, TZ, LZ and found significantly higher expression on TZ compared to DZ in tonsils **(**Figure 10**g-h).** Given the expression of CXCR4, Ki67 and CD83 on TZ in human tonsils and $HPV^+$ HNSCC, future studies should assess whether

TZ GC B cells in humans are analogous to GZ GC B cells in mice. CD27 expression was previously shown to be higher on DZ GC B cells in human tonsil[145]. Indeed, we observed significantly higher CD27 expression on DZ compared to LZ in tonsils and observed a similar trend in HPV$^+$ HNSCC but it was not significant **(**Figure 10**h).**

Next, we compared ICAM1 and CD40, as these may be important for $T_{FH}$ interactions in the LZ. We observed significantly higher expression of ICAM1 and CD40 on LZ compared to DZ in both tonsils and HPV$^+$ HNSCC tumors, however, ICAM1 was not significantly different between LZ and TZ **(Figure 10g-h).** CD40 expression was significantly higher on the LZ compared to the TZ in tonsils but not in HPV$^+$ HNSCC (**Fig. Figure 10g-h)**. Our initial assessment of SEMA4A expression revealed that LZ GC B cells expressed significantly higher SEMA4A expression compared to DZ in HNSCC tumors **(Figure 10e).** Interestingly, we found increased SEMA4A expression on TZ GC B cells compared to DZ in tonsils but not significantly different between TZ and LZ **(Figure 10g-h).** We found a similar trend in HPV$^+$ HNSCC, although it did not reach statistical significance **(Figure 10g-h).** A complete understanding of the transitional state of GC B cells in humans will contribute to identification of the signals that lead to egress from GC reactions, additional factors that contribute to the cycling between TZ, DZ and LZ, and additional cues that are necessary for a bonified GC reaction in the TME. Cues that are known to be important for GC formation and polarization include expression of BCL6, FOXO1 and S1PR1[150]. The TZ GC B cell subset in humans is likely akin to the “gray” zone (GZ) GC B cell in mice given similar protein expression profiles[292]. Therefore, transition from LZ, TZ and DZ in humans may be governed by similar genes.

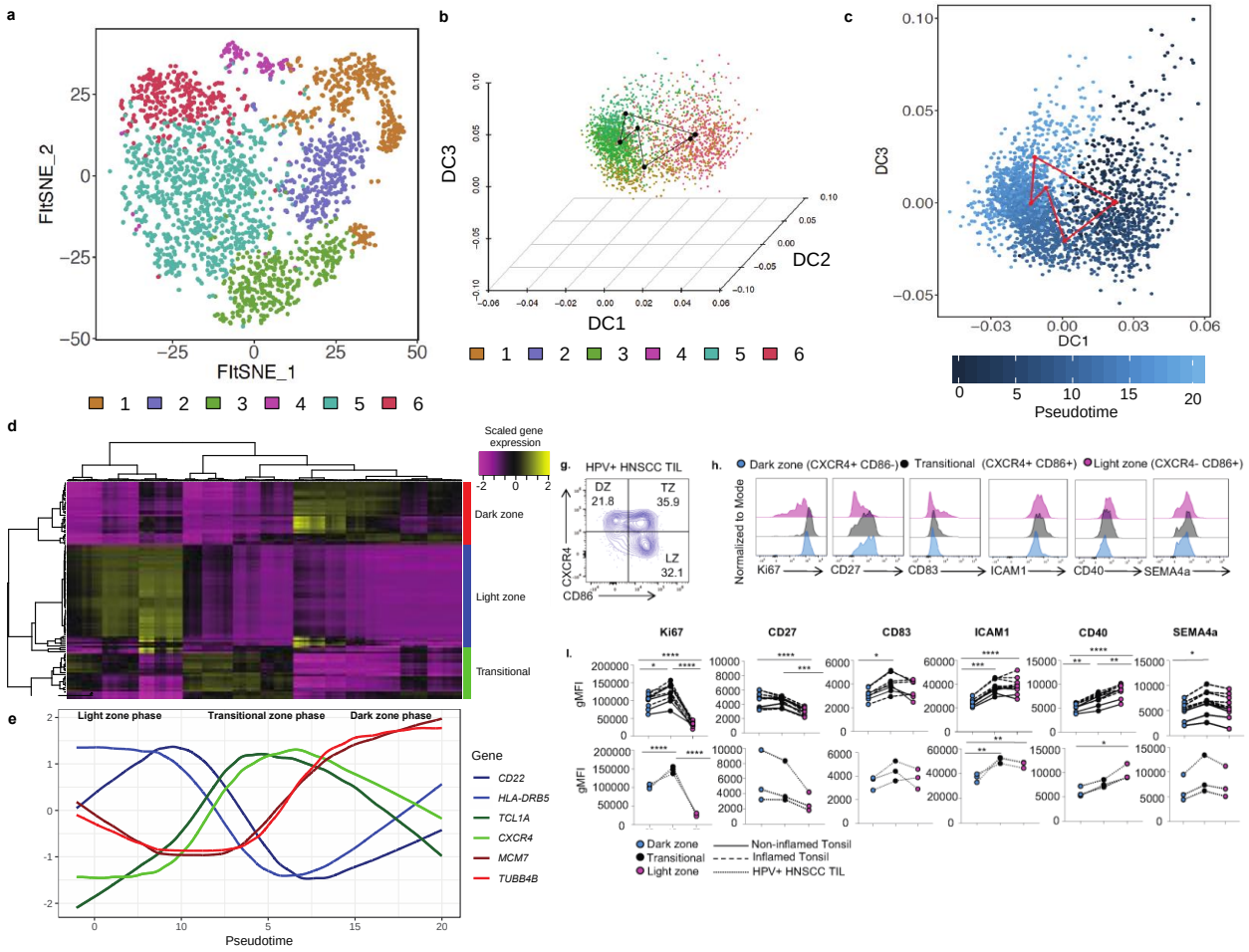


**Figure 10: Cyclical pseudotime modeling of germinal center B cell reactions reveals waves of gene expression.**

a. FItSNE showing 6 clusters of germinal center B cells (i.e. cells from clusters 17 and 18 from Fig. 1A/D). b. Three-dimensional diffusion map embedding of germinal center B cells, with cells colored by their cluster identities from (a). Black dots represent the centroid of each cluster, and the lines connecting the black dots represent the circular path through germinal center reactions. c. DCs 1 and 3 captured most the information required to reconstruct the circular trajectory of germinal center B cells (left panel). Pseudotemporal ordering was inferred by fitting the equivalent of a nonparametric principal component from the center of the trajectory using the assumption that the data is on a closed curve (right panel). d. Loess regression was used to fit curves for the

top 20 differentially expressed genes across GC B cell clusters as a function of pseudotime inferred in (c). Genes were found to cluster into 3 distinct groups by fit with pseudotime. Clusters were defined as dark zone, light zone and transitional. Analysis in a-d is derived from 6 healthy blood donors, 5 tonsils, and 27 HNSCC patients. e. Marker genes derived from (d), with scaled gene expression plotted as a function of time. Blue genes correspond to light zone (LZ) GC B cells, green genes correspond to B cells moving between LZ and dark zone (DZ) GC B cells, and red genes correspond to DZ GC B cells. f. Representative flow plot showing gating strategy for LZ, DZ and TZ populations. CD38+ $IgD^-$ $BCL6^+$ (GC B cells) were then gated on CXCR4 and CD86. Dark zone (DZ) $CXCR4^+$ $CD86^-$, "Transitional" (TZ) ($CXCR4^+CD86^+$) and Light zone (LZ) ($CXCR4^-CD86^+$) were identified. g. Representative plots comparing expression of the three distinct GC TIL-B populations, DZ (blue- filled histogram), TZ (black-filled histogram) LZ (pink-filled histogram) h. Scatter plots quantifying differences in geometric mean fluorescence intensity of indicated key markers on the three distinct GC B cell populations in tonsils and HPV+ HNSCC. Statistical analysis by ordinary one-way ANOVA followed by Tukeys multiple comparisons test. *P=0.02, **P=0.002, ***P=0.0002, ****P=<0.0001.

### 3.3.5 Tertiary lymphoid structures are associated with better survival in HNSCC

To complement the transcriptional analysis of GC reactions in HNSCC tumors, we evaluated the number of TLS with GC in HNSCC tumors, as GCs are paramount for maximal B cell immunity[139]. In counting TLS with GCs outside the tumor, we found elevated TLS with GC in $HPV^+$ and $HPV^-$ tumors **(Figure 11a-b, Table 3, Cohort 3).** However, these TLS with GCs were increased intratumorally and peritumorally in $HPV^+$ patients **(Figure 11c).** Of note, an intratumoral increase in TLS with GCs in $HPV^+$ HNSCC supports previous studies in other virally induced human tumors[293]. Furthermore, TLS

with GC in the tumor correlated with increased survival in both $HPV^+$ and $HPV^-$ disease **(Figure** 11**d),** but more discretely in $HPV^+$ disease. We also performed multivariate survival analysis including TLS with GC, HPV status, and disease burden (as measured by the number of positive nodes;

Appendix Figure 9**).** In addition, we revealed that $HPV^+$ HNSCC patients with increased disease burden (i.e. primary and secondary disease) had significantly less tumor TLS in their primary disease compared to those individuals with primary disease alone **(Figure 11e).** This suggests that tumor TLS could potentially be important for reducing tumor recurrence at the same site of the primary tumor (secondary disease). We also found that former and current smokers with the $HPV^+$ cohort of patients had increased TLS compared to never smokers **(Figure 11f)**. This indicates the importance of other environmental cues in TLS formation in cancer. Finally, we analyzed the key cell-cell neighborhoods associated with TLS with GC vs. TLS without GC in HNSCC **(Figure 11g).** In TLS with GC, TIL-Bs interact with other TIL-Bs and $CD4^+$ $T_{conv}$ TIL, which is in line with the working definition of an active GC. Interestingly, an evaluation of TLS without GC in HNSCC revealed that TIL-Bs were not frequently in the same neighborhood with $CD4^+$ $T_{conv}$, and instead $CD8^+$ TIL and $T_{regs}$ were implicated as a dominant interaction. These results demonstrate that in TLS with GC, the spatial patterning becomes distinct from well-infiltrated tumors where immune cells are found in aggregates.

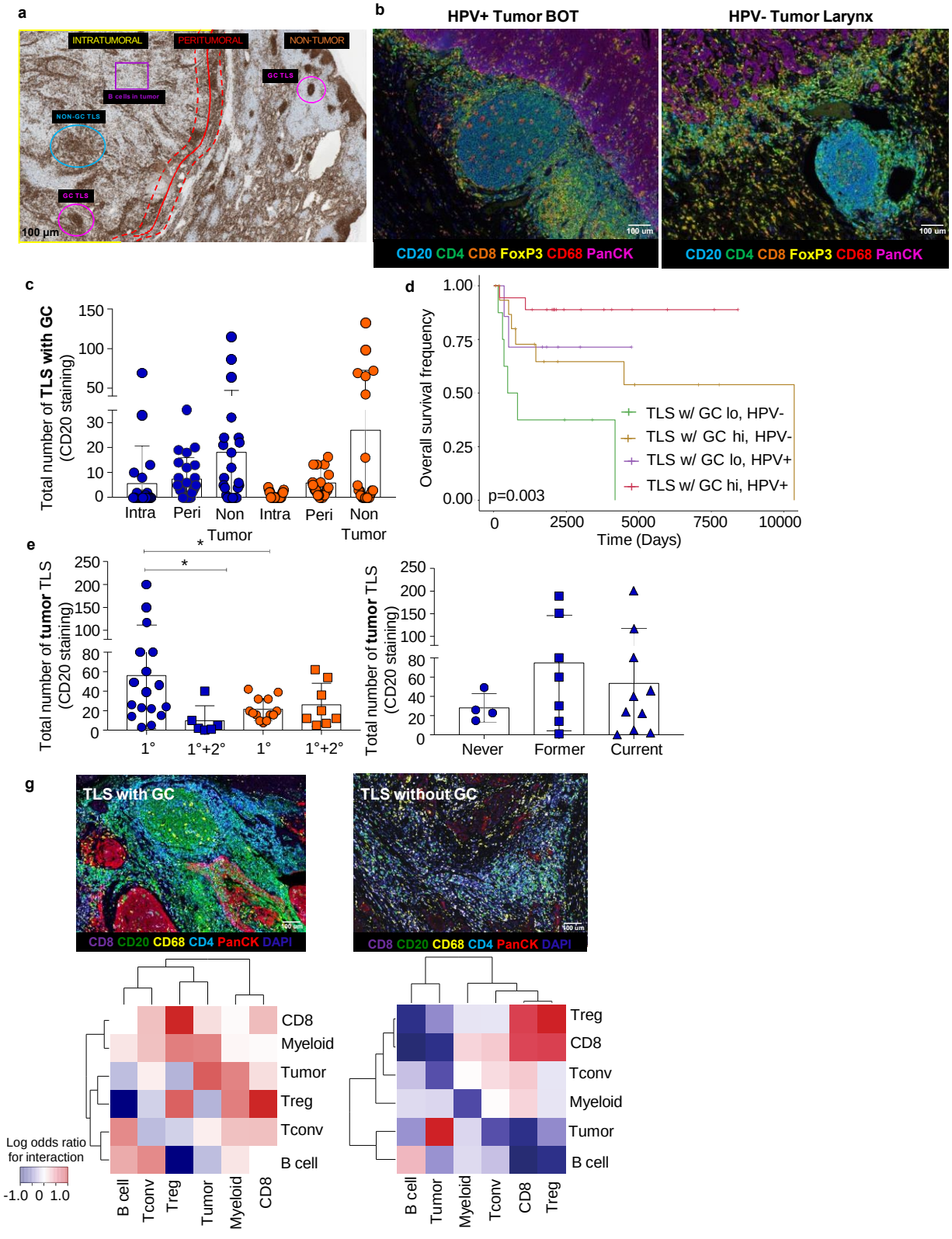
a
INTRATUMORAL
PERITUMORAL
NON-TUMOR
GC TLS
B cells in tumor
NON-GC TLS
GC TLS
100 µm
b
HPV+ Tumor BOT
HPV- Tumor Larynx
CD20 CD4 CD8 FoxP3 CD68 PanCK
CD20 CD4 CD8 FoxP3 CD68 PanCK
c
Total number of TLS with GC (CD20 staining)
Intra
Peri
Non Tumor
Intra
Peri
Non Tumor
d
Overall survival frequency
TLS w/ GC lo, HPV-
TLS w/ GC hi, HPV-
TLS w/ GC lo, HPV+
TLS w/ GC hi, HPV+
p=0.003
Time (Days)
e
Total number of tumor TLS (CD20 staining)
1°
1°+2°
1°
1°+2°
Total number of tumor TLS (CD20 staining)
Never
Former
Current
g
TLS with GC
CD8 CD20 CD68 CD4 PanCK DAPI
TLS without GC
CD8 CD20 CD68 CD4 PanCK DAPI
Log odds ratio for interaction
-1.0 0 1.0
CD8
Myeloid
Tumor
Treg
Tconv
B cell
B cell
Tconv
Treg
Tumor
Myeloid
CD8
Treg
CD8
Tconv
Myeloid
Tumor
B cell
B cell
Tumor
Myeloid
Tconv
CD8
Treg

**Figure 11: Increased TLS with GC within HPV+ HNSCC patients correlate with increased patient survival.**

a. Annotated tumor section stained for CD20 via single-plex IHC from a HNSCC patient (20x magnification). Annotations for tumor (intratumoral and peritumoral) and non-tumor areas are indicated. Blue circle =TLS without GC, Pink circle = TLS with GC, Purple square = TIL-B infiltrate within tumor bed b. Representative Vectra staining for TLS with GC within HPV+ and HPV- HNSCC tumors. BOT = base of tongue. c. TLS with GC are increased intratumorally (intra) and peritumorally (peri) in HPV+ HNSCC patients. Differences in intra vs. peri TLS with GC trended toward an increase in HPV+ HNSCC patients. Data are presented as mean values +/- SEM. d. TLS with GC in the tumors of HPV+ and HPV- HNSCC patients correlate with increased patient survival. Cox proportional hazard was used to evaluate overall survival based on high versus low frequencies of TLS with GC and HPV status ($p=0.003$, log rank test). The hazard ratio for high versus low TLS with GC was 0.32, and the hazard ratio for HPV+ versus HPV- was 0.27. e. Total number of tumor TLS are increased in HPV+ patients that do not progress to secondary disease. Total tumor TLS (via $CD20^+$ staining) were compared by primary disease (1°) vs. primary and secondary disease (1°+2°). n=50, 25 HPV+, 25 HPV-.*P=0.0336 and 0.0281, Student's 2 sided t test. Data are presented as mean values +/- SEM. f. Total number of tumor TLS are increased in former and current smokers that are also HPV+. Total tumor TLS (via $CD20^+$ staining) were compared in HPV+ patients that were never smokers vs. former or current smokers. Data are presented as mean values +/- SEM. g. Cell-cell neighborhoods in TLS with GC are distinct compared to TLS without GC (Methods). Top panels show a TLS with GC (left) and a TLS without GC (right). Bottom panels show the odds ratio of proximity to other cell types (Methods), with red representing a high probability of interaction with a given cell type and blue a low probability of interaction.

## 3.4 Discussion

In this study, we sought to perform an in-depth analysis of B cells in the TME of patients with HNSCC, with the goal of improving our understanding of the immunobiology of B cells and the potential role they have in generating baseline antitumor immune responses. Our study integrated new technical approaches across three cohorts of patient samples (n=124) and suggests that not only higher numbers of TIL-Bs, but also the specific phenotype and localization of TIL-Bs in the TME contribute to overall survival. Interestingly, we have implicated SEMA4A$^{+}$ GC TIL-Bs and TLS with GC as increased in HPV$^{+}$ HNSCC patients compared to HPV$^{-}$. Further, we also identified CD4$^{+}$ $T_{FH}$ in the TME of HNSCC, which complements findings in breast and colorectal cancer[294–296]. The correlation we observed between LZ B Cells and $T_{FH}$ in the TME extends this finding further, demonstrating the importance of crosstalk between CD4$^{+}$ T cells and GC TIL-Bs and the need for CD4$^{+}$ T cell help for GC TIL-B survival in the TME of HNSCC. Our single-cell transcriptional characterization of TIL-B populations uncovered numerous states of B cells in the TME and revealed distinct differences between HPV$^{+}$ and HPV$^{-}$ HNSCC. These differences should be considered in the development of a B cell-focused immunotherapy for HNSCC.

B cells are a heterogenous population with phenotypically and functionally distinct subsets. Thus, characterization of TIL-B phenotypes in treatment naïve patients is a critical first step in the development of B cell-focused immunotherapies. However, B cell targeted therapies may need to enhance certain subsets of B cells while inhibiting others, necessitating more dissection of the change in TIL-B phenotypes following therapy. For example, in melanoma, patients who did not respond to standard of care immunotherapy

i.e. anti-PD1 and/or anti-CTLA4 had significantly more naïve B cells than responders[122]. In this context, our findings suggest that driving naïve TIL-Bs towards activated and GC phenotypes could be one way to complement current immunotherapeutic strategies.

Functional assessment of TIL-B subpopulations is also needed to better inform potential targeting strategies. TIL-Bs in HNSCC have the potential to contribute to antitumor immunity in a number of ways including presenting tumor antigen to $CD4^+$ T cells[297,298]. In NSCLC, TIL-Bs were shown to present tumor antigen to and influence the phenotype of CD4+ T cells *in vitro*[127]. A $T_{H1}$ $CD4^+$ TIL phenotype following antigen presentation correlated with activated TIL-Bs in NSCLC patients while "exhausted" TIL-Bs correlated with $T_{regs}$[127]. We hypothesize that GC TIL-B in $HPV^+$ HNSCC may be more equipped to present antigen to $CD4^+$ T cells given their presence in TLS with GC and expression of CD40, CD86 and ICAM1, which are key proteins involved in interactions with $T_{FH}$ cells. Additionally, TIL-Bs in HNSCC could potentially enhance antitumor immunity through production of tumor specific antibodies that can activate NK mediated antibody-dependent cellular cytotoxicity (ADCC)[83,244,250]. Memory B cells, which are largely responsible for responding to secondary stimuli and differentiating into antibody secreting cells are increased in both $HPV^+$ and $HPV^-$ HNSCC. Future studies in HNSCC should assess whether memory TIL-Bs can respond to antigen stimulation and differentiate into antibody secreting cells. Given the suppressive TME of $HPV^-$ HNSCC and significant increase in $T_{regs}$, it is possible memory TIL-B function could be impaired or suppressed. However, if memory TIL-B produce antibodies in HNSCC patients, antigen specificity of those antibodies should be addressed. It is unclear whether antibodies produced in $HPV^+$ or $HPV^-$ HNSCC are tumor-reactive or self-reactive. However,

antibodies in the serum of HPV$^+$ HNSCC patients have been shown to have specificity to early and late antigens of HPV16[250]. Additionally, recent studies have shown that antibodies produce by TIL-Bs within the TME of HPV$^+$ HNSCC have specificity to HPV viral antigens E2, E6 and E7[246]. Whether these HPV-specific antibodies play a role in the anti-tumor response remains to be determined.

One function for TIL-Bs that is definitively correlated with increased survival and immunotherapeutic response in cancer patients is their role in TLS[156,158,162,203,299]. TLS formation and maintenance in tumors is an active area of investigation. Early studies reveal that common mechanisms of lymphoid organogenesis such as the presence of inflammatory cytokines and interactions of immune cells with tissue-resident stromal cells such as fibroblasts and mesenchymal stem cells are important for TLS initiation[125,156,162,300,301]. Our study identifies a potential mechanism for TLS formation in tumors through the identification of Sema4a expression on GC TIL-Bs within TLS. Sema4a is a membrane bound glycoprotein that is important for T cell co-stimulation and an important driver of $T_{h2}$ responses in humans, and was recently found to be expressed on human GC B cells in SLOs[291]. Further, Sema4a can interact with non-immune receptor Plexin D1 which is expressed on endothelial cells and immune receptor T cell, Ig domain, mucin domain-2 (Tim-2) and neuropilin-1 (NRP1) expressed by T cells[302–306]. Thus, Sema4a may play a central role in generating immune aggregates via TIL-B interactions with endothelial and T cells. In fact, CD4$^+$ $T_{FH}$ express high levels of NRP1[305]. Future studies should more thoroughly characterize the factors that lead to the creation of effective TLS, or conversely the factors that inhibit TLS formation in the TME, especially because TLS are both predictive [209,299,307] of and correlated with response to

immunotherapy[122,158,195]. There are a multitude of ways in which B cells can contribute to antitumor immunity, and it will be important to link B cell subsets with specific antitumor function to inform therapeutic strategies.

Current immunotherapeutic regimens aim to re-invigorate exhausted $CD8^+$ TIL within the TME[308]. Overall, our findings suggest that the presence of GC TIL-Bs within TLS in treatment naive patients is associated with better outcomes. Focusing on driving TIL-Bs into TLS with GC is a potentially paradigm-shifting step towards new immunotherapies. For example, we found that Sema4a may be a better marker of both early-stage and functional TLS in the TME compared with the canonical GC B cell marker BCL6. As such, determining ways to drive Sema4a expression on TIL-B and determining which ligands are required to nucleate TLS is an obvious next step for B cell mediated immunotherapy development. These findings are likely to stimulate future studies involving Sema4a in other cancers that have reported GC TIL-Bs such as lung cancer and melanoma[122,203,210]. In addition, formation of TLS with GC both peritumorally and intratumorally is paramount for increased patient survival and are increased in $HPV^+$ HNSCC. Thus, our study provides a rationale to assess Sema4a expression on GC TIL-Bs and in TLS of other virally induced cancers such as HCC, MCC, and cervical cancer where Sema4a expression on GC TIL-Bs has not yet been reported. Future studies should seek to evaluate how viral infection impacts the development and maintenance of GC TIL-B and TLS with GC in virally induced cancers. Further, additional environmental factors (i.e. the microbiome of the oral cavity and oropharynx) should be queried in future studies. Lastly, improved analysis of spatial relationships will be paramount as our data suggest that GC biology within TLS is associated with favorable antitumor immunity.

Beyond cancer, our dissection of B cell biology can inform strategies aimed at enhancing vaccine responses, or conversely disrupting the generation of B-cell mediated immune activation to suppress autoimmunity. Ultimately, this study highlights the significance of phenotypes and spatial patterns of TIL-Bs in both virally and carcinogen induced HNSCC and suggests that future studies should investigate if therapeutic enhancement of humoral immunity in HNSCC can complement current immunotherapeutic strategies

## 3.5 Author contributions

TCB conceived the project. TCB and DAAV obtained funding. ATR, ARC, DAAV, and TCB interpreted data and wrote the manuscript. ATR performed flow cytometry experiments and analyzed flow cytometry data. ARC performed scRNAseq experiments, analyzed scRNAseq data and immunofluorescence data, and performed statistical analyses. SRK and IA performed flow cytometric experiments. SaO performed multispectral immunofluorescence staining (within the lab of co-mentor StO). CHLK helped with scRNAseq experiments (in the laboratory of RLF). CL performed analysis and quantification of IHC images. AL performed IHC image analysis and interpretation (with TCB). RLF, UD, SK and RJS identified patients and collected specimens. RLF provided feedback and clinical interpretation of the data. HA and LCG performed the confocal microscopy experiments. TT and ZQ performed scRNAseq experiments; RL provided input on scRNAseq experimental design and library preparation. All authors reviewed and approved the manuscript.

# 4.0 Prevalence of intratumoral and circulating extrafollicular b cells is associated with disease progression in cancer patients

Data within this chapter are unpublished but a manuscript containing these data is in preparation

## 4.1 Summary

Many patients with recurrent/metastatic (R/M) cancer fail to produce a durable response to immunotherapy and other cancer treatments. Thus, there is a need to identify new biomarkers that can help predict risk of recurrence and monitor disease progression to determine if a therapy is effective. Memory B cells (MBCs) have been shown to correlate with survival in a variety of solid tumors and predict response to anti-PD1 therapy, but their origin, function and biomarker potential in tumors remains poorly understood. We addressed these questions by assessing the prevalence, phenotype, and function of germinal center and extrafollicular (EF) associated MBC populations in tumors and peripheral blood of patients with locally advanced (LA) head and neck squamous cell carcinoma (HNSCC) and peripheral blood of patients with metastatic melanoma and lung cancer. Here, we report an expansion of EF associated double negative (DN) MBC subsets: Tbet $^{+/-}$ CD11c$^{-}$ CD21$^{-}$ (DN3) and Tbet$^{+}$ CD11c$^{+}$ CD21$^{-}$ (DN2) in the periphery of patients with HNSCC, melanoma, and lung cancer. DN3 EF MBCs are hyporesponsive to antigen stimulation, represent poor antibody producers and fail to differentiate into

antibody secreting cells (ASC) while GC derived MBC subsets retain these functions. Circulating DN3 and DN2 share a B cell exhaustion-like program in cancer patients. Higher frequency of intratumoral DN3 EF MBCs in HNSCC is associated with advanced tumor stage. Levels of circulating DN3 EF MBCs can predict disease outcome following immunotherapy in melanoma patients. These findings support further clinical assessment of EF B cell responses in cancer and their potential to be used as biomarkers to monitor disease progression following treatment.

## 4.2 Introduction

B cells and tertiary lymphoid structures (TLS) were recently shown to predict response to immune checkpoint inhibitors (ICI) and survival in cancer[122,158,309,310]. Further, maturity of B cells and TLS can predict the risk of recurrence in cancer patients[210,213,293]. These studies highlight the biomarker potential of B cells and TLS. Current evidence suggests that B cells may also represent a new immunotherapeutic target that could be used in combination with current T cell-based immunotherapies[36,76,127,156,246,310]. One key obstacle to designing and developing B cell focused immunotherapies is that the direct anti-tumor role of B cell human cancer remains poorly understood. Further, it is not clear which B cell subpopulations and B cell specific pathways to therapeutically target given the number of B cell subpopulations within in the B cell compartment across tumor types and the lack of physiologically relevant pre-clinical models to test the impact of B cells on tumor clearance.

One of the major B cell subpopulations that infiltrate human tumors are memory B cells (MBC). MBCs are an important B cell subset for establishing life-long protection against pathogens. There are several key characteristics of MBCs that make them effective in this role: (1) increased lifespan, (2) faster proliferation and/or differentiation following antigen or polyclonal stimulation, and (3) expression of somatically mutated and affinity matured Ig genes. Intratumoral MBCs have been shown to be the predominant infiltrating B cell in non-small cell lung cancer (NSCLC), metastatic melanoma (MEL), breast cancer (BRCA), colorectal (CRC) and hepatocellular carcinoma (HCC) and head and neck squamous cell carcinoma (HNSCC) [76,122,203,226,311–313]. MEL patients who responded to ICI had a higher proportion of class switched memory B cells (SW) (MBC) defined by CD27 expression and lack of IgD prior to treatment. These studies suggest that enhancing effector function of MBC may be of therapeutic value and the MBC compartment could be used to monitor how tumors respond to therapy in patients.

It is not yet clear whether MBCs are recruited to the TME or generated locally in tumors. In non-cancer tissues, MBCs arise from antigen-experienced B cells participating in GC reactions or extrafollicular (EF) responses. GC responses result in $CD27^+$ MBC subsets and EF responses typically result in $CD27^-$ MBC subsets. GC derived MBC included (1) class-switched: $IgD^-$ express either IgA or IgG; can be activated ($CD21^-$ $CD95^+$) or resting ($CD21^+CD95^-$), (2) non-class-switched: $IgD^+IgM^+$, and (3) IgM-only[314–316] **(**Appendix Figure 10). EF responses result in CD27- IgD- MBCs also referred to as double negative (DN) MBCs **(**Appendix Figure 10**)**. MBCs generated from this pathway also undergo somatic hypermutation (SMH) and isotype class-switching. Chronic human infections such as HIV and malaria and autoimmune disorders are associated with a large

accumulation of DN2 or atypical MBC ($CD11c^+$ $Tbet^+CD21^-$) in the peripheral blood (PBL) of patients **(**Appendix Figure 11**).** In HIV, DN2 are generated in LN areas outside of GCs and have low mutation frequencies and HIV-neutralizing capacity[317]. Recently, DN2 MBCs were shown to be expanded in PBL of patients with severe COVID-19[318]. Additionally, these patients also had accumulation of a novel EF associated DN population termed DN3 ($CD11c^-$ $CD21^-$)[318]. However, the phenotype of DN3 MBCs in COVID was not well described. DN2 MBCs have increased expression of a variety of inhibitory receptors (IRs), abnormal expression of transcription factor Tbet and altered homing receptors (CD11c and CXCR3) but appear to have undergone class-switching as they express a predominant IgG isotype[251,317,319–325]. Chronic antigen exposure is hypothesized to drive upregulation of IRs, which inhibit MBC effector functions including BCR signaling, differentiation, cytokine production and antibody production[319,325,326]. Recent transcriptomic analysis showed that DN2 MBCs in HIV, malaria, and SLE share gene expression profiles suggesting a common driver of these cells in chronic diseases[324].Of note, this aberrant accumulation of DN2 MBCs in infections like HIV and malaria is thought to contribute to poor immunity against these diseases[321].

DN MBCs have been reported in some human solid tumors but their phenotype, function, origin, and impact on the tumor microenvironment (TME) remains unclear[121,205,327,328]. The intratumoral DN2 phenotype has been largely uncharacterized in the TME beyond low CD27 and CD21 expression and it's not clear if DN3 MBCs are present in tumors. However, in HCC, intratumoral DN2s do express IgG and functional tumor necrosis factor (TNF)-related apoptosis-inducing ligand (TRAIL)[205]. Signals driving GC or EF responses are not well understood but murine models of infection have reveal

that some pathogens induce GC responses while some induce EF or both and certain cytokines promote either response. It will be important to determine the differences in MBCs from GC and EF responses in patients as GCs are not present in all tumor types. This will also help determine which and whether MBC responses should be enhanced therapeutically.

In this study, we evaluated the presence and function of GC derived MBCs (SW) versus EF derived MBC (DN2 and DN3) in HPV driven (HPV+) and carcinogen (HPV-) driven head and neck squamous cell carcinoma (HNSCC) tumors to assess how the TME effects activation of GC or EF pathways. Through adoption of a new gating strategy recently published in COVID-19 studies, we identified an increase in a novel EF associated MBC subset (DN3) in cancer patients. Additionally, we surveyed levels of DN2 and DN3 MBCs in the peripheral blood of HNSCC, MEL, and lung cancer patients to determine if DN2 accumulate in the periphery of cancer patients. We included a cohort of 35 MEL patients who were later treated with anti-PD1 therapy (Nivolumab) and a cohort of 28 NSCLC patients who were treated with either chemotherapy, anti-PD1 therapy or combination so we could assess the prognostic value of circulating MBCs.

We hypothesized that GC derived MBCs would be increased in HPV+ HNSCC, HPV- HNSCC TME would favor EF differentiation and thus higher levels of DN2 and DN3 would be observed in HPV- patients. We also hypothesized that circulating DN2 and DN3 would be elevated in cancer patients and correlate with poor prognosis. We predict that GC derived SW and DN1 MBCs would be more functional than DN2 or DN3. We performed comprehensive characterization of MBC in patient tumors and PBL, and relevant healthy tissues using 24-parameter spectral flow cytometry panels, in vitro

functional assays, and correlative clinical analyses. Overall, our findings provide insight into the signals in the TME that may drive activation of GC vs EF pathways, providing a rationale for bolstering GC derived SW MBC function in cancer as an immunotherapy and using circulating EF MBCs as biomarkers for response to standard-of-care and immunotherapy.

## 4.3 Results

### 4.3.1 Extrafollicular derived B cell subpopulations are abundant in cancer patients and may predict disease outcome

To compare the abundance of B cell subpopulations derived from GCs versus EF responses in the TME and periphery of cancer patients, we performed spectral flow cytometry using spectral cytometry panels (Table 5) on tumor and blood specimens isolated from HPV+ and HPV- HNSCC patients**.** We also collected peripheral blood (PBL) for these analyses from patients with metastatic melanoma (MEL), primary and metastatic lung adenocarcinoma and squamous cell carcinoma (LUAD/LUSC) and non-small cell lung cancer (NSCLC) to compare the memory B cell compartment across multiple tumor types. We refer to LUAD/LUSC/NSCLC patients here as (LU) for brevity. HNSCC specimens were from patients with locally advanced disease. MEL and LU PBL specimens used here were collected prior to patients receiving chemotherapy, immunotherapy, or a combination of both. We included these samples although we did

not have access to matching tumor so that we could assess prognostic potential of circulating GC and EF associated B cell populations. We also collected tonsils from patients with tonsilitis, health donor spleen, and healthy PBL as tissue controls. Additionally, we used PBL from HIV+ individuals as a positive control for detecting EF B responses.

To exclude GC B cells and plasmablasts (PB) populations, expressing CD27 and lacking IgD, we first gated on $CD38^-$ $CD19^+CD20^+$ cells and then used CD27 and IgD to distinguish GC- and EF- associated B cell subpopulations (**Figure 12a).** Class-switched MBC (SW MBC) which are $CD27^+IgD^-$ were significantly increased in HNSCC tumors and peripheral blood compared to tonsils and HD and HIV+ PBL (**Figure 12b).** We did not observe a significant increase in SW MBCs in the PBL of MEL and LU patients **(Figure 12b).** Double negative MBC (DN) which are $CD27^-IgD^-$ were increased in HNSCC tumors (TIL) and PBL, and LU PBL compared to HD PBL **(Figure 12b).** DN MBC can be further subdivided using the markers CD11c and CD21: DN1 ($CD21^+CD11c^-$), DN2 ($CD21^-CD11c^+$) and DN3 ($CD21^-CD11c^-$). DN1 B cells are thought to be a MBCs precursor generated from GCs. DN3 B cells are a novel EF associated B cell subset recently identified and shown to be expanded in the PBL of patients with severe COVID-19, but not previously reported in cancer[318]. We observed a significant increase in DN3 B cells in HNSCC TIL and PBL compared to HD PBL, but not in non-cancer tissue. DN3 B cells were also significantly increased in MEL and LU PBL compared HD PBL **(Figure 12c).** DN3 frequency were slightly higher in cancer patient PBL than HIV+ PBL but did not reach statistical significance **(Figure 12c).** DN2 B cells were more abundant in HIV+ PBMCs compared to HNSCC TIL and patient PBL **(Figure 12c).** Strikingly**,** we observed a

significant increase in DN2 in patient PBL compared to HNSCC TIL **(Figure 12c).** DN1 B cells were significantly reduced in HIV+ PBL and MEL PBL compared to HD PBL, but this was not observed in HNSCC or LU patient PBL **(Appendix Figure 12)**

Next, we sought to determine the relationship between GC- and EF- associated DN subsets in TIL and PBL, we observed an inverse correlation between DN3 and DN1 in HNSCC TIL and PBL **(Figure 12d).** We observed a similar correlation between DN3 and DN1 in the PBL of MEL and LU patients **(Appendix Figure 12).** DN2 and DN3 were inversely correlated in HNSCC, MEL but positively correlated in LU patients **(**Appendix Figure 12**).** These data suggest that more EF B cell responses may indicate a decrease in GC responses in cancer patients. HNSCC patients with a higher freq of DN3 in their tumors also have a higher frequency of DN3 in their PBL **(Figure 12e)** suggesting that DN3 may be generated in TIL and migrate into the periphery. Lastly, we wanted to determine the clinical significance of DN3 B cells in cancer patients. For our cohort of LA HNSCC tumors, we correlated DN3 frequency with pathological tumor stage (T1, T2, T3, T4). We compared patients with early-stage tumors (T1) with patients who had a more advanced stage tumor (T2-T4). HNSCC patients with T stage T2-T4 had significantly higher than those with early stage (T1) **(Figure 12 f).** Having a higher ratio of DN3 B cells to DN1 B cells is also associate with advance stage tumors **(Figure 12g).** We observed a similar trend in the PBL of HNSCC patients **(Appendix Figure 12)** To assess whether the frequency of circulating DN3, DN2 or DN1 could predict outcomes, we grouped MEL patients based on their tumor response to anti-PD1 therapy. MEL patients with disease progression (PD) following therapy had a higher frequency of DN3 MBC and fewer DN1

MBC in their blood before therapy compared to those with no evidence of disease (NED) or stable disease (SD) **(Figure 12 h).** There was a trend that patients with stable disease had higher DN2s than PD or NED patients **(Figure 12h).** LU patients with LA primary tumors and metastatic disease had similar levels of SW, DN3 and DN2 MBCs **(**Appendix Figure 13**).** We did not observe a significant trend in terms of response to therapy in LU patients but there was a slight increase in DN2 MBCs in patients whose tumors progressed following chemotherapy (**Appendix Figure 13).** Together, EF B cell responses are elevated in cancer patients with more advanced disease, and this may represent prognostic indicator of immunotherapeutic response.

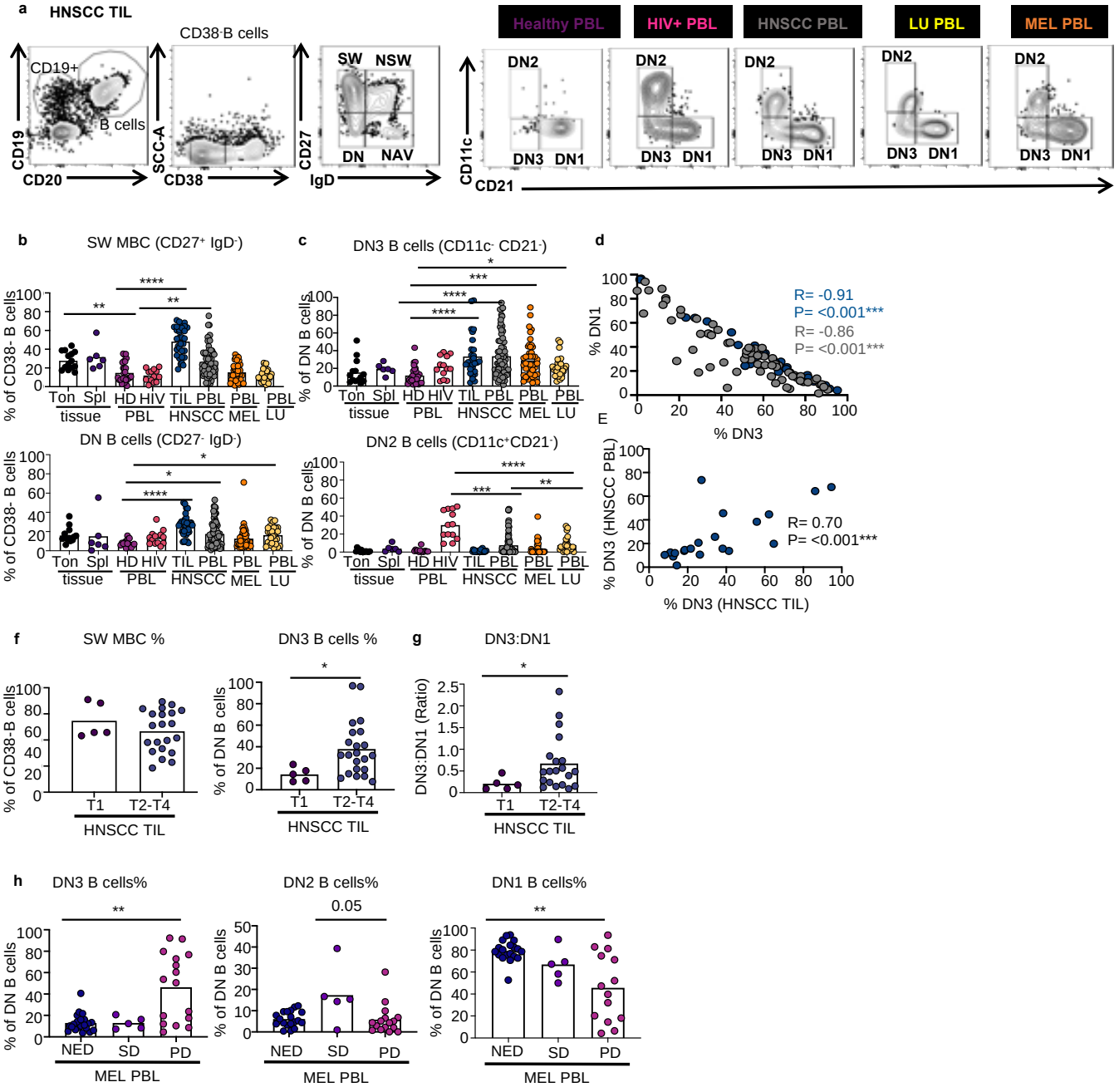
a
HNSCC TIL
CD38-B cells
CD19+
B cells
CD19
CD20
SCC-A
CD38
SW NSW
DN NAV
CD27
IgD
Healthy PBL
HIV+ PBL
HNSCC PBL
LU PBL
MEL PBL
DN2
DN3 DN1
CD11c
CD21
b
SW MBC (CD27+ IgD-)
% of CD38- B cells
Ton Spl HD HIV TIL PBL PBL PBL
tissue PBL HNSCC MEL LU
DN B cells (CD27- IgD-)
c
DN3 B cells (CD11c- CD21-)
% of DN B cells
DN2 B cells (CD11c+CD21-)
d
% DN1
% DN3
R= -0.91
P= <0.001***
R= -0.86
P= <0.001***
E
% DN3 (HNSCC PBL)
% DN3 (HNSCC TIL)
R= 0.70
P= <0.001***
f
SW MBC %
% of CD38-B cells
T1 T2-T4
HNSCC TIL
DN3 B cells %
% of DN B cells
g
DN3:DN1
DN3:DN1 (Ratio)
h
DN3 B cells%
DN2 B cells%
DN1 B cells%
NED SD PD
MEL PBL

**Figure 12: Increased presence of intratumoral and circulating extrafollicular B cells is associated with disease progression and may be predictive of disease outcome in cancer patients.**

**(a)** Representative flow cytometry gating of strategy for memory B cell subsets is shown for tumor (TIL) and blood samples from patients with head and neck squamous cell carcinoma (HNSCC), metastatic melanoma and lung cancer. Live cells are first gated on CD19+ CD20+ CD38- to excluded activated or antibody secreting B cells. B cell subsets are classified as followed: Class-switched memory B cells (SW), Non-class switched memory B cells (NSW), Double negative B cells (DN). DN B cells can be subdivided into : Double negative 1(DN1) Double negative 2 (DN2), and Double negative 3 (DN3). **(b)** Quantification graphs of the frequency SW, total DN **(c)** and DN3, DN2 B cell population in normal tissues and treatment naive patient tumor and blood samples. Control tissues include normal spleen (Spl) (n=6), inflamed tonsil (Ton) (n=14) , healthy donor (HD) PBL (n=27), PBL from patients with HIV (n=14). Cancer patient samples include tumor (TIL) (n=28) and PBL (n=71) from HNSCC, PBL from metastatic melanoma (n=46) and lung cancer patients (n=26). Data were analyzed by a non-parametric Kruskal-Wallis test with multiple comparisons to HD PBL.****p=<0.0001, ***p=0.0001, **p=0.002, *p=0.02 **(d)** Frequency are DN1 inversely related to DN3 in tumors and PBL of patients with HNSCC. Frequencies from tumor are overlaid in blue and PBL are overlaid in grey. Spearman's nonparametric correlation analysis results are reported. **(e)** Frequency of intratumoral DN3 is positively correlated with circulating DN3 B cells in patients with HNSCC. Spearman's nonparametric correlation analysis results are reported. **(f)** Quantification graphs of frequency of SW, DN3 and (**g)** ratio of DN3 to DN1 in HNSCC patient tumors grouped by pathology-defined T stage (Tumor stage) (range 1-4). Data were analyzed by Mann-Whitney. *p=0.02. **(h)** Quantification graphs of frequency of DN3, DN2, DN1 in metastatic melanoma patient PBL grouped by disease outcome. Blood was collected before patients went on immunotherapy treatment. NED= no evidence of disease, SD= Stable disease, PD=progressive disease. Data were analyzed by a non-parametric Kruskal-Wallis test with multiple comparisons of mean rank of each group to another. **p=0.003

### 4.3.2 Tumor location and environment may drive extrafollicular responses in HNSCC

The antigen stimuli that lead to dominance of GC or EF responses during immune response to infection remains poorly understood[329]. However, murine models of infection have revealed that EF responses are dominant in some infection models such as salmonella , while others have more GC responses such as influenza[329,330]. In the case of human HIV infection, both EF and GC responses are observed[317,329]. Cytokines play an important role in driving EF or GC responses. IL-12, TNF-α, and IFN-γ, promote EF response over GC. IL-21 is key for initiation and maturation of B cells and CD4+ T into GC B cells and CD4+ TFH respectively. However, in the absence of CD40 stimulation IL-21 with BCR stimulation can induce EF B cell phenotypes from naïve B cells. TLR7 and TLR9 appear to promote both types of responses but TLR9 favors EF responses in mice and humans in vitro[317,329,331].

Even less is known about drivers of EF and GC responses in cancer. However, intratumoral B cells with a GC phenotype have been described in MEL, NSCLC, HNSCC, HCC, and BRCA[36,122,198,203,210,246,332,333]. Additionally, intratumoral MBCs are the predominant B cell subpopulation and quite heterogenous in a variety of tumor types including NSCLC, metastatic MEL, HNSC, BRCA, CRC and HCC making up >60% of all intratumoral B cells[122,198,203,311,333,334]. To address impact of the TME on the presence and phenotype of MBC produced from GC and EF responses, we compared frequency of SW, DN1 and DN3 MBCs in HPV+ and HPV- HNSCC tumors. We previously showed that HPV+ tumors have more GCs and TLS than HPV- tumors **(Chapter 3).** We hypothesized that HPV- tumors would have more EF- derived MBCs than $HPV^+$. $HPV^+$ tumors arise in

the oropharynx and HPV$^-$ tumors arise in the oral cavity, larynx, hypopharynx, and nasopharynx **(**Figure 13**a).** We observed that DN3 were significantly increased in HPV$^-$ HNSCC tumors while DN1 B cells were significantly increased in HPV$^+$ **(**Figure 13**b).** There was not a significant difference in SW MBC between HPV$^+$ and HPV$^-$ **(**Figure 13**b)** or the ratio of DN:SW B cells **(**Figure 13**c)** however, the ratio of DN3:DN1 is significantly higher in HPV- tumors **(**Figure 13**c)**. We next compared expression of tissue-resident, GC homing and antigen experience markers on SW and DN3. Expression CD45RB and CD69 distinguishes four subsets of CD27$^+$ tissue resident MBCs that are not present in PBL[335]. CD27$^+$CD45RB$^+$ CD69$^+$ were significantly increased in gut tissues compared to other MBC subsets which was not observed in other tissues as spleen, Tonsil, LN and bone marrow (BM). CD45RB and CD69 DP cells were not present in the CD27$^-$ B cell compartment[335]. Strikingly, we observed co-expression of CD45RB and CD69 in both SW and DN3 MBCs in HNSCC tumors however it was significantly less than SW MBCs **(Figure 13d).** DN3 B cells in tonsil and LN trended to have less co-expression than intratumoral DN3 **(Figure 13d).** CXCR5 expression is important for B cell trafficking into tissues and is increased following activation via antigen and CD40 signaling. We observed a reduction in CXCR5 expression on DN3 B cells compared to SW MBC in HNSCC TIL and inflamed tonsil **(Figure 13e).** CD95 expression is also increased on B cells during activation and is often used to mark B cells that are antigen experienced. CD95 is expressed at comparable levels on SW and DN3 MBCs in HNSCC TIL **(Figure 13f)** and with a modest increase SW MBC in HNSCC TIL compared to SW in inflamed tonsil and normal LN. These data suggest that presence of SW and DN3 MBCs may be influenced by the TME and that the HPV- TME may favor EF B cell differentiation.

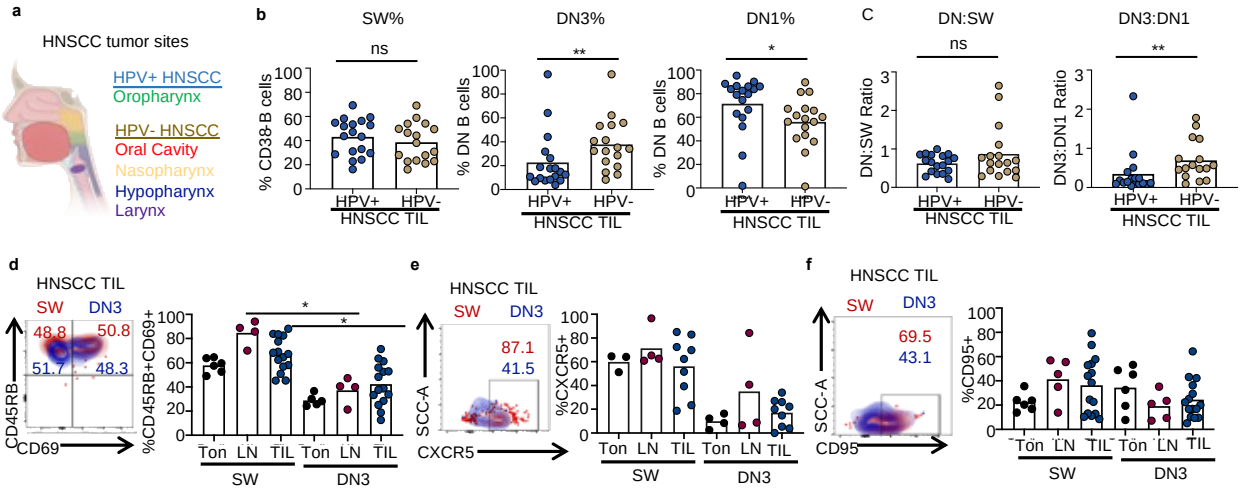


**Figure 13: Presence of tissue-resident DN3 B cells is increased in HPV- tumors**

**(a)** Schematic of grouping HNSCC patient tumors by location. HPV+ tumors occur in the oropharynx (Base of tongue (BOT), Tonsils and soft palate) HPV- tumors occur in the oral cavity (mouth, gums, lips, tongue, hard palate), Larynx, Nasopharynx and hypopharynx. Created with Biorender.com **(b)** Quantification graphs of frequency of SW, DN3 and DN1 in HPV+ tumors (n=18) vs HPV- tumors (n=17). Data analyzed by Mann Whitney. **p=0.007, *p=0.01. **(c)** Quantification graphs of ratio of total DN population versus SW population and ratio of DN3 to DN1 within the DN population. Data analyzed by Mann Whitney. **p=0.004. **(d)** Representative flow gating of co-expression of CD45RB and CD69 in B cell subsets in HNSCC tumor specimens (n=15). Gating on SW MBC is overlaid in red. Gating on DN3 B cells is overlaid in blue. Quantification graphs of each marker on SW or DN3 is displayed as indicated. Bar graphs include inflamed Tonsil (Ton) n= 6 and healthy lymph nodes (LN) n=5 as positive tissue controls. *p=0.02 **(e)** Representative flow gating of CXCR5 and **(f)** CD95 in B cell subsets in HNSCC tumor specimens (n=9) and n= (15). Quantification graphs of each marker on SW or DN3 is displayed as indicated.

### 4.3.3 Intratumoral and circulating extrafollicular-derived MBCs have markedly reduced effector function compared to GC-derived MBC

DN2 MBCs in HIV and malaria infected individuals were shown to be hyporesponsive to antigen stimulation. Additionally, DN2 MBC did not secrete antibodies, cytokines, or differentiate into antibody secreting cells (ASC) when stimulated. SW MBC in these patients retained these key MBC effector functions[319,325]. We hypothesized that SW and DN2 MBCs in cancer patients would behave similarly to those in chronic infection. While DN3 MBC function was not directly assessed in previous studies, the association of DN3 with the EF pathway suggests they may behave similarly to DN2s[318]. Given the positive correlation of DN3 in matched tumor and PBL of HNSCC patients, we compared functional readouts on TIL and PBL samples whenever possible. Assays that required isolating B cell subpopulations were performed on PBL samples as these demanded higher cell yields. We first assessed BCR responsiveness in GC derived or EF derived MBC subsets. We measured BCR signaling by quantifying the net change in phosphorylation of spleen tyrosine kinase (Syk) and B cell linker protein (BLNK) , which are phosphorylated early in the BCR signal transduction pathway[336] **(Figure 14a).** SW, DN1 Naïve B cells from HNSCC TIL were responsive to stimulation and there was no significant difference in the phosphorylation of Syk or BLNK **(Figure 14b).** However, we did observe that DN3 MBCs were hyporesponsive to stimulation and had significantly lower levels of phosphorylation of Syk and BLNK when compared to Naïve or SW MBC **(Figure 14b).** A similar trend was observed in HNSCC PBL; however, SW MBCs were more responsive to BCR stimulation than their Naïve counterparts **(Figure 14b).** Circulating DN3 and DN2 MBC were hyporesponsive to BCR stimulation compared to all

other subsets **(Figure 14b).** We also compared levels of phosphorylated Syk and BLNK in SW and DN3 in patients to HD PBL. We found that levels of phosphorylation of Syk and BLNK were significantly lower in SW MBC from HNSCC TIL and PBL as well as MEL PBL compared to HD but DN3 MBC cells were hyporesponsive in both HD and patient samples **(Figure 14c).** These results indicated that early BCR signaling events are diminished in DN3 and DN2 MBCs, and thus suggest that EF MBCs may have reduced capacity mediate effector functions in response to BCR crosslinking.

To gain insight into factors that may drive EF differentiation vs GC differentiation in cancer, we assessed differences in immunoglobulin (Ig) isotype distribution in GC-derived and EF- derived MBC subsets via flow cytometry as isotype switching is induced both by distinct antigen signals and cytokines **(Figure 14a).** Based on previous studies in chronic infection, DN2 MBCs predominately express IgG but can also express IgM[319,321]. We hypothesized that DN2 and DN3 MBCs in patients would have similar Ig isotype distributions. In HNSCC TIL, SW MBCs predominately expressed IgG and a smaller percentage of SW MBCs expressed IgA **(Figure 15b).** There was an almost equal distribution of IgG+ and IgM+ DN3 MBCs in HNSCC TIL **(Figure 15b).** Strikingly, we saw that circulating SW, DN3, and DN2 in HNSCC were predominately IgG-expressing, and that a fair portion of cells were IgA+ with very little IgM expression (**Figure 15b).** Given the predominance of IgG switching in these subsets, we next assessed IgG subclass distribution in these subsets. SW MBC is HNSCC TIL had an almost equal distribution of IgG1 and IgG2 expression , while DN3 MBCs were predominately IgG1 **(Figure 15c).** A similar distribution of IgG subclass in TIL was observed in circulating SW and DN3 with DN2 MBCs being predominately IgG1 **(Figure 15c).** To determine the capacity of these

subsets to secrete antibodies of different Isotypes and differentiate into antibody secreting cells (ASC), we purified SW and DN3 B cells using FACS (Methods) and stimulated them for five days withCpG (TLR-9 agonist), IL-2, IL-15, IL-10 and soluble CD40 ligand to induce both differentiation and antibody secretion, as previously described[264]. Circulating DN3 MBCs produced significantly less IgG1, IgG2, IgA and IgM compared to their SW MBC counterparts within the same patient **(Figure 15d).** Circulating DN3 MBCs were also unable to differentiate into ASCs when stimulated **(Figure 15e).** These data suggest that unique signals may be involved in driving SW and DN3 MBC differentiation in cancer and further differentiation of DN3s may be diminished in cancer patients.

T cell dysfunction in the TME has been shown to be mediated both by T cell intrinsic factors such as overexpression of inhibitory receptors including LAG3 PD1, and CTLA4 and environmental factors (i.e. suppressive cytokines, adenosine, glucose restriction, and hypoxia)[337–342]. Little is known about the effects of environmental factors on B cell function within tumors. To gain insight into this, we assayed the metabolic capacity of intratumoral and circulating GC derived and EF derived MBC subsets by measuring mitochondrial mass and glucose uptake, as mitochondrial stress and glucose avidity have been implicated in immune cell dysfunction[340,342,343]. Cells were isolated from HNSCC TIL and PBL and given fluorescent glucose analog 2-NBDG ex vivo and then subsequently stained with a flow cytometry panel containing surface markers of MBC subsets and Mitotracker deep red FM (MitoDRED) dye **(Figure 16a and c).** There was significantly higher percentage of intratumoral DN3 MBCs that took up glucose than SW, DN1 or naïve B cells in HNSCC **(Figure 16b).** DN1 MBCs also took up more glucose than SW or Naïve but this trend failed to reach statistical significance **(Figure 16b).**

Surprisingly, only circulating DN3 MBCs took up glucose in HNSCC PBL **(**Figure 16**b).** We observed a modest decrease in uptake of MitoDRED in intratumoral DN1 and DN3 **(Figure 16d).** However, there was not a clear trend in MitoDRED staining in circulating B cell subsets **(Figure 16d).** These data suggest that intratumoral DN3 B cells have a higher glucose avidity and may be under mitochondrial stress in the TME. Taken together, these data suggest that GC-derived MBC subsets appear to be more functional than EF-derived subsets in cancer. Further, dysfunction of intratumoral EF MBC may be driven by TME factors.

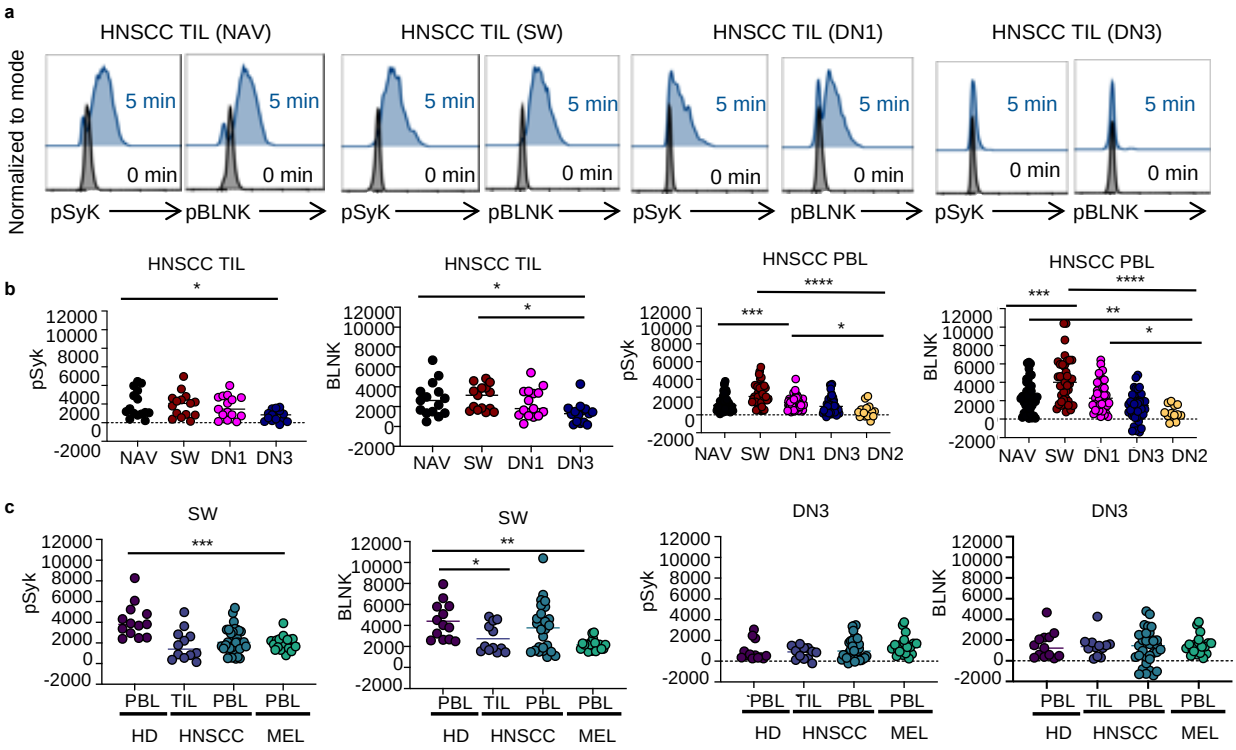


**Figure 14: Circulating and intratumoral extrafollicular B cell subsets are hyporesponsive to BCR stimulation**

**(a)** Representative histogram of phosphorylated SyK and BLNK in naïve (NAV), switched memory (SW), double negative 1 (DN1), double negative 3 (DN3) in HNSCC tumor. Untreated sample is overlaid in black and anti-Ig treated sample is overlaid in blue. **(b)** Quantification of phosphorylated BLNK and Syk in NAV, SW, DN3 ,DN1 and double negative 2 (DN2) in HNSCC tumors (n=15) and PBL (n=43) following 5 mins of stimulation with a pan anti-Ig (20 ug/ml) antibody. Scatter plots are of the net geometric mean fluorescence intensity (gMFI) calculated by subtracting the gMFI of the untreated from the treated cells. Cells were stimulated in bulk and then data was analyzed via flow cytometry. B cell subsets were first gated and then analyzed for phosphorylated BLNK and Syk. Data were analyzed by a non-parametric Kruskal-Wallis test with multiple comparisons of mean rank of each group to another.*p=0.03, **p=0.006; *p=0.01, **p=0.004, ***p=0.0004, ****p=<0.0001 **(c)** Quantification of phosphorylation of BLNK and Syk in SW and DN3 between HD PBL(n=13) and HNSCC TIL, PBL and MEL PBL (n=19). Data were analyzed by a non-parametric Kruskal-Wallis test with multiple comparisons of mean rank of each group to another.*p= 0.02, **p= 0.002, ***p=0.0004.

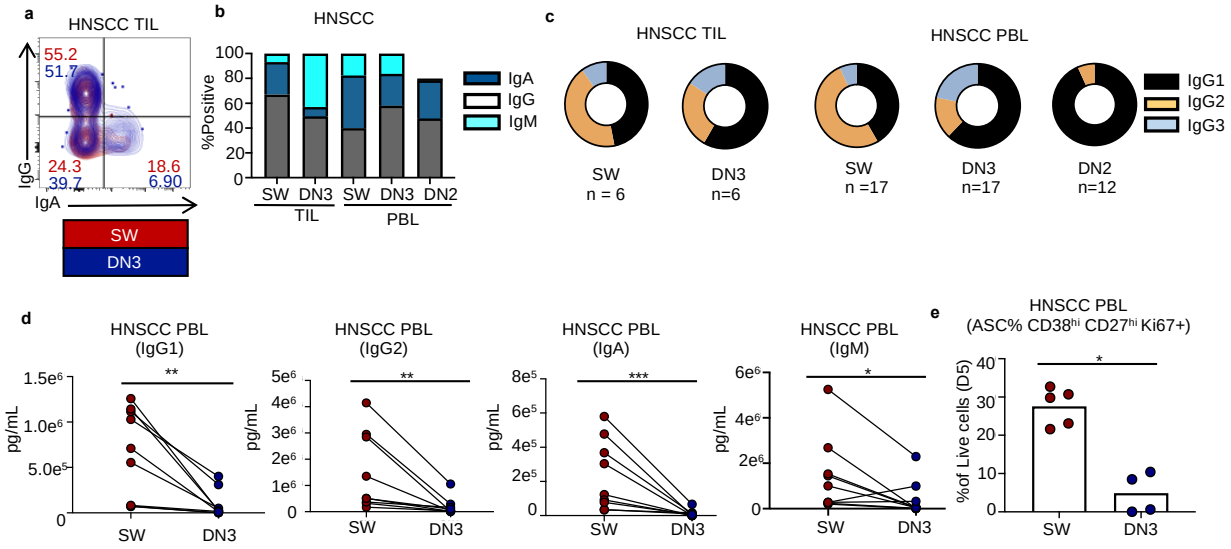


**Figure 15: Circulating and intratumoral GC and EF B cell subsets are isotype-switched but EF B cells are poor antibody producers**

**(a)** Respresentative flow plot depicting IgG and IgA expression on SW and DN3 in HNSCC TIL. SW are overlaid in red and DN3 are overlaid in blue. IgG-IgA- gate was then gated for IgM (not shown) to graph frequencied of all three isotypes in stacked bar graph **(b)** percentages of IgA, IgG and IgM were normalized in graph pad prism to equal 100%. **(c)** Donut graphs showing the summary of IgG subclasses expressed by SW, DN3 and DN2 in HNSCC TIL and PBL. Number of patients contributing to summary graphs is displayed under each repsective graph.**(d)** In vitro antibody production assay comparing secretion of IgG1, IgG2, IgA, IgM by SW and DN3 following stimulation with CpG (ODN2006), IL-2, IL-10, soluble CD40 ligand (sCD40L), and IL-15 for 5 days. SW and DN3 were sorted from HNSCC patient PBL via FACS and Ig secretion was measured by Luminex. **(e)** In vitro differentiation assay comparing antibody secreting cell formation by SW and DN3 from HNSCC patient PBL. Cells were stimulated with the same cocktail defined in panel 15 d. Data were analyzed by Mann-whitney. ***p=0.0002, **p=0.002, *p=0.02

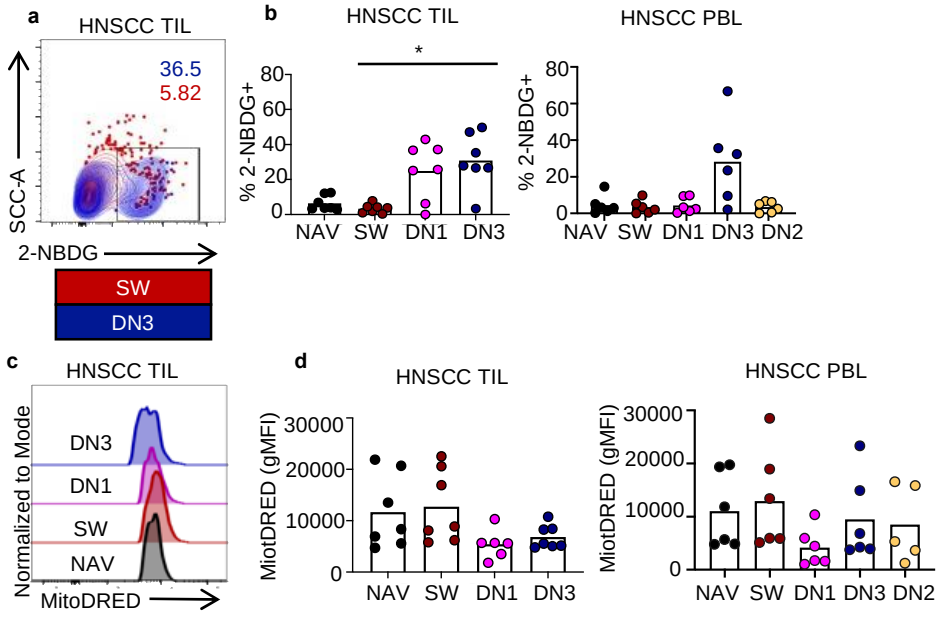


**Figure 16: Hyporesponsiveness of intratumoral DN3 B cells to stimulation may be due to mitochondria stress and glucose avidity**

**(a)** Representative flow gating of 2-NBDG (glucose analogy dye) on B cell subsets in HNSCC TIL specimen .SW MBC are overlaid in red. DN3 overlaid in blue. **(b)** Quantification of Ex vivo glucose uptake (2-NBDG) by NAV, SW, DN1, DN2, DN3 subsets in HNSCC patient TIL n=6 and PBL n=5. Data were analyzed using a non-parametric Kruskal-Wallis test with multiple comparisons of each column mean rank to one another. *p=0.01.**(c)** Representative histogram of Mitotracker deep red (MitoDRED) on B cell subsets in HNSCC TIL. Bar charts showing quantification of Ex vivo staining of) in NAV, SW, DN1, DN2, DN3 subsets from HNSCC TIL and PBL. gMFI of MitoDRED in positive cells is reported.

### 4.3.4 Circulating DN3 and DN2 share a B cell exhaustion-like expression profile that may be driven by Th1 cytokine signals in cancer patients

DN2 MBCs in HIV/HBV/malaria infection and autoimmunity are characterized by expression of inhibitory receptors (IRs), homing receptors, and transcription factors that are not present in SW MBC. Fc receptor-like 4 (FcRL4) and 5 (FcRL5) are B cell specific IRs that induce B cell dysfunction by inhibiting BCR signaling through recruitment of tyrosine phosphatases SHP-1and SHP-2[344]. The in vivo ligands for FcRL4 and FcRL5 are IgA and IgG respectively[345]. DN2 in HIV predominately express FcRL4 while DN2 in malaria, HBV, and SLE express FcRL5[251,283,322]. Leukocyte-associated immunoglobulin-like receptor 1 (LAIR-1) and CD85J also known as immunoglobulin (Ig)-like transcripts 2 (ILT2) are IRs that have been shown to inhibit BCR signaling as well as downregulate Ig and cytokine production[346]. LAIR-1 recognizes collagens, proteins that have collagen domains, and complement protein C1q[347,348]. CD85J binds major histocompatibility complex (MHC) 1 proteins or viral MHC 1 homologues[346]. CD72 is another IR mainly expressed on B cells that negatively regulates BCR signaling and binds to CD100 or Semaphorin 4D (Sema4D) expressed on myeloid cells[349]. The importance of IRs in mediating B cell dysfunction in these diseases is evident in studies where IRs were downregulated via siRNA in HIV patients, BCR signaling, proliferation cytokine and antibody functions were rescued[350]. Expression of IRs on DN2 are thought to be driven by chronic antigen stimulation and Th1 associated cytokines such as IFN-γ[321]. DN2 also express Th1 associated transcription factor Tbet and TOX which has been implicated in mediating T cell exhaustion[324,351–353].

Expression of IRs, Tbet and Tox have not been evaluated previously in DN MBC in cancer patients. Additionally, expression of these factors have not been evaluated in intratumoral GC-derived MBC subsets. To address these questions, we analyzed the expression of Tbet, Tox, LAIR1, FcRL4, FcRL5, CD85J and CD72 expression on GC derived and EF derived MBC subsets in HNSCC TIL and PBL and PBL from MEL and LU cancer patients **(Figure 17a).** We used HIV+ PBL as a positive control for expression of these proteins. Tox and CD72 were added to our validation analysis following our intial investigation into this expression profile so we were only able to characterize their expression in HNSCC. We observed co-expression of Tbet, FcRL5, CD85J and LAIR1 on circulating DN2 B cells in HNSCC, MEL, and LU patients (Figure **17b).** Circulating DN3 MBCs also expressed Tbet, CD85J and LAIR1 but not FcRL5 **(Figure 17b).** However, expression was significantly lower in DN3s compared to DN2s **(Figure 17b).** When we compared expression of Tbet, Tox, LAIR1, FcRL4, FcRL5, CD85J and CD72 in intratumoral DN3s versus circulating DN3s in HNSCC and found that there was modest expression of these proteins in TIL but significantly higher expression in circulating DN3s. **(Figure 17c and d)**. Circulating and intratumoral SW, did not express Tbet, FcRL5, and CD85J but do express some level of LAIR1 and CD72. We also observed some IR expression on Naïve B cells in HNSCC TIL and PBL in some patients **(Appendix Figure 14).** Strikingly**,** CD85J was increased in Naïve B cells in HNSCC, and LU samples but not in HD controls**.** These data suggest that circulating DN3 and DN2s in cancer patients may be generated by a similar mechanism to those in chronic infection but intratumoral DN3 B cells may receive additional signals or may lack signals which in turn may alter their expression profiles. Naïve B cells may also be dysfunctional in HNSCC patients.

Next, we used our previously published HNSCC scRNA seq data set to determine if cytokines differentially associated with GC versus EF differentiation were present and/or distinct between HPV+ and HPV- HNSCC as we see more DN3 MBCs in HPV- HNSCC. We also wanted to delineate the potential source of cytokines in HNSCC. We first used gene set enrichment analysis (GSEA) to identify and cluster all the immune cell types in HNSCC which is projected on a UMAP **(Figure 18a)** and used differential gene expression analysis to detect cytokine transcript which we displayed as feature plots **(Figure 18b).** Although detection of cytokine transcripts is limited in scRNA seq data sets, we were able to detect IFN-γ (*IFNG*), IL-6, and IL-18 in HPV+ and HPV- TIL **(**Figure 18b). Not surprisingly IL-6 and IL-18 expression was detected in the macrophage/monocyte compartment while IFN-γ was detected in the T cell compartment **(Figure 18b).** IL-18 was shown to work in concert with antigen, CpG , IFN-γ and IL-12 stimulation to induce differentiate of Naïve B cells and to some degree from MBCs into DN2 MBCs with Tbet, FcRL5, CD95, CXCR3 expression from tonsillar B cells in vitro[331]. IL-6 is important for generation of GC-TFH cells[354].These data suggest that signals for both types of responses may be present in HNSCC but additional factors may govern dominance of GC vs EF responses in patients.

Previous studies in SLE and HIV have highlight that DN2 cells arise from naïve B cells receiving EF signals, but it is not clear if DN3s are generated from naïve B cells via the EF pathway in cancer or how they arose in COVID-19 infection where they were first described. In some tumor types, including HPV- HNSCC the pool of naïve B cells is greatly diminished[36,121]. Persistent activation of resting SW MBCs $CD27^{+}CD21^{+}$ could potentially result in the DN3 phenotype as CD21 is downregulated upon activation and

CD27 can be cleaved by matrix metalloproteinases (MMPs) ,which have been shown to be elevated in several human cancers[355]. Indeed, patients with chronic infection, autoimmunity also have high plasma levels of soluble sCD27[356–359]. To gain insight into the origin and phenotype differences between DN3 MBCs and DN2 MBCs, we isolated SW MBCs, DN3 MBCs and naïve B cells from healthy donor spleen, and HNSCC PBL and stimulated with EF signals: IFN-γ, BAFF, IL-21, and TLR-7 with or without BCR stimulation using anti-Ig. We assessed frequency and phenotype of DN2 and DN3 generated from these parent populations. After 3 days, cells were also restimulated with just cytokines and TLR7 and harvested at day 7 to assess plasmablast (PB) differentiation , as previously described[283]**.** Total CD27+ MBC and Naïve B cells were isolated from a positive and negative selection kit, respectively, from HD PBL **(**Appendix Figure 15**)** and used in this assay. Magnetic isolation kits were used on HD PBL given the total cell demands (~200 million total cells) to acquire enough MBCs and low. Frequency of DN3 MBCs.

We first gated non-PB cells ($CD27^{+/-}$ $CD38^{+/-}$) and PB ($CD27^{hi}$ $CD38^{hi}$) from CD19+ cells **(Appendix Figure 15)** and then gated DN cells (CD27-IgD-). DN2 and DN3 MBCs were then gated using CD11c and CD21 **(Figure 19a).** We found that both SW MBCs, Naive B and DN3 MBCs cells could generate B cells with a DN2 phenotype (CD11c+CD21-) at comparable levels in HNSCC PBL but SW MBCs in spleen generated the most DN2 MBCs compared to Naïve or DN3 MBCs **(Figure 19b).** HNSCC PBL SW, DN3 and Naïve B cells generated fewer DN2s overall compared to HD spleen populations **(Figure 19b).** Co-stimulation of TLR7 and BCR is required generate high levels of DN2 MBCs in spleen and HNSCC PBL **(Figure 19b).** Naïve B cells produced more DN MBCs

with a DN3 phenotype (CD11c-CD21-) than SW MBCs in Spleen and HNSCC PBL **(Figure 19c).** A DN3 phenotype could be induced with or without antigen stimulation from naïve or SW MBC in HNSCC PBL, but BCR stimulation was required for Naïve B cells to produce high levels of DN3 in HD spleen **(Figure 19c).** PB's were more readily generated from SW MBCs at Day 7 but this was markedly reduced in SW MBC from HNSCC PBL **(Figure 19d).** Tbet and Tox expression in DN3 MBCs require co-stimulation of TLR7 and BCR but CD95, CD72 did not **(Figure 19e; Appendix Figure 15).** Taken together, these data suggest that Naïve B cells undergoing EF differentiation may be the primary source of circulating DN2 MBCs in cancer patients. SW MBC and Naïve B cells may generate DN3 MBCs in either a BCR independent and dependent manner. Incomplete EF signals may account for the accumulation DN3 MBCs in tumors and lack of DN2 MBCs as well as the variation in Tbet, TOX and IR expression in these subsets in cancer patients. In vitro derived DN2 and DN3 B cells share expression of Tbet, CD95 and CD72 as those detected ex vivo in patients. However, it is unclear if in vitro derived DN2 and DN3 B cells. are dysfunctional in the same manner as ex vivo DN2 and DN3 B cells.

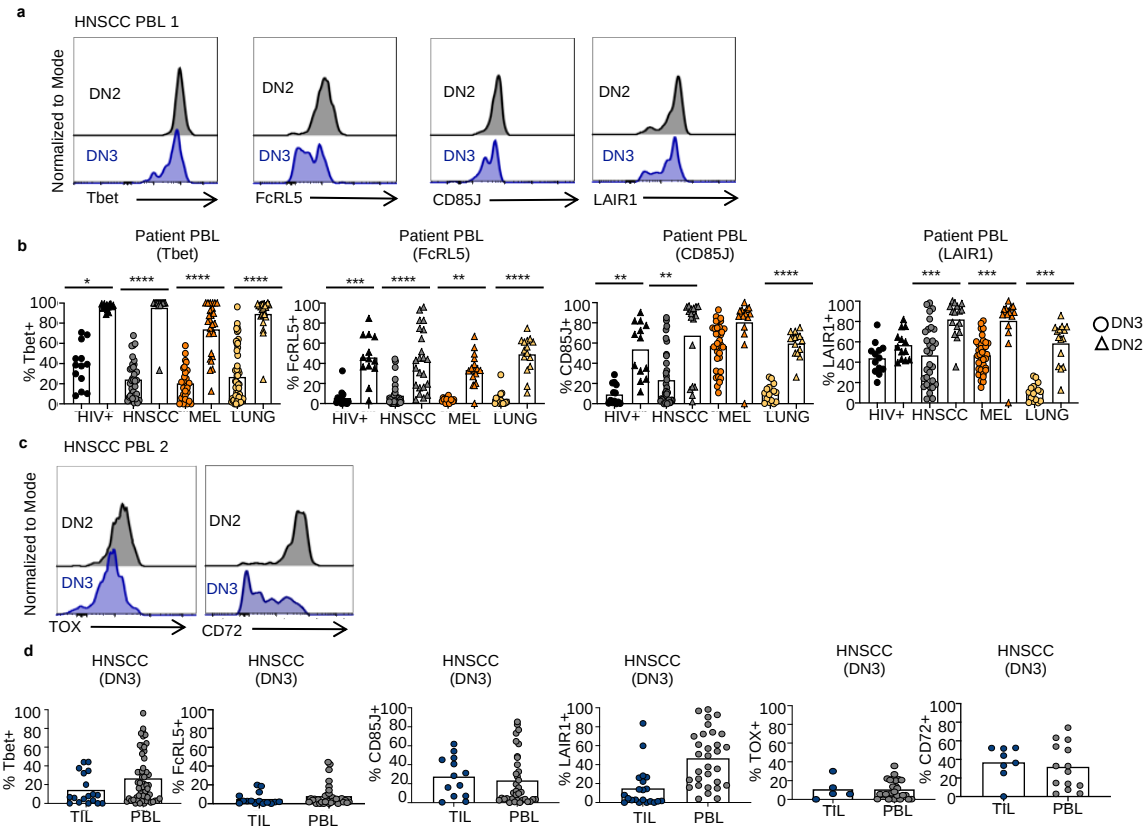


**Figure 17: Circulating DN3 and DN2 B cells in cancer patients co-express Tbet, Tox, and inhibitory receptors but intratumoral DN3 B cells do not**

**(a)** Representative histograms of expression of Tbet, FcRL5, CD85J, LAIR1 on extrafollicular B cell subsets. DN3 is overlaid in blue. DN2 is overlaid in black. **(b)** Quantification of Tbet , FcRL5, CD85J, LAIR1 on DN3 and DN2 in HIV+ PBL n=12, HNSCC PBL n=57, MEL PBL n=36 LUNG PBL n=23.*p=0.02,**p=0.009,***p=0.0002, ****p=<0.0001. **(c)** Representative histograms of expression of Tox and CD72 on extrafollicular B cell subsets. DN3 is overlaid in blue. DN2 is overlaid in black. **(D**) Comparison of Tbet, FcRL5, CD85J, LAIR1, TOX and CD72 on DN3 in HNSCC tumors n=18 and PBL n=57. For TOX. and CD72 a subset of HNSCC patients were stained: n= 5 (TIL) n=12 (PBL).

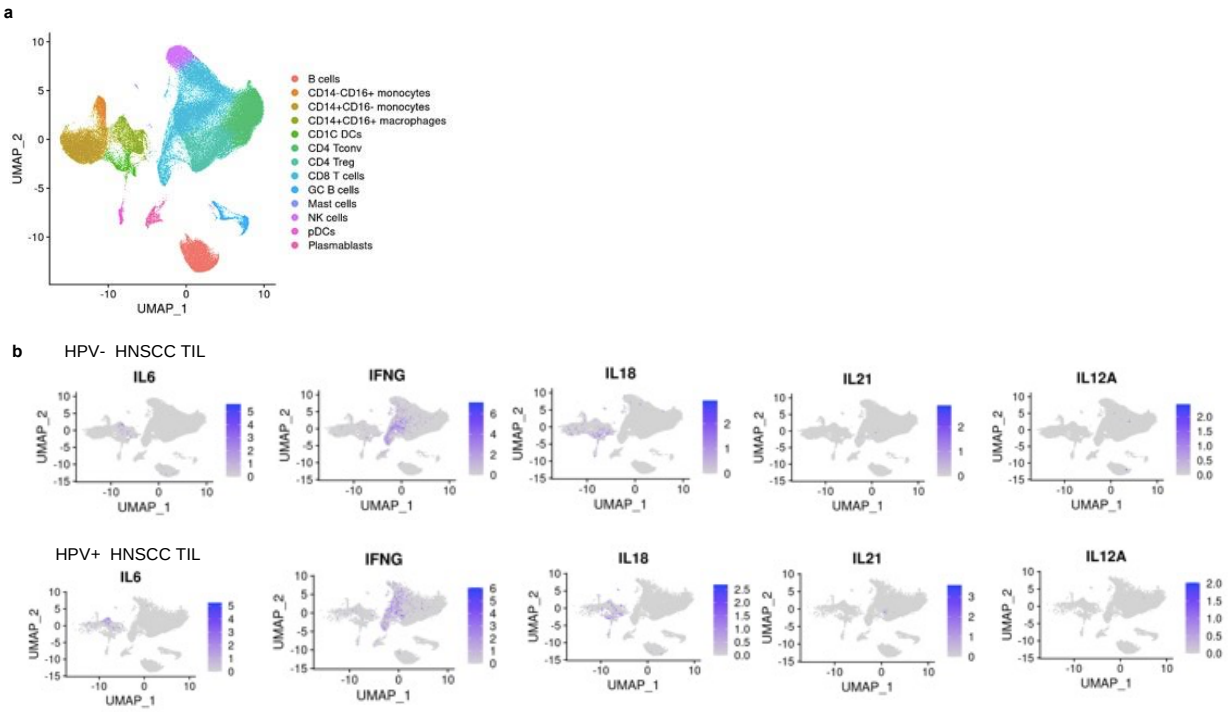


**Figure 18: scRNA seq analysis of cytokines in HPV+ and HPV- HNSCC tumors and PBL**

**(A)** UMAP projection of overall immune cell types in HNSCC. (**B)** Feature plots of IL-6, IFN-γ, IL-18, IL-21, and IL-12A in HPV- and HPV+ TIL.

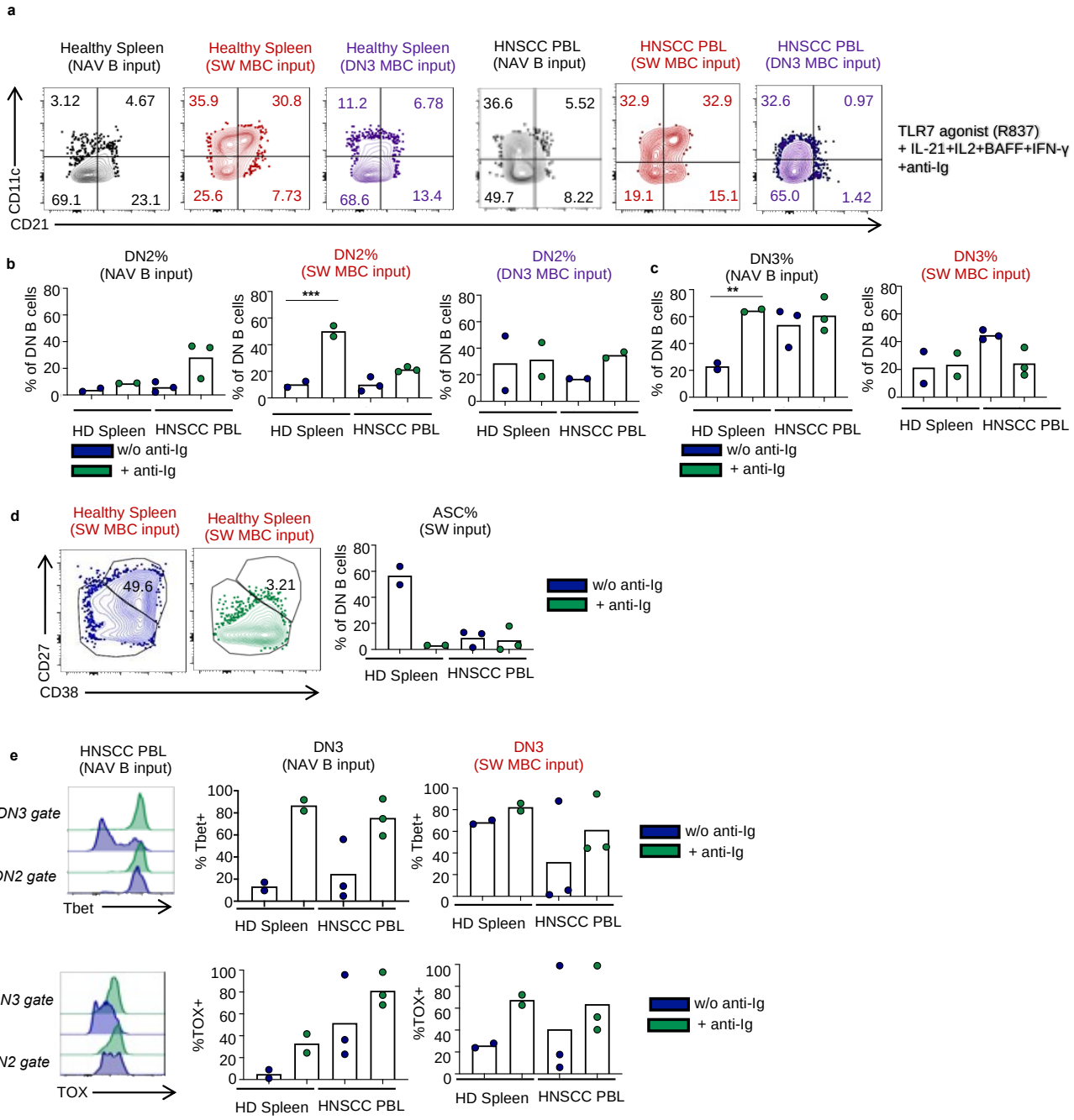


**Figure 19: TLR7 and cytokines induce differentiation of Naïve B cells and SW MBCs into DN3, DN2 and ASC in vitro**

**(a)** Representative flow gating strategy of DN3 and DN2 phenotypes in Healthy donor spleen (HD) and HNSCC PBL following stimulation of Naïve , SW or DN3 B cells with with TLR7 agonist (R837), recombinant IL21, IFN-y, IL-2 and BAFF with or without BCR sitmulation for 3 days. Stimulation with BCR (anti-Ig) is shown. **(b)** Quantification of DN2s generated from Naïve, SW or DN3 from HD spleen (n=2) and HNSCC

PBL (n=3). **(c)** Quantification of DN3s generated from Naïve or SW. **(d)** Representative flow gating strategy and quantification of plasmablasts (CD27hi CD38hi) in HNSCC PBL following stimulation of SW MBC with stimulation cocktail as described in (a). **(e**) Representative histgrams overlaying expression of Tbet and Tox, induced by the indicated stimulation condtions in cells from both DN2 and DN3 generated from Naïve B cells and quantification of Tbet, Tox in DN3 MBCs generated from Naïve and SW MBCs.

## 4.4 Discussion

In this study, we report expansion of a unique EF-associated MBC population (DN3), only previously identified in patients with severe COVID-19, in the periphery of cancer patients and its association with poor immunotherapeutic response. DN3 MBCs have markedly reduced effector function compared to GC derived MBCs which may be the result of active immunosuppression in the TME. DN3 MBC are more prevalent in HNSCC patients with HPV- tumors, suggesting that environmental factors in this TME may support EF differentiation over GC formation as DN3 MBCs are negatively correlated with GC-derived subsets. Intratumoral SW and DN3 MBCs display a similar isotype distribution suggesting that they may be exposed to some of the same extrinsic signals that induce isotype switching. Expression of IRs, Tbet and TOX are unique to DN3 and DN2 MBC. Our in vitro analysis of EF differentiation demonstrated that expression of IRs, Tbet and Tox require antigen stimulation, thus DN3 and SW MBC may have different antigen specificities, or they are exposed to factors that alter their expression profile in cancer patients. Our study supports further evaluation of environmental factors that lead to dominance of GC or EF maturation of B cells in cancer by tabulating the products of these pathways in tumors and peripheral blood in cancers that have unique microenvironments. Additionally, we provide a scoring system for assessing the ex vivo function of tumor-infiltrating B cells that provides a framework for future clinical evaluation of B cell subsets as immunotherapeutic targets **(Figure 20a).** Lastly, our work supports the concept of using the B cell compartment as a biomarker to monitor patient response to cancer therapies.

Mechanistic studies evaluating the direct effect of B cell effector function on tumor progression or clearance are currently lacking. However, we and others have provided evidence that B cells and TLS may support anti-tumor immunity as the absence of these in patients is associated with poor prognosis, higher risk of recurrence and poor immunotherapeutic response[122,195,210,213,293]. Within tumor-associated TLS, GCs form and produce local antigen specific ASCs[203,246,310]. In HNSCC patients with HPV+ tumors, antibodies are directed at HPV antigens and these ASCs are generated locally in tumors[246]. The absence of GCs in TLS in HNSCC is associated with poorer outcomes. In renal cell carcinoma (RCC), IgG-and IgA-producing ASCs disseminate into the tumor beds and TLS+ tumors have increased IgG-stained tumor cells and apoptotic tumor cells which correlated with survival and ICI response[310].These findings support the idea of developing B cell focused immunotherapies that bolster GC formation and TLS development which would be expected to improve anti-tumor immunity.

We provide further support of this notion in this study by assessing effector function of GC-derived MBC subsets from cancer patients. SW MBCs isolated from HNSCC tumors and PBL are responsive to antigen stimulation ex vivo, class switch to effector Ig isotype (IgG1) and can further differentiate upon stimulation. Intratumoral and circulating SW MBCs do not appear to be impeded by the suppressive TME like their T cell counterparts as they have intact mitochondria and low glucose avidity[338,340,343]. Additionally, there is little to no expression of inhibitory receptors on intratumoral or circulating SW MBC. While we assessed some effector functions of SW MBCs in cancer patients there are still many unanswered questions regarding our understanding of B cell function in the TME. B cells can also act as antigen presenting cells, produce cytokines

and induce TLS formation. Whether SW MBCs can present tumor antigen to $CD4^+$ or $CD8^+$ T cells in tumors remains unclear. Preliminary data from our lab has revealed that SW MBC isolated from healthy LNs, and patient tumors can present exogenous antigen to autologous CD4 T cells when stimulated with CD40 agonist in vitro **(**Appendix Figure 16**).** Future studies should assess the antigen presentation capabilities of tumor-associated GC derived MBCs. Further, it is not clear if SW MBC have the capacity to produce TLS -inducing factors such as LT and additional cytokines. While DN3 MBCs may have reduced BCR signaling and antibody production capabilities, they could potentially have other effector functions including antigen presentation, cytokine production, or a regulatory role that impact disease outcome.

Drivers of GC and EF B cell responses have not been well described in cancer. Intratumoral and circulating EF associated MBCs (DN3 and DN2) are more prevalent in HNSCC patients with HPV- tumors. This suggests that there may be factors in the HPV- TME that favor EF differentiation especially considering our previous data that shows that GC formation in HPV- disease is diminished but the mature B cell subsets are present. One confounding factor within the HNSCC TME is the presence of EF B cells could be driven by response to the local microbial environment as these tumors occur in mucosal tissues. BCR sequencing of SW and DN3 MBCs from HNSCC could determine if there are B cell clones that infiltrate tumors with BCR specificity to viral or bacterial pathogens as we identified both IgG1 and IgG2 + SW and DN3 MBCs in HNSCC patients.

The role of tumor-associated antigens (TAAs) including neoantigens or self-antigens in driving GC or EF fate decision by B cells is not well characterized and should be further evaluated. This could be addressed by determining tumor antigen specificity of

intratumoral and circulating SW and DN3 MBCs, clonal relationship of SW and DN3 MBCs in cancer patients. This will be important in determining whether EF B cell subpopulations have therapeutic value (tumor specificity; tumor reactive antibodies) and if their function should be rescued in the TME, or if the EF pathway should be instead antagonized in patients especially given our data that shows that EF B cells correlate with poor response. Recently, IgG tumor reactive antibodies against self-antigens (autoantibodies) were shown to be bound to tumor cells in situ in at least 34 tumor types including HNSCC and are also present in patient serum[360,361]. This study examined high-grade serous ovarian cancer (HGSOC) further and determined that autoantibodies directed at MMP-14 isolated from HGSOC patients could kill tumor cells, IgG1+ B cells and ASC were found in TLS-like structures and that the presence IgG coated tumor cells correlated with better survival. It is possible that SW and DN3 MBC in cancer patients could represent autoreactive B cell clones responding to self-antigens expressed on tumor cells in HNSCC. Whether the SW or DN3 MBCs were generated in the locally in the TME or recruited in from the surrounding normal tissue remains unclear but in situ detection of SW and DN3 MBCs in FFPE tissues could be used to determine their spatial location within the TME.

It's not yet clear why DN3 MBC in PBL have a different phenotype than those that infiltrate the tumor. One way to address this question would be to assess levels of soluble factors in patient plasma and serum such as cytokines and correlate these with the quantity and phenotype of circulating DN3 MBC. There may be novel tumor-associated markers expressed on intratumoral DN3 MBCs that provide insight into their origin and potential function in the TME that are not yet appreciated**.** Future studies should assess

differential gene expression between intratumoral and circulating DN3 MBCs in cancer. This may be best achieve by performing Cellular Indexing of Transcriptomes and Epitopes by Sequencing (CITE-seq) on B cells from cancer patients. Whether EF B responses have a negative impact on the TME remains unclear. However, our data suggest that having more EF responses may be reflective of poor disease control as patients who have higher tumor stage and exhibit disease progression following treatment have more intratumoral and circulating EF B cells. Pre-clinical modeling of GC and EF B cell responses in cancer should be prioritized as this will help clarify the impact of B cells on tumor growth and immune-mediated clearance.

In conclusion, we provide insights into the functional role of B cells within the TME by comparing BCR responsiveness, metabolic fitness, isotype distribution, differentiation and antibody production in distinct B cell subsets that are generated from distinct maturation pathways. Our study suggests that bolstering GC maturation of B cells in the TME may be a viable therapeutic option that complements ICI. We provide further rationale for using the B cell compartment as a biomarker to monitor tumor progression in response to therapy.

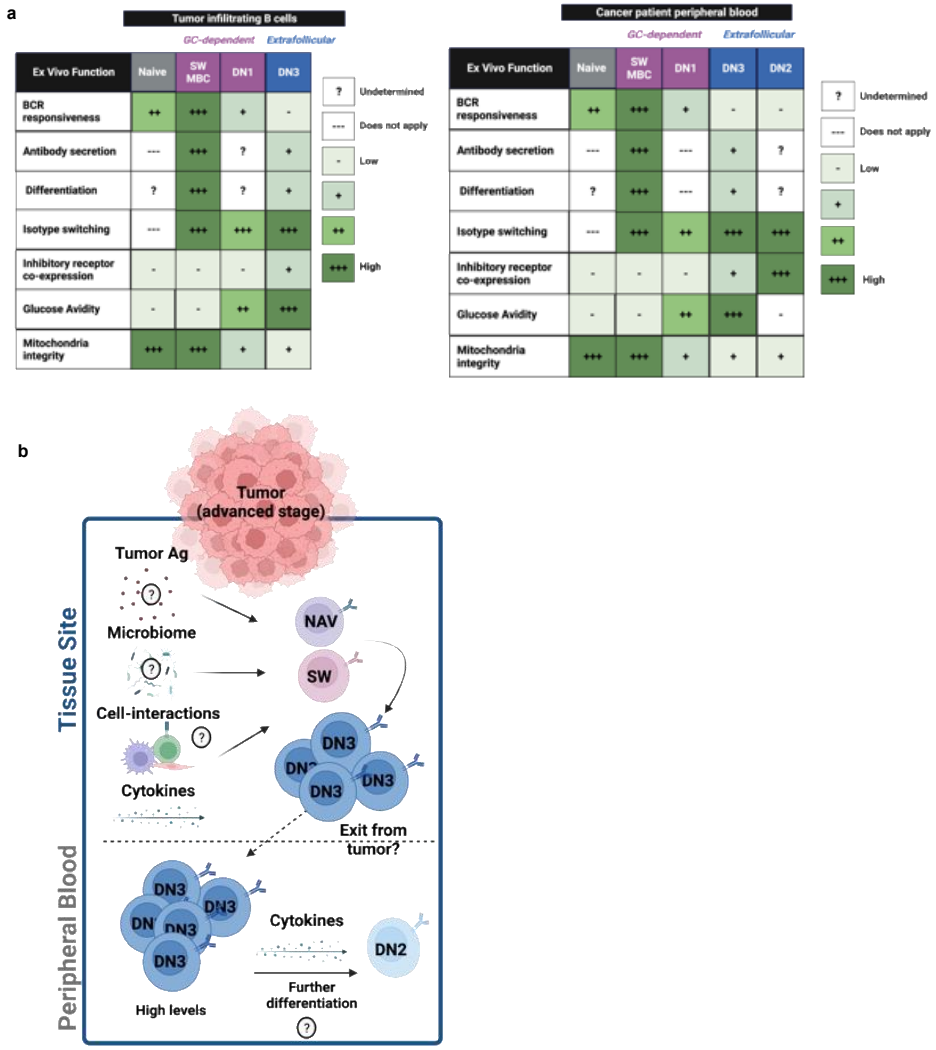


**Figure 20: Summary of ex vivo function and proposed origin of EF MBC subsets in cancer**

**(a)** Chart depicting functions of memory B cells (MBC) evaluated in our in vitro functional assays for intratumoral (left) and circulating memory B cell subsets (right). **(b)** Summary figure depicting a proposed orgin of DN3 and DN2 MBCs in cancer patients. Antigens from tumor or local microbiome , cytokines from local T cells and Myeloid cells could potentially induce extrafollicular differentiation of Naïve or SW MBCs into DN3 MBCs. Lack of additional signals may prevent further differentiation into DN2s or ASC. DN3 MBCs may migrate from tumor due to systemic inflammation in cancer patients and further differenentiate into DN2 MBCs in some patients. Created in Biorender.com

## 4.5 Author contributions

ATR and TCB conceived the project. TCB and ATR obtained funding. ATR, and TCB, DAAV interpreted data and wrote the manuscript. ATR, FK, AR, SRK performed flow cytometry experiments and analyzed flow cytometry data. ARC performed scRNAseq experiments and bioinformatic analysis, ATR and SRK performed in vitro functional assays. AS, RLF, GR, JK, UD provided clinical samples and helped with clinical correlate analysis.

## 5.0 Future directions

Portions of this section (5.1.1) were compiled and published in the second edition of *Cancer Immunotherapy: Principles and Practice* in the following book chapter *Cancer:*

**Ruffin AT**, Bruno TC. Harnessing B cells and tertiary lymphoid structures for antitumor immunity. In: Butterfield LH, Kaufman HL, Marincola FM, Ascierto PA, Puri RK, eds. Cancer immunotherapy principles and practice. New York, NY: Springer Publishing Company; 2021. doi:10.1891/9780826137432.0042. Copyright license ID (1223908-1)

## 5.1 Summary

My dissertation work expands our understanding of how different TMEs impact the composition of B cells within tumors, their function and the clinical significance of B cell maturation and TLS formation in cancer. Further, I have identified key biomarkers of functional and dysfunctional B cell subsets and correlated these subsets with patients' therapeutic responses and survival. I demonstrate the importance of GC presence in TLS and the relevance of GC-independent B cell maturation via the extrafollicular pathway in cancer. Briefly, the composition of B cells is distinct when comparing tumors from HNSCC patients with HPV+ vs HPV- tumors. GC and TLS occur more frequently in HPV+ patients and are associated with better survival. TLS w/GC frequency is reduced in HNSCC patients with recurrent disease which further highlights the importance of GCs and TLS in anti-tumor immunity. EF-associated MBCs (DN3 MBCs) correlate with advanced tumor stage in HNSCC and poor immunotherapeutic response in melanoma, which may be indicative of worse disease control as these cells accumulate in the blood of HNSCC, melanoma and lung cancer patients. EF MBCs are dysfunctional in HNSCC, while GC derived MBCs retain effector function. I provide further rationale that supports using the B cell compartment to define additional biomarkers for monitoring cancer progression and that these may represent a new immunotherapeutic target. In this section, I summarize the effects of current immunotherapeutics on B cells to provide a platform to develop future treatment regimens targeting B cells for therapeutic gain.

### 5.1.1 B cell-based immunotherapy: The next generation

Given the strong correlation between TIL-B cells and TLS with patient survival in many cancers and response to current immunotherapies, I would argue that it is important to consider the B cell compartment in the design of new cancer immunotherapies. It will be critical to first develop preclinical models that can assess the direct effect of B cell and TLS presence on tumor clearance and or progression. Therapeutically enhancing antitumor functions of B cells and/or blocking/depleting immunosuppressive B cell populations in tandem with T cell targeting strategies could be beneficial for patients. Further, rescuing B cell populations whose function may be impaired by the TME may also be a viable therapeutic option. Lastly, inducing TLS formation in patients with immunologically “cold” tumors could enhance responses to current immunotherapies. The current evidence suggest that the B cell compartment could be used in addition to T cells to inform decisions on which patients should receive immunotherapy. There’s also emerging evidence that suggest that traditional cancer treatments such as chemotherapy, radiation and hormone therapies can impact B cells and TLS. Future studies should continue to evaluate the effects of current cancer treatments on B cells. I would assert that the B cell compartment could be used to assess and help generate chemotherapy drugs that induce immunogenic cell death in tumors and immunogenic modulation of tumors which would result in increased tumor clearance by the immune system. I would propose that leveraging current therapeutic modalities such as monoclonal antibodies (mAb), adoptive cell therapy (ACT), cytokine-based therapy, and cancer vaccines to target B cells and induce TLS formation would be a great starting point.

#### 5.1.1.1 Effects of current therapies on B cells

Standard of care treatments for cancer patients including radiation, chemotherapy, and hormone therapies have all been shown to impact antitumor immunity[362–364]. These studies have been largely focused on T cells, but B cells and TLS can also be affected. For example, corticosteroids are often given to LUSC patients treated with chemotherapy to manage side effects, however, TLS density is greatly impaired in chemotherapy-naïve LUSC patients treated with corticosteroids before surgery[210]. Notably, in chemotherapy-treated LUSC patients, TLS density was similar to untreated patients, but GC formation was significantly impaired[210]. In patients with HGSOC metastases, chemotherapy enhanced MBC cell responses[365]. Radiotherapy enhanced activation of B cells , GC formation and increased tumor-specific B cell and PC differentiation in a murine model of HNSC[196]. More studies should assess the changes that B cells and TLS can undergo following standard therapies as these could be leveraged in combinatorial treatments with immunotherapies directed at B cells.

Therapeutic monoclonal antibodies (mAbs) targeting the PD1/PDL1 pathway have had remarkable success in cancer patients. While blocking this pathway on T cells enhances antitumor responses in patients, the effects of anti-PD1 and anti-PDL1 mAbs have been severely understudied in the context of B cell responses in tumors. Both human and murine B cells express PD1 and PDL1[276,366–368]. There is a basal level of PD1 on resting B cell populations (naive and MBC) within non-diseased PBL and lymph node and is significantly upregulated after stimulation[366]. In HCC, PD1 marks an immunosuppressive B cell population that suppress $CD8^+$ T cell responses[276]. Recently, we learned that B cell and TLS correlate with superior response to anti-PD1 therapy in

MEL, RCC and STS patients, although it is not clear if anti-PD1 is acting directly on B cells[122,158,195]. PD1 is also expressed on TFH cells and is important for GC B cell survival and differentiation into PC[116,369,370]. PDL1 is also used to mark $B_{reg}$ subsets in many tumors and non-diseased tissues[186,371,372]. In HNSCC, anti-PDL1 enhanced B cell antibody responses, GC formation, and B cell clonality in mice and antibody responses in patients who responded to ICB[196]. Thus, more studies should assess direct effects of ICB, especially anti-PD1 and anti-PDL1 on TIL-Bs in patients.

#### 5.1.1.2 How do we target B cell and TLS as a form of immunotherapy?

There is overwhelming evidence that TLS may support antitumor responses and patients without TLS have overall poor prognosis and are non-responsive to ICB[122,156–158,309]. However, it is not yet clear why TLS form in some patients and not others. Extensive studies in mice and human models of infection and autoimmune disease reveal the key events needed for TLS formation, including: (1) inflammatory cytokine expression, (2) lymphoid chemokine production by stromal cells, and (3) HEV development[156,157,159,373]. Developing therapies that can initiate one or more of these events in patients without TLS could be a promising new avenue for therapeutic intervention. Inducing inflammatory cytokine expression could be accomplished using stimulator of interferon response cGAMP interactor 1 (STING1) agonists (Figure 34.3)[374–376]. STING1 is an endoplasmic reticulum (ER) resident protein important for sensing cytoplasmic double-stranded DNA (dsDNA) during viral and bacterial infection and promoting type 1 interferon gene expression (IFN-α/β, IL-6 TNF-α) through canonical and non-canonical NFκB signaling pathways[374–376]. There are at least 15 STING agonists being investigated in clinical trials as single agents and in combination with ICB for

treating cancer patients due to the success of STING agonists to promote antitumor activity in pre-clinical models[374–376]. Type 1 IFNs regulate chemokines such as CXCL13 which are important for TLS formations, which suggests that STING agonists could be used for TLS induction[71,377]. Indeed, in vivo models using STING agonists to induce TLS are being developed[378].

Tumor necrosis factor superfamily member 14 (TNSF14) or LIGHT is an activation inducible inflammatory cytokine homologous to lymphotoxins that binds to herpesvirus entry mediator (HVEM) and LTβR. LIGHT provides costimulation to T cells via HVEM and can induce SLO formation through LTβR signaling[379,380]. Further, activated $CD4^+$ and $CD8^+$ T cells, NK cells and monocytes can also express membrane-bound LIGHT, suggesting it also has immunomodulatory functions[379]. Additionally, LIGHT can enhance CD40L costimulation of B cells whereby it increases IgM and IgG production and proliferation of naïve and MBCs which express HVEM[381]. In a murine model of spontaneous pancreatic neuroendocrine tumors, LIGHT fused to a vascular targeting peptide (VTP) was used to study de novo TLS formation[382]. VTP aided in targeting delivery of LIGHT to angiogenic tumor blood vessels. LIGHT-VTP fusion protein was able to normalize blood vessels, enhance immune cell infiltration, and induced TLS formation[382]. Thus, LIGHT could be a potential pathway for TLS induction in patients.

Recombinant cytokines, IFN-α (rIFN-α) and IL-2 (rIL-2), were some of the first FDA approved immunotherapies to treat several malignancies[383]. Given the potent antitumor activity of these pro-inflammatory cytokines and their role in TLS formation and maintenance, delivering specific TLS-associated cytokines to the TME could be used to induce TLS in patients. rLT-α and rTNF-α can induce chemokine expression (CXCL13,

CCL19, CCL21) in stromal cells and macrophages which is important for recruiting immune cells[71,156,164,300]. rIL-21 and rIL-7 could potentially play an important role in GC formation, B cell differentiation, and $T_{FH}$ development within the TME and TLS[75,384,385]. Several clinical trials are ongoing to assess rIL-21 and rTNF-α in combination with other cancer therapies and ICB[383]. One key consideration for TLS inducing therapies will be also developing delivery vehicles that can deliver therapies to the TME and minimize off target effects and toxicities that can be associated with cytokine mediated inflammation. Additionally, future therapies will need to consider how to induce GC formation over EF differentiation (if desirable) within TLS. As previously discussed, GC formation within TLS correlates with better survival in HPV+ and HPV- HNSCC patients. However, products of the EF differentiation pathway (DN2 and DN3 B cells) are associated with more advanced disease particularly in HPV- HNSCC. A major question, which was posed in chapter 4, is what antigens in the TME lead to GC formation over EF differentiation in tumors? Given that GCs do not form readily in all tumor types, is EF differentiation of B cells sufficient to generate mature B cells? One experiment that could be done to elucidate this would be to identify what antigens are recognized by the B cell receptor (BCR) from B cell subsets (SW, DN3, DN2) in both HPV+ and HPV- HNSCC tumors and peripheral blood. It may be that products from GC vs EF pathways have an entirely distinct BCR repertoires within these two patient cohorts. If true, this would suggest that BCR stimulation through cancer associated antigens or microbial-associated antigens may be drivers of EF over GC responses and vice versa in cancer patients. This experiment would also allow one to assess the replication histories and levels of SHM to determine if activation of the EF pathway in cancer can produce affinity matured B cells. This finding would help determine

the relevance of this differentiation pathway for B cells in cancer. New spatial transcriptomic platforms 10X Visium and Nanostring DSP may allow researchers to identify genes and pathways that are important for GCs or EF differentiation in TLS within tumors[386,387]. Further, scRNA seq of DN3 MBCs could identify uniquely expressed markers that may be of therapeutic value.

Adoptive cell therapy (ACT) is a form of cellular immunotherapy that harnesses the natural ability to T cells to kill tumors, by isolating and reinfusing T cells to patients after (1) expanding naturally occurring tumor-specific T cells, (2) engineering T cells to have a TCR directed at specific tumor antigens (3) or creating a chimeric antigen receptor (CAR) that can bypass the need for tumor antigens to be presented on MHC[388]. There is evidence suggesting that ACT mechanisms could be employed with B cells to harness their ability to present tumor antigens, potentially directly kill tumor cells, and generate long-lasting protective tumor-specific antibodies[389]. The CD40L/CD40 signaling pathway is a key stimulator of the antigen presentation capacity in B cells[127,175,179,390]. Ligation of CD40 increases B cell proliferation and expression of costimulatory molecules (CD86, CD27, MHC molecules)[179,297,389,391]. There are several studies that show that antigen presenting B cells can be generated from PBL using CD40 agonistic antibodies, soluble CD40 ligand, and CD40L expressing cell lines[389]. In fact, a few early-stage clinical trials have shown that CD40- activated B cells could be used in ACT in RCC and metastatic MEL[392,393]. B cells are isolated from PBL, activated and expanded in a CD40L culture, pulsed with tumor antigen and reinfused into the patient[389]. In addition to CD40 activation, TLR-9 agonists (CpG ODN) can induce antibody production and B cell differentiation when coupled with cytokines (IL-2, IL-10, IL-15) which could be used to enhance tumor-

specific antibody production by B cells[394,395]. When coupled with IFN-α, TLR-9 agonist can induce expression of functional TRAIL on B cells, which could license B cells with cytotoxic capabilities as an ACT[192]. Lastly, CRISPR/Cas9 technology could potentially be used to engineer B cells from patients to express BCRs to different tumor-specific antigens and subsequently be used as an B cell-based ACT/vaccine. This technique has already been developed and employed to generate pathogen-specific antibodies to respiratory syncytial virus (RSV) that protect against re-infection in mouse models and can be used on human primary B cells from blood to produce RSV-specific antibodies[396]. In this technique, CRISPR/Cas9 technology replaces endogenous membrane antibody, with an engineered monoclonal antibody (emAb) that recognizes RSV antigens[396]. These emAb engineered B cells can also be expanded using traditional methods and PC differentiation can also be induced[396].

With anti-CTLA4 and anti-PD1 mAbs only being successful in a subset of patients with certain forms of cancer, development of new mAbs targeting other immune checkpoints as well as costimulatory molecules have been prioritized for translation into the clinic. While most of these are still T cell and tumor cell focused, markers of interest such as CD27, PDL1 and CD73 are also expressed on B cells and could be leveraged in B cell-based immunotherapies. CD27 is expressed on MBC subsets and is important for B cell differentiation and antibody production. Two CD27 therapeutic agonistic antibodies have been developed and are in current clinical trials: Varlilumab (anti-CD27) and CDX-527 (anti-CD27 and anti-PDL1bispecific) have shown efficacy in boosting T cell responses in solid tumors, however, effects on B cells with these therapies has not yet been reported[397,398]. Additionally, other molecules that are in clinical trials that are also

important for B cell activation, antibody production and proliferation and could affect B cells include CD73 (CPI-006), CD319 or SLAMF7 (elotuzumab)[399–404]. Pathways that inhibit B cell function could be considered for the development of new B cell therapeutics such as inhibitory receptors unique to B cells including CD72, FcRL4 and FcRL5, CD22, which could rescue dysfunctional B cell populations[344,405,406]. We showed in this thesis that IRs CD72, FcRL5 mark DN3 and DN2 MBCs and these populations are dysfunctional in HNSCC. Future studies could explore using blocking antibodies to specific IRs to rescue B cell functions in these cells such as BCR signaling, antibody production and differentiation into ASC. Sema4a/NRP1 axis is currently being investigated in the clinic in the context of intratumoral $T_{regs}$[407].We showed that Sema4a expressed on B cells during activation but its role on intratumoral B cells has yet to be explored. It is not clear whether Sema4a on GC intratumoral B cells is playing a role in interactions with $T_{FH}$ or $T_{regs}$ or both in the TME of HNSCC as both can express NRP1. It is also not yet clear Sema4a expression is a feature of GC intratumoral B cells in other human cancers which could be easily determined by mining scRNA seq data from other tumor types. Additionally, Tregs are not a prominent feature in TLS in human tumors, but they are present in TLS a mouse model of LUAD[408]. Sema4a can enhance CD4 T helper 2 polarization of Naïve $CD4^+$ T cells stimulated in Th2 skewing conditions. Future studies should assess the role of Sema4a in polarization of TFH and or Tregs. This could be done using in vitro assays that co-culture Sema4a + B cells or APCs with Naïve CD4+ T cells and phenotyping $T_{regs}$ vs $T_{FH}$ signatures and cytokines. **(**Figure 21**).**

Early murine models led researchers to believe that intratumoral B cells only promoted tumor progression with no role in the antitumor response. However, as reviewed here, intratumoral B cells and TLS may support antitumor responses in humans and correlate with better overall survival and therapeutic response. The increased heterogeneity of B cells within tumors should be further explored across tumor types to determine which B cell subsets can support antitumor function by T cells. Antigen specificity of intratumoral B cells remains poorly understood but several methods exist to explore this further. Whether antibodies from intratumoral B cells have antitumor capabilities is a major knowledge gap for the field. Linking intratumoral B cell phenotypes to antigen presentation function, tumor-specific antibody production and cytokine production will aid in the development of B cell-based therapies. It will be paramount to prioritize further studies to investigate the role of B cells and TLS in vivo to better understand how to coordinate B and T cell immune responses using immunotherapy. This will hopefully ensure more patients can benefit from cancer immunotherapy.

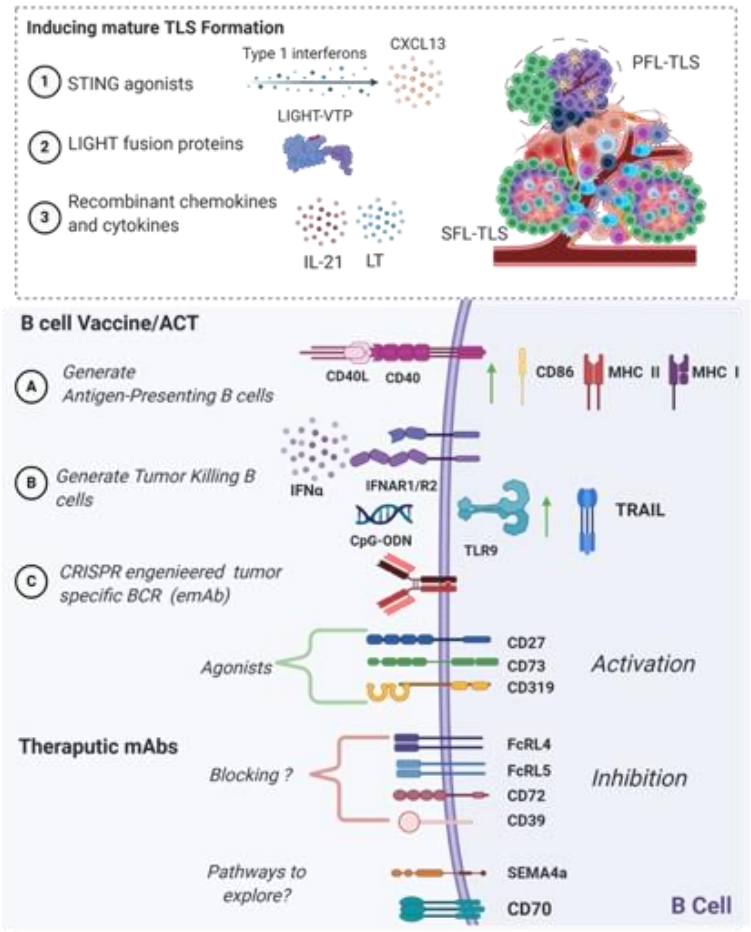


**Figure 21: Targeting B cells and TLS for cancer immunotherapy**

B cell /TLS axis may provide new and exciting avenues for developing B cell-based immunotherapies. This schematic list potential mechanisms that could be leveraged for future therapeutics. Inducing TLS: (1) STING Agonists: Compounds that can induce activation of the STING pathway (stimulator of interferon genes) are being investigated as a potential immunotherapy as this pathway leads to induction of type 1 interferons and promote antitumor immunity through T cell s in pre-clinical models. Type 1 interferons also regulate chemokines and cytokines important for TLS formation suggesting this pathway could be leveraged to induce TLS. Using STING agonist for inducing TLS is an active area of research. (2) LIGHT fusion protein: Tumor necrosis factor superfamily member 14 (TNFSF14) or LIGHT is a secreted protein important for TLS formation. Fusing LIGHT to vascular targeting peptide (VTP) allowed for de novo TLS formation in solid tumors in mice. (3) Recombinant cytokines/chemokines : Delivering recombinant

cytokines that are important for TLS formation and maintenance such as lymphotoxin , IL-21, IL-7 to tumors without TLS could induce TLS in these patients. IL-21 is important in regulating GC reactions and B cell differentiation and thus could be used to mature TLS in patients. Recombinant IL-21 as an immunotherapy is actively being investigated in clinical trials. B cell Vaccines/ Adoptive Cell Therapy: (A) Generating Antigen presenting cells: Activating B cells from patient tumors or blood via CD40, pulsing these CD40-activated B cells with tumor Ag and then transferring them back to the patient as an ACT. (B) Generating Tumor killing B cells: Activating B cells isolated from patient tumors or blood via CpG-ODN (TLR-9 agonist) and IFN-α which induce TRAIL expression on B cells and then transferring them back to patient as ACT. (C) CRISPR engineering tumor specific BCRs: Using CRISPR cas 9 technology to engineer B cells and plasma cells to target specific tumor Ag to use as a B cell vaccine. Therapeutic mAbs: Leveraging current immunotherapies that target activation pathways in B cells. mAb against CD27, CD73, CD319 are actively being investigated in clinical trials to target other immune cell types but are also important for B cell function. Sema4a and CD70 have not been well investigated in the TME for B cells but are also important for B cells in normal tissues. Developing new mAbs to targeting pathways that inhibit B cell function or are immunosuppressive

# Appendix A

## B cell signatures and tertiary lymphoid structures contribute to outcome in head and neck squamous cell carcinoma

This was a collaborative project with many members of the Vignali, Bruno, and Ferris labs. I was an equal contributor along with Dr. Anthony Cillo. This work was published in *Nature Communications* in 2021. Supplementary data tables and figures referenced in Chapter 3 are provided in this appendix.

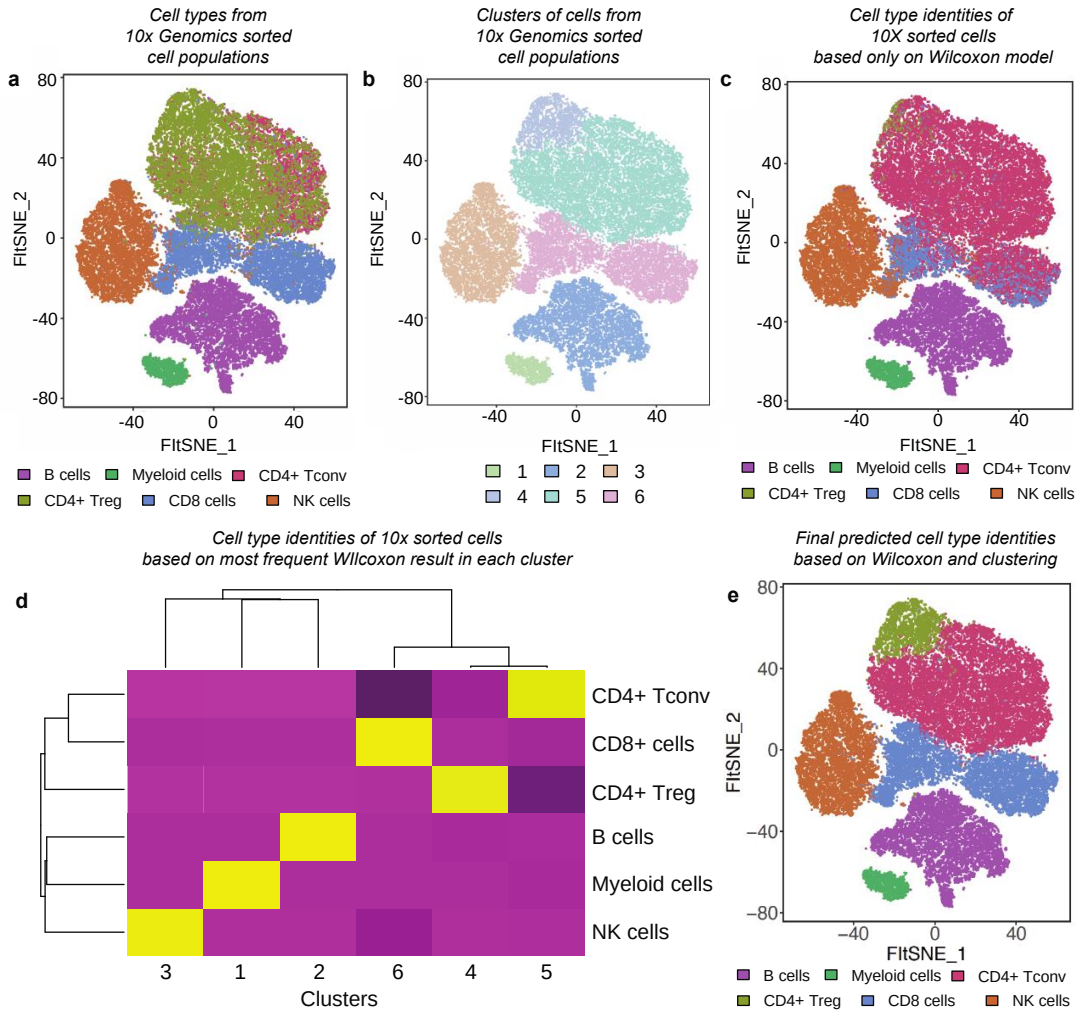


f

*Metrics of cell type predictions from Wilcoxon and clustering model using sorted cells from 10X Genomics*

| | B cells | Myeloid cells | CD4+ Tconv | CD4+ Treg | CD8+ cells | NK cells |
|---|---|---|---|---|---|---|
| Sensitivity | 1.000 | 0.987 | 0.976 | 0.928 | 0.990 | 0.985 |
| Specificity | 0.999 | 1.000 | 1.000 | 1.000 | 0.981 | 0.997 |
| Pos Pred Value | 0.997 | 0.996 | 1.000 | 1.000 | 0.926 | 0.987 |
| Neg Pred Value | 1.000 | 1.000 | 0.987 | 0.995 | 0.998 | 0.997 |
| Prevalence | 0.191 | 0.032 | 0.354 | 0.068 | 0.194 | 0.161 |
| Detection Rate | 0.191 | 0.031 | 0.346 | 0.063 | 0.192 | 0.158 |
| Detection Prevalence | 0.192 | 0.031 | 0.346 | 0.063 | 0.208 | 0.161 |
| Balanced Accuracy | 1.000 | 0.993 | 0.988 | 0.964 | 0.986 | 0.991 |

**Appendix Figure 1: Validation of a combination Wilcoxon rank sum test and clustering based method for identification of cell types**

Publicly available data from sorted populations of immune cells was combined, and a classification algorithm was employed to identify cells types. **a.** FItSNE plot of combined purified B cells, CD14+ monocytes, CD4+ helper T cells, CD4+ Treg, CD8+ T cells, and CD4+ regulatory T cells. **b.** Same FItSNE

plot as (a), but showing clustering results. Clusters were strongly associated with cell types of purified populations. CD4+ Treg, despite overlapping with CD4+ Tconv as a purified population, were strongly associated with cluster 5, suggesting that the sorted population of CD4+ Treg were mixed with CD4+ Tconv. **c.** Raw results from testing of the Wilcoxon rank sum from known cell populations. Individual cells were scored for enrichment of markers associated with each purified cell population. Some clusters were readily identifiable as pure populations using just the Wilcoxon based enrichment, but mixtures of T cells were evident. **d.** Heatmap showing the association between inferred lineage type from the Wilcoxon rank sum scores and the clusters. Each cluster largely consisted of a major lineage when looking at the aggregate Wilcoxon rank sum test across clusters. **e.** Inferred cell types based on the association between Wilcoxon scores and clusters from (d). Cell type inference agreed strongly with results of clustering from (b). **f.** Confusion matrix comparing the inferred cell types to the ground truth. The sensitivity, specificity, and accuracy were between 0.93 and 1.0 for all lineages.

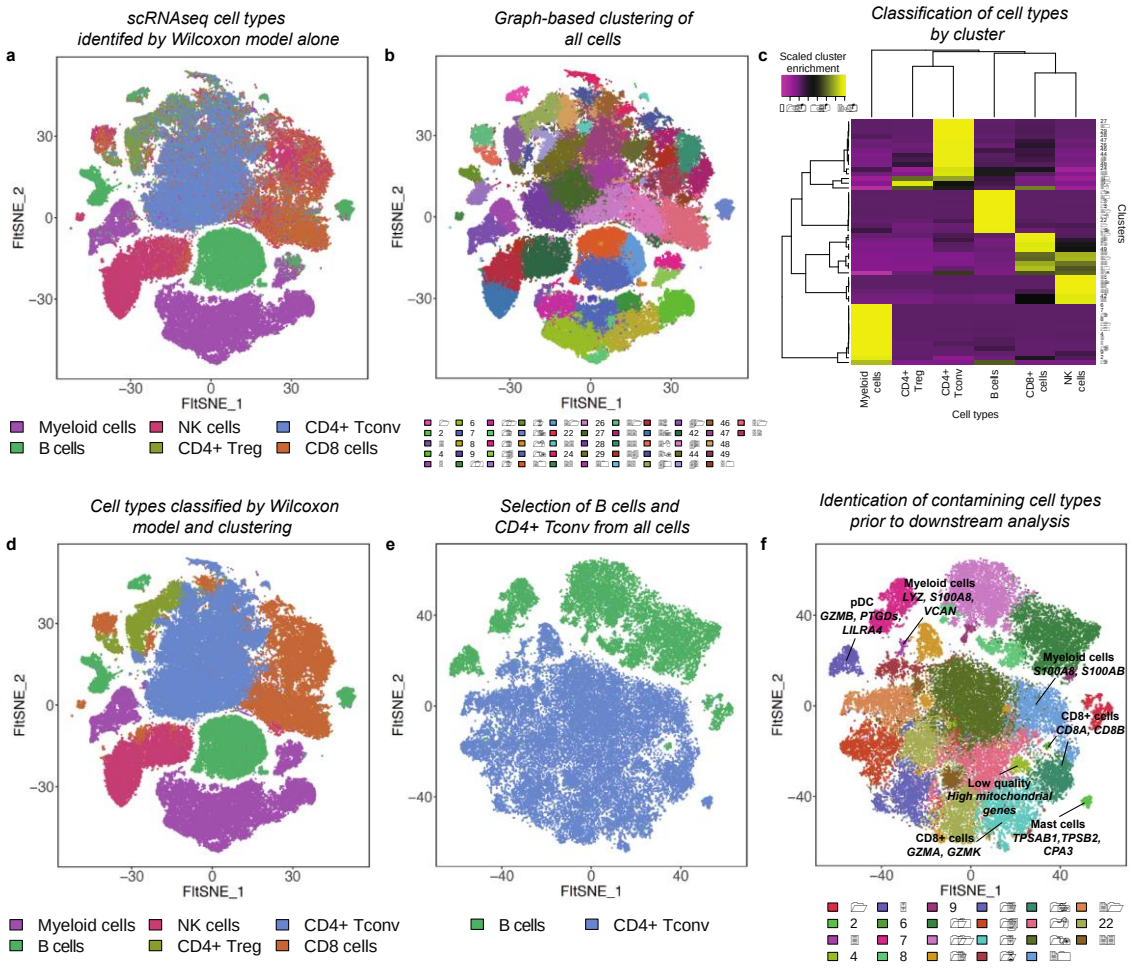


**Appendix Figure 2: Identification of cell types from patients and controls using the combination Wilcoxon rank sum test and clustering based approach.**

**a**. Raw results from the Wilcoxon scores derived for each individual cell. Certain populations are highly accurately inferred from this first step, while others exhibit mixtures of cell types. **b**. Results of Louvian clustering revealed a total of 52 clusters from all the cells in the dataset. **c.** Heatmap showing the relationship between cluster and inferred cell types from (a) and (b). **d.** Results of the combination of Wilcoxon scoring and cluster association from (a-c). Major lineages are grouped together in FItSNE space, allowing the isolation of B cells and CD4+ Tconv for downstream analysis. e. B cells and CD4+ Tconv were bioinformatically isolated from D) and were projected in a new FItSNE space and colored by their inferred cell types. **f.** Identities of cell clusters were cross-checked by investigating differentially expressed genes across lineages. Contaminating lineages (i.e. those that are not B or CD4+ Tconv) and cell types that were

not present in the training dataset (e.g. plasmacytoid dendritic cells [pDC], mast cells) were identified and removed, leaving only highly purified B and CD4+ Tconv for downstream analysis.

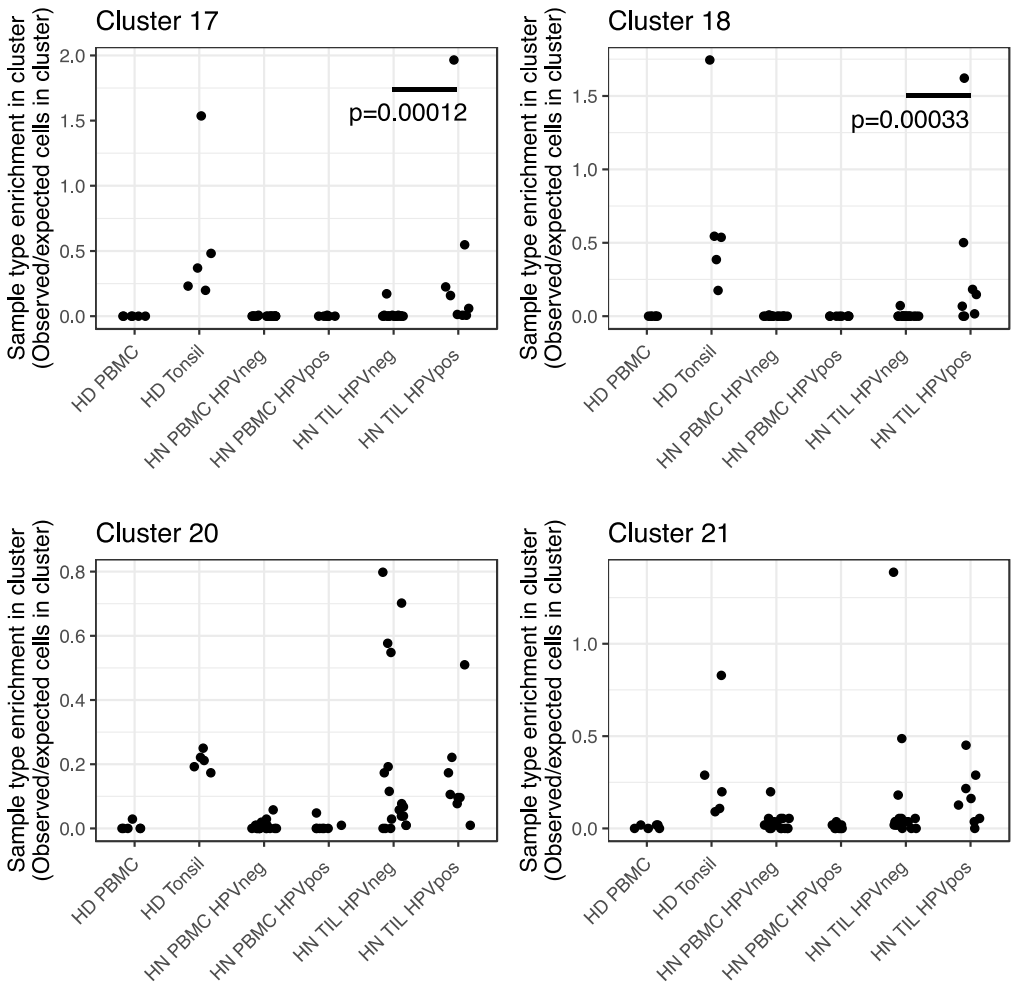


**Appendix Figure 3: Statistical assessment of observed versus expected number of cells in germinal center and plasma cell clusters.**

We first performed ANOVA tests to determine if there were differences between patient groups in a given cluster, and we found that clusters 17 ($p=0.00033$), 18 ($p<0.0001$) and 20 ($p=0.0025$) had at least one group that was different, while cluster 21 did not ($p=0.067$). Within clusters 17, 18 and 20 we tested whether there was any difference between TIL samples from HPV– versus HPV+ patients by Wilcoxon rank sum test and found that there were significantly higher frequencies of germinal center B cells in clusters 17 and 18. There was no different between HPV– versus HPV+ patients in for plasma cells in cluster 20.

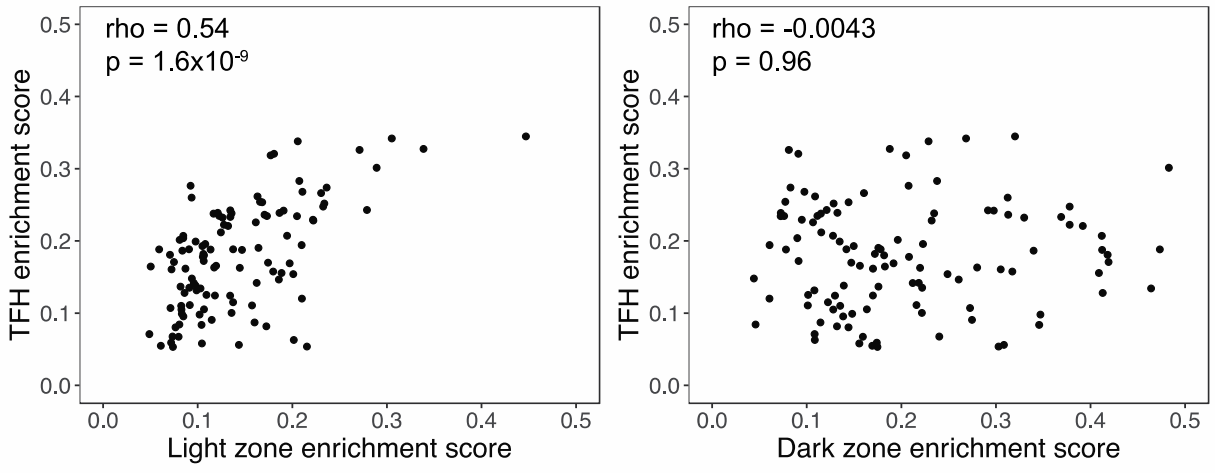


**Appendix Figure 4: Relationship between germinal center cell states and TFH cells in samples from The Cancer Genome Atlas.**

Light zone B cells were significantly correlated with TFH cells (left panel), but there was no relationship between dark zone B cells and TFH cells (right panel). Spearman's correlation was used, and p values are two-tailed.

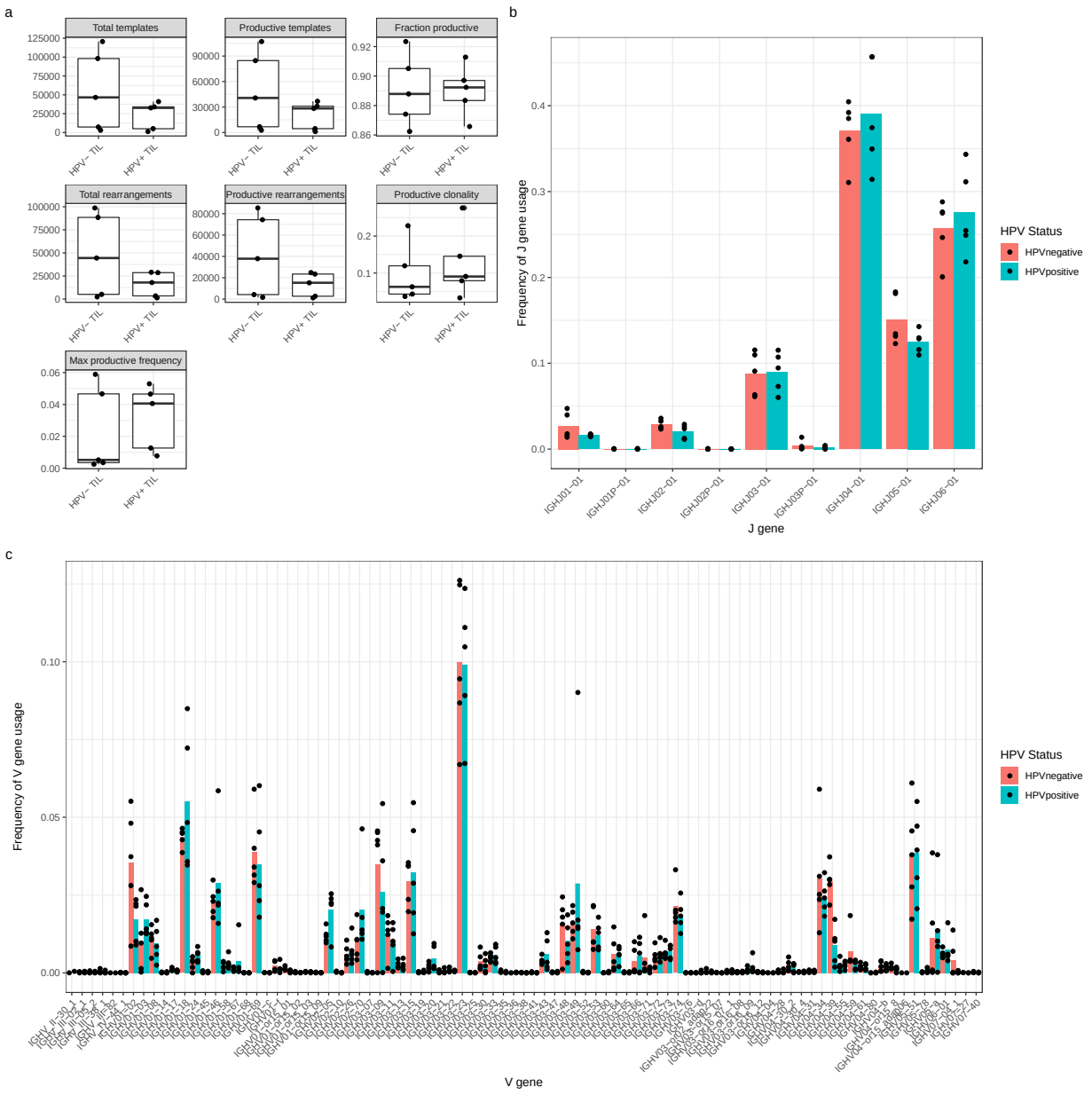


**Appendix Figure 5: Adaptive BCR sequencing reveals no difference in clonality or other metrics between HPV– and HPV+ TIL.**

a. There were no statistically significant differences by Wilcoxon rank sum test in BCR templates, rearrangements or clonality between HPV– and HPV+ TIL. BCR metrics were assessed from N=5 patients in each group. The line in the middle of the boxplot indicates the median, the top and bottom of the boxplot indicate the first and third quartiles, and the whiskers indicate 95% confidence intervals. b. There were no significant differences in J gene usage for BCRs between HPV+ and HPV– TIL. J gene usage was assessed from N=5 patients in each group and compared by Wilcoxon rank sum test. c. There were no significant

differences in V gene usage between BCRs from HPV– and HPV+ TIL. V gene usage was assessed from N=5 patients in each group and compared by Wilcoxon rank sum test.

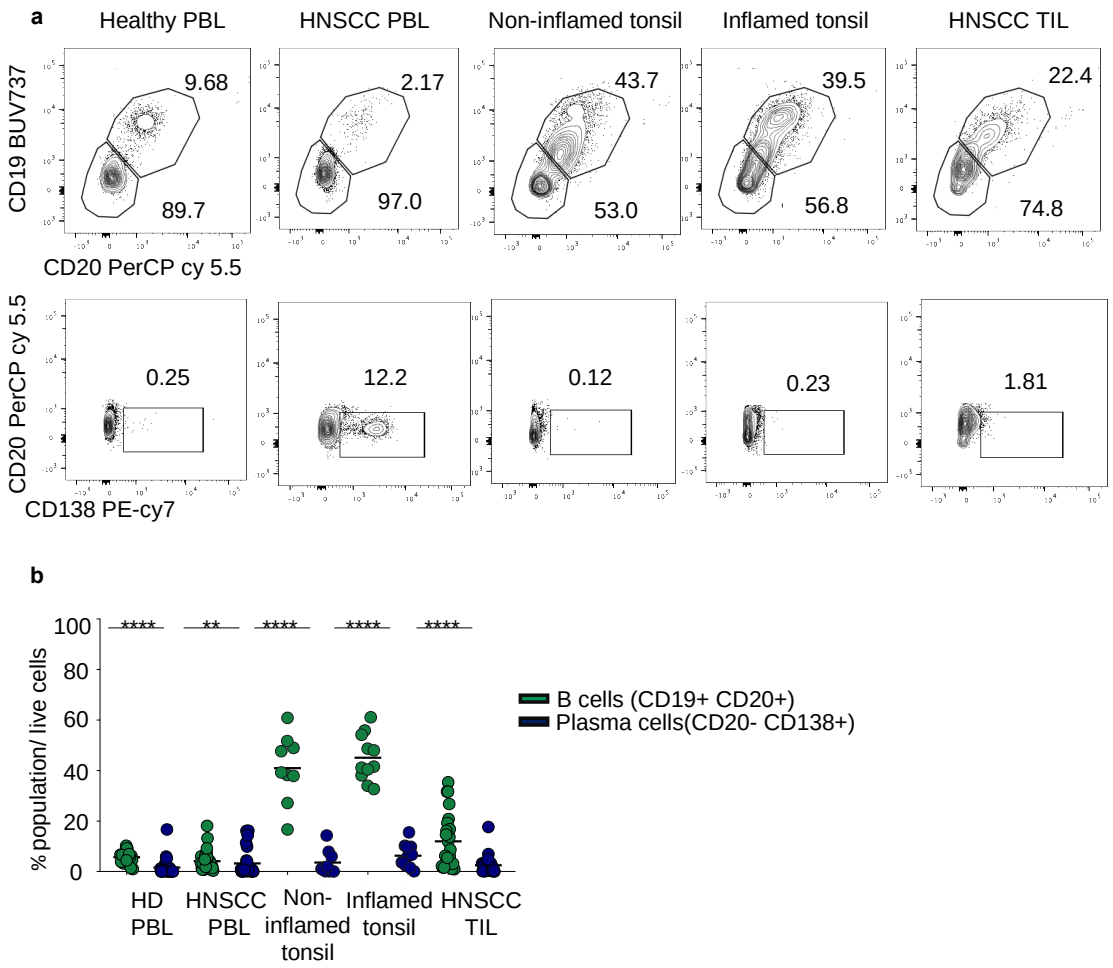


**Appendix Figure 6: B cells are significantly increased compared to plasma cells in HNSCC patients.**

**a.** Representative flow plots for quantification of B cell frequency compared to plasma cell frequency from a separate cohort of tonsils, healthy PBMCs, HNSCC TIL, and HNSCC PBMC. **b.** Scatter plot showing the frequency of B cells compared to plasma cells in healthy PBL (n=22), non-inflamed tonsils (n=9), inflamed tonsil (n=11), HNSCC tumor (n=23), HNSCC PBMCs (n=30). Statistical analysis by Students Two-sided T-test (Mann-Whitney). ****P=<0.0001, **P=0.003

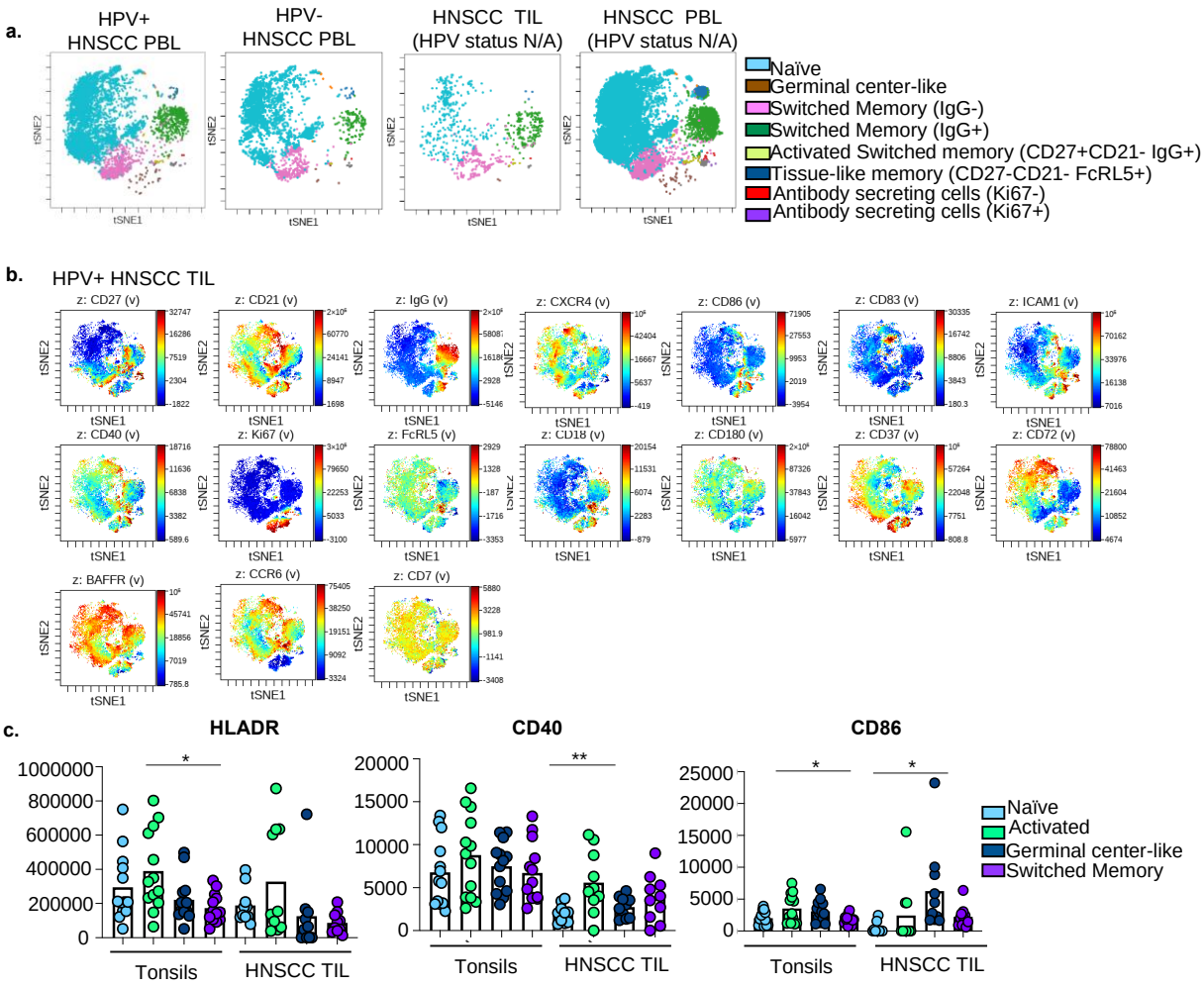


**Appendix Figure 7: Additional high dimensional analysis of HNSCC cohort 2.**

**a.** tSNE plots showing additional samples that were analyzed using Cytobank with patients from HNSCC cohort 2. Included were matched HPV+ (n=3) and HPV-PBMC (n=2). An additional set of HNSCC TIL (n=3) and PBL (n=14) were also included, however HPV status in these patients was not evaluated (HPV status N/A). b. Individual feature plots from HPV+ HNSCC patients demonstrating expression level of additional markers used to identify B cell subpopulations. **c.** Bar plot showing mean fluorescent intensity of HLADR, CD86, CD40 on B cell subsets. Statistical analysis by one-way ANOVA followed by Tukeys multiple. comparison.*P=0.03,**P=0.002.

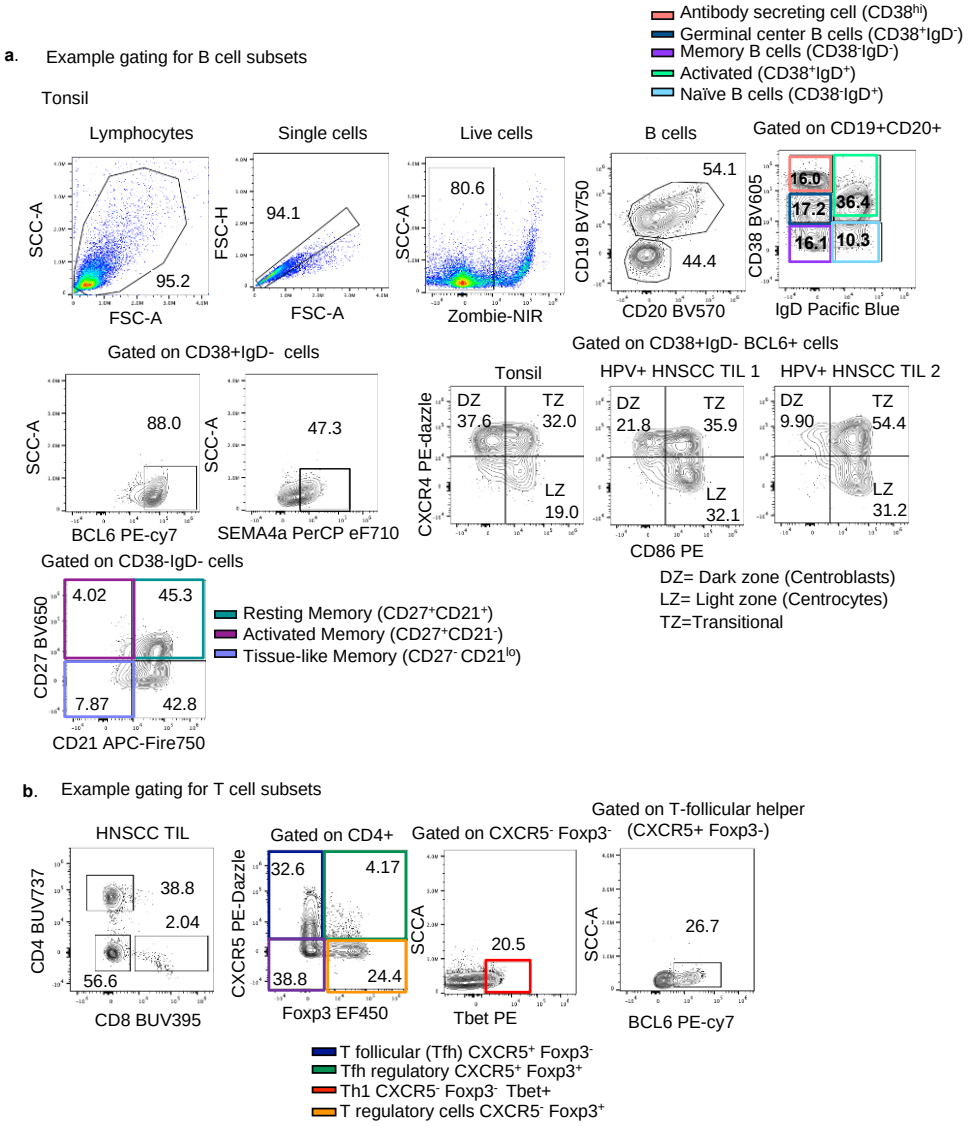


**Appendix Figure 8: Flow cytometry gating strategy for B cell and T cell profiling.**

**a.** Representative flow cytometry plots for analysis of samples stained with 25 parameter Cytek Aurora panel (Fig. 2 and 4). **b.** Representative flow cytometry plots for analysis of samples stained with T cell panel (Fig. 2c).

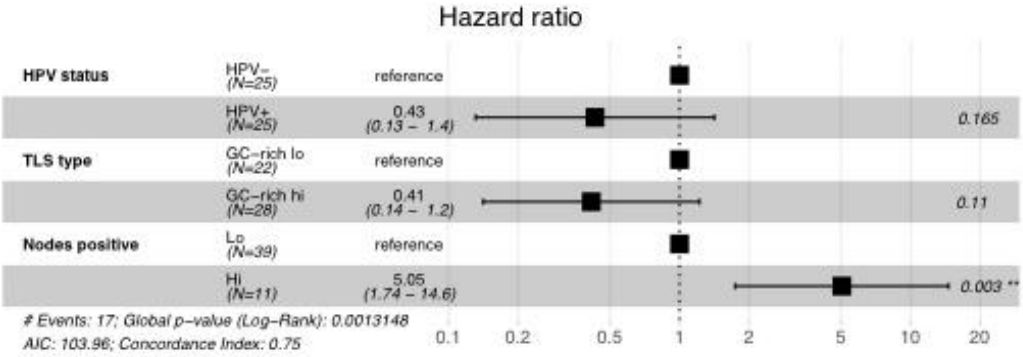


**Appendix Figure 9: Multivariate survival analysis for TLS, HPV status, and disease burden.**

Multivariate survival analysis based on HPV status, TLS type (i.e. either high TLS with GC or low TLS with GC) and disease burden as measured by the number of positive nodes. This multivariate analysis was significant with a log-rank p value of 0.0013; however, given the relatively small size of this dataset, neither the HPV status or TLS type were statistically significant after correcting for disease burden. Both HPV+ disease and high TLS with GC trended towards better outcomes.

**Table 1: Clinical characteristics of prospective patient cohort for single-cell RNAseq and immunofluorescence (Cohort 1)**

| | Healthy PBMCs | Healthy Tonsils | HNSCC |
|---|---|---|---|
| | N=6 | N=5 | N=27 |
| **Demographics** | | | |
| Median Age | 55(29-56) | 38(28-53) | 60(15-80) |
| Sex N (%) Female | 3(50%) | 0(0%) | 6(22.2%) |
| Race N (%) African American N(%); N (%) Caucasian | 0(0%); 6(100%) | 0(0%); 5(100%) | 0(0%); 26(99%) |
| **Tumor p16 Status** | | | |
| p16+ N (%) | N/A | N/A | 9(33.3%) |
| p16- N (%) | N/A | N/A | 18(66.7% |
| NE N (%) | N/A | N/A | 0(0%) |
| **Site of primary tumor** | | | |
| Tonsil N(%) | N/A | N/A | 3(11.1%) |
| Tongue N(%) | N/A | N/A | 8 (29.6%) |
| Base of Tongue N(%) | N/A | N/A | 4(14.8%) |
| Larynx N(%) | N/A | N/A | 3(11.1%) |
| Other N(%) | N/A | N/A | 9(33.3%) |
| **Pathalogical Staging** | N/A | N/A | |
| TX N(%) | N/A | N/A | 1(3.7%) |
| T0 N(%) | N/A | N/A | 0(0%) |
| T1-T2 N(%) | N/A | N/A | 10(37%) |
| T3-T4A. N(%) | N/A | N/A | 15 (55.6%) |
| Unknown N(%) | N/A | N/A | 1 (3.7%) |
| **Pathalogical Node** | | | |
| NX N(%) | N/A | N/A | 0 (0%) |
| N0 N(%) | N/A | N/A | 8(29.6%) |
| N1-N2 N(%) | N/A | N/A | 6(22.2%) |
| N2A-N2C N(%) | N/A | N/A | 10(37.0%) |
| N3-N3B N(%) | N/A | N/A | 2(7.4%) |
| Unknown N(%) | N/A | N/A | 1(3.7%) |
| **Tobacco Use** | | | |
| Yes N(%) | 0(0%) | 1(20%) | 14(52%) |
| No N(%) | 4(66.7%) | 1(20%) | 8(29.6%) |
| Former N(%) | 2(33.3%) | 3(60%) | 4(14.8%) |
| **ETOH use** | | | |
| Never N(%) | 0(0%) | 0(0%) | 0(0%) |
| Yes N(%) | 2(33.3%) | 0(40%) | 9(33.3%) |
| No N(%) | 1(16.7) | 2(40%) | 11(25.6%) |
| Occasional N(%) | 3(50%) | 1(20%) | 4(14.8%) |
| Former N(%) | 0(0%) | 0(0%) | 0(0%) |
| Unknown N(%) | 0(0%) | 2(40%) | 3(11.1%) |

**Table 2: Clinical characteristics of prospective patient cohort for spectral flow cytometry and protein validation (Cohort 2)**

| | Tonsils | HNSCC |
|---|---|---|
| | N=24 | N=43 |
| **Demographics** | | |
| Median Age | 31(18-52) | 57 (36-81) |
| Sex N (%) Female | 13(54.2%) | 13(30.2%) |
| Race N (%) African American N(%); N (%) Caucasian | 7(29.2%); 17(70.8%) | 1(2.2%); 42(97.7%) |
| **Tumor p16 Status** | | |
| p16+ N (%) | N/A | 12(28%) |
| p16- N (%) | N/A | 8 (18.6%) |
| NE N (%) | N/A | 23(53.4%) |
| **Site of primary tumor** | | |
| Tonsil N(%) | N/A | 7(16.3%) |
| Tongue N(%) | N/A | 8(18.6%) |
| Base of Tongue N(%) | N/A | 6(13.9%) |
| Larynx N(%) | N/A | 7(16.3%) |
| Mouth (N%) | N/A | 6(13.9%) |
| Other (N%) | N/A | 9(20.9%) |
| **Pathalogical Staging** | | |
| TX N(%) | N/A | 11(25.6%) |
| T0 N(%) | NA | 1(2.33%) |
| T1-T2 N(%) | NA | 10(23.3%) |
| T3-T4A N(%) | NA | 21(48.8%) |
| **Pathalogical Node** | | |
| NX N(%) | N/A | 12(27.9%) |
| N0 N(%) | N/A | 11(25.6%) |
| N1-N2 N(%) | N/A | 10(23.2%) |
| N2A-N2C N(%) | N/A | 4(9.3%) |
| N3-N3B N(%) | N/A | 6 (14%) |
| **Tobacco Use** | | |
| Yes N(%) | 6(25%) | 22(51.2%) |
| No N(%) | 13(54.2%) | 7(16.3%) |
| Former N(%) | 5(20.8%) | 14(32.5%) |
| **ETOH use** | | |
| Never N(%) | 1(4.2%) | 0(0%) |
| Yes N(%) | 13(54.2%) | 28(65.1%) |
| No N(%) | 8(33.3%) | 7(16.3%) |
| Occasional N(%) | 0(0%) | 8(18.6%) |
| Former N(%) | 2(8.3%) | 0(0%) |

**Table 3: Clinical characteristics of retrospective patient cohort for IHC and TLS analysis (Cohort 3)**

| | HNSCC |
|---|---|
| | N=50 |
| **Demographics** | |
| Median Age | 60(37-82) |
| Sex N (%) Female | 6(12%) |
| Race N (%) African American N(%); N (%) Caucasian | 3(6%);47(94%) |
| **Tumor p16 Status** | |
| p16+ N (%) | 25(50%) |
| p16- N (%) | 25(50%) |
| NE N (%) | 0(0%) |
| **Site of primary tumor** | |
| Tonsil N(%) | 25(50%) |
| Tongue N(%) | 4(8%) |
| Base of Tongue N(%) | 21(42%) |
| Larynx N(%) | 0(0%) |
| Other N(%) | 0(0%) |
| **Pathalogical Staging** | |
| TX N(%) | 0(0%) |
| T0 N(%) | 0(0%) |
| T1-T2 N(%) | 34(68%) |
| T3-T4 N(%) | 12(24%) |
| Unknown N(%) | 4(8%) |
| **Pathalogical Node** | |
| NX N(%) | 0(0%) |
| N0 N(%) | 12(24%) |
| N1-N2 N(%) | 15(30%) |
| N2A-N2C N(%) | 18(72%) |
| N3-N3B N(%) | 0(0%) |
| Unknown N(%) | 5(10%) |
| **Tobacco Use** | |
| Yes N(%) | 23(46%) |
| No N(%) | 6(12%) |
| Former N(%) | 14(28%) |
| Unknown N(%) | 7(14%) |
| **ETOH use** | |
| Never N(%) | 0(0%) |
| Yes N(%) | 27(54%) |
| No N(%) | 8(16%) |
| Occasional N(%) | 2(4%) |
| Former N(%) | 3(6%) |
| Unknown N(%) | 10(20%) |

# Table 4: Flow cytometry antibody panels (Chapter 3)

| Panel 1 | | | | Panel 3 | | | |
|---|---|---|---|---|---|---|---|
| VENDOR | CAT# | ANTIBODY/DYE | CLONE | VENDOR | CAT# | ANTIBODY/DYE | CLONE |
| BD bioscience | 741136 | BUV496 Mouse Anti-Human CD7 | (M-T701) | Biolegend | 302262 | Brilliant Violet 750™ anti-human CD19 Antibody | (HIB19) |
| BD bioscience | 748443 | BUV563 Mouse Anti-Human CD268 (BAFF Receptor) | (11C1) | ThermoFisher | 62-0209-42 | CD20 Monoclonal Antibody Super Bright 436, eBioscience™ | (2H7) |
| BD bioscience | 751138 | BUV615 Mouse Anti-Human CD38 | (HIT2) | Biolegend | 348224 | Pacific Blue™ anti-human IgD Antibody | (IA6-2) |
| BD bioscience | 751680 | BUV661 Mouse Anti-Human CD27 | (O323) | BD bioscience | 566146 | BD Horizon™ BV480 Mouse Anti-Human IgM | (G20-127) |
| BD bioscience | 741858 | BUV737 Mouse Anti-Human IgG | (G18-145) | Biolegend | 302825 | Brilliant Violet 570™ anti-human CD27 Antibody | (O323) |
| BD bioscience | 742007 | BUV805 Mouse Anti-Human CD19 | (HIB19) | BD bioscience | 740414 | BV605 Mouse Anti-Human CD23 | (M-L233) |
| Biolegend | 366314 | APC/Fire™ 750 anti-human CD18 Antibody | (CBR LFA-1/2) | Biolegend | 305440 | Brilliant Violet 711™ anti-human CD86 Antibody | (IT2.2) |
| Biolegend | 362906 | Alexa Fluor® 488 anti-human CD191 (CCR1) Antibody | (5F10B29) | Biolegend | 306526 | PE/Dazzle™ 594 anti-human CD184 (CXCR4) Antibody | (12G5) |
| BD bioscience | 742397 | BD OptiBuild™ BV421 Mouse Anti-Human CD37 | (M-B371) | ThermoFisher | 46-9753-41 | PerCP/EF710 anti-human SEMA4A | (clone 5E3) |
| BD bioscience | 746638 | BV480 Mouse Anti-Human CD54 (ICAM-1) | (HA58) | Biolegend | 340304 | PE anti-human CD307e (FcRL5) Antibody | (509f6) |
| BD bioscience | 743625 | BD OptiBuild™ BV510 Mouse Anti-Human CD180 | (G28-8) | Biolegend | 340202 | Purified anti-human CD307d (FcRL4) Antibody | (413D12) |
| BD bioscience | 743796 | BD OptiBuild™ BV605 Mouse Anti-Human CD72 | (J4-117) | Biolegend | 304010 | PE/Cyanine5 anti-human CD45 Antibody | (HI30) |
| BD bioscience | 563922 | BD Horizon™ BV650 Mouse Anti-Human CD196 (CCR6) | (11A9) | Biolegend | 342804 | PerCP/Cyanine5.5 anti-human CD305 (LAIR1) Antibody | (NKTA255) |
| BD bioscience | 747484 | BD OptiBuild™ BV750 Mouse Anti-Human IgD | ( IA6-2) | BD bioscience | 565156 | BD Horizon™ BB515 Mouse Anti-Human CD70 | (Ki-24) |
| BD bioscience | 740969 | BD OptiBuild™ BV786 Mouse Anti-Human CD21 | (B-ly4) | Biolegend | 310932 | Brilliant Violet 785™ anti-human CD69 Antibody | (FN50) |
| BD bioscience | 551058 | PE-Cy™5 Mouse Anti-Human CD83 | (HB15e) | BD bioscience | 740570 | BV650 Mouse Anti-Human CD22 | (HIB22) |
| BD bioscience | 564071 | BUV395 Mouse Anti-Ki-67 | (B56) | Biolegend | 307620 | Alexa Fluor® 488 anti-human HLA-DR Antibody | (L243) |
| ThermoFisher | 46-9753-41 | PerCP/EF710 anti-human SEMA4A | (clone 5E3) | Biolegend | 356518 | Brilliant Violet 510™ anti-human CD138 (Syndecan-1) Antibody | (MI15) |
| Biolegend | 305406 | PE anti-human CD86 Antibody | (IT2.2) | BD bioscience | 566670 | Alexa Fluor® 647 Mouse Anti-Human VISTA | (MIH65) |
| BD bioscience | 563582 | PE-Cy™7 Mouse Anti-Bcl-6 | (K112-91) | Biolegend | 356608 | PE/Cyanine7 anti-human CD38 Antibody | (HB-7) |
| Biolegend | 302332 | Brilliant Violet 570™ anti-human CD20 Antibody | (2H7) | **Panel 4** | | | |
| Biolegend | 300330 | Pacific Blue™ anti-human CD3 Antibody | (HIT3a) | BD biosciences | 565972 | BD Horizon™ BUV395 Mouse Anti-Human HLA-DR | (G46-6) |
| Biolegend | 340306 | APC anti-human CD307e (FcRL5) | (509f6) | BD biosciences | 612757 | BD Horizon™ BUV737 Mouse Anti-Human CD19 | (SJ25C1) |
| Biolegend | 334328 | Alexa Fluor® 700 anti-human CD40 | (5C3) | Biolegend | 305432 | Brilliant Violet 510™ anti-human CD86 Antibody | (IT2.2) |
| BD bioscience | 752351 | BD OptiBuild™ BUV615 Mouse Anti-Human CD38 | (HB7) | Biolegend | 302828 | Brilliant Violet 650™ anti-human CD27 Antibody | (O323) |
| **Panel 2** | | | | Biolegend | 329722 | Brilliant Violet 711™ anti-human CD274 (B7-H1, PD-L1) Antibody | (29E.2A3) |
| Biolegend | 302262 | Brilliant Violet 750™ anti-human CD19 Antibody | (HIB19) | Biolegend | 310932 | Brilliant Violet 785™ anti-human CD69 Antibody | (FN50) |
| Biolegend | 302332 | Brilliant Violet 570™ anti-human CD20 Antibody | (2H7) | Biolegend | 354906 | APC anti-human CD21 Antibody | (Bu32) |
| Biolegend | 354920 | APC/Fire™ 750 anti-human CD21 Antibody | (Bu32) | Biolegend | 334328 | Alexa Fluor® 700 anti-human CD40 Antibody | (5C3) |
| Biolegend | 302828 | Brilliant Violet 650™ anti-human CD27 Antibody | (O323) | Biolegend | 356604 | PE anti-human CD38 Antibody | (HB-7) |
| Biolegend | 348224 | Pacific Blue™ anti-human IgD Antibody | (IA6-2) | ThermoFisher | 61-2799-42 | CD279 (PD-1) Monoclonal Antibody PE-eFluor 610 | (eBioJ105 (J105)) |
| BD bioscience | 566146 | BD Horizon™ BV480 Mouse Anti-Human IgM | (G20-127) | Biolegend | 356513 | PE/Cyanine7 anti-human CD138 (Syndecan-1) Antibody | (MI15) |
| Biolegend | 340304 | PE anti-human CD307e (FcRL5) Antibody | (509f6) | Biolegend | 302326 | PerCP/Cyanine5.5 anti-human CD20 Antibody | (2H7) |
| Biolegend | 340202 | Purified anti-human CD307d (FcRL4) Antibody | (413D12) | Miltenyi | 130-113-475 | FITC anti-human IgA | (IS11-8E10) |
| Biolegend | 328214 | Brilliant Violet 421™ anti-human CD39 Antibody | (A1) | **Panel 5** | | | |
| BD bioscience | 563198 | BV510 Mouse Anti-Human CD73 | (AD2) | BD biosciences | 741823 | BD OptiBuild™ BUV737 Mouse Anti-Human CD4 | (RPA-T4) |
| Biolegend | 644835 | Brilliant Violet 785™ anti-T-bet Antibody | (4B10) | BD biosciences | 563795 | BD Horizon™ BUV395 Mouse Anti-Human CD8 | (RPA-T8) |
| Biolegend | 301614 | APC anti-human CD11c Antibody | (clone 3.9) | Biolegend | 644820 | Brilliant Violet 711™ anti-T-bet Antibody | (4B10) |
| BD bioscience | 565153 | BB515 Mouse Anti-Human LAIR-1 (CD305) | (DX26) | BD biosciences | 563582 | BD Pharmingen™ PE-Cy™7 Mouse Anti-Bcl-6 | (K112-91) |
| Biolegend | 307621 | Alexa Fluor® 647 anti-human HLA-DR Antibody | (L243) | Biolegend | 356928 | PE/Dazzle™ 594 anti-human CD185 (CXCR5) Antibody | (J252D4) |
| Biolegend | 334328 | Alexa Fluor® 700 anti-human CD40 Antibody | (5C3) | ThermoFisher | 48-4776-42 | FOXP3 Monoclonal Antibody eFluor 450, eBioscience™ | (PCH101) |
| Biolegend | 306526 | PE/Dazzle™ 594 anti-human CD184 (CXCR4) Antibody | (12G5) | Biolegend | 302828 | Brilliant Violet 650™ anti-human CD27 Antibody | (O323) |
| Biolegend | 305440 | Brilliant Violet 711™ anti-human CD86 Antibody | (IT2.2) | **Panel 6** | | | |
| Biolegend | 3556641 | Brilliant Violet 605™ anti-human CD38 Antibody | (HB-7) | Biolegend | 300514 | APC anti-human CD4 Antibody | (RPA-T4) |
| Biolegend | 356513 | PE/Cyanine7 anti-human CD138 (Syndecan-1) Antibody | (MI15) | Biolegend | 301012 | PE/Cyanine7 anti-human CD8a Antibody | (RPA-T8) |
| BD bioscience | 612856 | BD Horizon™ BUV737 Mouse Anti-Human CD70 | (Ki-24) | Biolegend | 644810 | PE anti-T-bet Antibody | (4B10) |
| BD bioscience | 744103 | BD OptiBuild™ BUV395 Mouse Anti-Human CD178 | (NOK1) | ThermoFisher | 48-4776-42 | FOXP3 Monoclonal Antibody eFluor 450, eBioscience™ | (PCH101) |
| Biolegend | 356912 | Alexa Fluor® 488 anti-human CD185 (CXCR5) Antibody | (J252D4) | Biolegend | 356928 | PE/Dazzle™ 594 anti-human CD185 (CXCR5) Antibody | (J252D4) |

# Appendix B

## Prevalence of intratumoral and circulating extrafollicular B cells is associated with disease progression in cancer patients

This project was a collaborative effort between the Bruno and Ferris labs with input from members of the Vignali lab (Drs. Anthony Cillo and Ashwin Somasundaram). A manuscript regarding these data is in preparation. Supplementary data, tables and figures referenced in Chapter 4 are in this appendix.

# Table 5: Flow cytometry antibody panels (Chapter 4)

| Cytek Aurora panel 1 | | | | |
|---|---|---|---|---|
| **Antigen** | **Flurophore** | **Vendor** | **Clone** | **Cat #** |
| FcRL4 | BUV395 | BD biosciences | (A1) | 747554 |
| LAIR1 | BUV615 | BD biosciences | (DX26) | 751585 |
| IgG | BUV737 | BD biosciences | (G18-145) | 741858 |
| CXCR3 | BUV805 | BD biosciences | (1C6/CXCR3) | 742048 |
| IgD | Pacific blue | Biolegend | (JAG-2) | 348224 |
| IgM | BV480 | Fisher (BD) | (G20-127) | 566146 |
| CD86 | BV510 | Biolegend | (IT2.2) | 305432 |
| CD20 | BV570 | Biolegend | (2H7) | 302332 |
| CD38 | BV605 | BD biosciences | (HIT2) | 303532 |
| PDL1 | BV711 | Biolegend | (29E.2A3) | 329722 |
| CD19 | BV750 | Biolegend | (HIB19) | 302262 |
| Granzyme B | FITC | Biolegend | (GB11) | 515403 |
| CD11b | Percp cy5.5 | Biolegend | (RPA-T8) | 301328 |
| Tbet | PE | Biolegend | (4B10) | 644810 |
| CD11c | PE-dazzle | Biolegend | 3.9) | 301642 |
| CD27 | PE-cy5 | Invitrogen | (O323) | 15-0279-42 |
| TRAIL | PE-cy7 | Biolegend | (RIK-2) | 308216 |
| FcRL5 | APC | Biolegend | (509f6) | 340306 |
| CD40 | AF700 | Biolegend | (5C3) | 334328 |
| Viability | Zombie NIR | Biolegend | | 423106 |
| **Cytek Aurora panel 2** | | | | |
| CXCR5 | BUV395 | BD biosciences | (RF8B2) | 740266 |
| LAIR1 | BUV615 | BD biosciences | (DX26) | 751585 |
| CD45RB | BUV563 | BD Biosciences | (MT4 6B6) | 748737 |
| CD38 | BUV615 | BD biosciences | (HIT2) | 751138 |
| CD69 | BUV661 | BD biosciences | (FN50) | 750213 |
| IgG | BUV737 | BD biosciences | (G18-145) | 741858 |
| CD19 | BUV805 | BD biosciences | (HIB19) | 742007 |
| CD95 | BV421 | Biolegend | (DX2) | 305624 |
| CD22 | BV510 | Biolegend | (HIB22) | 302526 |
| IgM | BV570 | Biolegend | (MHM-88) | 314517 |
| FcRL4 | BV650 | Biolegend | (A1) | 747557 |
| CD86 | BV711 | Biolegend | (IT2.2) | 305440 |
| FcRL5 | PE-cy5 | Biolegend (in house conjugation) | (509f6) | 340302 |
| CD21 | BV786 | BD biosciences | (B-ly4) | 740969 |
| IgA | FITC | Miltenyi | (IS11-8E10) | 130-113-475 |
| CD85j | PerCP-Cy5.5 | Biolegend | (GHI/75) | 333714 |
| Tbet | PE | Biolegend | (4B10) | 644810 |
| CD11c | PE/Dazzle594 | Biolegend | 3.9) | 301642 |
| IgD | BV750 | Biolegend | (IA6-2) | 747484 |
| TRAIL | PE-Cy7 | Biolegend | (RIK-2) | 308216 |
| CD40 | Alexa Fluor 700 | Biolegend | (5C3) | 334328 |
| CD11b | APC-Cy7 | Biolegend | (ICRF44) | 301342 |
| CD20 | Spark NIR 685 | Biolegend | (2H7) | 302366 |
| CD27 | APC/Fire 810 | Biolegend | (Bu32) | 354920 |
| Viability | Zombie NIR | | | 423106 |
| **Panel 3 (Fortessa II)** | | | | |
| CD19 | BUV737 | BD biosciences | (SJ25C1) | 612756 |
| CD20 | BUV395 | BD biosciences | (2H7) | 563782 |
| CD21 | BV786 | BD biosciences | (B-ly4) | 740969 |
| CD27 | PE-cy5 | Invitrogen | (O323) | 15-0279-42 |
| CD11c | BV650 | Biolegend | 3.9) | 301638 |
| CXCR5 | AF488 | Biolegend | (J252D4) | 356912 |
| IgD | Pacific Blue | Biolegend | (JAG-2) | 348224 |
| CD38 | PE-cy7 | Biolegend | (HB-7) | 356608 |
| CD138 | BV510 | Biolegend | (M-115) | 356518 |
| Tbet | PE-dazzle | Biolegend | (4B10) | 644828 |
| TOX | PE | Invitrogen | (TXRX10) | 12-6502-82 |
| TCF7/TCF1 | Alexa fluor 647 | Biolegend | (7F11A10) | 655204 |
| Ki67 | BV711 | Biolegend | (Ki-67) | 350516 |
| Viability | APC-cy7 | BD biosciences | | 565388 |
| **Panel 4 (Fortessa II)** | | | | |
| CD19 | APC | Biolegend | (HIB19) | 302212 |
| CD20 | BUV395 | BD biosciences | (2H7) | 563782 |
| CD21 | BV786 | BD biosciences | (B-ly4) | 740969 |
| CD27 | PE-cy5 | Invitrogen | (O323) | 15-0279-42 |
| FcRL4 | BV650 | Biolegend | (A1) | 747557 |
| LAIR1 | BB515 | BD biosciences | (CD305) | 565153 |
| IgD | Pacfic Blue | Biolegend | (JAG-2) | 348224 |
| CD85J | PE-cy7 | Biolegend | (HB-7) | 356608 |
| FcRL5 | BUV737 | BD biosciences | (G18-145) | 741858 |
| CD11c | PE-dazzle | Biolegend | 3.9) | 301642 |
| CD86 | BV711 | Biolegend | (IT2.2) | 305440 |
| Tbet | PE | Biolegend | (4B10) | 644810 |
| Viability | APC-cy7 | BD biosciences | | 565388 |

| In vitro EF differentiation assay panel | | | | |
|---|---|---|---|---|
| **Antigen** | **Flurophore** | **Vendor** | **Clone** | **Cat #** |
| CD19 | BUV805 | BD biosciences | (HIB19) | 742007 |
| CD20 | BUV395 | BD biosciences | (2H7) | 563782 |
| CD27 | PE-cy5 | Invitrogen | (O323) | 15-0279-42 |
| CD38 | BUV615 | BD biosciences | (HIT2) | 751138 |
| CD11c | APC | Biolegend | 3.9) | 301614 |
| IgD | BV750 | Biolegend | (IA6-2) | 747484 |
| CD138 | PE-cy7 | Biolegend | (M115) | 356514 |
| FcRL5 | BUV737 | BD biosciences | (G18-145) | 741858 |
| FcRL4 | BV650 | Biolegend | (A1) | 747557 |
| CD95 | BV421 | Biolegend | (DX2) | 305624 |
| CD72 | BV605 | BD biosciences | (J4-117) | 743796 |
| CD21 | APC-FIRE 750 | Biolegend | (Bu32) | 354920 |
| Ki67 | BV711 | Biolegend | (Ki-67) | 350516 |
| Tbet | PE-dazzle | Biolegend | (4B10) | 644828 |
| TOX | PE | Invitrogen | (TXRX10) | 12-6502-82 |
| Viability | Zombie NIR | | | 423106 |
| **BCR signaling panel (Cytek Aurora)** | | | | |
| CD19 | BUV805 | BD biosciences | (HIB19) | 742007 |
| CD20 | BV570 | Biolegend | (2H7) | 302332 |
| CD38 | BUV615 | BD biosciences | (HIT2) | 751138 |
| CD27 | PE-cy5 | Invitrogen | (O323) | 15-0279-42 |
| IgD | Pacific blue | Biolegend | (JAG-2) | 348224 |
| CD21 | BV786 | BD biosciences | (B-ly4) | 740969 |
| CD11c | PE-dazzle | Biolegend | 3.9) | 301642 |
| FcRL4 | BV650 | Biolegend | (A1) | 747557 |
| FcRL5 | BUV737 | BD biosciences | (G18-145) | 741858 |
| TRAIL | PE-cy7 | Biolegend | (RIK-2) | 308216 |
| LAIR1 | BB515 | BD biosciences | (CD305) | 565153 |
| Tbet | BV711 | Biolegend | (4B10) | 644820 |
| pSyk | Alexa fluor 647 | BD biosciences | (PY319)/(PY352) | 557817 |
| pBLNK | PE | BD biosciences | (J117-1278) | 558442 |
| **Antigen presentation assay panel (Fortessa II)** | | | | |
| CD4 | BUV395 | BD biosciences | (RPA-T4) | 564724 |
| CD19 | BUV737 | BD biosciences | (SJ25C1) | 612756 |
| CD3 | FITC | Biolegend | (HIT3) | 300306 |
| CTV | | Thermofisher | | C34571 |
| PD1 | PerCP cy5.5 | Biolegend | (EH12.1) | 561273 |
| CXCR5 | PE-dazzle | Biolegend | (JS52D4) | 356928 |
| Tbet | PE | Biolegend | (4B10) | 644810 |
| Foxp3 | APC | Thermofisher | (PCH101) | 17-4776-42 |
| Ki67 | BV711 | Biolegend | (Ki-67) | 350516 |
| BCL6 | PE-cy7 | BD biosciences | (K112-91) | 563582 |
| Viability | APC-cy7 | BD biosciences | | 565388 |
| **Mitotracker and 2-NBDG staining panel ( Fortessa II)** | | | | |
| CD19 | BUV737 | BD biosciences | (SJ25C1) | 612756 |
| CD20 | BUV395 | BD biosciences | (2H7) | 563782 |
| CD27 | PE-cy5 | Invitrogen | (O323) | 15-0279-42 |
| IgD | Pacificblue | Biolegend | (JAG-2) | 348224 |
| CD21 | BV786 | BD biosciences | (B-ly4) | 740969 |
| CXCR5 | PE-dazzle | Biolegend | (JS52D4) | 356928 |
| Mitotracker Deep Red FM | | Thermofisher | | M22425 |
| 2-NBDG | | Cayman Chem | | 11046 |
| CD85J | PE-cy7 | Biolegend | (HB-7) | 356608 |
| FcRL5 | PE | Biolegend | (509f6) | 340304 |
| Viability | APC-cy7 | | | 565388 |
| **IgG isotype panel (Cytek Aurora)** | | | | |
| CD19 | BUV805 | BD biosciences | (HIB19) | 742007 |
| CD20 | BUV395 | BD biosciences | (2H7) | 563782 |
| CD21 | APC-Fire 750 | Biolegend | (Bu32) | 354920 |
| IgD | BV750 | Biolegend | (IA6-2) | 747484 |
| CD38 | BUV615 | BD biosciences | (HIT2) | 751138 |
| IgG1 | PE | Southern Biotech | | 9054-09 |
| IgG3 | Alexa fluor 647 | Southern Biotech | | 9210-31 |
| IgG2 | Alexa fluor 488 | Southern Biotech | | 9070-30 |
| CD11c | PE-dazzle | Biolegend | 3.9) | 301642 |
| FcRL4 | BV650 | Biolegend | (A1) | 747557 |
| FcRL5 | BUV737 | BD biosciences | (G18-145) | 741858 |
| CD85J | PE-cy7 | Biolegend | (HB-7) | 356608 |
| LAIR1 | BUV496 | BD biosciences | (DX26) | 750755 |
| CD72 | BV605 | BD biosciences | (J4-117) | 743796 |
| CD95 | BV421 | Biolegend | (DX2) | 305624 |
| CD27 | PE-cy5 | Invitrogen | (O323) | 15-0279-42 |
| Viability | Zombie NIR | | | 423106 |

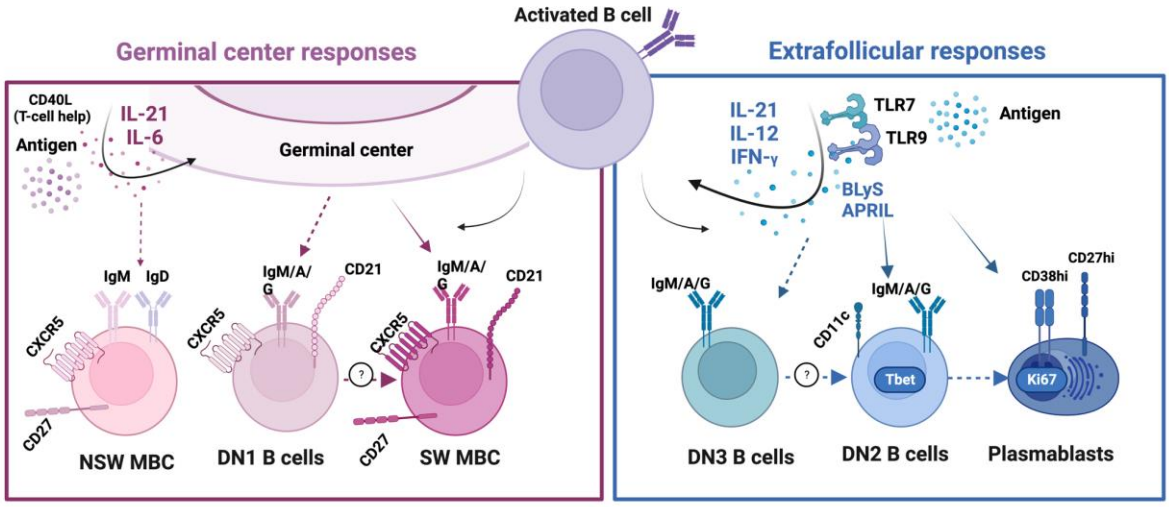


**Appendix Figure 10: Comparision of germinal center and extrafolliicular B cell differentiation pathways**

B cells that encounter their cognate antigen become activated and participate in germinal center (GC) or extrafollicular (EF) repsonses. T cell interaction and soluble factors can influence dominace of GC or EF responses. CD40 stimulation by CD4+ T follicular helper (TFH) cells promotes GC formation. IL-21 and IL-6 promote TFH differentiation and IL-21 acts directly on B cells to promote GC B cell differentiation. GC reponses produce class switch (SW) memory B cells (MBC) and non-class switched (NSW) MBC. Double negative 1 (DN1) MBC are thought to be SW MBC precursor cells. Th1 associated cytokines IL-12, IFN-γ,TNF-α, IL-2 have been shown to drive EF repsonses[321,330]. TLR ligands have been associated with EF responses in autoimmune disorders such as SLE but few studies address the direct role of TLR7/9 on directing either GC or EF responses[283,329]. BLys (BAFF) and April tend to promote EF responses. Both EF and GC responses result in isotype switched mature B cells. EF reponses result in CD27- MBC subsets (DN3 and DN2) and short-lived plasmablasts.

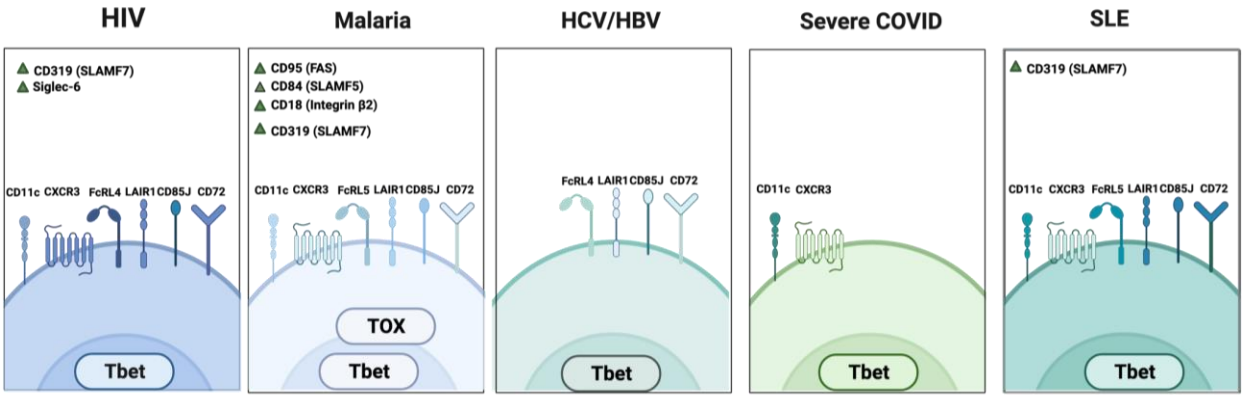


**Appendix Figure 11: Comparision of DN2 MBC phenotype in different diseases**

Accumulation of double negative 2 (DN2) MBCs or atypical MBC in peripheral blood is a prominent feature of chronic infection and autoimmune disorders. DN2 MBC express transciption factor Tbet and homing receptors CD11c and CXCR3 which are not found in CD27+ MBC subsets. DN2 MBCs express a host of inhibitory receptors including FcRL4, FcRL5, LAIR1, CD85J, CD72, SLAM proteins. Expression of IRs can vary between diseases which is not competely understood. IR expression has not been fully evaluated in COVID-19 and sars-cov2 infection. Overexpression of IRs is thought to mediated dysfunction of DN2 MBCs in chronic infection.

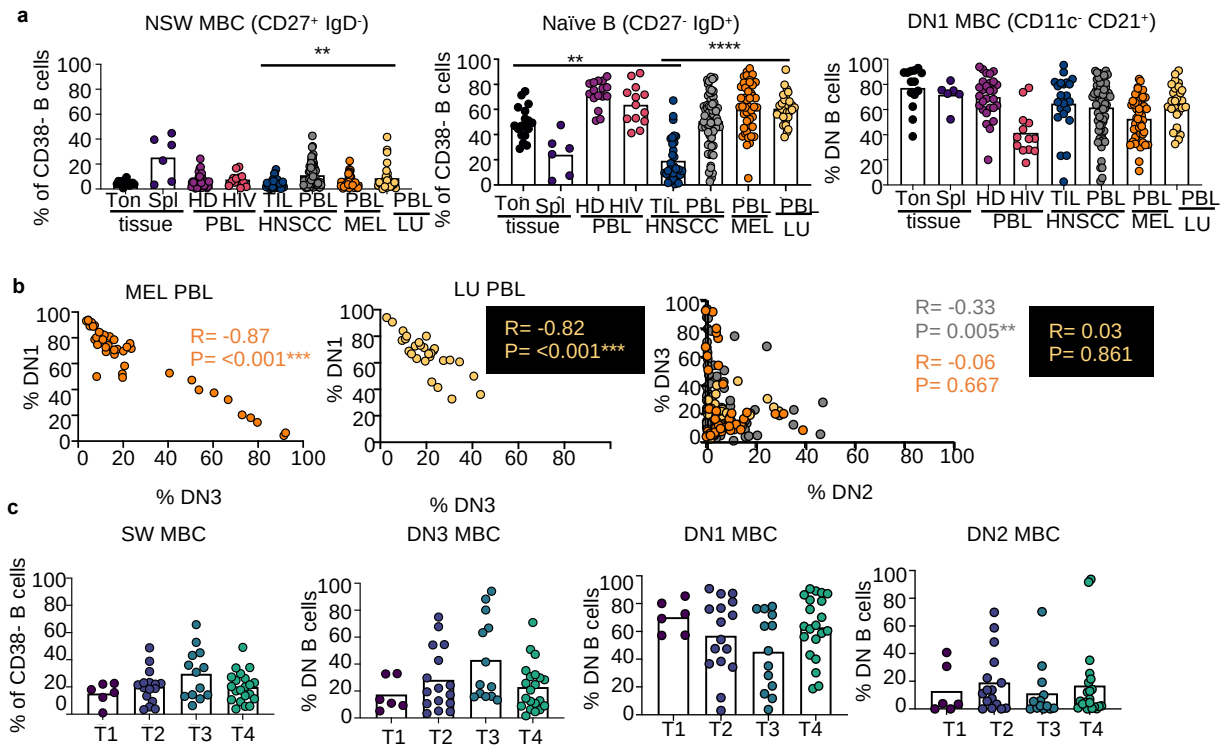


**Appendix Figure 12: Additional quantification and clinical correaltion of GC and EF derived B cell subsets**

**(a)** Quantification graphs of the frequency NSW, Naïve and DN1 B cell populations in normal tissues and treatment naive patient tumor and blood samples. Control tissues include normal spleen (Spl) (n=6), inflamed tonsil (Ton) (n=14) , healthy donor (HD) PBL (n=27), PBL from patients with HIV (n=14). Cancer patient samples include tumor (TIL) (n=28) and PBL (n=71) from HNSCC, PBL from metastatic melanoma (n=46) and lung cancer patients (n=26). Data were analyzed by a non-parametric Kruskal-Wallis test with multiple comparisons to HD PBL.****p=<0.0001, ***p=0.0001, **p=0.002, *p=0.02 **(b)** Frequency are DN1 inversely related to DN3 and DN2 in PBL of patients with MEL, LU and HNSCC. Frequencies from MEL PBL are overlaid in orange, HNSCC PBL are overlaid in grey and LU PBL are overlaid in yellow. Spearman's nonparametric correlation analysis results are reported. **(c)** Quantiication graphs of frequency of SW, DN3 DN2 and DN1 in HNSCC patient PBL grouped by pathology-defined T stage (Tumor stage) (range 1-4).

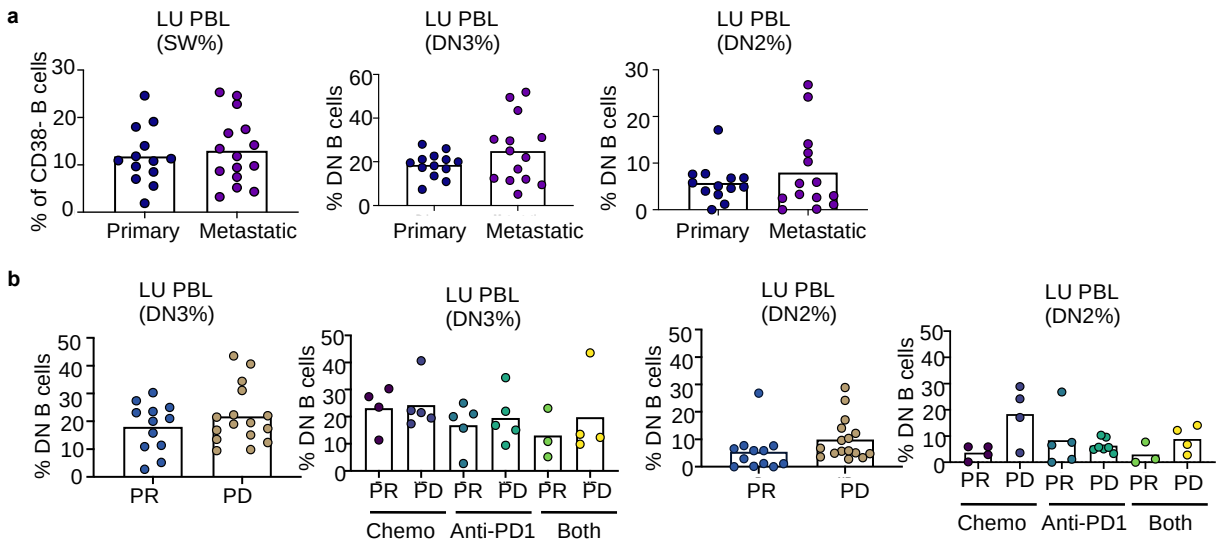


**Appendix Figure 13: Clinical correlation of EF subsets in Lung cancer patient cohort**

**(a)** Quantification of SW, DN3, DN2 frequency in LU PBL grouped by patients primary locally advanced tumors or metastatic tumors. Data analysis by non-parametric Mann-whitney test. No significant differences observed. **(b)** Quantification of DN3, DN2 frequency in LU PBL grouped by overall repsonse in patients (Left graph) and patients seperated by treatment type. Chemo= Chemotherapy; Both= anti-PD1+ Chemotherapy

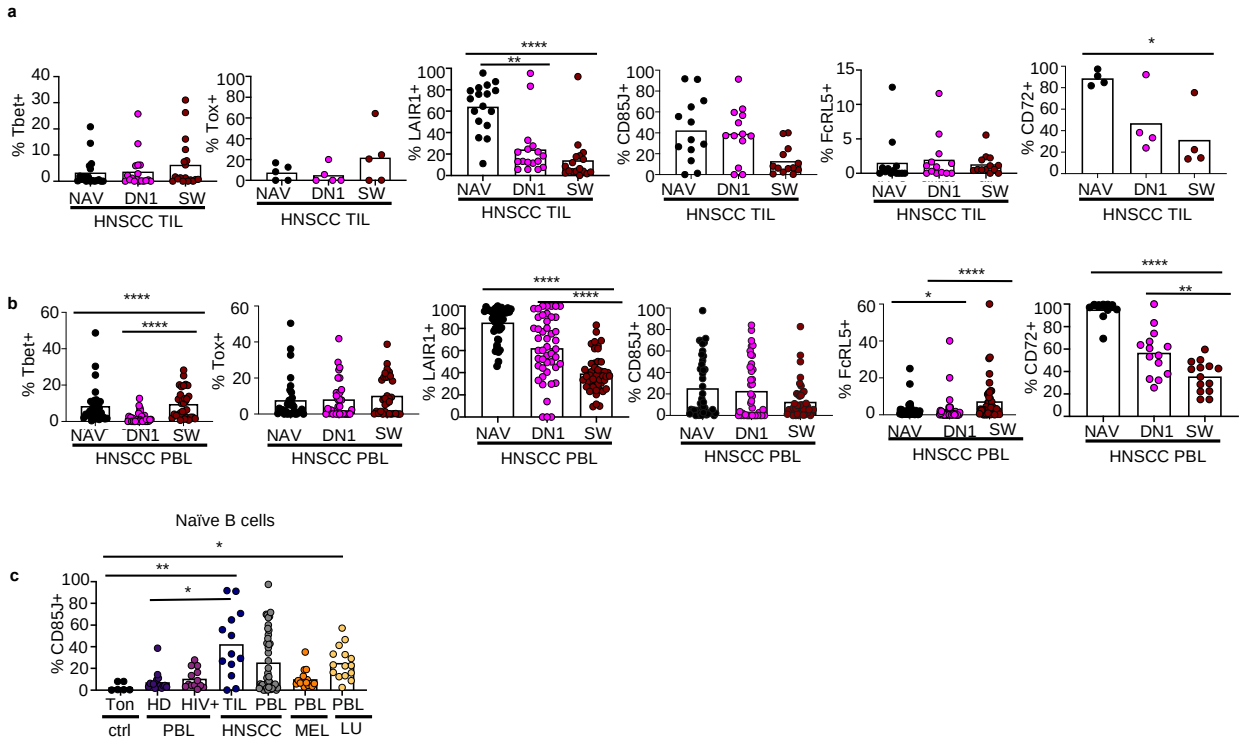


**Appendix Figure 14: Quantification of B cell exhaustion-like program in SW, Naïve, DN1 subsets**

**(a)** Quantification graphs of Tbet, Tox, LAIR1, CD85J, FcRL5, CD72 on Naïve (NAV), DN1 MBC, and SW MBC in HNSCC TIL (**b)** HNSCC PBL. Data analysis by non-parametric Krullis Walls test and dunn's multiple comparisons. (add in P values) **(c)** Comparision of CD85J frequency on Naïve B cells in HNSCC TIL and PBL, MEL PBL, LU PBL and control tissues. Data analysis by non-parametric Krullis Walls test and dunn's multiple comparisons. (add in P values)

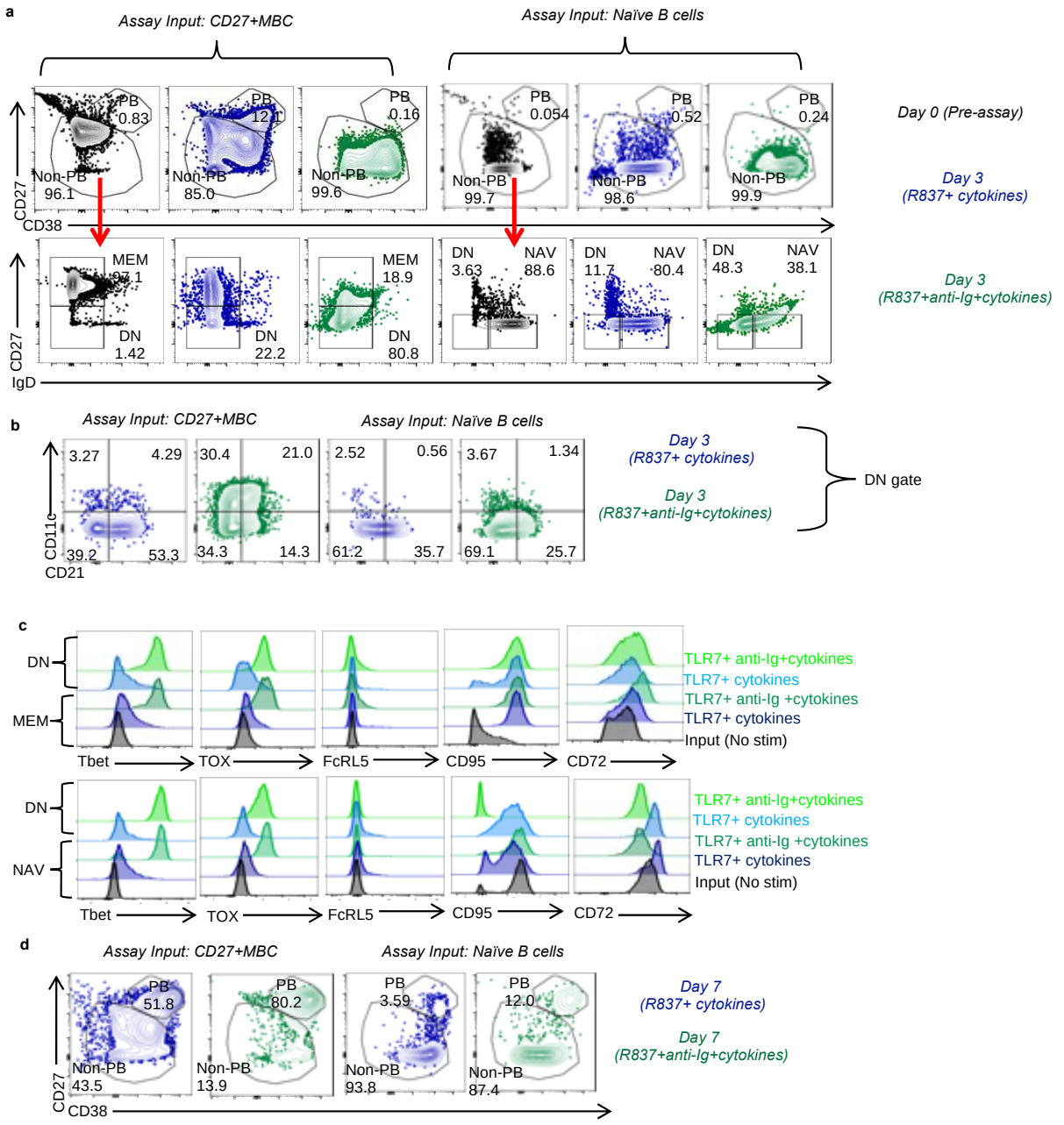


**Appendix Figure 15: Gating stategy for in vitro EF differentiation assay**

**(a)** Representative flow gating strategy of CD27+ MBC and Naïve B cells before sorting (pre-assay) and 3-day post stimulation (HD PBL control). Live CD19+ cells were then gated on CD27 and CD38 to distinguish plasmablasts (PB) and Non-PB cells. Non-PB cells are then gated for CD27 and IgD to distinguish MBC, DN and Naïve cells pre and post stimulation. Stimulation conditions are labeled as indicated. R837 is a TLR7 agonist. Cytokines included IFN-γ, IL21, IL2, and BAFF. **(b)** Representative flow gating strategy of

DN subsets. DN cells were then gated on CD11c and CD21. **(c)** Representative histograms of expression of Tbet, Tox , FcRL5, CD95, CD72 on DN gate (CD27-IgD- cells) and memory gate (MEM) (CD27+IgD- cells). **(d)** Representative gating of Plasmablast (PB) at Day 7 harvest.

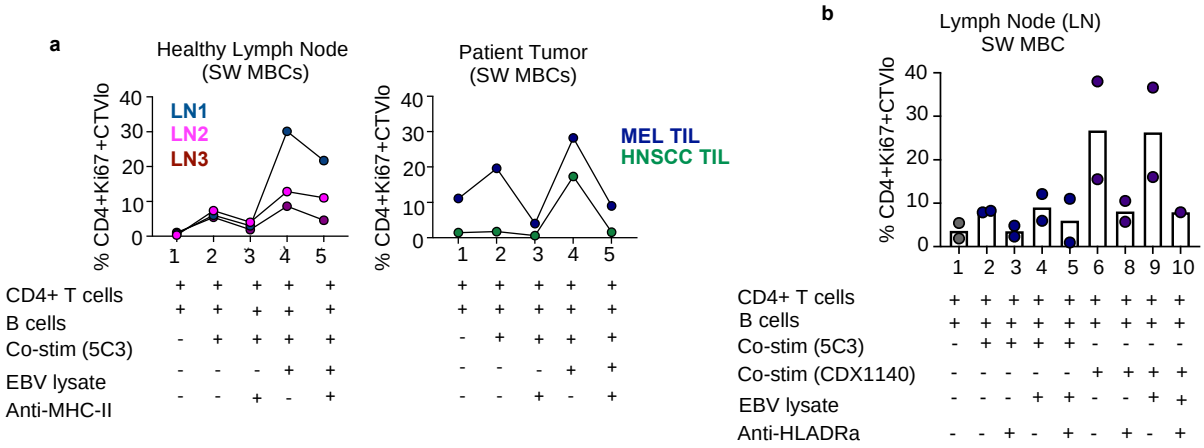


**Appendix Figure 16: in vitro antigen presentation assay**

**(a)** Quantification of Ki67+ CD4+ CTVlo T cells following antigen presentation by class-switched MBC (CD27+IgD-) (SW MBC). CD4 T cells were co-cultured with autologous SW MBC and incubated with or without costimulatory antibodies (Co-stim) (anti-CD40; clone 5C3) (anti-CD28) and/or exogenous antigen (EBV lysate) for 5 days. Proliferation by CD4+ T cells via antigen presentation was confirmed using a pan-MHCII antibody. Left graph= HD Lymph node (n=3) and Right graph patient tumor n=1 Melanoma (MEL TIL) n=1 (HNSCC TIL) **(b)** Quantification of Ki67+ CD4+ T CTVlo cells following antigen presentatio by class-switched MBC (CD27+IgD-) (SW MBC) comparing commercial CD40 agonist (5C3) to theraputic CD40 agonist (CDX1140) (Celldex Theraputics). Proliferation by CD4 via Antigen presentation was confirmed using a HLADRα antibody for more effcient blocking.

## Bibliography


1. Anand, P. *et al.* Cancer is a preventable disease that requires major lifestyle changes. *Pharm. Res.* **25,** 2097–2116 (2008).
2. Bray, F. *et al.* Global cancer statistics 2018: GLOBOCAN estimates of incidence and mortality worldwide for 36 cancers in 185 countries. *CA Cancer J Clin* **68,** 394–424 (2018).
3. Categories of Cancer | SEER Training. at <https://training.seer.cancer.gov/disease/categories/>
4. Hanahan, D. & Weinberg, R. A. The hallmarks of cancer. *Cell* **100,** 57–70 (2000).
5. Hanahan, D. & Weinberg, R. A. Hallmarks of cancer: the next generation. *Cell* **144,** 646–674 (2011).
6. Hanahan, D. Hallmarks of cancer: new dimensions. *Cancer Discov.* **12,** 31–46 (2022).
7. Bhat, A. A. *et al.* Tumor microenvironment: an evil nexus promoting aggressive head and neck squamous cell carcinoma and avenue for targeted therapy. *Signal Transduct. Target. Ther.* **6,** 12 (2021).
8. Luo, Z. *et al.* Tumor microenvironment: The culprit for ovarian cancer metastasis? *Cancer Lett.* **377,** 174–182 (2016).
9. Valkenburg, K. C., de Groot, A. E. & Pienta, K. J. Targeting the tumour stroma to improve cancer therapy. *Nat. Rev. Clin. Oncol.* **15,** 366–381 (2018).
10. Chen, D. S. & Mellman, I. Oncology meets immunology: the cancer-immunity cycle. *Immunity* **39,** 1–10 (2013).
11. Fabian, K. P., Wolfson, B. & Hodge, J. W. From Immunogenic Cell Death to

Immunogenic Modulation: Select Chemotherapy Regimens Induce a Spectrum of Immune-Enhancing Activities in the Tumor Microenvironment. *Front. Oncol.* **11,** 728018 (2021).

12. Fucikova, J. *et al.* Detection of immunogenic cell death and its relevance for cancer therapy. *Cell Death Dis.* **11,** 1013 (2020).
13. Topalian, S. L. *et al.* Safety, activity, and immune correlates of anti-PD-1 antibody in cancer. *N. Engl. J. Med.* **366,** 2443–2454 (2012).
14. Wu, X. *et al.* Application of PD-1 Blockade in Cancer Immunotherapy. *Comput Struct Biotechnol J* **17,** 661–674 (2019).
15. Johnson, D. E. *et al.* Head and neck squamous cell carcinoma. *Nat. Rev. Dis. Primers* **6,** 92 (2020).
16. Ferlay, J. *et al.* Estimating the global cancer incidence and mortality in 2018: GLOBOCAN sources and methods. *Int. J. Cancer* **144,** 1941–1953 (2019).
17. Welters, M. J. P., Santegoets, S. J. & van der Burg, S. H. The tumor microenvironment and immunotherapy of oropharyngeal squamous cell carcinoma. *Front. Oncol.* **10,** 545385 (2020).
18. Leemans, C. R., Braakhuis, B. J. M. & Brakenhoff, R. H. The molecular biology of head and neck cancer. *Nat. Rev. Cancer* **11,** 9–22 (2011).
19. Cancer Genome Atlas Network. Comprehensive genomic characterization of head and neck squamous cell carcinomas. *Nature* **517,** 576–582 (2015).
20. Hoppe-Seyler, K., Bossler, F., Braun, J. A., Herrmann, A. L. & Hoppe-Seyler, F. The HPV E6/E7 oncogenes: key factors for viral carcinogenesis and therapeutic targets. *Trends Microbiol.* **26,** 158–168 (2018).

21. Mittal, S. & Banks, L. Molecular mechanisms underlying human papillomavirus E6 and E7 oncoprotein-induced cell transformation. *Mutat. Res. Rev. Mutat. Res.* **772,** 23–35 (2017).

22. Seiwert, T. Y. *et al.* Integrative and comparative genomic analysis of HPV-positive and HPV-negative head and neck squamous cell carcinomas. *Clin. Cancer Res.* **21,** 632–641 (2015).

23. Osborne, C., Wilson, P. & Tripathy, D. Oncogenes and tumor suppressor genes in breast cancer: potential diagnostic and therapeutic applications. *Oncologist* **9,** 361–377 (2004).

24. Chen, J. Signaling pathways in HPV-associated cancers and therapeutic implications. *Rev Med Virol* **25 Suppl 1,** 24–53 (2015).

25. Yang, D.-H., Wildeman, A. G. & Sharom, F. J. Overexpression, purification, and structural analysis of the hydrophobic E5 protein from human papillomavirus type 16. *Protein Expr. Purif.* **30,** 1–10 (2003).

26. Brimer, N., Lyons, C. & Vande Pol, S. B. Association of E6AP (UBE3A) with human papillomavirus type 11 E6 protein. *Virology* **358,** 303–310 (2007).

27. Massimi, P., Gammoh, N., Thomas, M. & Banks, L. HPV E6 specifically targets different cellular pools of its PDZ domain-containing tumour suppressor substrates for proteasome-mediated degradation. *Oncogene* **23,** 8033–8039 (2004).

28. Kabsch, K. & Alonso, A. The human papillomavirus type 16 E5 protein impairs TRAIL- and FasL-mediated apoptosis in HaCaT cells by different mechanisms. *J. Virol.* **76,** 12162–12172 (2002).

29. Kabsch, K. *et al.* The HPV-16 E5 protein inhibits TRAIL- and FasL-mediated

apoptosis in human keratinocyte raft cultures. *Intervirology* **47,** 48–56 (2004).

30. Kürten, C. H. L. *et al.* Investigating immune and non-immune cell interactions in head and neck tumors by single-cell RNA sequencing. *Nat. Commun.* **12,** 7338 (2021).
31. Fakhry, C. *et al.* Improved survival of patients with human papillomavirus-positive head and neck squamous cell carcinoma in a prospective clinical trial. *J. Natl. Cancer Inst.* **100,** 261–269 (2008).
32. Vermorken, J. B. *et al.* Impact of tumor HPV status on outcome in patients with recurrent and/or metastatic squamous cell carcinoma of the head and neck receiving chemotherapy with or without cetuximab: retrospective analysis of the phase III EXTREME trial. *Ann. Oncol.* **25,** 801–807 (2014).
33. Ferris, R. L. *et al.* Nivolumab vs investigator's choice in recurrent or metastatic squamous cell carcinoma of the head and neck: 2-year long-term survival update of CheckMate 141 with analyses by tumor PD-L1 expression. *Oral Oncol* **81,** 45–51 (2018).
34. Ferris, R. L. *et al.* Nivolumab for Recurrent Squamous-Cell Carcinoma of the Head and Neck. *N. Engl. J. Med.* **375,** 1856–1867 (2016).
35. Wood, O. *et al.* Gene expression analysis of TIL rich HPV-driven head and neck tumors reveals a distinct B-cell signature when compared to HPV independent tumors. *Oncotarget* **7,** 56781–56797 (2016).
36. Cillo, A. R. *et al.* Immune Landscape of Viral- and Carcinogen-Driven Head and Neck Cancer. *Immunity* **52,** 183–199.e9 (2020).
37. Mito, I. *et al.* Comprehensive analysis of immune cell enrichment in the tumor

microenvironment of head and neck squamous cell carcinoma. *Sci. Rep.* **11,** 16134 (2021).

38. Mandal, R. *et al.* The head and neck cancer immune landscape and its immunotherapeutic implications. *JCI Insight* **1,** e89829 (2016).
39. Jiang, A.-M. *et al.* Tumor Mutation Burden, Immune Cell Infiltration, and Construction of Immune-Related Genes Prognostic Model in Head and Neck Cancer. *Int J Med Sci* **18,** 226–238 (2021).
40. Chen, X. *et al.* Immunological network analysis in HPV associated head and neck squamous cancer and implications for disease prognosis. *Mol. Immunol.* **96,** 28–36 (2018).
41. Li, L. *et al.* Comprehensive immunogenomic landscape analysis of prognosis-related genes in head and neck cancer. *Sci. Rep.* **10,** 6395 (2020).
42. Wuerdemann, N. *et al.* LAG-3, TIM-3 and VISTA Expression on Tumor-Infiltrating Lymphocytes in Oropharyngeal Squamous Cell Carcinoma-Potential Biomarkers for Targeted Therapy Concepts. *Int. J. Mol. Sci.* **22,** (2020).
43. Lechner, A. *et al.* Characterization of tumor-associated T-lymphocyte subsets and immune checkpoint molecules in head and neck squamous cell carcinoma. *Oncotarget* **8,** 44418–44433 (2017).
44. Liu, Z. *et al.* Novel Effector Phenotype of Tim-3+ Regulatory T Cells Leads to Enhanced Suppressive Function in Head and Neck Cancer Patients. *Clin. Cancer Res.* **24,** 4529–4538 (2018).
45. Liu, J.-F. *et al.* Blockade of TIM3 relieves immunosuppression through reducing regulatory T cells in head and neck cancer. *J Exp Clin Cancer Res* **37,** 44 (2018).

46. Duhen, T. *et al.* Co-expression of CD39 and CD103 identifies tumor-reactive CD8 T cells in human solid tumors. *Nat. Commun.* **9,** 2724 (2018).

47. Hwang, B., Lee, J. H. & Bang, D. Single-cell RNA sequencing technologies and bioinformatics pipelines. *Exp Mol Med* **50,** 1–14 (2018).

48. Kuksin, M. *et al.* Applications of single-cell and bulk RNA sequencing in onco-immunology. *Eur. J. Cancer* **149,** 193–210 (2021).

49. Chaudhry, F. *et al.* Single-Cell RNA Sequencing of the Cardiovascular System: New Looks for Old Diseases. *Front. Cardiovasc. Med.* **6,** 173 (2019).

50. Li, X. & Wang, C.-Y. From bulk, single-cell to spatial RNA sequencing. *Int. J. Oral Sci.* **13,** 36 (2021).

51. Puram, S. V. *et al.* Single-Cell Transcriptomic Analysis of Primary and Metastatic Tumor Ecosystems in Head and Neck Cancer. *Cell* **171,** 1611–1624.e24 (2017).

52. Nordfors, C. *et al.* CD8+ and CD4+ tumour infiltrating lymphocytes in relation to human papillomavirus status and clinical outcome in tonsillar and base of tongue squamous cell carcinoma. *Eur. J. Cancer* **49,** 2522–2530 (2013).

53. Wuerdemann, N. *et al.* PD-L1 Expression and a High Tumor Infiltrate of CD8+ Lymphocytes Predict Outcome in Patients with Oropharyngeal Squamous Cells Carcinoma. *Int. J. Mol. Sci.* **21,** (2020).

54. Zhou, Z. *et al.* PD-L1 in Combination with CD8+TIL and HIF-1α are Promising Prognosis Predictors of Head and Neck Squamous Cell Carcinoma. *Cancer Manag Res* **12,** 13233–13239 (2020).

55. McKinney, E. F. & Smith, K. G. T cell exhaustion and immune-mediated disease-the potential for therapeutic exhaustion. *Curr. Opin. Immunol.* **43,** 74–80 (2016).

56. Wherry, E. J. & Kurachi, M. Molecular and cellular insights into T cell exhaustion. *Nat. Rev. Immunol.* **15,** 486–499 (2015).

57. Wherry, E. J. T cell exhaustion. *Nat. Immunol.* **12,** 492–499 (2011).

58. Beltra, J.-C. *et al.* Developmental relationships of four exhausted CD8+ T cell subsets reveals underlying transcriptional and epigenetic landscape control mechanisms. *Immunity* **52,** 825–841.e8 (2020).

59. Eberhardt, C. S. *et al.* Functional HPV-specific PD-1+ stem-like CD8 T cells in head and neck cancer. *Nature* **597,** 279–284 (2021).

60. Wang, D. *et al.* A comprehensive profile of TCF1+ progenitor and TCF1- terminally exhausted PD-1+CD8+ T cells in head and neck squamous cell carcinoma: implications for prognosis and immunotherapy. *Int. J. Oral Sci.* **14,** 8 (2022).

61. Borst, J., Ahrends, T., Bąbała, N., Melief, C. J. M. & Kastenmüller, W. CD4+ T cell help in cancer immunology and immunotherapy. *Nat. Rev. Immunol.* **18,** 635–647 (2018).

62. Tay, R. E., Richardson, E. K. & Toh, H. C. Revisiting the role of CD4+ T cells in cancer immunotherapy-new insights into old paradigms. *Cancer Gene Ther* **28,** 5–17 (2021).

63. Tesmer, L. A., Lundy, S. K., Sarkar, S. & Fox, D. A. Th17 cells in human disease. *Immunol. Rev.* **223,** 87–113 (2008).

64. Ye, J., Livergood, R. S. & Peng, G. The role and regulation of human Th17 cells in tumor immunity. *Am. J. Pathol.* **182,** 10–20 (2013).

65. Gameiro, S. F. *et al.* Treatment-naïve HPV+ head and neck cancers display a T-cell-inflamed phenotype distinct from their HPV- counterparts that has implications

for immunotherapy. *Oncoimmunology* **7,** e1498439 (2018).

66. Bhatt, K. H. *et al.* Profiling HPV-16-specific T cell responses reveals broad antigen reactivities in oropharyngeal cancer patients. *J. Exp. Med.* **217,** (2020).
67. Albers, A. *et al.* Antitumor activity of human papillomavirus type 16 E7-specific T cells against virally infected squamous cell carcinoma of the head and neck. *Cancer Res.* **65,** 11146–11155 (2005).
68. Welters, M. J. P. *et al.* Intratumoral HPV16-Specific T Cells Constitute a Type I-Oriented Tumor Microenvironment to Improve Survival in HPV16-Driven Oropharyngeal Cancer. *Clin. Cancer Res.* **24,** 634–647 (2018).
69. Kesselring, R., Thiel, A., Pries, R., Trenkle, T. & Wollenberg, B. Human Th17 cells can be induced through head and neck cancer and have a functional impact on HNSCC development. *Br. J. Cancer* **103,** 1245–1254 (2010).
70. Li, C., Zhao, Y., Zhang, W. & Zhang, W. Increased prevalence of T(H)17 cells in the peripheral blood of patients with head and neck squamous cell carcinoma. *Oral Surg. Oral Med. Oral Pathol. Oral Radiol. Endod.* **112,** 81–89 (2011).
71. Yang, M. *et al.* CXCL13 shapes immunoactive tumor microenvironment and enhances the efficacy of PD-1 checkpoint blockade in high-grade serous ovarian cancer. *J. Immunother. Cancer* **9,** (2021).
72. Niogret, J. *et al.* Follicular helper-T cells restore CD8+-dependent antitumor immunity and anti-PD-L1/PD-1 efficacy. *J. Immunother. Cancer* **9,** (2021).
73. Kim, S. T. *et al.* Human extrafollicular CD4+ th cells help memory B cells produce igs. *J. Immunol.* **201,** 1359–1372 (2018).
74. Tahiliani, V., Hutchinson, T. E., Abboud, G., Croft, M. & Salek-Ardakani, S. OX40

Cooperates with ICOS To Amplify Follicular Th Cell Development and Germinal Center Reactions during Infection. *J. Immunol.* **198,** 218–228 (2017).

75. Zotos, D. *et al.* IL-21 regulates germinal center B cell differentiation and proliferation through a B cell-intrinsic mechanism. *J. Exp. Med.* **207,** 365–378 (2010).
76. Ruffin, A. T. *et al.* B cell signatures and tertiary lymphoid structures contribute to outcome in head and neck squamous cell carcinoma. *Nat. Commun.* **12,** 3349 (2021).
77. Dadey, R. E., Workman, C. J. & Vignali, D. A. A. Regulatory T cells in the tumor microenvironment. *Adv. Exp. Med. Biol.* **1273,** 105–134 (2020).
78. Sawant, D. V. *et al.* Adaptive plasticity of IL-10+ and IL-35+ Treg cells cooperatively promotes tumor T cell exhaustion. *Nat. Immunol.* **20,** 724–735 (2019).
79. Jie, H. B. *et al.* Intratumoral regulatory T cells upregulate immunosuppressive molecules in head and neck cancer patients. *Br. J. Cancer* **109,** 2629–2635 (2013).
80. Chuckran, C. A. *et al.* Prevalence of intratumoral regulatory T cells expressing neuropilin-1 is associated with poorer outcomes in patients with cancer. *Sci. Transl. Med.* **13,** eabf8495 (2021).
81. Strauss, L., Bergmann, C., Gooding, W., Johnson, J. T. & Whiteside, T. L. The frequency and suppressor function of CD4+CD25highFoxp3+ T cells in the circulation of patients with squamous cell carcinoma of the head and neck. *Clin. Cancer Res.* **13,** 6301–6311 (2007).
82. Jie, H.-B. *et al.* CTLA-4$^{+}$ Regulatory T Cells Increased in Cetuximab-Treated Head and Neck Cancer Patients Suppress NK Cell Cytotoxicity and Correlate with Poor Prognosis. *Cancer Res.* **75,** 2200–2210 (2015).

83. Wang, W., Erbe, A. K., Hank, J. A., Morris, Z. S. & Sondel, P. M. NK Cell-Mediated Antibody-Dependent Cellular Cytotoxicity in Cancer Immunotherapy. *Front. Immunol.* **6,** 368 (2015).

84. Bald, T., Krummel, M. F., Smyth, M. J. & Barry, K. C. The NK cell-cancer cycle: advances and new challenges in NK cell-based immunotherapies. *Nat. Immunol.* **21,** 835–847 (2020).

85. Vujanovic, L. *et al.* Virally infected and matured human dendritic cells activate natural killer cells via cooperative activity of plasma membrane-bound TNF and IL-15. *Blood* **116,** 575–583 (2010).

86. Barry, K. C. *et al.* A natural killer-dendritic cell axis defines checkpoint therapy-responsive tumor microenvironments. *Nat. Med.* **24,** 1178–1191 (2018).

87. Concha-Benavente, F. *et al.* PD-L1 Mediates Dysfunction in Activated PD-1+ NK Cells in Head and Neck Cancer Patients. *Cancer Immunol Res* **6,** 1548–1560 (2018).

88. Charap, A. J. *et al.* Landscape of natural killer cell activity in head and neck squamous cell carcinoma. *J. Immunother. Cancer* **8,** (2020).

89. Merad, M., Sathe, P., Helft, J., Miller, J. & Mortha, A. The dendritic cell lineage: ontogeny and function of dendritic cells and their subsets in the steady state and the inflamed setting. *Annu. Rev. Immunol.* **31,** 563–604 (2013).

90. Veglia, F. & Gabrilovich, D. I. Dendritic cells in cancer: the role revisited. *Curr. Opin. Immunol.* **45,** 43–51 (2017).

91. Ma, Y., Shurin, G. V., Peiyuan, Z. & Shurin, M. R. Dendritic cells in the cancer microenvironment. *J. Cancer* **4,** 36–44 (2013).

92. Villani, A.-C. *et al.* Single-cell RNA-seq reveals new types of human blood dendritic cells, monocytes, and progenitors. *Science* **356,** (2017).

93. Gerhard, G. M., Bill, R., Messemaker, M., Klein, A. M. & Pittet, M. J. Tumor-infiltrating dendritic cell states are conserved across solid human cancers. *J. Exp. Med.* **218,** (2021).

94. Jardim, J. F., Gondak, R., Galvis, M. M., Pinto, C. A. L. & Kowalski, L. P. A decreased peritumoral CD1a+ cell number predicts a worse prognosis in oral squamous cell carcinoma. *Histopathology* **72,** 905–913 (2018).

95. Reichert, T. *et al.* The Number of Intratumoral Dendritic Cells and.

96. Partlová, S. *et al.* Distinct patterns of intratumoral immune cell infiltrates in patients with HPV-associated compared to non-virally induced head and neck squamous cell carcinoma. *Oncoimmunology* **4,** e965570 (2015).

97. Mosser, D. M. & Edwards, J. P. Exploring the full spectrum of macrophage activation. *Nat. Rev. Immunol.* **8,** 958–969 (2008).

98. Utispan, K. & Koontongkaew, S. Fibroblasts and macrophages: Key players in the head and neck cancer microenvironment. *Journal of Oral Biosciences* **59,** 23–30 (2017).

99. Hu, Y. *et al.* Tumor-associated macrophages correlate with the clinicopathological features and poor outcomes via inducing epithelial to mesenchymal transition in oral squamous cell carcinoma. *J Exp Clin Cancer Res* **35,** 12 (2016).

100. Mantovani, A., Marchesi, F., Malesci, A., Laghi, L. & Allavena, P. Tumour-associated macrophages as treatment targets in oncology. *Nat. Rev. Clin. Oncol.* **14,** 399–416 (2017).

101. Zhang, Q. *et al.* Integrated analysis of single-cell RNA-seq and bulk RNA-seq reveals distinct cancer-associated fibroblasts in head and neck squamous cell carcinoma. *Ann Transl Med* **9,** 1017 (2021).
102. Knops, A. M. *et al.* Cancer-Associated Fibroblast Density, Prognostic Characteristics, and Recurrence in Head and Neck Squamous Cell Carcinoma: A Meta-Analysis. *Front. Oncol.* **10,** 565306 (2020).
103. Zhou, B. *et al.* A role for cancer-associated fibroblasts in inducing the epithelial-to-mesenchymal transition in human tongue squamous cell carcinoma. *J Oral Pathol Med* **43,** 585–592 (2014).
104. Costea, D. E. *et al.* Identification of two distinct carcinoma-associated fibroblast subtypes with differential tumor-promoting abilities in oral squamous cell carcinoma. *Cancer Res.* **73,** 3888–3901 (2013).
105. Bienkowska, K. J., Hanley, C. J. & Thomas, G. J. Cancer-Associated Fibroblasts in Oral Cancer: A Current Perspective on Function and Potential for Therapeutic Targeting. *Front. Oral. Health* **2,** 686337 (2021).
106. Kumar, D. *et al.* Cancer-Associated Fibroblasts Drive Glycolysis in a Targetable Signaling Loop Implicated in Head and Neck Squamous Cell Carcinoma Progression. *Cancer Res.* **78,** 3769–3782 (2018).
107. Kang, S. H. *et al.* Cancer-Associated Fibroblast Subgroups Showing Differential Promoting Effect on HNSCC Progression. *Cancers (Basel)* **13,** (2021).
108. Wheeler, S. E. *et al.* Enhancement of head and neck squamous cell carcinoma proliferation, invasion, and metastasis by tumor-associated fibroblasts in preclinical models. *Head Neck* **36,** 385–392 (2014).

109. Wu, X. *et al.* Mesenchymal stromal cell therapies: immunomodulatory properties and clinical progress. *Stem Cell Res Ther* **11,** 345 (2020).

110. Kansy, B. A. *et al.* The bidirectional tumor--mesenchymal stromal cell interaction promotes the progression of head and neck cancer. *Stem Cell Res Ther* **5,** 95 (2014).

111. Liu, C. *et al.* Bone marrow mesenchymal stem cells interact with head and neck squamous cell carcinoma cells to promote cancer progression and drug resistance. *Neoplasia* **23,** 118–128 (2021).

112. Liotta, F. *et al.* Mesenchymal stem cells are enriched in head neck squamous cell carcinoma, correlates with tumour size and inhibit T-cell proliferation. *Br. J. Cancer* **112,** 745–754 (2015).

113. Mazzoni, A. *et al.* Human T cells interacting with HNSCC-derived mesenchymal stromal cells acquire tissue-resident memory like properties. *Eur. J. Immunol.* **50,** 1571–1579 (2020).

114. Pieper, K., Grimbacher, B. & Eibel, H. B-cell biology and development. *J. Allergy Clin. Immunol.* **131,** 959–971 (2013).

115. León, B., Ballesteros-Tato, A., Misra, R. S., Wojciechowski, W. & Lund, F. E. Unraveling effector functions of B cells during infection: the hidden world beyond antibody production. *Infect Disord Drug Targets* **12,** 213–221 (2012).

116. Hoffman, W., Lakkis, F. G. & Chalasani, G. B cells, antibodies, and more. *Clin. J. Am. Soc. Nephrol.* **11,** 137–154 (2016).

117. Turner, J. S. *et al.* Human germinal centres engage memory and naive B cells after influenza vaccination. *Nature* **586,** 127–132 (2020).

118. Jegaskanda, S. *et al.* Intranasal live influenza vaccine priming elicits localized B cell responses in mediastinal lymph nodes. *J. Virol.* **92,** (2018).
119. Pauli, N. T., Henry Dunand, C. J. & Wilson, P. C. Exploiting human memory B cell heterogeneity for improved vaccine efficacy. *Front. Immunol.* **2,** 77 (2011).
120. Lin, Z. *et al.* Pan-cancer analysis of genomic properties and clinical outcome associated with tumor tertiary lymphoid structure. *Sci. Rep.* **10,** 21530 (2020).
121. Hu, Q. *et al.* Atlas of breast cancer infiltrated B-lymphocytes revealed by paired single-cell RNA-sequencing and antigen receptor profiling. *Nat. Commun.* **12,** 2186 (2021).
122. Helmink, B. A. *et al.* B cells and tertiary lymphoid structures promote immunotherapy response. *Nature* **577,** 549–555 (2020).
123. Lundgren, S., Berntsson, J., Nodin, B., Micke, P. & Jirström, K. Prognostic impact of tumour-associated B cells and plasma cells in epithelial ovarian cancer. *J Ovarian Res* **9,** 21 (2016).
124. Santoiemma, P. P. & Powell, D. J. Tumor infiltrating lymphocytes in ovarian cancer. *Cancer Biol. Ther.* **16,** 807–820 (2015).
125. Germain, C., Gnjatic, S. & Dieu-Nosjean, M.-C. Tertiary Lymphoid Structure-Associated B Cells are Key Players in Anti-Tumor Immunity. *Front. Immunol.* **6,** 67 (2015).
126. Tang, A. *et al.* B cells promote tumor progression in a mouse model of HPV-mediated cervical cancer. *Int. J. Cancer* **139,** 1358–1371 (2016).
127. Bruno, T. C. *et al.* Antigen-Presenting Intratumoral B Cells Affect CD4+ TIL Phenotypes in Non-Small Cell Lung Cancer Patients. *Cancer Immunol Res* **5,** 898–

907 (2017).

128. Schlößer, H. A. *et al.* B cells in esophago-gastric adenocarcinoma are highly differentiated, organize in tertiary lymphoid structures and produce tumor-specific antibodies. *Oncoimmunology* **8,** e1512458 (2019).
129. Yuen, G. J., Demissie, E. & Pillai, S. B lymphocytes and cancer: a love-hate relationship. *Trends Cancer* **2,** 747–757 (2016).
130. LeBien, T. W. & Tedder, T. F. B lymphocytes: how they develop and function. *Blood* **112,** 1570–1580 (2008).
131. Kaminski, D. A., Wei, C., Qian, Y., Rosenberg, A. F. & Sanz, I. Advances in human B cell phenotypic profiling. *Front. Immunol.* **3,** 302 (2012).
132. Dono, M. *et al.* The human marginal zone B cell. *Ann. N. Y. Acad. Sci.* **987,** 117–124 (2003).
133. Tull, T. J. *et al.* Human marginal zone B cell development from early T2 progenitors. *J. Exp. Med.* **218,** (2021).
134. Pillai, S. & Cariappa, A. The follicular versus marginal zone B lymphocyte cell fate decision. *Nat. Rev. Immunol.* **9,** 767–777 (2009).
135. Siu, J. H. Y. *et al.* Two subsets of human marginal zone B cells resolved by global analysis of lymphoid tissues and blood. *Sci. Immunol.* **7,** eabm9060 (2022).
136. Avery, D. T. *et al.* BAFF selectively enhances the survival of plasmablasts generated from human memory B cells. *J. Clin. Invest.* **112,** 286–297 (2003).
137. in *Immunology Guidebook* 311–338 (Elsevier, 2004). doi:10.1016/B978-012198382-6/50033-9
138. Adler, L. N. *et al.* The Other Function: Class II-Restricted Antigen Presentation by B

Cells. *Front. Immunol.* **8,** 319 (2017).

139. Mesin, L., Ersching, J. & Victora, G. D. Germinal center B cell dynamics. *Immunity* **45,** 471–482 (2016).
140. De Silva, N. S. & Klein, U. Dynamics of B cells in germinal centres. *Nat. Rev. Immunol.* **15,** 137–148 (2015).
141. Warnatz, K. *et al.* Severe deficiency of switched memory B cells (CD271IgM2IgD2) in subgroups of patients with common variable immunodeficiency: a new approach to classify a heterogeneous disease.
142. Unger, S. *et al.* Ill-defined germinal centers and severely reduced plasma cells are histological hallmarks of lymphadenopathy in patients with common variable immunodeficiency. *J. Clin. Immunol.* **34,** 615–626 (2014).
143. Batista, F. D. & Harwood, N. E. The who, how and where of antigen presentation to B cells. *Nat. Rev. Immunol.* **9,** 15–27 (2009).
144. Allen, C. D. C., Okada, T. & Cyster, J. G. Germinal-center organization and cellular dynamics. *Immunity* **27,** 190–202 (2007).
145. Victora, G. D. *et al.* Identification of human germinal center light and dark zone cells and their relationship to human B-cell lymphomas. *Blood* **120,** 2240–2248 (2012).
146. Roco, J. A. *et al.* Class-Switch Recombination Occurs Infrequently in Germinal Centers. *Immunity* **51,** 337–350.e7 (2019).
147. Rodda, L. B., Bannard, O., Ludewig, B., Nagasawa, T. & Cyster, J. G. Phenotypic and Morphological Properties of Germinal Center Dark Zone Cxcl12-Expressing Reticular Cells. *J. Immunol.* **195,** 4781–4791 (2015).
148. Recaldin, T. & Fear, D. J. Transcription factors regulating B cell fate in the germinal

centre. *Clin. Exp. Immunol.* **183,** 65–75 (2016).

149. Brescia, P. *et al.* MEF2B instructs germinal center development and acts as an oncogene in B cell lymphomagenesis. *Cancer Cell* **34,** 453–465.e9 (2018).
150. Song, S. & Matthias, P. D. The transcriptional regulation of germinal center formation. *Front. Immunol.* **9,** 2026 (2018).
151. Ise, W. *et al.* The transcription factor BATF controls the global regulators of class-switch recombination in both B cells and T cells. *Nat. Immunol.* **12,** 536–543 (2011).
152. Severino, P. *et al.* Human Lymph Node-Derived Fibroblastic and Double-Negative Reticular Cells Alter Their Chemokines and Cytokines Expression Profile Following Inflammatory Stimuli. *Front. Immunol.* **8,** 141 (2017).
153. Silva-Cayetano, A. & Linterman, M. A. Stromal cell control of conventional and ectopic germinal centre reactions. *Curr. Opin. Immunol.* **64,** 26–33 (2020).
154. Denton, A. E. & Linterman, M. A. Stromal networking: cellular connections in the germinal centre. *Curr. Opin. Immunol.* **45,** 103–111 (2017).
155. Bannard, O. *et al.* Germinal center centroblasts transition to a centrocyte phenotype according to a timed program and depend on the dark zone for effective selection. *Immunity* **39,** 912–924 (2013).
156. Sautès-Fridman, C., Petitprez, F., Calderaro, J. & Fridman, W. H. Tertiary lymphoid structures in the era of cancer immunotherapy. *Nat. Rev. Cancer* **19,** 307–325 (2019).
157. Dieu-Nosjean, M.-C. *et al.* Tertiary lymphoid structures, drivers of the anti-tumor responses in human cancers. *Immunol. Rev.* **271,** 260–275 (2016).
158. Cabrita, R. *et al.* Tertiary lymphoid structures improve immunotherapy and survival

in melanoma. *Nature* **577,** 561–565 (2020).

159. Dieu-Nosjean, M.-C., Goc, J., Giraldo, N. A., Sautès-Fridman, C. & Fridman, W. H. Tertiary lymphoid structures in cancer and beyond. *Trends Immunol.* **35,** 571–580 (2014).

160. Drayton, D. L., Liao, S., Mounzer, R. H. & Ruddle, N. H. Lymphoid organ development: from ontogeny to neogenesis. *Nat. Immunol.* **7,** 344–353 (2006).

161. Alsughayyir, J., Pettigrew, G. J. & Motallebzadeh, R. Spoiling for a Fight: B Lymphocytes As Initiator and Effector Populations within Tertiary Lymphoid Organs in Autoimmunity and Transplantation. *Front. Immunol.* **8,** 1639 (2017).

162. Sautès-Fridman, C. *et al.* Tertiary lymphoid structures in cancers: prognostic value, regulation, and manipulation for therapeutic intervention. *Front. Immunol.* **7,** 407 (2016).

163. Lochner, M. *et al.* Microbiota-induced tertiary lymphoid tissues aggravate inflammatory disease in the absence of RORgamma t and LTi cells. *J. Exp. Med.* **208,** 125–134 (2011).

164. Guedj, K. *et al.* M1 macrophages act as LTβR-independent lymphoid tissue inducer cells during atherosclerosis-related lymphoid neogenesis. *Cardiovasc. Res.* **101,** 434–443 (2014).

165. van Erp, E. A., Luytjes, W., Ferwerda, G. & van Kasteren, P. B. Fc-Mediated Antibody Effector Functions During Respiratory Syncytial Virus Infection and Disease. *Front. Immunol.* **10,** 548 (2019).

166. Lu, L. L., Suscovich, T. J., Fortune, S. M. & Alter, G. Beyond binding: antibody effector functions in infectious diseases. *Nat. Rev. Immunol.* **18,** 46–61 (2018).

167. Sharonov, G. V., Serebrovskaya, E. O., Yuzhakova, D. V., Britanova, O. V. & Chudakov, D. M. B cells, plasma cells and antibody repertoires in the tumour microenvironment. *Nat. Rev. Immunol.* **20,** 294–307 (2020).

168. Trouw, L. A., Pickering, M. C. & Blom, A. M. The complement system as a potential therapeutic target in rheumatic disease. *Nat. Rev. Rheumatol.* **13,** 538–547 (2017).

169. Vidarsson, G., Dekkers, G. & Rispens, T. IgG subclasses and allotypes: from structure to effector functions. *Front. Immunol.* **5,** 520 (2014).

170. Xu, Z., Zan, H., Pone, E. J., Mai, T. & Casali, P. Immunoglobulin class-switch DNA recombination: induction, targeting and beyond. *Nat. Rev. Immunol.* **12,** 517–531 (2012).

171. Steffen, U. *et al.* IgA subclasses have different effector functions associated with distinct glycosylation profiles. *Nat. Commun.* **11,** 120 (2020).

172. Moens, L. & Tangye, S. G. Cytokine-Mediated Regulation of Plasma Cell Generation: IL-21 Takes Center Stage. *Front. Immunol.* **5,** 65 (2014).

173. Mackay, F. & Browning, J. L. BAFF: a fundamental survival factor for B cells. *Nat. Rev. Immunol.* **2,** 465–475 (2002).

174. Rodríguez-Pinto, D. B cells as antigen presenting cells. *Cell Immunol.* **238,** 67–75 (2005).

175. Chen, X. & Jensen, P. E. The role of B lymphocytes as antigen-presenting cells. *Arch. Immunol. Ther. Exp. (Warsz.)* **56,** 77–83 (2008).

176. Yuseff, M.-I., Pierobon, P., Reversat, A. & Lennon-Duménil, A.-M. How B cells capture, process and present antigens: a crucial role for cell polarity. *Nat. Rev. Immunol.* **13,** 475–486 (2013).

177. von Bergwelt-Baildon, M. S. *et al.* Human primary and memory cytotoxic T lymphocyte responses are efficiently induced by means of CD40-activated B cells as antigen-presenting cells: potential for clinical application. *Blood* **99,** 3319–3325 (2002).

178. Hong, S. *et al.* B Cells Are the Dominant Antigen-Presenting Cells that Activate Naive CD4+ T Cells upon Immunization with a Virus-Derived Nanoparticle Antigen. *Immunity* **49,** 695–708.e4 (2018).

179. Lapointe, R., Bellemare-Pelletier, A., Housseau, F., Thibodeau, J. & Hwu, P. CD40-stimulated B lymphocytes pulsed with tumor antigens are effective antigen-presenting cells that can generate specific T cells. *Cancer Res.* **63,** 2836–2843 (2003).

180. Shen, P. & Fillatreau, S. Antibody-independent functions of B cells: a focus on cytokines. *Nat. Rev. Immunol.* **15,** 441–451 (2015).

181. Zhou, P., Liang, K. & Yu, D. Germinal center TFH cells: T(w)o be or not t(w)o be, IL-6 is the answer. *Sci. Immunol.* **4,** (2019).

182. Huggins, J. *et al.* CpG DNA activation and plasma-cell differentiation of CD27- naive human B cells. *Blood* **109,** 1611–1619 (2007).

183. Lighaam, L. C. *et al.* In vitro-Induced Human IL-10+ B Cells Do Not Show a Subset-Defining Marker Signature and Plastically Co-express IL-10 With Pro-Inflammatory Cytokines. *Front. Immunol.* **9,** 1913 (2018).

184. Glass, M. C. *et al.* Human IL-10-producing B cells have diverse states that are induced from multiple B cell subsets. *Cell Rep.* **39,** 110728 (2022).

185. Rosser, E. C. & Mauri, C. Regulatory B cells: origin, phenotype, and function.

*Immunity* **42,** 607–612 (2015).

186. Sarvaria, A., Madrigal, J. A. & Saudemont, A. B cell regulation in cancer and anti-tumor immunity. *Cell Mol Immunol* **14,** 662–674 (2017).
187. Hagn, M. *et al.* Human B cells differentiate into granzyme B-secreting cytotoxic B lymphocytes upon incomplete T-cell help. *Immunol. Cell Biol.* **90,** 457–467 (2012).
188. Hagn, M. *et al.* Human B cells secrete granzyme B when recognizing viral antigens in the context of the acute phase cytokine IL-21. *J. Immunol.* **183,** 1838–1845 (2009).
189. Lindner, S. *et al.* Interleukin 21-induced granzyme B-expressing B cells infiltrate tumors and regulate T cells. *Cancer Res.* **73,** 2468–2479 (2013).
190. Janjic, B. M., Kulkarni, A., Ferris, R. L., Vujanovic, L. & Vujanovic, N. L. Human B Cells Mediate Innate Anti-Cancer Cytotoxicity Through Concurrent Engagement of Multiple TNF Superfamily Ligands. *Front. Immunol.* **13,** 837842 (2022).
191. Tao, H. *et al.* Antitumor effector B cells directly kill tumor cells via the Fas/FasL pathway and are regulated by IL-10. *Eur. J. Immunol.* **45,** 999–1009 (2015).
192. Kemp, T. J., Moore, J. M. & Griffith, T. S. Human B cells express functional TRAIL/Apo-2 ligand after CpG-containing oligodeoxynucleotide stimulation. *J. Immunol.* **173,** 892–899 (2004).
193. Lundy, S. K., Klinker, M. W. & Fox, D. A. Killer B lymphocytes and their fas ligand positive exosomes as inducers of immune tolerance. *Front. Immunol.* **6,** 122 (2015).
194. Lundy, S. K. Killer B lymphocytes: the evidence and the potential. *Inflamm Res* **58,** 345–357 (2009).
195. Petitprez, F. *et al.* B cells are associated with survival and immunotherapy response

in sarcoma. *Nature* **577,** 556–560 (2020).

196. Kim, S. S. *et al.* B Cells Improve Overall Survival in HPV-Associated Squamous Cell Carcinomas and Are Activated by Radiation and PD-1 Blockade. *Clin. Cancer Res.* **26,** 3345–3359 (2020).
197. Ladányi, A. *et al.* Prognostic impact of B-cell density in cutaneous melanoma. *Cancer Immunol. Immunother.* **60,** 1729–1738 (2011).
198. Garaud, S. *et al.* Tumor infiltrating B-cells signal functional humoral immune responses in breast cancer. *JCI Insight* **5,** (2019).
199. DiLillo, D. J., Yanaba, K. & Tedder, T. F. B cells are required for optimal CD4+ and CD8+ T cell tumor immunity: therapeutic B cell depletion enhances B16 melanoma growth in mice. *J. Immunol.* **184,** 4006–4016 (2010).
200. Inoue, S., Leitner, W. W., Golding, B. & Scott, D. Inhibitory effects of B cells on antitumor immunity. *Cancer Res.* **66,** 7741–7747 (2006).
201. Cui, C. *et al.* Neoantigen-driven B cell and CD4 T follicular helper cell collaboration promotes anti-tumor CD8 T cell responses. *Cell* **184,** 6101–6118.e13 (2021).
202. Edin, S. *et al.* The Prognostic Importance of CD20+ B lymphocytes in Colorectal Cancer and the Relation to Other Immune Cell subsets. *Sci. Rep.* **9,** 19997 (2019).
203. Germain, C. *et al.* Presence of B cells in tertiary lymphoid structures is associated with a protective immunity in patients with lung cancer. *Am. J. Respir. Crit. Care Med.* **189,** 832–844 (2014).
204. Mahmoud, S. M. A. *et al.* The prognostic significance of B lymphocytes in invasive carcinoma of the breast. *Breast Cancer Res. Treat.* **132,** 545–553 (2012).
205. Shi, J.-Y. *et al.* Margin-infiltrating CD20(+) B cells display an atypical memory

phenotype and correlate with favorable prognosis in hepatocellular carcinoma. *Clin. Cancer Res.* **19,** 5994–6005 (2013).

206. Kroeger, D. R., Milne, K. & Nelson, B. H. Tumor-Infiltrating Plasma Cells Are Associated with Tertiary Lymphoid Structures, Cytolytic T-Cell Responses, and Superior Prognosis in Ovarian Cancer. *Clin. Cancer Res.* **22,** 3005–3015 (2016).
207. Fristedt, R. *et al.* Prognostic impact of tumour-associated B cells and plasma cells in oesophageal and gastric adenocarcinoma. *J. Gastrointest. Oncol.* **7,** 848–859 (2016).
208. Sofopoulos, M. *et al.* The prognostic significance of peritumoral tertiary lymphoid structures in breast cancer. *Cancer Immunol. Immunother.* **68,** 1733–1745 (2019).
209. Dieu-Nosjean, M.-C. *et al.* Long-term survival for patients with non-small-cell lung cancer with intratumoral lymphoid structures. *J. Clin. Oncol.* **26,** 4410–4417 (2008).
210. Siliņa, K. *et al.* Germinal centers determine the prognostic relevance of tertiary lymphoid structures and are impaired by corticosteroids in lung squamous cell carcinoma. *Cancer Res.* **78,** 1308–1320 (2018).
211. Li, Q. *et al.* Prognostic value of tertiary lymphoid structure and tumour infiltrating lymphocytes in oral squamous cell carcinoma. *Int. J. Oral Sci.* **12,** 24 (2020).
212. Remark, R. *et al.* Characteristics and clinical impacts of the immune environments in colorectal and renal cell carcinoma lung metastases: influence of tumor origin. *Clin. Cancer Res.* **19,** 4079–4091 (2013).
213. Posch, F. *et al.* Maturation of tertiary lymphoid structures and recurrence of stage II and III colorectal cancer. *Oncoimmunology* **7,** e1378844 (2018).
214. Gopalakrishnan, V., Helmink, B. A., Spencer, C. N., Reuben, A. & Wargo, J. A. The

influence of the gut microbiome on cancer, immunity, and cancer immunotherapy. *Cancer Cell* **33,** 570–580 (2018).

215. Overacre-Delgoffe, A. E. *et al.* Microbiome-specific T follicular helper cells drive tertiary lymphoid structures and anti-tumor immunity against colorectal cancer. *BioRxiv* (2021). doi:10.1101/2021.01.27.428417
216. Prabhakaran, S. *et al.* Evaluation of invasive breast cancer samples using a 12-chemokine gene expression score: correlation with clinical outcomes. *Breast Cancer Res.* **19,** 71 (2017).
217. Pavoni, E. *et al.* Tumor-infiltrating B lymphocytes as an efficient source of highly specific immunoglobulins recognizing tumor cells. *BMC Biotechnol.* **7,** 70 (2007).
218. Reuschenbach, M., von Knebel Doeberitz, M. & Wentzensen, N. A systematic review of humoral immune responses against tumor antigens. *Cancer Immunol. Immunother.* **58,** 1535–1544 (2009).
219. Budiu, R. A. *et al.* Soluble MUC1 and serum MUC1-specific antibodies are potential prognostic biomarkers for platinum-resistant ovarian cancer. *Cancer Immunol. Immunother.* **60,** 975–984 (2011).
220. Bouillez, A. *et al.* MUC1-C promotes the suppressive immune microenvironment in non-small cell lung cancer. *Oncoimmunology* **6,** e1338998 (2017).
221. Fremd, C. *et al.* Mucin 1-specific B cell immune responses and their impact on overall survival in breast cancer patients. *Oncoimmunology* **5,** e1057387 (2016).
222. Hamanaka, Y. *et al.* Circulating anti-MUC1 IgG antibodies as a favorable prognostic factor for pancreatic cancer. *Int. J. Cancer* **103,** 97–100 (2003).
223. Blixt, O. *et al.* Autoantibodies to aberrantly glycosylated MUC1 in early stage breast

cancer are associated with a better prognosis. *Breast Cancer Res.* **13,** R25 (2011).

224. Ohue, Y. *et al.* Serum Antibody Against NY-ESO-1 and XAGE1 Antigens Potentially Predicts Clinical Responses to Anti-Programmed Cell Death-1 Therapy in NSCLC. *J. Thorac. Oncol.* **14,** 2071–2083 (2019).
225. Daudi, S. *et al.* Expression and immune responses to MAGE antigens predict survival in epithelial ovarian cancer. *PLoS One* **9,** e104099 (2014).
226. Lechner, A. *et al.* Tumor-associated B cells and humoral immune response in head and neck squamous cell carcinoma. *Oncoimmunology* **8,** 1535293 (2019).
227. Hansen, M. H., Nielsen, H. & Ditzel, H. J. The tumor-infiltrating B cell response in medullary breast cancer is oligoclonal and directed against the autoantigen actin exposed on the surface of apoptotic cancer cells. *Proc. Natl. Acad. Sci. USA* **98,** 12659–12664 (2001).
228. Hansen, M. H., Nielsen, H. V. & Ditzel, H. J. Translocation of an intracellular antigen to the surface of medullary breast cancer cells early in apoptosis allows for an antigen-driven antibody response elicited by tumor-infiltrating B cells. *J. Immunol.* **169,** 2701–2711 (2002).
229. Angelopoulou, K., Yu, H., Bharaj, B., Giai, M. & Diamandis, E. P. p53 gene mutation, tumor p53 protein overexpression, and serum p53 autoantibody generation in patients with breast cancer. *Clin. Biochem.* **33,** 53–62 (2000).
230. Ralhan, R. *et al.* Circulating p53 antibodies as early markers of oral cancer: correlation with p53 alterations. *Clin. Cancer Res.* **4,** 2147–2152 (1998).
231. Stockert, E. *et al.* A survey of the humoral immune response of cancer patients to a panel of human tumor antigens. *J. Exp. Med.* **187,** 1349–1354 (1998).

232. Kumar, S., Mohan, A. & Guleria, R. Prognostic implications of circulating anti-p53 antibodies in lung cancer--a review. *Eur. J. Cancer Care (Engl.)* **18,** 248–254 (2009).

233. Werner, J. A. *et al.* p53 serum antibodies as prognostic indicator in head and neck cancer. *Cancer Immunol. Immunother.* **44,** 112–116 (1997).

234. Tabuchi, Y. *et al.* Protective effect of naturally occurring anti-HER2 autoantibodies on breast cancer. *Breast Cancer Res. Treat.* **157,** 55–63 (2016).

235. Knutson, K. L. *et al.* Improved Survival of HER2+ Breast Cancer Patients Treated with Trastuzumab and Chemotherapy Is Associated with Host Antibody Immunity against the HER2 Intracellular Domain. *Cancer Res.* **76,** 3702–3710 (2016).

236. Sasada, T., Azuma, K., Ohtake, J. & Fujimoto, Y. Immune responses to epidermal growth factor receptor (EGFR) and their application for cancer treatment. *Front. Pharmacol.* **7,** 405 (2016).

237. Azuma, K. *et al.* Humoral immune responses to EGFR-derived peptides predict progression-free and overall survival of non-small cell lung cancer patients receiving gefitinib. *PLoS One* **9,** e86667 (2014).

238. Amornsiripanitch, N. *et al.* Complement factor H autoantibodies are associated with early stage NSCLC. *Clin. Cancer Res.* **16,** 3226–3231 (2010).

239. Dai, L., Lei, N., Liu, M. & Zhang, J.-Y. Autoantibodies to tumor-associated antigens as biomarkers in human hepatocellular carcinoma (HCC). *Exp Hematol Oncol* **2,** 15 (2013).

240. Yang, B., Li, X., Ren, T. & Yin, Y. Autoantibodies as diagnostic biomarkers for lung cancer: A systematic review. *Cell Death Discov.* **5,** 126 (2019).

241. Garaud, S. *et al.* Antigen Specificity and Clinical Significance of IgG and IgA

Autoantibodies Produced in situ by Tumor-Infiltrating B Cells in Breast Cancer. *Front. Immunol.* **9,** 2660 (2018).

242. Fischer, E. *et al.* Cryptic epitopes induce high-titer humoral immune response in patients with cancer. *J. Immunol.* **185,** 3095–3102 (2010).
243. Nonomura, C. *et al.* Identification of a neoantigen epitope in a melanoma patient with good response to anti-PD-1 antibody therapy. *Immunol. Lett.* **208,** 52–59 (2019).
244. DeFalco, J. *et al.* Non-progressing cancer patients have persistent B cell responses expressing shared antibody paratopes that target public tumor antigens. *Clin. Immunol.* **187,** 37–45 (2018).
245. Paulson, K. G. *et al.* Antibodies to merkel cell polyomavirus T antigen oncoproteins reflect tumor burden in merkel cell carcinoma patients. *Cancer Res.* **70,** 8388–8397 (2010).
246. Wieland, A. *et al.* Defining HPV-specific B cell responses in patients with head and neck cancer. *Nature* **597,** 274–278 (2021).
247. Watanabe, Y., Harada, S., Saito, I. & Miyamura, T. Prevalence of antibody against the core protein of hepatitis C virus in patients with hepatocellular carcinoma. *Int. J. Cancer* **48,** 340–343 (1991).
248. Dalagiorgou, G. *et al.* High levels of HCV core+1 antibodies in HCV patients with hepatocellular carcinoma. *J. Gen. Virol.* **92,** 1343–1351 (2011).
249. Chen, Y. & Tian, Z. HBV-Induced Immune Imbalance in the Development of HCC. *Front. Immunol.* **10,** 2048 (2019).
250. Broglie, M. A. *et al.* Evaluation of type-specific antibodies to high risk-human

papillomavirus (HPV) proteins in patients with oropharyngeal cancer. *Oral Oncol* **70,** 43–50 (2017).

251. Poonia, B., Ayithan, N., Nandi, M., Masur, H. & Kottilil, S. HBV induces inhibitory FcRL receptor on B cells and dysregulates B cell-T follicular helper cell axis. *Sci. Rep.* **8,** 15296 (2018).
252. Wang, X. D. *et al.* Decreased CD27 on B lymphocytes in patients with primary hepatocellular carcinoma. *J Int Med Res* **40,** 307–316 (2012).
253. Boonyaratanakornkit, J. & Taylor, J. J. Techniques to Study Antigen-Specific B Cell Responses. *Front. Immunol.* **10,** 1694 (2019).
254. Moody, M. A. & Haynes, B. F. Antigen-specific B cell detection reagents: use and quality control. *Cytometry A* **73,** 1086–1092 (2008).
255. Jahnmatz, P. *et al.* Multiplex analysis of antigen-specific memory B cells in humans using reversed B-cell FluoroSpot. *J. Immunol. Methods* **478,** 112715 (2020).
256. Gilbert, A. E. *et al.* Monitoring the systemic human memory B cell compartment of melanoma patients for anti-tumor IgG antibodies. *PLoS One* **6,** e19330 (2011).
257. Kurai, J. *et al.* Antibody-dependent cellular cytotoxicity mediated by cetuximab against lung cancer cell lines. *Clin. Cancer Res.* **13,** 1552–1561 (2007).
258. López-Albaitero, A. *et al.* Role of polymorphic Fc gamma receptor IIIa and EGFR expression level in cetuximab mediated, NK cell dependent in vitro cytotoxicity of head and neck squamous cell carcinoma cells. *Cancer Immunol. Immunother.* **58,** 1853–1864 (2009).
259. Chung, S. *et al.* Characterization of in vitro antibody-dependent cell-mediated cytotoxicity activity of therapeutic antibodies - impact of effector cells. *J. Immunol.*

*Methods* **407,** 63–75 (2014).

260. DiLillo, D. J. & Ravetch, J. V. Fc-Receptor Interactions Regulate Both Cytotoxic and Immunomodulatory Therapeutic Antibody Effector Functions. *Cancer Immunol Res* **3,** 704–713 (2015).
261. Roumenina, L. T., Daugan, M. V., Petitprez, F., Sautès-Fridman, C. & Fridman, W. H. Context-dependent roles of complement in cancer. *Nat. Rev. Cancer* **19,** 698–715 (2019).
262. Zhang, R., Liu, Q., Li, T., Liao, Q. & Zhao, Y. Role of the complement system in the tumor microenvironment. *Cancer Cell Int.* **19,** 300 (2019).
263. Brezicka, F., Einbeigi, Z. & Bergman, B. Functional assessment in vitro of human-complement-dependent antibody-induced cytotoxicity of neoplastic cells. *Cancer Immunol. Immunother.* **49,** 235–242 (2000).
264. Jourdan, M. *et al.* An in vitro model of differentiation of memory B cells into plasmablasts and plasma cells including detailed phenotypic and molecular characterization. *Blood* **114,** 5173–5181 (2009).
265. Ruffell, B. & Coussens, L. M. Macrophages and therapeutic resistance in cancer. *Cancer Cell* **27,** 462–472 (2015).
266. Shimabukuro-Vornhagen, A. *et al.* Antigen-presenting human B cells are expanded in inflammatory conditions. *J. Leukoc. Biol.* **101,** 577–587 (2017).
267. Gururajan, M., Sindhava, V. & Bondada, S. B cells and immunological tolerance. *Antibodies (Basel)* **3,** 116–129 (2014).
268. Evans, D. E., Munks, M. W., Purkerson, J. M. & Parker, D. C. Resting B lymphocytes as APC for naive T lymphocytes: dependence on CD40 ligand/CD40. *J. Immunol.*

**164,** 688–697 (2000).

269. Deola, S. *et al.* Helper B cells promote cytotoxic T cell survival and proliferation independently of antigen presentation through CD27/CD70 interactions. *J. Immunol.* **180,** 1362–1372 (2008).
270. Hladíková, K. *et al.* Tumor-infiltrating B cells affect the progression of oropharyngeal squamous cell carcinoma via cell-to-cell interactions with CD8+ T cells. *J. Immunother. Cancer* **7,** 261 (2019).
271. Fillatreau, S. B cells and their cytokine activities implications in human diseases. *Clin. Immunol.* **186,** 26–31 (2018).
272. Duddy, M. E., Alter, A. & Bar-Or, A. Distinct profiles of human B cell effector cytokines: a role in immune regulation? *J. Immunol.* **172,** 3422–3427 (2004).
273. Zhou, X., Su, Y.-X., Lao, X.-M., Liang, Y.-J. & Liao, G.-Q. CD19(+)IL-10(+) regulatory B cells affect survival of tongue squamous cell carcinoma patients and induce resting CD4(+) T cells to CD4(+)Foxp3(+) regulatory T cells. *Oral Oncol* **53,** 27–35 (2016).
274. Ouyang, F.-Z. *et al.* Dendritic cell-elicited B-cell activation fosters immune privilege via IL-10 signals in hepatocellular carcinoma. *Nat. Commun.* **7,** 13453 (2016).
275. Chen, Z. *et al.* Role of regulatory B cells in the progression of cervical cancer. *Mediators Inflamm.* **2019,** 6519427 (2019).
276. Xiao, X. *et al.* PD-1hi Identifies a Novel Regulatory B-cell Population in Human Hepatoma That Promotes Disease Progression. *Cancer Discov.* **6,** 546–559 (2016).
277. Wang, K., Liu, J. & Li, J. IL-35-producing B cells in gastric cancer patients. *Medicine* **97,** e0710 (2018).

278. Linderman, G. C., Rachh, M., Hoskins, J. G., Steinerberger, S. & Kluger, Y. Fast interpolation-based t-SNE for improved visualization of single-cell RNA-seq data. *Nat. Methods* **16,** 243–245 (2019).

279. Haghverdi, L., Büttner, M., Wolf, F. A., Buettner, F. & Theis, F. J. Diffusion pseudotime robustly reconstructs lineage branching. *Nat. Methods* **13,** 845–848 (2016).

280. Street, K. *et al.* Slingshot: cell lineage and pseudotime inference for single-cell transcriptomics. *BMC Genomics* **19,** 477 (2018).

281. Goltsev, Y. *et al.* Deep Profiling of Mouse Splenic Architecture with CODEX Multiplexed Imaging. *Cell* **174,** 968–981.e15 (2018).

282. Ruffin, A. T. *et al.* B cell signatures and tertiary lymphoid structures contribute to outcomes in head and neck squamous cell carcinoma. *Zenodo* (2021). doi:10.5281/zenodo.4599815

283. Jenks, S. A. *et al.* Distinct Effector B Cells Induced by Unregulated Toll-like Receptor 7 Contribute to Pathogenic Responses in Systemic Lupus Erythematosus. *Immunity* **49,** 725–739.e6 (2018).

284. Miller, N. J. *et al.* Merkel cell polyomavirus-specific immune responses in patients with Merkel cell carcinoma receiving anti-PD-1 therapy. *J. Immunother. Cancer* **6,** 131 (2018).

285. Zur Hausen, A., Rennspiess, D., Winnepenninckx, V., Speel, E.-J. & Kurz, A. K. Early B-cell differentiation in Merkel cell carcinomas: clues to cellular ancestry. *Cancer Res.* **73,** 4982–4987 (2013).

286. Dok, R. & Nuyts, S. HPV positive head and neck cancers: molecular pathogenesis

and evolving treatment strategies. *Cancers (Basel)* **8,** (2016).

287. Weinberger, P. M. *et al.* Molecular classification identifies a subset of human papillomavirus--associated oropharyngeal cancers with favorable prognosis. *J. Clin. Oncol.* **24,** 736–747 (2006).
288. Pitzalis, C., Jones, G. W., Bombardieri, M. & Jones, S. A. Ectopic lymphoid-like structures in infection, cancer and autoimmunity. *Nat. Rev. Immunol.* **14,** 447–462 (2014).
289. Neyt, K., Perros, F., GeurtsvanKessel, C. H., Hammad, H. & Lambrecht, B. N. Tertiary lymphoid organs in infection and autoimmunity. *Trends Immunol.* **33,** 297–305 (2012).
290. Castino, G. F. *et al.* Spatial distribution of B cells predicts prognosis in human pancreatic adenocarcinoma. *Oncoimmunology* **5,** e1085147 (2016).
291. Lu, N. *et al.* Human Semaphorin-4A drives Th2 responses by binding to receptor ILT-4. *Nat. Commun.* **9,** 742 (2018).
292. Kennedy, D. E. *et al.* Novel specialized cell state and spatial compartments within the germinal center. *Nat. Immunol.* **21,** 660–670 (2020).
293. Calderaro, J. *et al.* Intra-tumoral tertiary lymphoid structures are associated with a low risk of early recurrence of hepatocellular carcinoma. *J. Hepatol.* **70,** 58–65 (2019).
294. Gu-Trantien, C. *et al.* $CD4^+$ follicular helper T cell infiltration predicts breast cancer survival. *J. Clin. Invest.* **123,** 2873–2892 (2013).
295. Gu-Trantien, C. *et al.* CXCL13-producing TFH cells link immune suppression and adaptive memory in human breast cancer. *JCI Insight* **2,** (2017).

296. Bindea, G. *et al.* Spatiotemporal dynamics of intratumoral immune cells reveal the immune landscape in human cancer. *Immunity* **39,** 782–795 (2013).

297. Rossetti, R. A. M. *et al.* B lymphocytes can be activated to act as antigen presenting cells to promote anti-tumor responses. *PLoS One* **13,** e0199034 (2018).

298. Nelson, B. H. CD20+ B cells: the other tumor-infiltrating lymphocytes. *J. Immunol.* **185,** 4977–4982 (2010).

299. Figenschau, S. L., Fismen, S., Fenton, K. A., Fenton, C. & Mortensen, E. S. Tertiary lymphoid structures are associated with higher tumor grade in primary operable breast cancer patients. *BMC Cancer* **15,** 101 (2015).

300. Luther, S. A. *et al.* Differing activities of homeostatic chemokines CCL19, CCL21, and CXCL12 in lymphocyte and dendritic cell recruitment and lymphoid neogenesis. *J. Immunol.* **169,** 424–433 (2002).

301. Cupovic, J. *et al.* Central Nervous System Stromal Cells Control Local CD8(+) T Cell Responses during Virus-Induced Neuroinflammation. *Immunity* **44,** 622–633 (2016).

302. van der Zwaag, B. *et al.* PLEXIN-D1, a novel plexin family member, is expressed in vascular endothelium and the central nervous system during mouse embryogenesis. *Dev. Dyn.* **225,** 336–343 (2002).

303. Delgoffe, G. M. *et al.* Stability and function of regulatory T cells is maintained by a neuropilin-1-semaphorin-4a axis. *Nature* **501,** 252–256 (2013).

304. Renand, A. *et al.* Neuropilin-1 expression characterizes T follicular helper (Tfh) cells activated during B cell differentiation in human secondary lymphoid organs. *PLoS One* **8,** e85589 (2013).

305. Battaglia, A. *et al.* Neuropilin-1 expression identifies a subset of regulatory T cells in

human lymph nodes that is modulated by preoperative chemoradiation therapy in cervical cancer. *Immunology* **123,** 129–138 (2008).

306. Sarris, M., Andersen, K. G., Randow, F., Mayr, L. & Betz, A. G. Neuropilin-1 expression on regulatory T cells enhances their interactions with dendritic cells during antigen recognition. *Immunity* **28,** 402–413 (2008).
307. Lee, H. J. *et al.* Tertiary lymphoid structures: prognostic significance and relationship with tumour-infiltrating lymphocytes in triple-negative breast cancer. *J. Clin. Pathol.* **69,** 422–430 (2016).
308. Im, S. J. *et al.* Defining CD8+ T cells that provide the proliferative burst after PD-1 therapy. *Nature* **537,** 417–421 (2016).
309. Sautès-Fridman, C. *et al.* Tertiary Lymphoid Structures and B cells: Clinical impact and therapeutic modulation in cancer. *Semin. Immunol.* **48,** 101406 (2020).
310. Meylan, M. *et al.* Tertiary lymphoid structures generate and propagate anti-tumor antibody-producing plasma cells in renal cell cancer. *Immunity* **55,** 527–541.e5 (2022).
311. Zhang, Z. *et al.* Landscape of infiltrating B cells and their clinical significance in human hepatocellular carcinoma. *Oncoimmunology* **8,** e1571388 (2019).
312. Berntsson, J., Nodin, B., Eberhard, J., Micke, P. & Jirström, K. Prognostic impact of tumour-infiltrating B cells and plasma cells in colorectal cancer. *Int. J. Cancer* **139,** 1129–1139 (2016).
313. Mullins, C. S., Gock, M., Krohn, M. & Linnebacher, M. Human colorectal carcinoma infiltrating B lymphocytes are active secretors of the immunoglobulin isotypes A, G, and M. *Cancers (Basel)* **11,** (2019).

314. Seifert, M. & Küppers, R. Human memory B cells. *Leukemia* **30,** 2283–2292 (2016).

315. Sanz, I., Wei, C., Lee, F. E.-H. & Anolik, J. Phenotypic and functional heterogeneity of human memory B cells. *Semin. Immunol.* **20,** 67–82 (2008).

316. Sanz, I. *et al.* Challenges and opportunities for consistent classification of human B cell and plasma cell populations. *Front. Immunol.* **10,** 2458 (2019).

317. Austin, J. W. *et al.* Overexpression of T-bet in HIV infection is associated with accumulation of B cells outside germinal centers and poor affinity maturation. *Sci. Transl. Med.* **11,** (2019).

318. Woodruff, M. C. *et al.* Extrafollicular B cell responses correlate with neutralizing antibodies and morbidity in COVID-19. *Nat. Immunol.* **21,** 1506–1516 (2020).

319. Portugal, S. *et al.* Malaria-associated atypical memory B cells exhibit markedly reduced B cell receptor signaling and effector function. *Elife* **4,** (2015).

320. Knox, J. J. *et al.* T-bet+ B cells are induced by human viral infections and dominate the HIV gp140 response. *JCI Insight* **2,** (2017).

321. Portugal, S., Obeng-Adjei, N., Moir, S., Crompton, P. D. & Pierce, S. K. Atypical memory B cells in human chronic infectious diseases: An interim report. *Cell Immunol.* **321,** 18–25 (2017).

322. Sullivan, R. T. *et al.* FCRL5 Delineates Functionally Impaired Memory B Cells Associated with Plasmodium falciparum Exposure. *PLoS Pathog.* **11,** e1004894 (2015).

323. Braddom, A. E., Batugedara, G., Bol, S. & Bunnik, E. M. Potential functions of atypical memory B cells in Plasmodium-exposed individuals. *Int. J. Parasitol.* **50,** 1033–1042 (2020).

324. Holla, P. *et al.* Shared transcriptional profiles of atypical B cells suggest common drivers of expansion and function in malaria, HIV, and autoimmunity. *Sci. Adv.* **7,** (2021).

325. Moir, S. *et al.* Evidence for HIV-associated B cell exhaustion in a dysfunctional memory B cell compartment in HIV-infected viremic individuals. *J. Exp. Med.* **205,** 1797–1805 (2008).

326. Knox, J. J., Kaplan, D. E. & Betts, M. R. T-bet-expressing B cells during HIV and HCV infections. *Cell Immunol.* **321,** 26–34 (2017).

327. Centuori, S. M. *et al.* Double-negative (CD27-IgD-) B cells are expanded in NSCLC and inversely correlate with affinity-matured B cell populations. *J. Transl. Med.* **16,** 30 (2018).

328. Nielsen, J. S. *et al.* CD20+ tumor-infiltrating lymphocytes have an atypical CD27- memory phenotype and together with CD8+ T cells promote favorable prognosis in ovarian cancer. *Clin. Cancer Res.* **18,** 3281–3292 (2012).

329. Elsner, R. A. & Shlomchik, M. J. Germinal center and extrafollicular B cell responses in vaccination, immunity, and autoimmunity. *Immunity* **53,** 1136–1150 (2020).

330. Elsner, R. A. & Shlomchik, M. J. IL-12 Blocks Tfh Cell Differentiation during Salmonella Infection, thereby Contributing to Germinal Center Suppression. *Cell Rep.* **29,** 2796–2809.e5 (2019).

331. Ambegaonkar, A. A., Nagata, S., Pierce, S. K. & Sohn, H. The Differentiation in vitro of Human Tonsil B Cells With the Phenotypic and Functional Characteristics of T-bet+ Atypical Memory B Cells in Malaria. *Front. Immunol.* **10,** 852 (2019).

332. Griss, J. *et al.* B cells sustain inflammation and predict response to immune

checkpoint blockade in human melanoma. *Nat. Commun.* **10,** 4186 (2019).

333. Ruffin, A. T. *et al.* Divergent cancer etiologies drive distinct B cell signatures and tertiary lymphoid structures. *BioRxiv* (2020). doi:10.1101/2020.05.29.123265

334. Shimabukuro-Vornhagen, A. *et al.* Characterization of tumor-associated B-cell subsets in patients with colorectal cancer. *Oncotarget* **5,** 4651–4664 (2014).

335. Weisel, N. M. *et al.* Comprehensive analyses of B-cell compartments across the human body reveal novel subsets and a gut-resident memory phenotype. *Blood* **136,** 2774–2785 (2020).

336. Burger, J. A. & Wiestner, A. Targeting B cell receptor signalling in cancer: preclinical and clinical advances. *Nat. Rev. Cancer* **18,** 148–167 (2018).

337. Andrews, L. P., Marciscano, A. E., Drake, C. G. & Vignali, D. A. A. LAG3 (CD223) as a cancer immunotherapy target. *Immunol. Rev.* **276,** 80–96 (2017).

338. Bengsch, B. *et al.* Bioenergetic Insufficiencies Due to Metabolic Alterations Regulated by the Inhibitory Receptor PD-1 Are an Early Driver of CD8(+) T Cell Exhaustion. *Immunity* **45,** 358–373 (2016).

339. Oida, T., Xu, L., Weiner, H. L., Kitani, A. & Strober, W. TGF-beta-mediated suppression by CD4+CD25+ T cells is facilitated by CTLA-4 signaling. *J. Immunol.* **177,** 2331–2339 (2006).

340. Watson, M. J. *et al.* Metabolic support of tumour-infiltrating regulatory T cells by lactic acid. *Nature* **591,** 645–651 (2021).

341. DePeaux, K. & Delgoffe, G. M. Metabolic barriers to cancer immunotherapy. *Nat. Rev. Immunol.* **21,** 785–797 (2021).

342. Scharping, N. E. *et al.* The tumor microenvironment represses T cell mitochondrial

biogenesis to drive intratumoral T cell metabolic insufficiency and dysfunction. *Immunity* **45,** 374–388 (2016).

343. Scharping, N. E. *et al.* Mitochondrial stress induced by continuous stimulation under hypoxia rapidly drives T cell exhaustion. *Nat. Immunol.* **22,** 205–215 (2021).
344. Haga, C. L., Ehrhardt, G. R. A., Boohaker, R. J., Davis, R. S. & Cooper, M. D. Fc receptor-like 5 inhibits B cell activation via SHP-1 tyrosine phosphatase recruitment. *Proc. Natl. Acad. Sci. USA* **104,** 9770–9775 (2007).
345. Wilson, T. J., Fuchs, A. & Colonna, M. Cutting edge: human FcRL4 and FcRL5 are receptors for IgA and IgG. *J. Immunol.* **188,** 4741–4745 (2012).
346. Merlo, A. *et al.* Inhibitory receptors CD85j, LAIR-1, and CD152 down-regulate immunoglobulin and cytokine production by human B lymphocytes. *Clin Diagn Lab Immunol* **12,** 705–712 (2005).
347. Son, M., Santiago-Schwarz, F., Al-Abed, Y. & Diamond, B. C1q limits dendritic cell differentiation and activation by engaging LAIR-1. *Proc. Natl. Acad. Sci. USA* **109,** E3160-7 (2012).
348. Carvalheiro, T. *et al.* Leukocyte associated immunoglobulin like receptor 1 regulation and function on monocytes and dendritic cells during inflammation. *Front. Immunol.* **11,** 1793 (2020).
349. Nitschke, L. & Tsubata, T. Molecular interactions regulate BCR signal inhibition by CD22 and CD72. *Trends Immunol.* **25,** 543–550 (2004).
350. Kardava, L. *et al.* Attenuation of HIV-associated human B cell exhaustion by siRNA downregulation of inhibitory receptors. *J. Clin. Invest.* **121,** 2614–2624 (2011).
351. Johnson, J. L. *et al.* The Transcription Factor T-bet Resolves Memory B Cell

Subsets with Distinct Tissue Distributions and Antibody Specificities in Mice and Humans. *Immunity* **52,** 842–855.e6 (2020).

352. Khan, O. *et al.* TOX transcriptionally and epigenetically programs CD8+ T cell exhaustion. *Nature* **571,** 211–218 (2019).
353. Myles, A., Gearhart, P. J. & Cancro, M. P. Signals that drive T-bet expression in B cells. *Cell Immunol.* **321,** 3–7 (2017).
354. Papillion, A. *et al.* Inhibition of IL-2 responsiveness by IL-6 is required for the generation of GC-TFH cells. *Sci. Immunol.* **4,** (2019).
355. Gobin, E. *et al.* A pan-cancer perspective of matrix metalloproteases (MMP) gene expression profile and their diagnostic/prognostic potential. *BMC Cancer* **19,** 581 (2019).
356. Castañeda, D. M., Salgado, D. M. & Narváez, C. F. B cells naturally induced during dengue virus infection release soluble CD27, the plasma level of which is associated with severe forms of pediatric dengue. *Virology* **497,** 136–145 (2016).
357. Widney, D. *et al.* Aberrant expression of CD27 and soluble CD27 (sCD27) in HIV infection and in AIDS-associated lymphoma. *Clin. Immunol.* **93,** 114–123 (1999).
358. Kato, K., Chu, P., Takahashi, S., Hamada, H. & Kipps, T. J. Metalloprotease inhibitors block release of soluble CD27 and enhance the immune stimulatory activity of chronic lymphocytic leukemia cells. *Exp. Hematol.* **35,** 434–442 (2007).
359. Bohnhorst, J. Ø. *et al.* Abnormal B cell differentiation in primary Sjögren's syndrome results in a depressed percentage of circulating memory B cells and elevated levels of soluble CD27 that correlate with Serum IgG concentration. *Clin. Immunol.* **103,** 79–88 (2002).

360. Mazor, R. D. *et al.* Tumor-reactive antibodies evolve from non-binding and autoreactive precursors. *Cell* **185,** 1208–1222.e21 (2022).

361. Macdonald, I. K., Parsy-Kowalska, C. B. & Chapman, C. J. Autoantibodies: opportunities for early cancer detection. *Trends Cancer* **3,** 198–213 (2017).

362. Emens, L. A. & Middleton, G. The interplay of immunotherapy and chemotherapy: harnessing potential synergies. *Cancer Immunol Res* **3,** 436–443 (2015).

363. Derer, A., Frey, B., Fietkau, R. & Gaipl, U. S. Immune-modulating properties of ionizing radiation: rationale for the treatment of cancer by combination radiotherapy and immune checkpoint inhibitors. *Cancer Immunol. Immunother.* **65,** 779–786 (2016).

364. Walle, T. *et al.* Radiation effects on antitumor immune responses: current perspectives and challenges. *Ther Adv Med Oncol* **10,** 1758834017742575 (2018).

365. Montfort, A. *et al.* A Strong B-cell Response Is Part of the Immune Landscape in Human High-Grade Serous Ovarian Metastases. *Clin. Cancer Res.* **23,** 250–262 (2017).

366. Thibult, M.-L. *et al.* PD-1 is a novel regulator of human B-cell activation. *Int. Immunol.* **25,** 129–137 (2013).

367. Wang, X. *et al.* PD-1-expressing B cells suppress CD4+ and CD8+ T cells via PD-1/PD-L1-dependent pathway. *Mol. Immunol.* **109,** 20–26 (2019).

368. Agata, Y. *et al.* Expression of the PD-1 antigen on the surface of stimulated mouse T and B lymphocytes. *Int. Immunol.* **8,** 765–772 (1996).

369. Good-Jacobson, K. L. *et al.* PD-1 regulates germinal center B cell survival and the formation and affinity of long-lived plasma cells. *Nat. Immunol.* **11,** 535–542 (2010).

370. Shi, J. *et al.* PD-1 Controls Follicular T Helper Cell Positioning and Function. *Immunity* **49,** 264–274.e4 (2018).

371. Schwartz, M., Zhang, Y. & Rosenblatt, J. D. B cell regulation of the anti-tumor response and role in carcinogenesis. *J. Immunother. Cancer* **4,** 40 (2016).

372. Wu, H. *et al.* PD-L1+ regulatory B cells act as a T cell suppressor in a PD-L1-dependent manner in melanoma patients with bone metastasis. *Mol. Immunol.* **119,** 83–91 (2020).

373. Pipi, E. *et al.* Tertiary lymphoid structures: autoimmunity goes local. *Front. Immunol.* **9,** 1952 (2018).

374. Chin, E. N. *et al.* Antitumor activity of a systemic STING-activating non-nucleotide cGAMP mimetic. *Science* **369,** 993–999 (2020).

375. Le Naour, J., Zitvogel, L., Galluzzi, L., Vacchelli, E. & Kroemer, G. Trial watch: STING agonists in cancer therapy. *Oncoimmunology* **9,** 1777624 (2020).

376. Pan, B.-S. *et al.* An orally available non-nucleotide STING agonist with antitumor activity. *Science* **369,** (2020).

377. Denton, A. E. *et al.* Type I interferon induces CXCL13 to support ectopic germinal center formation. *J. Exp. Med.* **216,** 621–637 (2019).

378. Chelvanambi, M., Fecek, R. J., Taylor, J. L. & Storkus, W. J. STING agonist-based treatment promotes vascular normalization and tertiary lymphoid structure formation in the therapeutic melanoma microenvironment. *J. Immunother. Cancer* **9,** (2021).

379. Cohavy, O., Zhou, J., Granger, S. W., Ware, C. F. & Targan, S. R. LIGHT expression by mucosal T cells may regulate IFN-gamma expression in the intestine. *J. Immunol.* **173,** 251–258 (2004).

380. Tang, H., Zhu, M., Qiao, J. & Fu, Y.-X. Lymphotoxin signalling in tertiary lymphoid structures and immunotherapy. *Cell Mol Immunol* **14,** 809–818 (2017).

381. Duhen, T. *et al.* LIGHT costimulates CD40 triggering and induces immunoglobulin secretion; a novel key partner in T cell-dependent B cell terminal differentiation. *Eur. J. Immunol.* **34,** 3534–3541 (2004).

382. Johansson-Percival, A. *et al.* De novo induction of intratumoral lymphoid structures and vessel normalization enhances immunotherapy in resistant tumors. *Nat. Immunol.* **18,** 1207–1217 (2017).

383. Berraondo, P. *et al.* Cytokines in clinical cancer immunotherapy. *Br. J. Cancer* **120,** 6–15 (2019).

384. Seo, Y. B. *et al.* Crucial roles of interleukin-7 in the development of T follicular helper cells and in the induction of humoral immunity. *J. Virol.* **88,** 8998–9009 (2014).

385. Avery, D. T. *et al.* B cell-intrinsic signaling through IL-21 receptor and STAT3 is required for establishing long-lived antibody responses in humans. *J. Exp. Med.* **207,** 155–171 (2010).

386. Fawkner-Corbett, D. *et al.* Spatiotemporal analysis of human intestinal development at single-cell resolution. *Cell* **184,** 810–826.e23 (2021).

387. Muñoz, N. M. *et al.* Molecularly targeted photothermal ablation improves tumor specificity and immune modulation in a rat model of hepatocellular carcinoma. *Commun. Biol.* **3,** 783 (2020).

388. Rohaan, M. W., Wilgenhof, S. & Haanen, J. B. A. G. Adoptive cellular therapies: the current landscape. *Virchows Arch* **474,** 449–461 (2019).

389. Wennhold, K., Shimabukuro-Vornhagen, A. & von Bergwelt-Baildon, M. B Cell-

Based Cancer Immunotherapy. *Transfus. Med. Hemother.* **46,** 36–46 (2019).

390. Néron, S. *et al.* B cell proliferation following CD40 stimulation results in the expression and activation of Src protein tyrosine kinase. *Int. Immunol.* **18,** 375–387 (2006).
391. von Bergwelt-Baildon, M. *et al.* CD40-activated B cells express full lymph node homing triad and induce T-cell chemotaxis: potential as cellular adjuvants. *Blood* **107,** 2786–2789 (2006).
392. Batista, F. D. & Neuberger, M. S. Affinity dependence of the B cell response to antigen: a threshold, a ceiling, and the importance of off-rate. *Immunity* **8,** 751–759 (1998).
393. Trefzer, U. *et al.* Hybrid cell vaccination for cancer immune therapy: first clinical trial with metastatic melanoma. *Int. J. Cancer* **85,** 618–626 (2000).
394. Geffroy-Luseau, A. *et al.* TLR9 ligand induces the generation of CD20+ plasmablasts and plasma cells from CD27+ memory B-cells. *Front. Immunol.* **2,** 83 (2011).
395. Henn, A. D. *et al.* Functionally Distinct Subpopulations of CpG-Activated Memory B Cells. *Sci. Rep.* **2,** 345 (2012).
396. Moffett, H. F. *et al.* B cells engineered to express pathogen-specific antibodies protect against infection. *Sci. Immunol.* **4,** (2019).
397. Burris, H. A. *et al.* Safety and Activity of Varlilumab, a Novel and First-in-Class Agonist Anti-CD27 Antibody, in Patients With Advanced Solid Tumors. *J. Clin. Oncol.* **35,** 2028–2036 (2017).
398. Starzer, A. M. & Berghoff, A. S. New emerging targets in cancer immunotherapy:

CD27 (TNFRSF7). *ESMO Open* **4,** e000629 (2020).

399. Lee, J. K., Mathew, S. O., Vaidya, S. V., Kumaresan, P. R. & Mathew, P. A. CS1 (CRACC, CD319) induces proliferation and autocrine cytokine expression on human B lymphocytes. *J. Immunol.* **179,** 4672–4678 (2007).
400. Magen, H. & Muchtar, E. Elotuzumab: the first approved monoclonal antibody for multiple myeloma treatment. *Ther. Adv. Hematol.* **7,** 187–195 (2016).
401. Airas, L. & Jalkanen, S. CD73 mediates adhesion of B cells to follicular dendritic cells. *Blood* **88,** 1755–1764 (1996).
402. Perrot, I. *et al.* Blocking antibodies targeting the CD39/CD73 immunosuppressive pathway unleash immune responses in combination cancer therapies. *Cell Rep.* **27,** 2411–2425.e9 (2019).
403. Conter, L. J., Song, E., Shlomchik, M. J. & Tomayko, M. M. CD73 expression is dynamically regulated in the germinal center and bone marrow plasma cells are diminished in its absence. *PLoS One* **9,** e92009 (2014).
404. Parra, M. *et al.* Memory CD73+IgM+ B cells protect against Plasmodium yoelii infection and express Granzyme B. *PLoS One* **15,** e0238493 (2020).
405. Li, H. *et al.* Fc receptor-like 4 and 5 define human atypical memory B cells. *Int. Immunol.* **32,** 755–770 (2020).
406. Tsubata, T. Role of inhibitory BCR co-receptors in immunity. *Infect Disord Drug Targets* **12,** 181–190 (2012).
407. Chuckran, C. A., Liu, C., Bruno, T. C., Workman, C. J. & Vignali, D. A. Neuropilin-1: a checkpoint target with unique implications for cancer immunology and immunotherapy. *J. Immunother. Cancer* **8,** (2020).

408. Joshi, N. S. *et al.* Regulatory T Cells in Tumor-Associated Tertiary Lymphoid Structures Suppress Anti-tumor T Cell Responses. *Immunity* **43,** 579–590 (2015).